

This document downloaded from
vulcanhammer.net **vulcanhammer.info**
Chet Aero Marine



Don't forget to visit our companion site
<http://www.vulcanhammer.org>

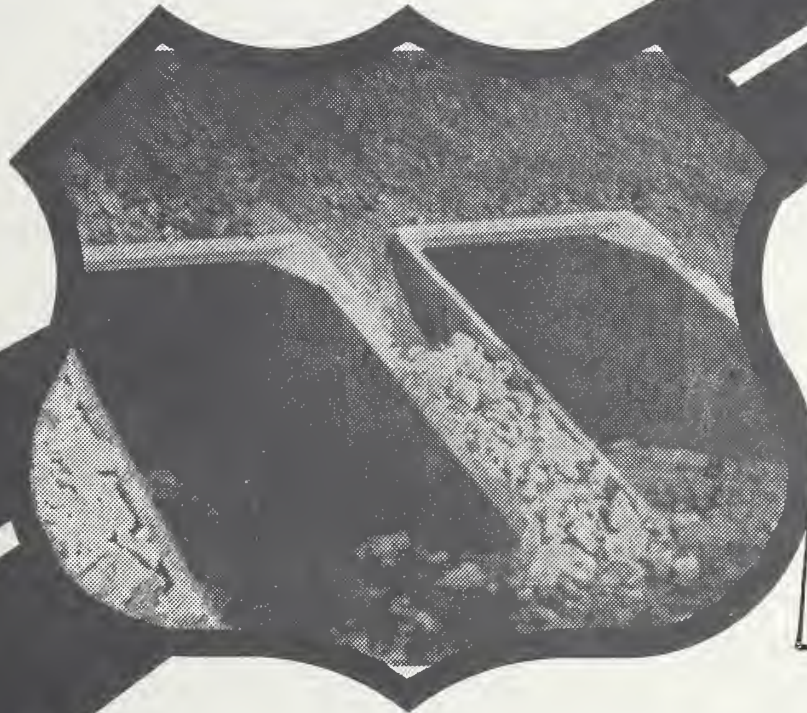
Use subject to the terms and conditions of the respective websites.

TE
662
.A3
no.
FHWA-
RD-
80-172

Report No. FHWA/RD-80/172

SHANDE-1980: BOX CULVERTS AND SOIL MODELS

May 1981
Final Report



Document is available to the public through
the National Technical Information Service,
Springfield, Virginia 22161

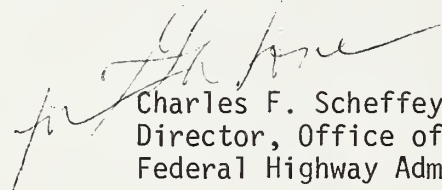


Prepared for
FEDERAL HIGHWAY ADMINISTRATION
Offices of Research & Development
Structures and Applied Mechanics Division
Washington, D.C. 20590

FOREWORD

This report presents the results of a study designed to extend the capability of the FHWA "CANDE" (Culvert Analysis and Design) computer program to include the capability for the automated finite element analysis for the structural design of precast reinforced concrete box culvert installations. The study also resulted in a new reinforced concrete model with loading through ultimate, unloading and redistribution of stresses due to cracking, as well as a new soil model (the so-called Duncan model). Included in the report is a User Manual Supplement and three (3) solved sample problems. Overlay instructions permit the program to be executed more efficiently and with less computer core storage requirements. This report will be of primary interest to supervisors, engineers, and consultants responsible for the design of culverts.

This report is being distributed under FHWA Bulletin with sufficient copies of the report to provide one copy to each regional office, one copy to each division, and one copy to each State highway department. Direct distribution is being made to the division offices.



Charles F. Scheffey
Director, Office of Research
Federal Highway Administration

NOTICE

This document is disseminated under the sponsorship of the Department of Transportation in the interest of information exchange. The United States Government assumes no liability for its contents or use thereof.

The contents of this report reflect the views of the authors, who are responsible for the facts and the accuracy of the data presented herein. The contents do not necessarily reflect the official views or policy of the Department of Transportation.

This report does not constitute a standard, specification, or regulation.

The United States Government does not endorse products or manufacturers. Trademarks or manufacturers' names appear herein only because they are considered essential to the object of this document.

662
A3
20.
FHWA - RD -

-172

Technical Report Documentation Page

1. Report No. FHWA/RD-80/172	2. Government Accession No.	3. Recipient's Catalog No.	
4. Title and Subtitle CANDE-1980: Box Culverts and Soil Models		5. Report Date May 1981	
6. Performing Organization Code		8. Performing Organization Report No.	
7. Author(s) Katona, M.G., Vittes, P.D., Lee, C.H., and Ho, H.T.		10. Work Unit No. (TRAIS) 35I3-241	
9. Performing Organization Name and Address University of Notre Dame Notre Dame, Indiana 46556		11. Contract or Grant No. DOT-FH-11-9408	
12. Sponsoring Agency Name and Address Offices of Research and Development Federal Highway Administration U.S. Department of Transportation Washington, D.C. 20590		13. Type of Report and Period Covered Final Report November 1978-October 1980	
15. Supplementary Notes George W. Ring, Contract Manager, HRS-14		DEPARTMENT OF SPONSORING AGENCY CODE TRANSPORTATION	
16. Abstract The CANDE computer program, introduced in 1976 for the structural design and analysis of buried culverts, is extended and enhanced in this work effort to include options for automated finite element analysis of precast, reinforced concrete box culverts, and new nonlinear soil models. User input instructions for the new options, now operative in the CANDE-1980 program, are provided in the appendix of this report along with example input/output data.		JAN 11 1982 LIBRARY	
Comparisons between CANDE-1980 predictions and the elastic analysis/design method used to develop the ASTM C789 design tables for precast box culverts revealed the importance of soil-structure interaction which is not taken into account in the latter method. As a general conclusion, the ASTM C 789 design tables provide safe designs (conservative) providing that good quality soil is used for backfill.			
The so-called Duncan soil model, employing hyperbolic functions for Young's modulus and bulk modulus, is a new soil model option in CANDE-1980. Standard soil model parameters, established from a large data base of triaxial tests, are stored in the program and can be used by simply identifying the type of soil and degree of compaction. In a similar manner, simplified data input options have also been developed for the overburden dependent soil model.			
In addition to user input instructions and example input/output data, the appendices also provide overlay instructions to reduce computer core storage requirements.			
17. Key Words Culverts, Box Culverts, Soil Models, Soil Structure Interaction	18. Distribution Statement No restrictions. This document is available through the National Technical Information Service, Springfield, Virginia 22161.		
19. Security Classif. (of this report) Unclassified	20. Security Classif. (of this page) Unclassified	21. No. of Pages 214	22. Price

ACKNOWLEDGMENTS

Representatives of industry, state highway departments, universities and research groups have been very helpful in providing information and constructive comments for this research effort. A special thank you is extended to Dr. James M. Duncan of the University of California for providing data and details of his soil model, and to Dr. Frank J. Heger of Simpson Gumpertz and Heger Inc. who, along with representatives of the American Concrete Pipe Association, supplied experimental data for out-of-ground tests. Mr. Robert Thacker provided consultation on overlaying the CANDE program on the IBM computers and programming the metric version of CANDE-1980.

TABLE OF CONTENTS

	<u>Page</u>
CHAPTER 1 - INTRODUCTION	1
1.1 Background	1
1.2 Objectives	2
1.3 Scope and Approach	2
CHAPTER 2 - REVIEW OF PRECAST BOX CULVERTS	4
2.1 Background	4
2.2 Development and rational of ASTM precast box culvert standards	5
CHAPTER 3 - REINFORCED CONCRETE MODEL	10
3.1 Objective	10
3.2 Assumptions, limitations and approach	10
3.3 Basic formulation for beam-rod element	12
3.4 Finite element interpolations	16
3.5 Stress-strain relationships	19
3.6 Section properties	23
3.7 Incremental solution strategy	24
3.8 Measures of reinforced concrete performance.	26
3.9 Standard parameters for concrete and reinforcement	29
CHAPTER 4 - EVALUATION OF REINFORCED CONCRETE MODEL FOR CIRCULAR PIPE LOADED IN THREE-EDGE BEARING	31
4.1 Preliminary investigations	31
4.2 Experimental tests	33
4.3 Analytical model and comparison of results	37
CHAPTER 5 - EVALUATION OF REINFORCED CONCRETE MODEL FOR BOX CULVERTS LOADED IN FOUR-EDGE BEARING	49
5.1 Experimental tests	49
5.2 CANDE model	53
5.3 Comparison of models with experiments	53
CHAPTER 6 - DEVELOPMENT OF LEVEL 2 BOX MESH	62
6.1 Parameters to define the models	62
6.2 Assumptions and limitations	67
CHAPTER 7 - EVALUATION OF CANDE BOX-SOIL SYSTEM	71
7.1 Sensitivity of soil parameters	71
7.2 Comparison with test data	79

TABLE OF CONTENTS (Continued)

	<u>Page</u>
CHAPTER 8 - EVALUATION OF ASTM C789 DESIGN TABLES WITH CANDE	85
8.1 Box section studies for dead load.	85
8.2 Box section studies with live loads	111
CHAPTER 9 - SOIL MODELS.	115
9.1 Duncan model representation of elastic parameters	117
9.2 CANDE solution strategy for Duncan model	121
9.3 Standard hyperbolic parameters	125
CHAPTER 10 - SUMMARY AND CONCLUSIONS	132
 APPENDICES	
A - Details of reinforced concrete model.	134
B - CANDE-1980; User Manual Supplement	147
C - Sample of input data and output	177
D - System overlay	202
REFERENCES	208

CHAPTER 1

INTRODUCTION

1.1 BACKGROUND

The CANDE computer program (Culvert ANalysis and Design) was first introduced in 1976 for the structural analysis and design of buried culverts (1,2,3). CANDE employs soil-structure interaction analysis and has a variety of options, such as; choice of culvert type (corrugated steel, corrugated aluminum, reinforced concrete, and plastic) and choice of analysis/design method (elasticity solution - level 1, automated finite element solution - level 2, and standard finite element solution - level 3). Other features include; linear and nonlinear culvert and soil models, incremental construction and soil-structure interface elements.

Since its introduction in 1976, the program has been widely distributed and used by state highway departments, federal agencies, consulting firms, industry, research laboratories, and universities in the United States and Canada. User responses have been very favorable along with encouragement and suggestions for extending the program's capabilities. In particular, it is observed that reinforced concrete box culverts have dramatically increased in use during recent years. To analyze these with CANDE (1976 version) requires level 3 analysis with time consuming finite element data preparation. Prior to this work, the automated finite element level 2 analysis was restricted to round or elliptical pipes. Thus, a desirable program extension is a level 2 analysis for box culverts with the capability to analyze through ultimate loading. A second observation is the wide spread popularity of the so-called Duncan soil model (26, 27, 28, 29) which has been developing over the last decade and is formulated on a large experimental data base for many types of soil. The above observations lead to the objectives of this work.

1.2 OBJECTIVES

The first major objective is to develop and incorporate into the CANDE program an automated finite element analysis solution method for buried, precast reinforced concrete box culverts, called here, "level 2 box" option. Included in this objective is validating the CANDE model with experimental data for loadings through ultimate and comparisons with other design/analysis methods.

The second major objective is to incorporate the Duncan soil model into the CANDE program with due regard to convergence problems and to provide options for simplified data input.

1.3 SCOPE AND APPROACH

To meet the above objectives, a step by step approach was undertaken for both major goals. First, for the development and validation of precast reinforced concrete box culverts, the steps are:

- (a) Review current design/analysis procedures to assess the state-of-the-art and to establish a comparative basis with CANDE (Chapter 2).
- (b) Reformulate the existing reinforced concrete model to include loading through ultimate, unloading, and redistribution of stresses due to concrete cracking (Chapter 3 and Appendix A).
- (c) Evaluate and validate the reinforced concrete model with out-of-ground experimental data including pipes with 3-edge bearing loads and boxes with 4-edge bearing loads (Chapters 4 and 5).
- (d) Develop an automated finite element solution method (level 2 box) for buried box culverts (box-soil model) with simplified input for embankment and trench installations (Chapter 6).
- (e) Evaluate and validate the box-soil model with available experimental data and parametric studies (Chapter 7).
- (f) Cross check the box-soil model predictions with current design/analysis procedures in step (a) and evaluate current design methods (Chapter 8).

Next, for the objective of incorporating the Duncan soil model and simplifying soil model input, the steps are (Chapter 9):

- (a) Evaluate the Duncan soil model to verify reasonable behavior in confined compression and triaxial loading.
- (b) Investigate iterative solution strategies to enhance convergence and incorporate the model into CANDE program.
- (c) Establish standard model parameters dependent on soil type and degree of compaction for the simplified data input option.
Also, simplify data input for the existing overburden dependent soil model.

All program modifications noted above have been incorporated into CANDE, hereafter called CANDE-1980 to distinguish it from the 1976 version. Appendix B provides input instructions to exercise the new options contained in CANDE-1980. These instructions are a supplement to the 1976 CANDE User Manual (2) and only need to be referred to if the new options are desired. In other words, the 1976 user manual is compatible with the CANDE-1980 program. Appendix C illustrates input-output data for some of the new options and Appendix D provides system overlay instructions to reduce core storage.

The CANDE-1980 program discussed herein is based on the English system of units. A companion program in metric units has been developed and is also available from FHWA.

CHAPTER 2

REVIEW OF PRECAST BOX CULVERTS

In this chapter a brief review on the development of precast reinforced concrete box culverts is presented along with a discussion of current design procedures. The intent is to acquaint the reader with precast box culverts, terminology and design concepts and to "set the stage" for the CANDE methodology presented in later chapters. For brevity, "reinforced concrete box culverts" will be referred to as "box culverts".

2.1 BACKGROUND

Precast box culverts, as opposed to cast-in-place box culverts, are relatively recent additions in culvert technology, coming into popular use within the last decade. For many years, cast-in-place box culverts have been used in installations with special requirements or by design preference. However, cast-in-place culverts have inherent disadvantages; high labor costs associated with cast-in-place construction, lengthy periods of traffic disruption, and minimal quality control often compensated for by conservative designs. Alternatively, plant-produced box culverts, manufactured under strict quality control and installed by rapid cut-and-fill procedures, can offset these disadvantages particularly if the box dimensions, reinforcement, ect., are standardized for manufacture.

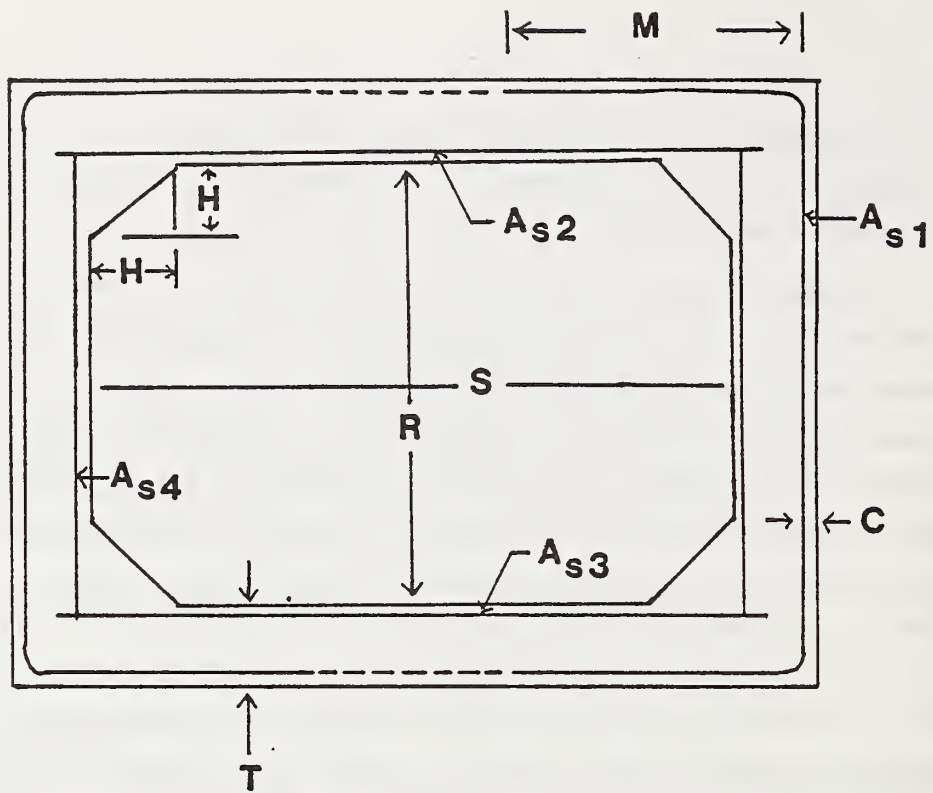
With the above motivation, the Virginia Department of Highways and the American Concrete Pipe Association (ACPA), with financial support from the Wire Reinforcement Institute, initiated a cooperative program, early in 1971, to develop manufacturing specifications and standard designs for precast box culverts. These specifications were to be adaptable as a national standard under the auspices of the American Society of Testing Materials (ASTM) and the American Association of State Highway and Transportation Officials (AASHTO). To this end, ACPA contracted

the consulting firm of Simpson, Gumpertz and Heger Inc. (SGH) to develop a computerized design program for precast box culverts in cooperation with ASTM committee C-13.

Ultimately, this effort culminated in the ASTM C789 and AASHTO M259 specifications on Precast Reinforced Concrete Box Sections for Culverts, Storm Drains and Sewers first published in 1974. These specifications were limited to box culverts with a minimum of two feet (0.61 m) of earth cover. Further developmental work by SGH resulted in the additional specifications: ASTM C850 and AASHTO M273 published in 1976 for precast box culvert installations with less than two feet of earth cover. The above ASTM and AASHTO specifications are essentially the same except for a few details which are apparently now resolved. For purposes of this study, the ASTM specifications will be used as reference. Design methods for precast box culverts, other than those embodied in ASTM or AASHTO specifications, will not be reviewed here since they are not standardized nor have they gained national acceptance. Recently, ACPA published a survey (Concrete Pipe News, June 1980) showing that usage of precast box culverts, designed by ASTM specifications, has increased dramatically within the last year. . . the number of projects and linear footage installed in 1979 is almost equal to the total for the previous five years!

2.2 DEVELOPMENT AND RATIONALE OF ASTM PRECAST BOX CULVERT STANDARDS

The SGH computerized design program (12) is the basis of the design rationale in the ASTM C789 design tables. A typical box cross-section is shown in Figure 2.1 along with nomenclature. The SGH design/analysis approach includes the following steps; (a) load distributions are assumed around the culvert in an attempt to simulate dead earth loads and live loads, (b) moment, shear, and thrust distributions are determined by standard matrix methods using elastic, uncracked concrete section properties, (c) in the design mode, steel areas are determined by an ultimate strength theory for bending and thrust, where ultimate moments and thrusts are obtained from step (b) multiplied by a load factor, (d) crack-width (0.01 inch allowable) is checked using a semi-empirical formula



A_{s1} = outer reinforcement

A_{s2} = top inner reinforcement

A_{s3} = bottom inner reinforcement

A_{s4} = side inner reinforcement

C = cover distance of reinforcement, uniform

H = haunch dimension

M = minimum length A_{s1} steel, top and bottom

R = rise distance, inside to inside

S = span distance, inside to inside

T = wall thickness, uniform

Figure 2.1. Typical Box Culvert Cross Section

controlled by steel stress at service loads, (e) ultimate shear stress ($2\sqrt{f'_c}$) is checked against the nominal shear stress obtained in step (b) multiplied by a load factor.

For the standard box sizes shown in Table 2.1, the SGH design program was used to generate the ASTM C789 design tables wherein steel reinforcement requirements are specified as a function of design earth cover beginning with a two foot minimum.

In a similar manner, ASTM C850 design tables were generated for earth covers less than two feet. Here, the SGH design procedure was modified to include requirements for longitudinal steel design due to concentrated live loads (see ASTM Symposium STP 630).

Although the SGH design/analysis program has not been validated with experimental data from buried box culverts, fairly good correlation with out-of-ground experimental tests has been reported (13). More will be said about these experiments in Chapter 5.

Experimental data for instrumented, buried box culverts is extremely limited. As of this writing, only two state highway departments (Kentucky and Illinois) are known to have undertaken experimental programs for instrumenting (settlement, soil pressure, and strain gages) buried box culvert installations. Other states have made visual inspection reports on the performance of buried box installations, but this data has marginal value for validating design/analysis procedures. Data from the Kentucky Department of Transportation was made available for this study and is used to evaluate the CANDE program in Chapter 7.

In summary, the ASTM design tables for buried, precast box culverts, which are based on the SGH design/analysis program, have not been previously validated with experimental data from buried installations. Nor have the tables been cross-checked with analytical procedures, such as CANDE, employing soil-structure interaction and the nonlinear nature of reinforced concrete. With this goal in mind, a step by step approach is presented in the following chapters. First, the theory of CANDE's nonlinear, reinforced concrete model is developed. Second, the model is

TABLE 2.1 Standard box sizes, ASTM C789

Span ft.	Rise, ft.										Wall Thickness in.
	2	3	4	5	6	7	8	9	10		
3	X	X									4
4	X	X	X								5
5		X	X	X							6
6		X	X	X	X						7
7			X	X	X	X					8
8			X	X	X	X	X				8
9				X	X	X	X	X			9
10					X	X	X	X	X	X	10

1 ft = 0.3048 m

1 in = 2.54 cm

validated with experimental data for out-of-ground conditions. Third, the reinforced concrete model is combined with soil system models and compared with experimental data from a buried installation. Last, the CANDE model is used to evaluate the ASTM design tables.

CHAPTER 3

REINFORCED CONCRETE MODEL

3.1 OBJECTIVE

A reinforced concrete, beam-rod member, whether it be part of a culvert or any other structural system, poses a difficult analysis problem due to the nonlinear material behavior of concrete in compression, cracking of concrete in tension, yielding of reinforcement steel, and the composite interaction of concrete and reinforcement. Matters are further complicated when the internal loading is not proportional, i.e., when the internal moment, shear and thrust at a particular cross section change in different proportions (including load reversals) during the loading history. Such is the case for buried culverts during the installation process.

In this chapter, the development of a reinforced concrete beam-rod element is developed in the context of a finite element formulation for CANDE-1980. This model is more general than the model in CANDE-1976 and includes; incremental loading through ultimate, unloading, and redistribution of stresses due to cracking.

The following presentation provides an overview of the model development emphasizing assumptions and limitations. Details of the numerical solution strategy are presented in Appendix A. Evaluation of the model with experimental data and other theories is presented in subsequent chapters.

3.2 ASSUMPTIONS, LIMITATIONS, AND APPROACH

Listed below are the fundamental assumptions for the reinforced concrete beam-rod element.

1. Geometry and loading conform to plane strain implying the beam-rod element is of unit width. Constant section properties are assumed through an element length, but may differ between elements.
2. Displacements and strains are small. No buckling considerations are included.
3. Planes remain plane in bending and shear deformation is negligible.
4. Concrete is linear in tension up to cracking. Cracked concrete cannot carry tension stresses and pre-crack stresses are redistributed. In compression, concrete is modeled with a trilinear stress-strain curve terminating at ultimate strain. Unloading is elastic.
5. Reinforcement steel is elastic-plastic and identical in compression and tension. Unloading is elastic.
6. Reinforcement steel is lumped into two discrete points near the top and bottom of the cross-section and deforms with the cross-section.
7. Element lengths are sufficiently small so that the current stress distribution through a cross-section is representative of the entire element for purposes of computing current section properties.
8. Loads are applied incrementally and sufficiently small so that the stress-strain relations (for both steel and concrete) can be regarded as incremental tangent relations determined iteratively over the load step.

In overall perspective, the developmental steps begin with an incremental statement of virtual work wherein the beam-rod assumptions are introduced along with standard finite element interpolation functions for axial and bending deflections. This results in a tangent element stiffness matrix and incremental load vector that can be assembled into a global set of system equations with unknown nodal degrees of freedom, and solved by standard techniques (1). However, the global matrix contains estimates of the bending and axial stiffness for each beam-rod element (as well as estimates for soil stiffness if nonlinear soil models are part of the system). Thus, each load step is repetitively solved (iterated), and the results are used to improve the stiffness estimates until convergence is achieved.

Prior to the first loading increment, the beam-rod element is assumed stress free and uncracked so initial stiffnesses correspond to an uncracked, elastic, transformed reinforced concrete cross-section. Upon applying the first load increment, the first tentative solution may indicate that some elements should have had reduced stiffnesses due to cracking or yielding of the section. Using the strain distribution at the beginning and end of the load step, new stiffness estimates are obtained and the process is iterated to convergence. Each subsequent load step is treated in a similar fashion where a history of maximum stress and strain is maintained for purposes of identifying unloading conditions.

The above assumptions and general approach are outlined in the following development.

3.3 BASIC FORMULATION FOR BEAM-ROD ELEMENT

In this section we consider an incremental virtual work statement for a unit width, beam-rod element with body forces given by:

$$\delta \Delta V_e = \delta \Delta U - \delta \Delta W \quad (3.1)$$

with $\delta \Delta U = \int \int \int \delta \epsilon \Delta \sigma \, dx dy =$ internal virtual work increment

$$\delta \Delta W = \int_x \int_y \delta \{ \begin{matrix} u \\ v \end{matrix} \}^T \{ \begin{matrix} \Delta f_1 \\ \Delta f_2 \end{matrix} \} dx dy = \text{external virtual work increment}$$

where σ = normal stress, x-direction
 ϵ = normal strain, x-direction
 u = longitudinal displacement, x-direction
 v = transverse displacement, y-direction
 f_1 = longitudinal body force, x-direction
 f_2 = transverse body force, y-direction
 x = space coordinate parallel to beam axis
 y = space coordinate transverse to beam axis
 δ = virtual symbol
 Δ = increment symbol

The above beam displacements are illustrated in Figure 3.1.

Introducing Bernouli-Euler beam kinematics (Assumptions 2 and 3), longitudinal displacements through a cross section may be arbitrarily decomposed into a uniform axial distribution, $u_0(x)$, plus a distribution proportional to slope, $v'(x)$, and linearly varying about some axis \bar{y} , i.e.:

$$u(x, y) = u_0(x) + v'(x) (\bar{y} - y) \quad 3.2$$

Later, when the above kinematic relation is incorporated into Equation 3.1, the axis \bar{y} will be chosen such that internal bending work is uncoupled from internal axial work,

Employing the small strain-displacement assumption, normal strain is:

$$\epsilon(x, y) = u'_0(x) + v''(x) (\bar{y} - y) \quad 3.3$$

where primes denote derivatives with respect to the argument.

To complete the field variable assumptions, a general, nonlinear stress-strain relationship is assumed in incremental form as:

$$\Delta \sigma = E'(\epsilon) \Delta \epsilon \quad 3.4$$

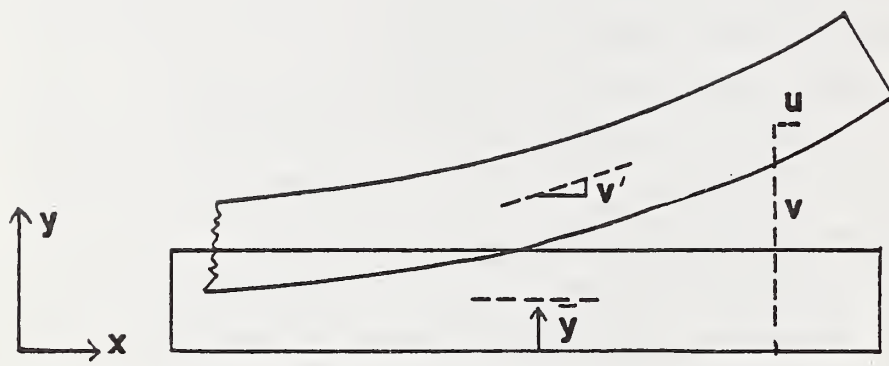


Figure 3.1 Deformation of Beam-Rod Element

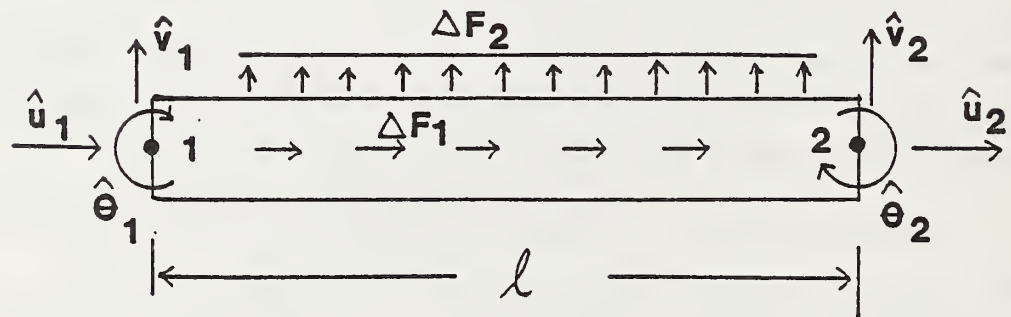


Figure 3.2 Nodal Degrees of Freedom
and Element Loading

Here $E'(\epsilon)$ is a tangent modulus relating increments of stress to increments of strain and is dependent on loading history. Naturally, the functional forms of $E'(\epsilon)$ are different for concrete and steel materials. However for clarity of presentation, the specific forms of $E'(\epsilon)$ will be deferred to a later section.

Using the incremental form of Equation 3.3 along with Equation 3.4 and integrating through the cross section, the internal virtual work increment may be expressed as:

$$\delta\Delta U = \int_x (\delta u'_0 EA^* \Delta u'_0 + \delta v'' EI^* v'' + EX^* (\delta v'' \Delta u'_0 + \delta u'_0 \Delta v'')) dx \quad 3.5$$

where $EA^* = \int_y E'(\epsilon) dy$ = effective axial stiffness 3.6

$$EI^* = \int_y E'(\epsilon) (\bar{y}-y)^2 dy = \text{effective bending stiffness} \quad 3.7$$

$$EX^* = \int_y E'(\epsilon) (\bar{y}-y) dy = \text{axial-bending coupling} \quad 3.8$$

The location of \bar{y} is now chosen so that the coupling term EX^* is zero. Thus, \bar{y} is given by:

$$\bar{y} = (\int_y E'(\epsilon) y dy) / EA^* \quad 3.9$$

This choice of \bar{y} is convenient because bending and axial deformations are uncoupled in the virtual work statement. However, it must be remembered that \bar{y} , like EA^* and EI^* , is dependent on $E'(\epsilon)$, thus these values change during each load step.

To complete the virtual work statement, the kinematic assumption (Equation 3.2) is introduced into the external virtual work incremental expression and integrated over the cross section to give:

$$\delta\Delta W = \int_x (\delta u'_0 \Delta F_1 + \delta v \Delta F_2 + \delta v' \Delta F_3) dx \quad 3.10$$

where $\Delta F_1 = \int_y \Delta f_1 dy$ = axial body force per unit length

$$\Delta F_2 = \int_y \Delta f_2 dy = \text{transverse body force per unit length}$$

$$\Delta F_3 = \int_y \Delta f_1 (\bar{y}-y) dy = \text{body moment per unit length}$$

The body moment, ΔF_3 , is generally nonzero except if the centroid of the axial body weight happens to coincide with the current location of \bar{y} . However, the magnitude of the body moment is usually negligible compared to the magnitude of internal moments which arise from transverse loading in culvert installations. Thus, the body moment is neglected in this study.

Equations 3.5 and 3.10 are the internal and external virtual work expressions for the beam-rod element with unknown displacement functions $u_0(x)$ and $v(x)$.

3.4 FINITE ELEMENT INTERPOLATIONS

Figure 3.2 shows a beam-rod element with three nodal degrees of freedom at each end node, an axial displacement, a vertical displacement, and a rotation. These degrees of freedom are used to define admissible interpolation functions for $u_0(x)$ and $v(x)$ in the context of a finite element formulation.

Specifically, the axially displacement, $u_0(x)$ is approximated with a two-point Lagrange interpolation function:

$$u_0(x) = \langle \phi_1 \phi_2 \rangle \begin{bmatrix} \hat{u}_1 \\ \hat{u}_2 \end{bmatrix} \quad 3.11$$

where \hat{u}_1 = axial displacement at node 1

\hat{u}_2 = axial displacement at node 2

$$\phi_1(x) = 1 - \beta$$

$$\phi_2(x) = \beta$$

$$\beta(x) = x/\ell$$

For transverse displacements, $v(x)$, a two-point Hermetian interpolation function is used.

$$v(x) = \begin{bmatrix} \alpha_1 & \alpha_2 & \alpha_3 & \alpha_4 \end{bmatrix} \begin{bmatrix} \hat{v}_1 \\ \hat{\theta}_1 \\ \hat{v}_2 \\ \hat{\theta}_2 \end{bmatrix} \quad 3.12$$

where \hat{v}_1 = transverse displacement at node 1

\hat{v}_2 = transverse displacement at node 2

$\hat{\theta}_1$ = rotation at node 1

$\hat{\theta}_2$ = rotation at node 2

$$\alpha_1(x) = 1 - 3\beta^2 + 2\beta^3$$

$$\alpha_2(x) = \beta(1-\beta)^2 \ell$$

$$\alpha_3(x) = 3\beta^2 - 2\beta^3$$

$$\alpha_4(x) = \beta^2 (\beta-1) \ell$$

Upon substituting the interpolation functions into the incremental virtual work expression, $\delta\Delta V_e = \delta\Delta U - \delta\Delta W$, we have:

$$\delta\Delta V_e = \langle \delta\hat{r} \rangle \{ [K_e] \{ \Delta\hat{r} \} - \{ \Delta P_e \} \} \quad 3.13$$

where

$$\{ \hat{r} \} = \begin{bmatrix} \hat{u}_1 \\ \hat{v}_1 \\ \hat{\theta}_1 \\ \hat{u}_2 \\ \hat{\theta}_2 \\ \hat{v}_2 \end{bmatrix} = \text{element degrees of freedom} \quad 3.14$$

$$\{\Delta P_e\} = \frac{\ell}{12} \begin{bmatrix} 6\Delta F_1 \\ 6\Delta F_2 \\ \ell\Delta F_2 \\ 6\Delta F_1 \\ 6\Delta F_2 \\ -\ell\Delta F_2 \end{bmatrix} = \text{element load vector} \quad 3.15$$

$$[K_e] = \begin{bmatrix} \frac{EA}{\ell}^* & 0 & 0 & \frac{-EA}{\ell}^* & 0 & 0 \\ 0 & \frac{12EI}{\ell^3}^* & \frac{6EI}{\ell^2}^* & 0 & \frac{-12EI}{\ell^3}^* & \frac{6EI}{\ell^2}^* \\ 0 & \frac{6EI}{\ell^2}^* & \frac{4EI}{\ell}^* & 0 & \frac{-6EI}{\ell^2}^* & \frac{2EI}{\ell}^* \\ \frac{-EA}{\ell}^* & 0 & 0 & \frac{EA}{\ell}^* & 0 & 0 \\ 0 & \frac{-12EI}{\ell^3}^* & \frac{6EI}{\ell^2}^* & 0 & \frac{12EI}{\ell^3}^* & \frac{-6EI}{\ell^2}^* \\ 0 & \frac{6EI}{\ell^2}^* & \frac{2EI}{\ell}^* & 0 & \frac{-6EI}{\ell^2}^* & \frac{4EI}{\ell}^* \end{bmatrix}$$

Symmetric.

(tangent element stiffness matrix)

The above tangent element stiffness and load vector are valid for the local beam coordinates. For assembling element contributions into the global coordinate system, standard coordinate transformation are employed.

Note that the tangent element stiffness matrix is identical in form to that obtained from standard matrix methods of structural analysis. However, the axial stiffness EA^* and bending stiffness EI^* (dependent on \bar{y}) are not constant and must be determined iteratively for each load step in accordance with Equations 3.6, 3.7, and 3.9. These equations are dependent on the concrete and steel stress-strain relationships discussed next.

3.5 STRESS-STRAIN RELATIONSHIPS

Concrete. The assumed stress-strain behavior for concrete is shown in Figure 3.3 where the trilinear curve is defined by the following input variables:

ϵ_t = concrete strain at initial tensile cracking
 ϵ_y = concrete strain at initial elastic limit
 ϵ'_c = concrete strain at onset of ultimate
 f'_c = unconfined compressive strength of concrete
 E_1 = Young's modulus in linear zone

With the above input variables, three additional parameters can be derived:

$$E_2 = (f'_c - E_1 \epsilon_y) / (\epsilon'_c - \epsilon_y) = \text{Young's modulus in yielding zone}$$
$$f_t = E_1 \epsilon_t = \text{initial tensile strength}$$
$$f_{yc} = E_1 \epsilon_y = \text{initial yield strength}$$

In tension the concrete is linear until the initial tensile strain exceeds the cracking strain limit ϵ_t . When cracking occurs, the tensile stress becomes abruptly zero (redistributed to noncracked portions). Once a point in the cross section is cracked, the crack does not heal, implying no tensile strength. Thus ϵ_t is set to zero for all subsequent reloading in tension.

For initial compression loading, the concrete begins to yield with hardening at stress f_{yc} . Perfect plasticity occurs at stress f'_c and continues through ultimate strain. Unloading is elastic and results in permanent plastic strains as indicated in Figure 3.4. Reloading is elastic until the stress reaches its previous maximum value after which it follows the original stress-strain curve. (See Figure 3.4).

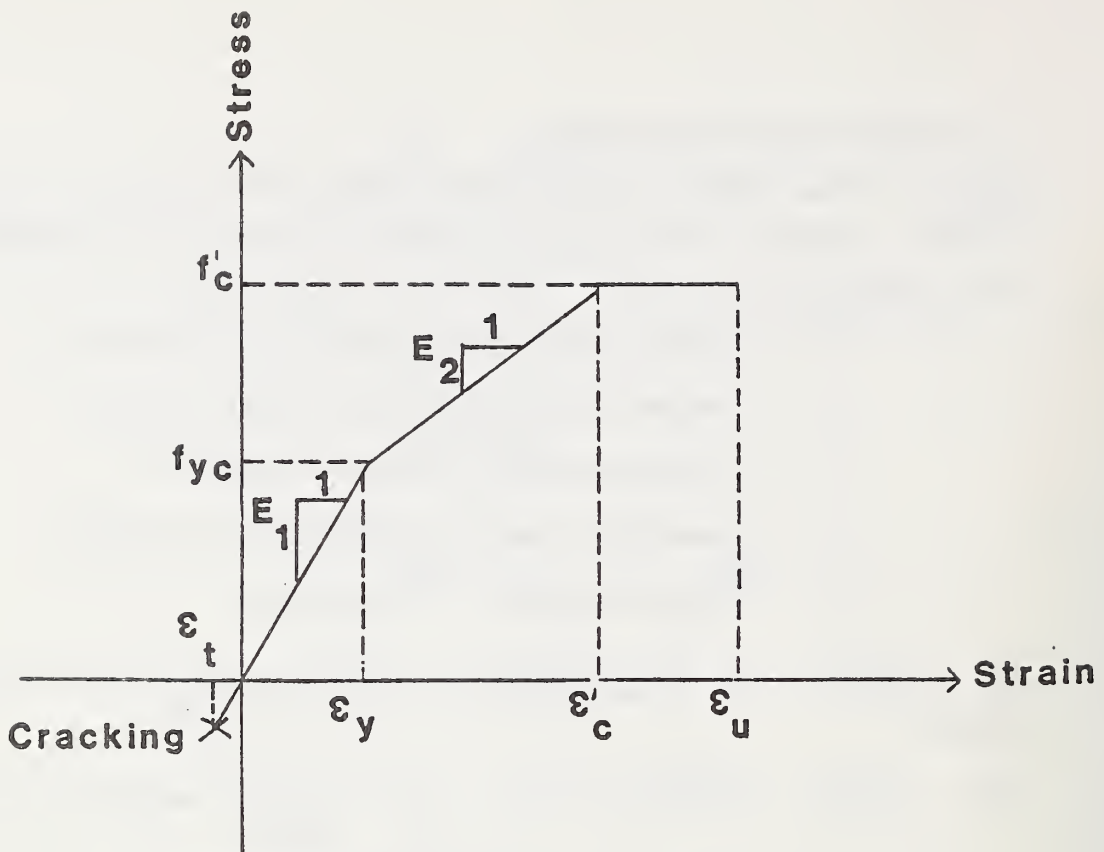


Figure 3.3 Idealized Stress-Strain Diagram for Concrete

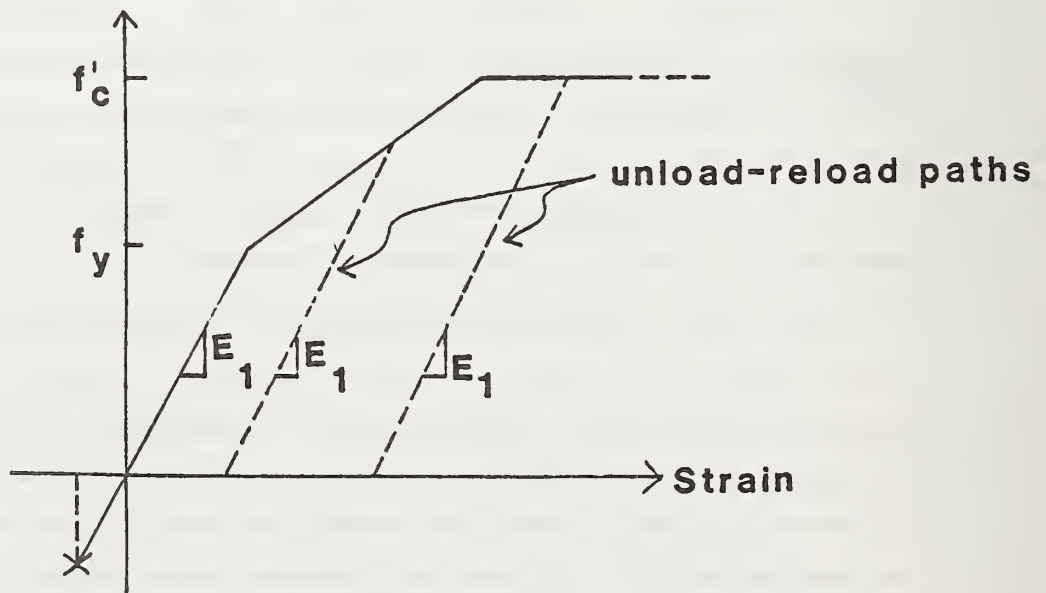


Figure 3.4 Elastic Unload-Reload for Concrete

With the above understanding, the tangent modulus relationship for concrete confined in a plane is expressed as:

$$E'_c(\epsilon) = E_c (1 - \alpha(\epsilon)) \quad 3.17$$

where $E_c = E_1 / (1 - \nu_c^2)$

with E_c = elastic, confined plane modulus of concrete

ν_c = Poisson's ratio of concrete (constant)

$\alpha(\epsilon)$ = dimensionless function of stress-strain history

The dimensionless function $\alpha(\epsilon)$ ranges in value from 0.0 (elastic response) to 1.0 (perfectly-plastic response), representing the non-linear effect of concrete. The actual value of $\alpha(\epsilon)$ to be used for any given load increment is dependent on; known values of stress and strain at the beginning of the step, known history parameters for cracking and yielding, and unknown values of stress and strain at the end of the step (iteration). Appendix A provides the details for determining $\alpha(\epsilon)$ for all loading histories.

Steel. The assumed stress-strain behavior for reinforcing steel is shown in Figure 3.5 where the elastic-plastic curve is characterized with two input variables:

E_0 = Young's modulus for steel

f_y = steel yield strength

Behavior in compression and tension is identical so that material is elastic whenever the stress magnitude is less than f_y . Nonhardening plastic flow occurs when the stress is equal to f_y . Unloading from the plastic range is elastic and results in permanent plastic strains (see Figure 3.5).

Similar to Equation 3.17 for concrete, the tangent modulus relationship for reinforcement steel confined in a plane is expressed as:

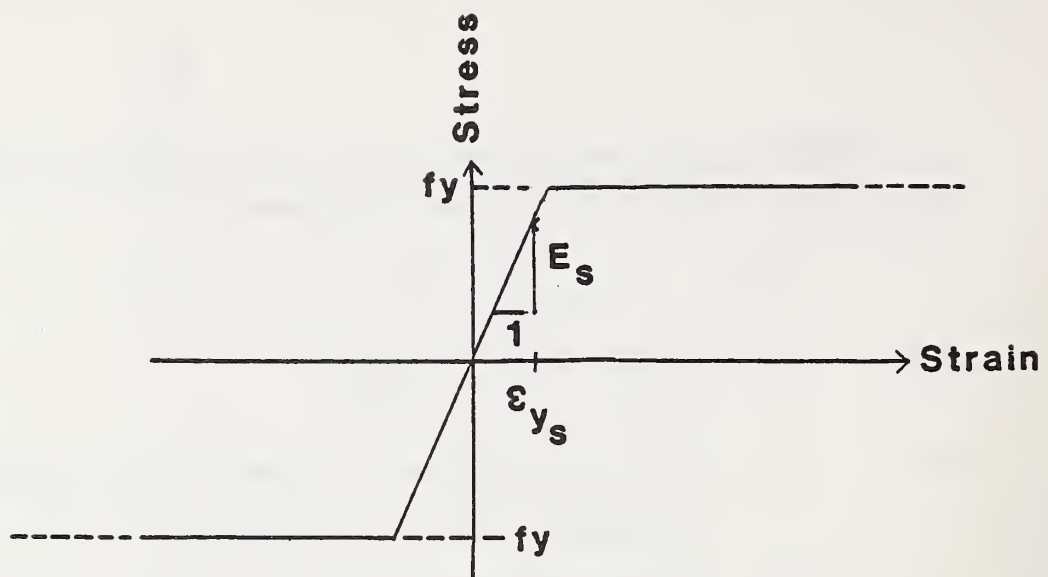


Figure 3.5 Idealized Stress-Strain Diagram for Reinforcing Steel

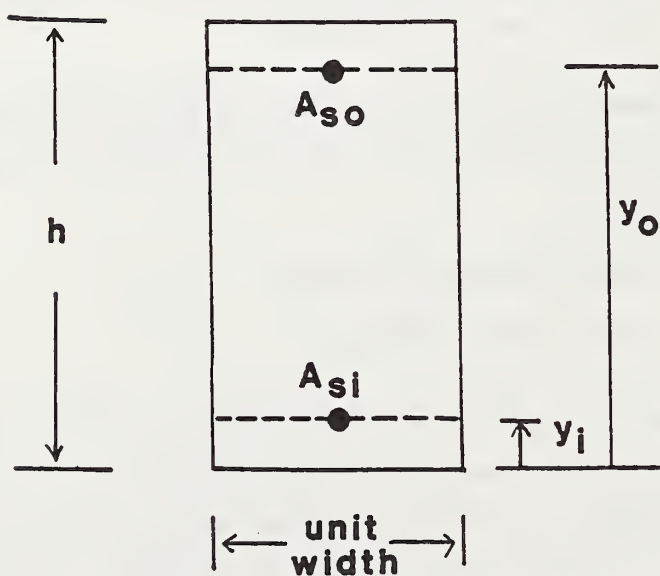


Figure 3.6 Reinforced Concrete Cross Section

$$E'_s(\varepsilon) = E_s (1 - \alpha(\varepsilon)) \quad 3.18$$

where $E_s = E_0 / (1 - \nu_s^2)$

with E_s = elastic, confined plane modulus of steel

ν_s = Poisson's ratio of steel (constant)

$\alpha(\varepsilon)$ = dimensionless function of stress-strain history

As in the case of concrete, the function $\alpha(\varepsilon)$ for steel ranges in value from 0.0 (elastic) to 1.0 (perfectly plastic) depending on stress-strain history and stress values at the beginning and end of each load step (see Appendix A).

3.6 SECTION PROPERTIES

Equations 3.17 and 3.18 represent the tangent modulus relationships for concrete and steel, respectively, which now can be used to evaluate current section properties EA^* , \bar{y} , and EI^* .

Referring to a typical cross section shown in Figure 3.6, the effective axial stiffness (Equation 3.6), the bending axis (Equation 3.9), and the effective bending stiffness (Equation 3.7) can be evaluated by separating the concrete and steel integration areas as shown below.

$$EA^* = \int_0^h E'_c(\varepsilon) dy + A_{si} E'_s(\varepsilon_i) + A_{s0} E'_s(\varepsilon_0) \quad 3.19$$

$$\bar{y} = \left(\int_0^h E'_c(\varepsilon) y dy + A_{si} E'_s(\varepsilon_i) y_i + A_{s0} E'_s(\varepsilon_0) y_0 \right) / EA^* \quad 3.20$$

$$EI^* = \int_0^h E'_c(\varepsilon) (\bar{y} - y)^2 dy + A_{si} E'_s(\varepsilon_i) (\bar{y} - y_i)^2 + A_{s0} E'_s(\varepsilon_0) (\bar{y} - y_0)^2 \quad 3.21$$

where A_{si} = bottom steel area per unit width
 A_{s0} = top steel area per unit width
 y_i = distance to A_{si} from bottom
 y_0 = distance to A_{s0} from bottom

The integrals containing $E'_c(\epsilon)$ represent the concrete contribution to section properties and are evaluated numerically with 11-point Simpson integration. A stress-strain history is maintained at each integration point for determining the current values of $\alpha(\epsilon)$. Steel contributions to section properties are governed by $E'_{s_i}(\epsilon_i)$ and $E'_{s_0}(\epsilon_0)$ representing the tangent steel modulus at the centroid of bottom and top steel reinforcement.

The above equations suggest that the concrete contributions are integrated over the entire section area irrespective of "holes" where steel exists, however, the algorithm used in this study accounts for these holes. These and other details of computing section properties are discussed in Appendix A.

3.7 INCREMENTAL SOLUTION STRATEGY

All the assumptions and derivations for the beam-rod element have been presented. An overview of the solution strategy is given next.

It is assumed that a converged solution is known at load step $i-1$ and it is desired to obtain a converged solution at load step i . Basically, the objective is to determine effective section properties, EI^* , \bar{y} , and EI^* for each beam-rod element.

A flow chart of the solution strategy is illustrated in Figure 3.7. The procedure begins by initially assuming the section properties are the same as the previous load step. Next, the system is assembled for the current load increment and trial solutions are obtained for moment and thrust increments in each element, given by:

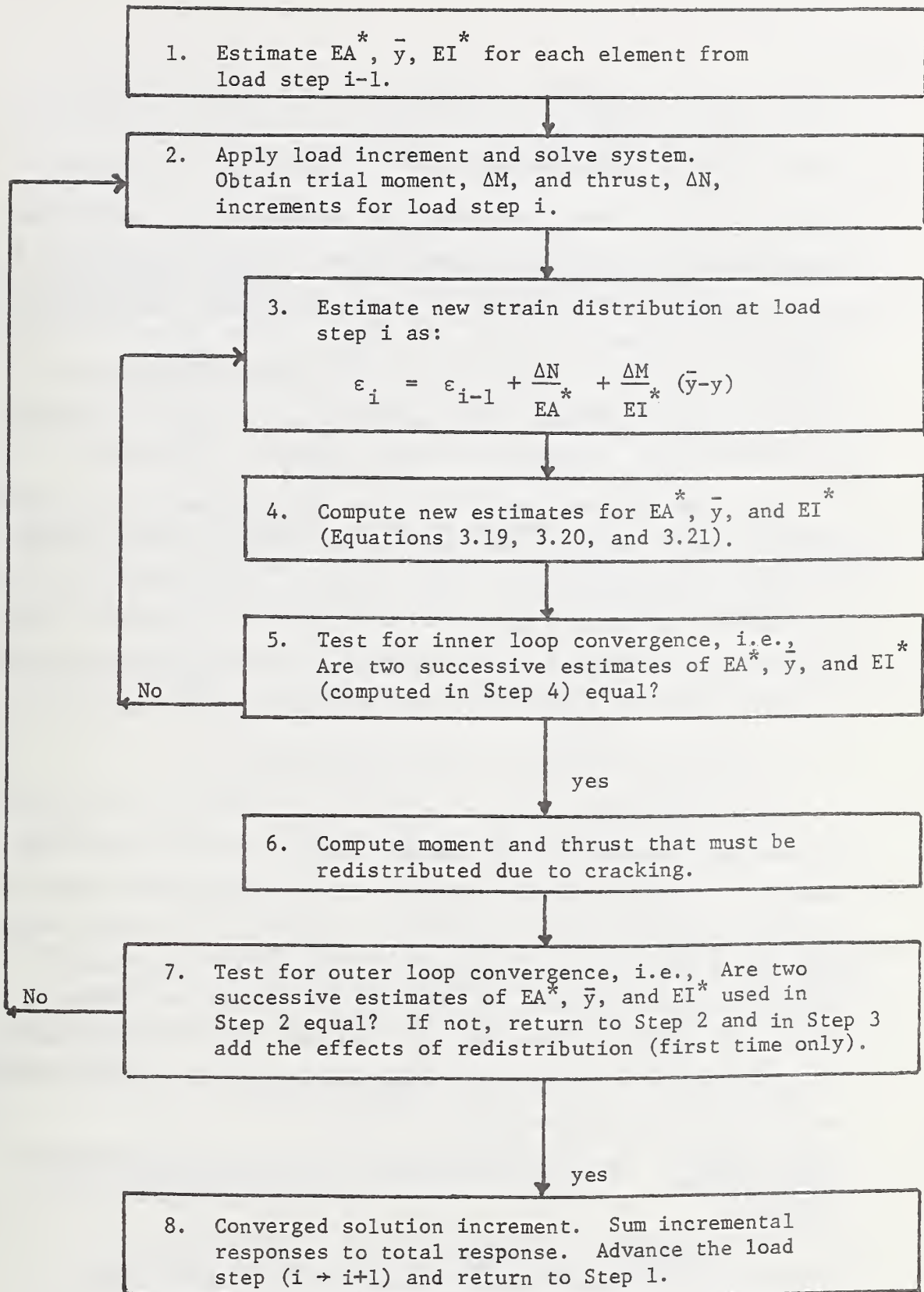


Figure 3.7. Flow chart of solution strategy.

$$\Delta N = \int_A \Delta \sigma \, dA = EA^* \Delta u' \Big|_0$$

$$\Delta M = \int_A \Delta \sigma (\bar{y} - y) \, dA = EI^* \Delta v''$$

Using the above relations together with Equation 3.3, a new strain distribution is estimated as shown in Step 3 of the flow chart. This, in turn, permits improving the estimates for section properties in the "inner loop" iteration; steps 3, 4, and 5. Here, ΔM and ΔN remain fixed (as estimated in Step 2) while the corresponding section properties are determined. Note that inner loop operations are at the element level, requiring no global assembly or solution.

Each time the inner loop converges, the converged section properties are used in Step 2 to get new global solutions for ΔM and ΔN . This process is called "outer loop" iteration and continues until two successive solutions are equal within a specified tolerance. When this occurs, convergence is achieved and the program advances to the next load step (see Appendix A for additional detail).

3.8 MEASURES OF REINFORCED CONCRETE PERFORMANCE

Once a converged solution is obtained, measures of structural distress are assessed by; (a) maximum tensile stress in steel (b), maximum compressive stress in concrete, (c) maximum shear stress in concrete, and (d) maximum crackwidth in concrete. The first three measures of distress are evaluated directly from the structural response predictions from the CANDE model, however the crackwidth prediction employs a semi-empirical approach. Each distress measure is normalized by a corresponding design criterion to produce performance factors as discussed below.

Steel Tension. The performance factor for steel reinforcing is given by:

$$PF_{\text{steel}} = f_y / f_{\text{max}}$$

where f_{max} = maximum steel stress (predicted)
 f_y = steel yield stress

For properly designed structures, this performance factor should be in the range of 1.5 to 2.0. When the steel begins to yield, the performance factor becomes 1.0 and remains there through ultimate loading.

Concrete Compression. For the outer concrete fibers experiencing compressive stress from thrust and bending, the performance factor is:

$$PF_{comp.} = f'_c / \sigma_{max}$$

where σ_{max} = maximum compressive stress (predicted)

f'_c = compressive strength of concrete

Proper designs should have this performance factor in the range 1.6 to 2.5. The performance factor remains at 1.0 when the concrete becomes perfectly plastic and remains there through ultimate loading.

Concrete Shear. Nominal shear stress through a cross section is used to define the shear performance factor, given by:

$$PF_{shear} = v_c / v_{max}$$

where v_{max} = nominal average shear stress on section

v_c = nominal concrete shear strength

Here v_{max} is computed by dividing the maximum predicted shear force by the concrete area minus the cover area of steel. This definition is consistent with the standard ACI measure of shear strength for beams given by:

$$v_c = 2.0 \sqrt{f'_c} \text{ (psi)}$$

Other measures of shear strength are examined in the next chapter with experimental data.

For proper design, the above performance factor should be in the range 1.7 to 2.7. In the absence of stirrups, shear failure (e.g. diagonal cracking) is assumed to occur when the performance

factor value is 1.0. Note that the CANDE model does not incorporate diagonal cracking into the stress-strain law, only flexural cracking.

Concrete Crackwidth. The crackwidth prediction, C_w , is a semi-empirical approach wherein the maximum tensile steel stress predicted by CANDE is used in an empirical formula proposed by Gergely and Lutz (10). Using 0.01 inches (0.0254 cm) as the design standard for allowable crackwidth, the cracking performance factor is defined as:

$$PF_{crack} = 0.01/C_w$$

where $C_w = 0.091\sqrt[3]{2t_b^2 S} (f_s - 5000)R$ (inches)

$R = 1.34 \times 10^{-6}$ (dimensionless number for culvert slabs).

t_b = concrete cover to steel centroid (inches)

f_s = tensile steel stress (psi)

S = spacing of reinforcement (inches)

The Gergely and Lutz formula for C_w was found to give good predictions for crackwidths in this study. This finding is further supported by Lloyd, Relaji and Kesler (11) in their experimental tests on one-way slabs with deformed wire, deformed wire fabric, and deformed bars. The new crackwidth formula defined above replaces the old crackwidth formula in CANDE-1976. The new formula can be made to be identical to the old by defining $S = 0.68/A_s t_b^2$ where A_s is tension steel reinforcement, in²/in.

Ultimate Loads. Ultimate loading in thrust and bending occurs in a beam-rod element when the reinforced concrete section cannot sustain any additional loading, i.e., all uncracked concrete is at maximum compressive strength f'_c and all reinforcement steel is yielding (plastic hinging). For a structure composed of beam-rod elements, such as a box culvert, ultimate loading occurs when a sufficient number of plastic hinges have formed to produce a collapse mechanism. This can be determined from the CANDE program by observing unrestrained deformation as the load is increased to ultimate.

Ultimate loading in shear is assumed to occur when the performance factor for shear in any beam-rod element becomes 1.0. If a structure fails in shear prior to flexural-thrust failures, the CANDE model is still capable of carrying load up to flexural-thrust failure because diagonal cracking is not included in the model development. Thus for loads exceeding concrete shear failure, it must be presumed that sufficient shear reinforcement (stirrups) is available.

3.9 STANDARD PARAMETERS FOR CONCRETE AND REINFORCEMENT

Based on investigations presented in subsequent chapters, a set of standard parameter values for concrete is given in Table 3.1 (see also Figure 3.3). Except for compressive strength f'_c and cracking strain ϵ_t , the parameters are assigned unique values, some of which are dependent on f'_c .

For subsequent analytical studies, the concrete will be characterized by specifying f'_c and ϵ_t . The remaining parameters are assigned the standard values shown in Table 3.1 unless stated otherwise.

Standard parameters for reinforcement steel are shown in Table 3.2 wherein the yield stress is considered as the primary variable.

Table 3.1 Standard Concrete Parameters

Parameter	Symbol	Value
Compressive strength	f'_c	3000 to 7000 (psi)
Elastic modulus	E_1	$33\sqrt{f'_c} (\gamma_c)^{1.5}$ (psi)
Cracking Strain	ϵ_t	0.0 to 0.0001 (in/in)
Initial yield strain	ϵ_y	$0.5 f'_c / E_1$ (in/in)
Strain at f'_c	ϵ'_c	0.002 (in/in)
Weight density	γ_c	150 (lbs/ft ³)
Poisson's ratio	ν_c	0.17 -

Table 3.2 Standard Steel Parameters

Parameter	Symbol	Value
Yield strength	f_y	30 to 90 ksi
Elastic modulus	E_0	29000 ksi
Poisson's ratio	ν_s	0.3 -

1 psi = 6.895 kPa

1 pcf = 157.1 N/m³

CHAPTER 4

EVALUATION OF REINFORCED CONCRETE MODEL FOR CIRCULAR PIPE LOADED IN THREE-EDGE BEARING

In this chapter the validity of the reinforced concrete model (presented in the previous chapter) is examined by comparing results with experimental data for circular pipe tested out-of-ground in three edge bearing, i.e., the so-called D-load test (ASTM C497-65T). The objective is to determine if the model can reasonably predict load-deflection histories, the load at which 0.01 inch (0.254 cm) crackwidths occur, and ultimate load.

4.1 PRELIMINARY INVESTIGATIONS

Prior to comparing the model performance with circular pipe test data, a preliminary study was undertaken for statically determinate, reinforced concrete beams with transverse loading and combined transverse with axial loading. The purpose of this preliminary study was to investigate the sensitivity of modeling parameters and to compare the model predictions with published experimental beam data (8,9) and conventional ultimate strength theories (4,5). Major findings from the preliminary study are listed below, additional detail is reported in Reference (6).

1. For all the beams studied, including both single and double reinforcement, the predicted ultimate moment capacity for transverse loading agreed within 1% to those computed in accordance with ACI 318-77.
2. Predicted load-deflection curves through ultimate were in close agreement with experimental data (8) obtained from two point loading of simply supported, rectangular beams with approximately 1.7% tension steel reinforcement.

3. In the presence of axial thrust loads, the predicted ultimate moment capacity was in good agreement with experimental data (9), wherein the ultimate moment capacity initially is increased as the axial thrust increased up to the balance point on the ultimate moment-thrust interaction diagram. Thereafter, the moment capacity steadily decreased to zero as thrust was increased to ultimate.
4. As expected, the predictions for ultimate thrust-moment capacity were not influenced by the model input parameters ϵ_t , ϵ_y , and ϵ'_c which describe the concrete stress-strain curve up to compressive strength. Only the strength parameters for concrete and steel (f'_c and f_y) influenced ultimate capacity. However, the load-deflection path to ultimate is influenced by ϵ_t , ϵ_y , and ϵ'_c and the initial elastic moduli values for steel and concrete.
5. The concrete cracking strain parameter ϵ_t was found to have a significant effect on the load-deformation curves for lightly reinforced beams (typical for culvert cross-sections). As the parameter ϵ_t decreases over a practical range (0.0001 to 0.0) the effective stiffness decreases resulting in greater deformations for the same load.
6. The compressive concrete strain parameters, ϵ_y , and ϵ'_c , also influence the shape of the load-deformation curves, but to a lesser extent than ϵ_t . As ϵ_y is decreased over the range 0.0008 to 0.0003 the deformations slightly increase. Conversely, as ϵ'_c is decreased over the range 0.0025 to 0.0015 deformations decrease.

These preliminary studies demonstrated that the reinforced concrete model was working properly and provided insights for modeling and interpreting results for the circular pipes in three-edge bearing discussed next.

4.2 EXPERIMENTAL TESTS

The out-of-ground test results used in this study were obtained from an experimental study by Heger and Saba (15), wherein they tested reinforced concrete circular pipes under three-edge bearing loadings as shown in Figure 4.1. Test results included; ultimate strength (load capacity), 0.01 inch cracking load, deflections, visual observations of crack development, and stresses in the reinforcing steel and in the concrete wall.

The pipe test program consisted of 39 pipe specimens with different wall and diameter dimensions and amounts of reinforcement. For some pipes, stirrup reinforcement was used to prevent diagonal tension failure. The unconfined compressive strength of concrete was obtained using cylinder and core tests, the tensile strength of concrete was obtained with a split cylinder test, and the ultimate tensile strength, yield strength and modulus of elasticity for the steel wires were obtained with tests carried out in accordance with the ASTM Specification A185-56T for Welded Steel Wire Fabric.

From the 39 pipes tested a subset of seven pipes are selected for this study. The subset represents the complete range of pipe dimensions and amounts of steel reinforcement used in the test program. Table 4.1 along with Figure 4.1 identifies the geometry of each selected pipe in three diameter groups; 48-inch, 72-inch and 108-inch pipes (1.22 m, 1.83 m and 2.74 m). Each diameter group has a constant wall thickness with different amounts of steel reinforcement. Ideally, each group should consist of low, medium, and high levels of steel reinforcement. However, the experiment did not include tests with medium levels of reinforcement for the 48-inch or 108-inch pipe. Thus all groups contain low and high reinforcement levels, but only the 72-inch pipe also has medium reinforcement. The first four columns of Table 4.2 shows measured strength properties of concrete and steel.

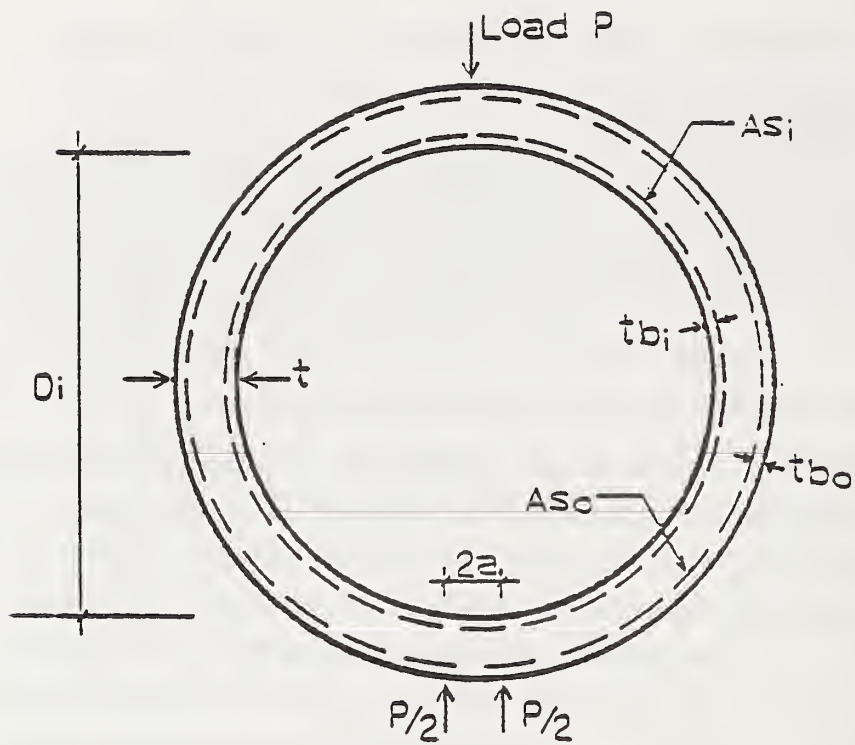


Figure 4.1 - Typical Cross Section of Circular Pipe.

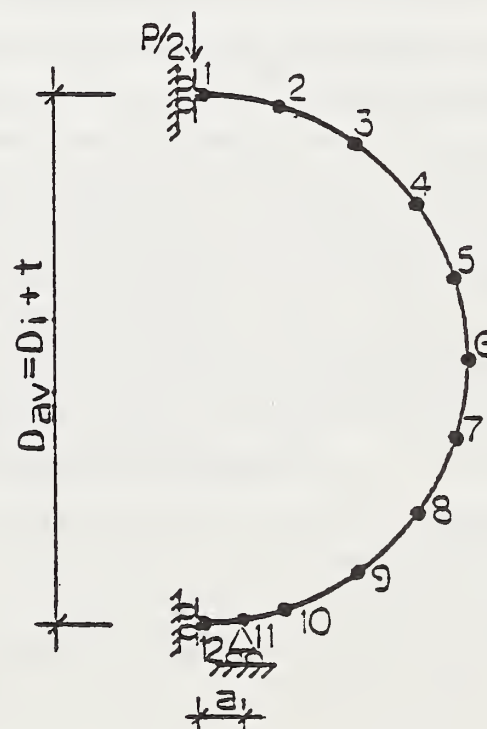


Figure 4.2 - Finite Element Model of Circular Pipe.

TABLE 4.1 - Geometric Characteristics of the Analyzed
Pipes to Compare Test and CANDE Results

Pipes	Di (in)	ti (in)	Asi (in ² /in)	Aso (in ² /in)	tbi (in)	tbo (in)	a (in)
J	48	5	.01683(L)	.01233(L)	1.10	1.09	2
K	48	5	.02708(H)	.01992(H)	1.13	1.11	2
B	72	7	.03142(L)	.02342(L)	1.14	1.12	3
G*	72	7	.05158(M)	.03692(M)	1.18	1.15	3
D	72	7	.07292(H)	.05158(H)	1.21	1.18	3
Q*	108	9	.05158(L)	.04000(L)	1.18	1.16	4.5
P	108	9	.10317(H)	.07383(H)	1.18	1.15	4.5

*
They have stirrup reinforcement

1 in = 2.54 cm

TABLE 4.2 - Material Properties Obtained From
Tests (15) for the Pipes to be Analyzed

Pipes	f'_c (psi) (cylinder)	f_t (psi)	f_{su}^* (psi)	f_{sy}^* (psi)	f'_c average (psi)	f_s^{**} average (psi)
J	1 4470	-	81800	79250	4600	80525
	2 4730	-				
K	1 4900	503	79400	77000	5225	78200
	2 5550	465				
B	1 4900	-	87300	82000	4400	84650
	2 4120	-				
	3 4640	-				
	4 3950	-				
G	1 4765	-	88650	85000	4760	86825
	2 4375	-				
	3 5136	-				
D	1 6090	-	86100	81500	5820	83800
	2 5550	-				
Q	1 5085	507	79100	75500	5810	77300
	2 6540	578				
P	1 5175	555	87325	85000	5095	86160
	2 5015	568				

* The average from the inner and outer reinforcement

** The average between the ultimate and yielding stresses

1 psi = 6.895 kPa

4.3 ANALYTICAL MODEL AND COMPARISON OF RESULTS

The circular pipe is idealized using the finite element model shown in Figure 4.2 composed of eleven beam-rod elements. For each of the seven pipes selected there are two or more test results using the same pipe with the same amount of reinforcement, where some of the material properties were obtained for each repeated test as shown in Table 4.2. For analytical predictions, concrete compressive strengths f'_c from repeated tests are averaged. The value of the steel yield stress used for analysis is taken as the average between the ultimate and yielding stresses obtained from the tests. Averaging the ultimate and yield stress of the reinforcement permits considering both ultimate load as well as the load-deflection curve within the limits of perfect plasticity. The last two columns in Table 4.2 show average strength values for concrete and steel used for analysis.

Except for the cracking strain parameter ϵ_t , the remaining material parameters for steel and concrete are assigned the standard values (Table 3.1 and 3.2). Since cracking strain is a sensitive parameter and not well established from the test data, two values are assumed for analysis; 0.00003 and 0.00008, under the assumption that actual values will be within this range.

In the following, the analytical predictions (CANDE) are compared with experimental results for load-deformation, cracking load, and ultimate load.

Load-Deformation. Figures 4.3 to 4.16 show predicted and measured vertical and horizontal deflections versus the applied load for each of the seven pipes. Each plot shows at least two "repeated" experimental tests, two predicted curves representing $\epsilon_t = 0.00003$ and 0.00008 , and the actual mode of failure; flexural or shear. Overall it is observed, the CANDE predictions generally bracket the experimental curves and follow the deformation trends quite well. Results are generally in better agreement when ultimate failure is in flexure rather than shear. For shear failures, the predicted deflections are generally less than

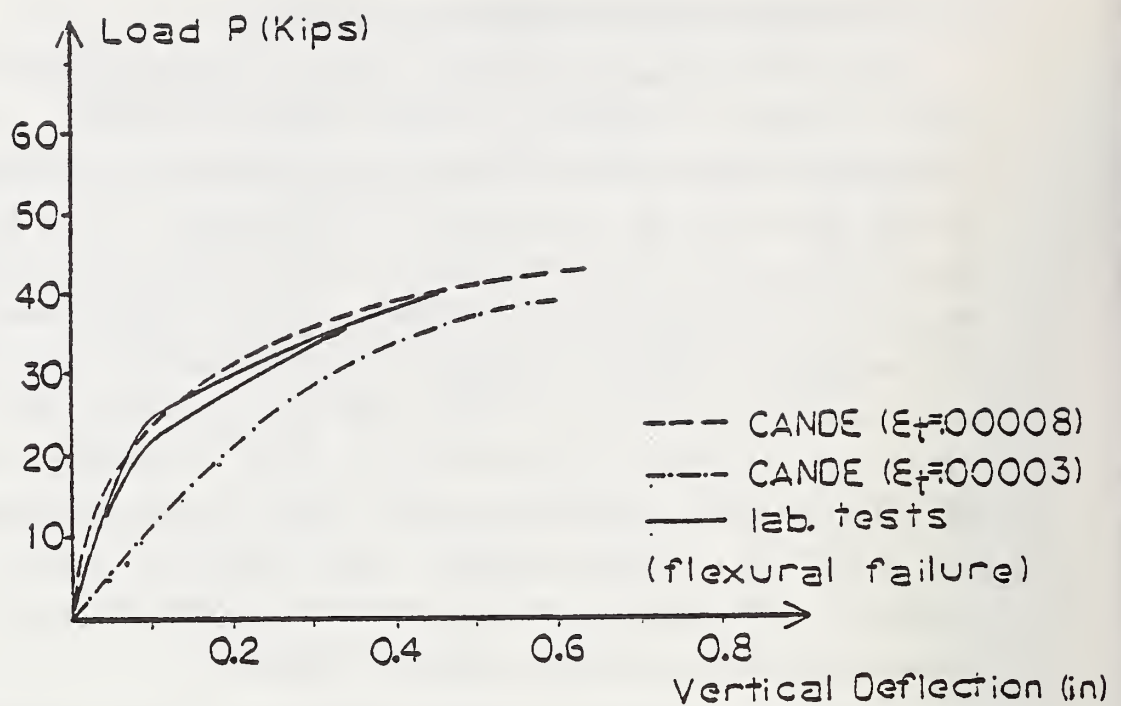


Figure 4.3 - Vertical Load - Vertical Deflection of Pipe J.

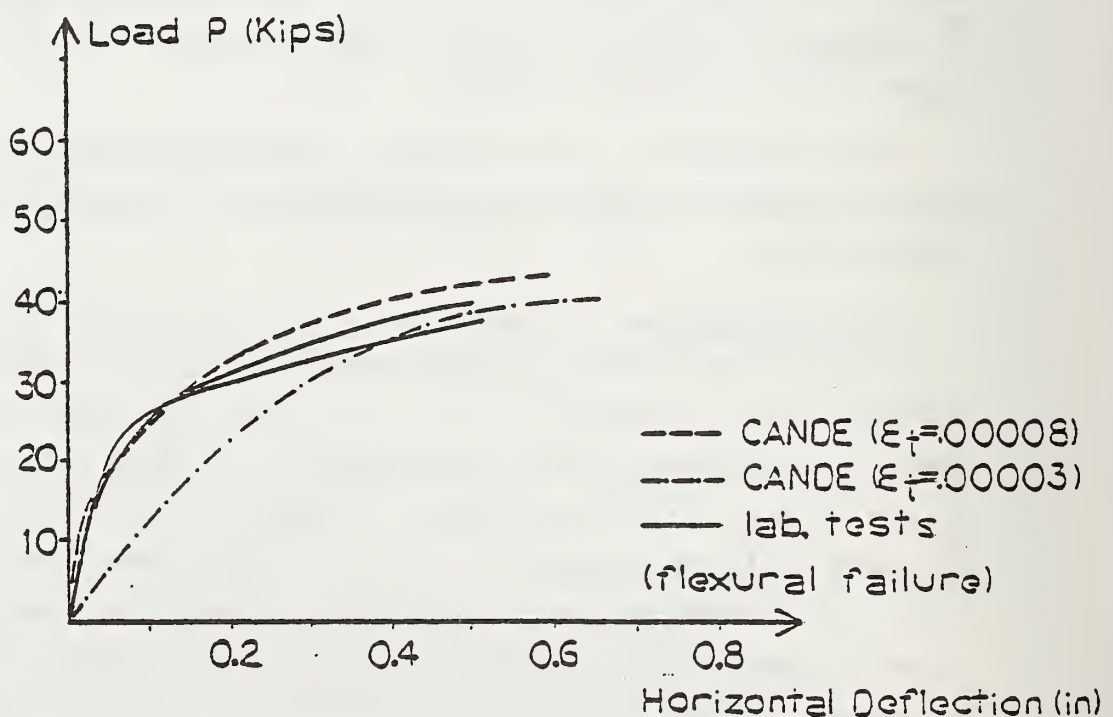


Figure 4.4 - Vertical Load - Horizontal Deflection of Pipe J.

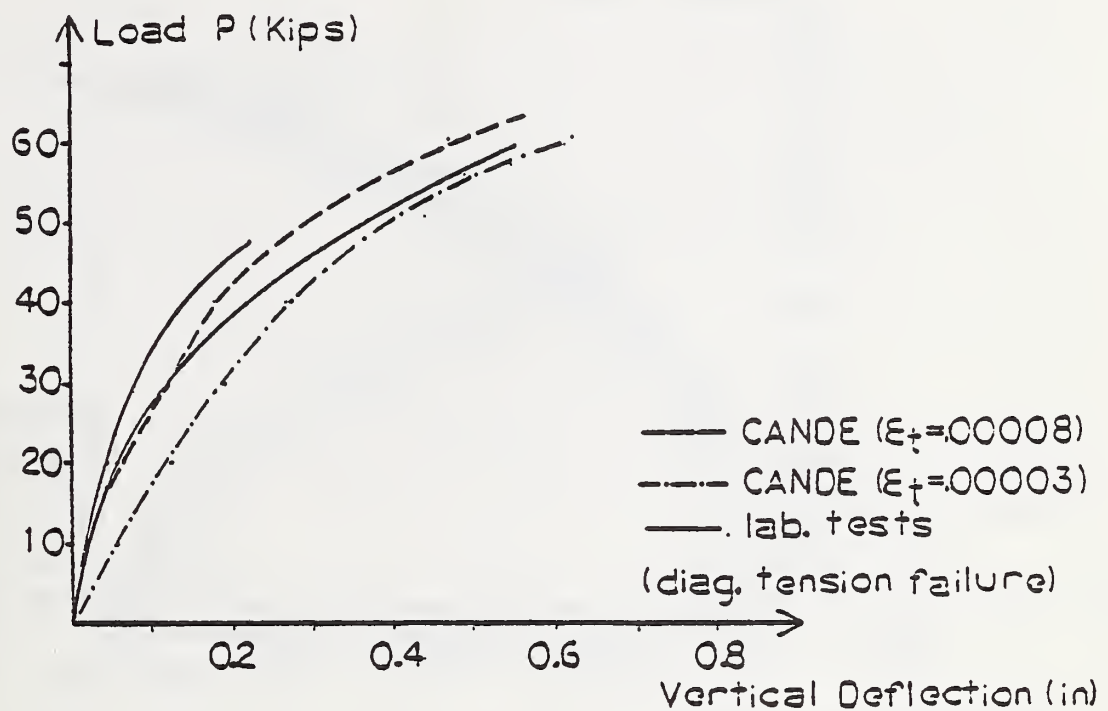


Figure 4.5 - Vertical Load - Vertical Deflection of Pipe K.

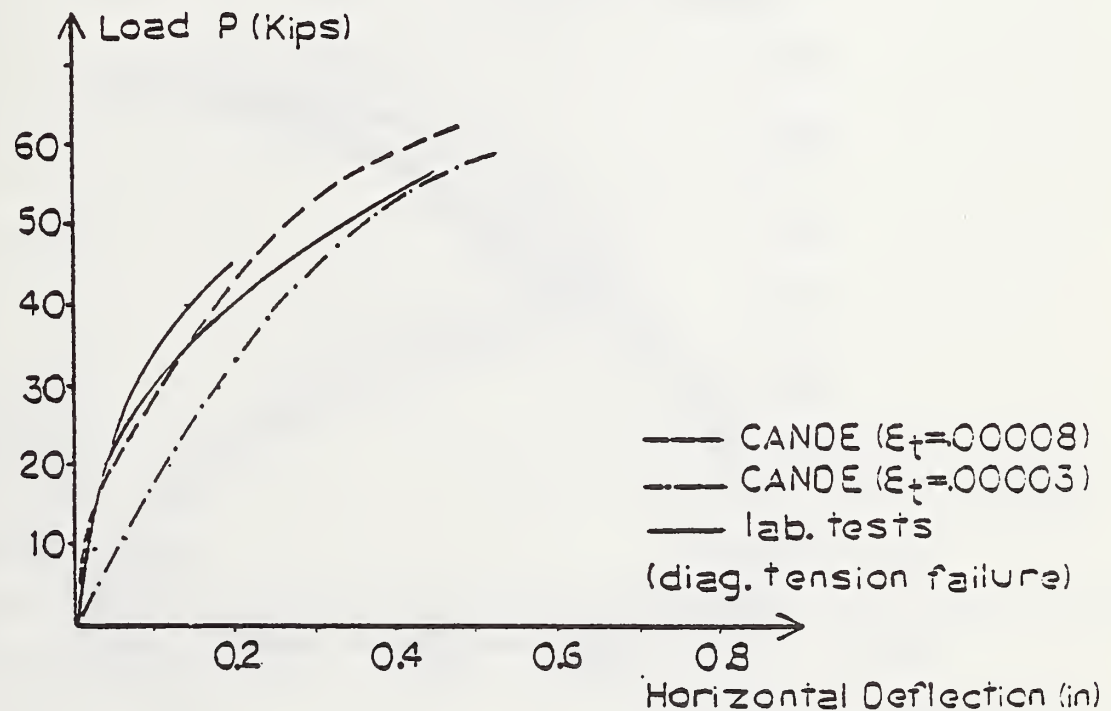


Figure 4.6 - Vertical Load - Horizontal Deflection of Pipe K.

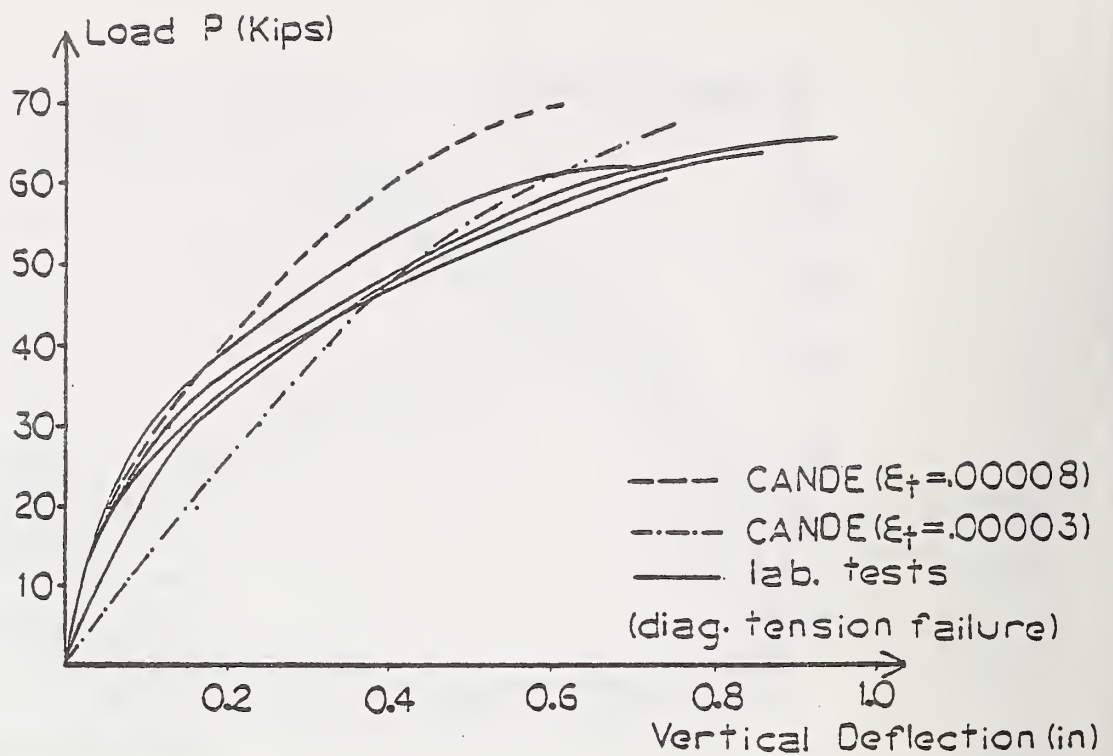


Figure 4.7 - Vertical Load - Vertical Deflection of Pipe B.

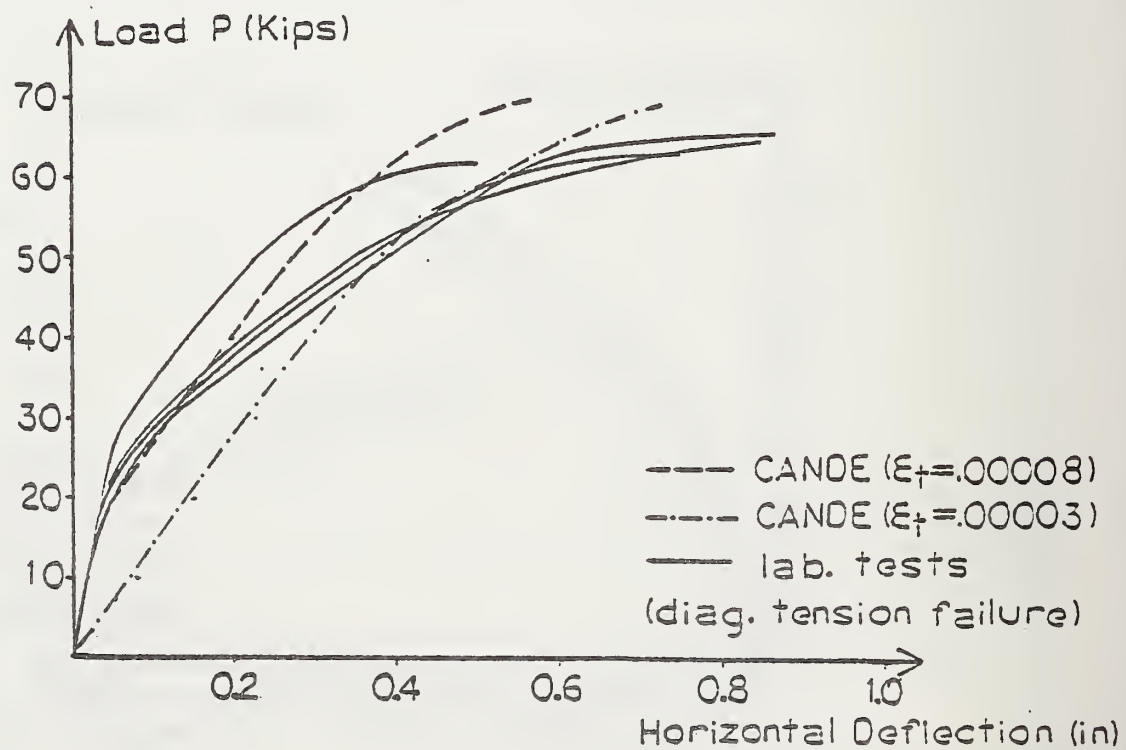


Figure 4.8 - Vertical Load - Horizontal Deflection of Pipe B.

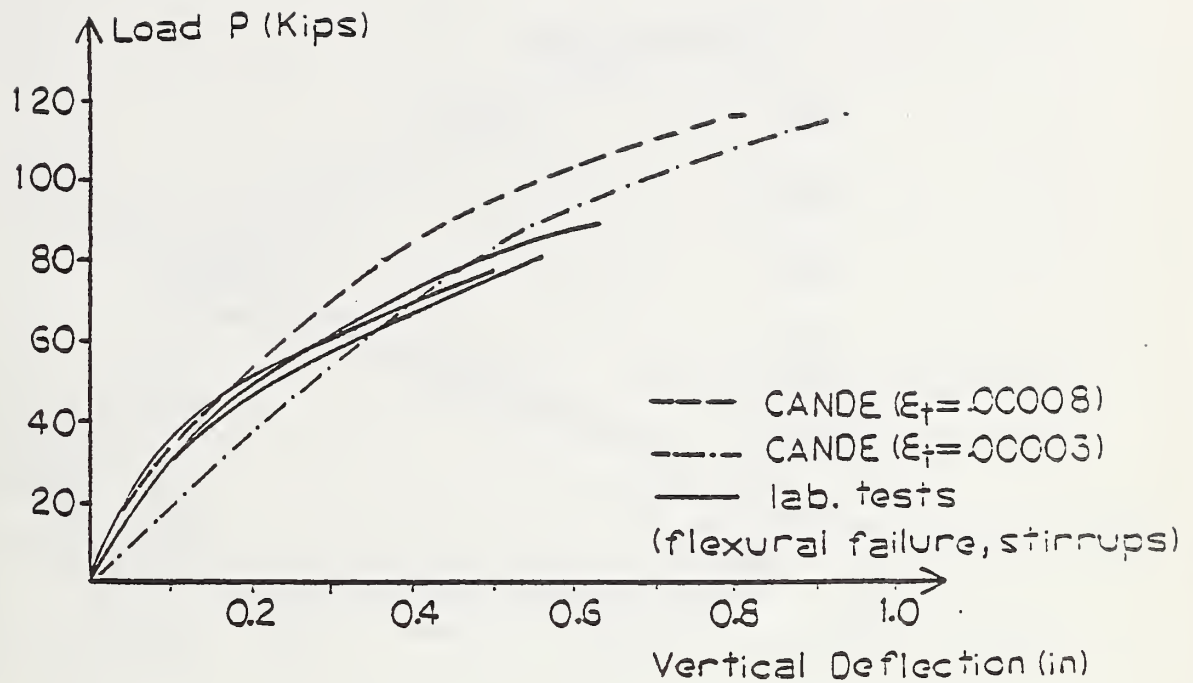


Figure 4.9 - Vertical Load - Vertical Deflection of Pipe G.

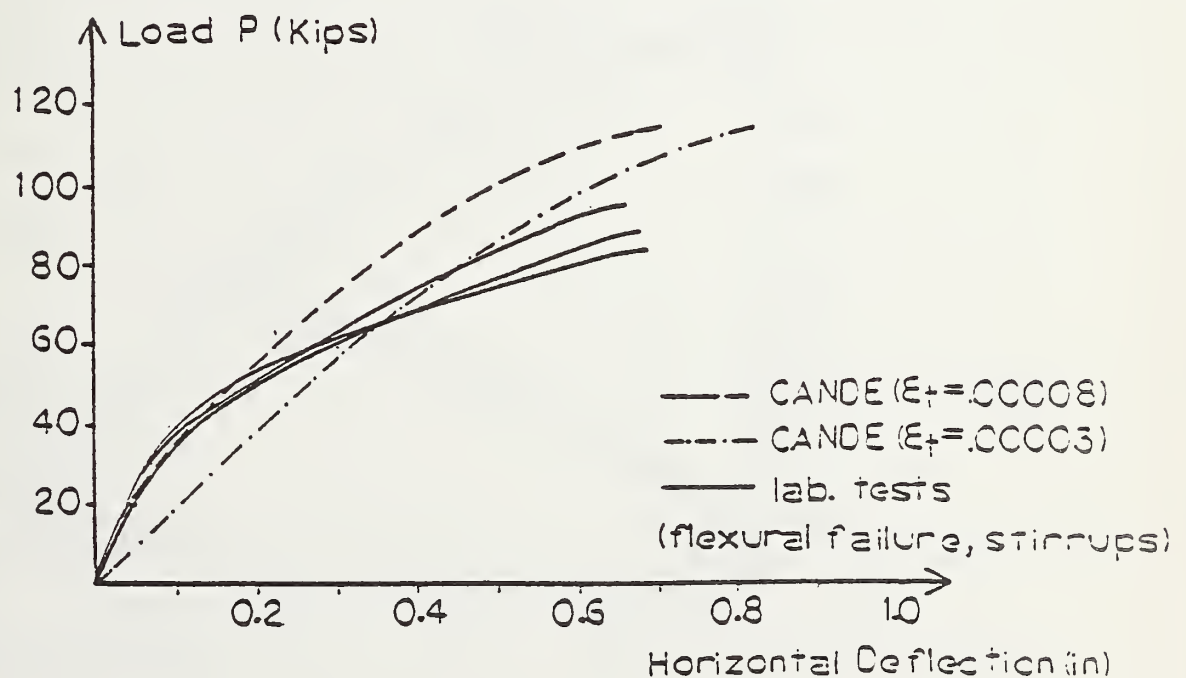


Figure 4.10 - Vertical Load - Horizontal Deflection of Pipe G.

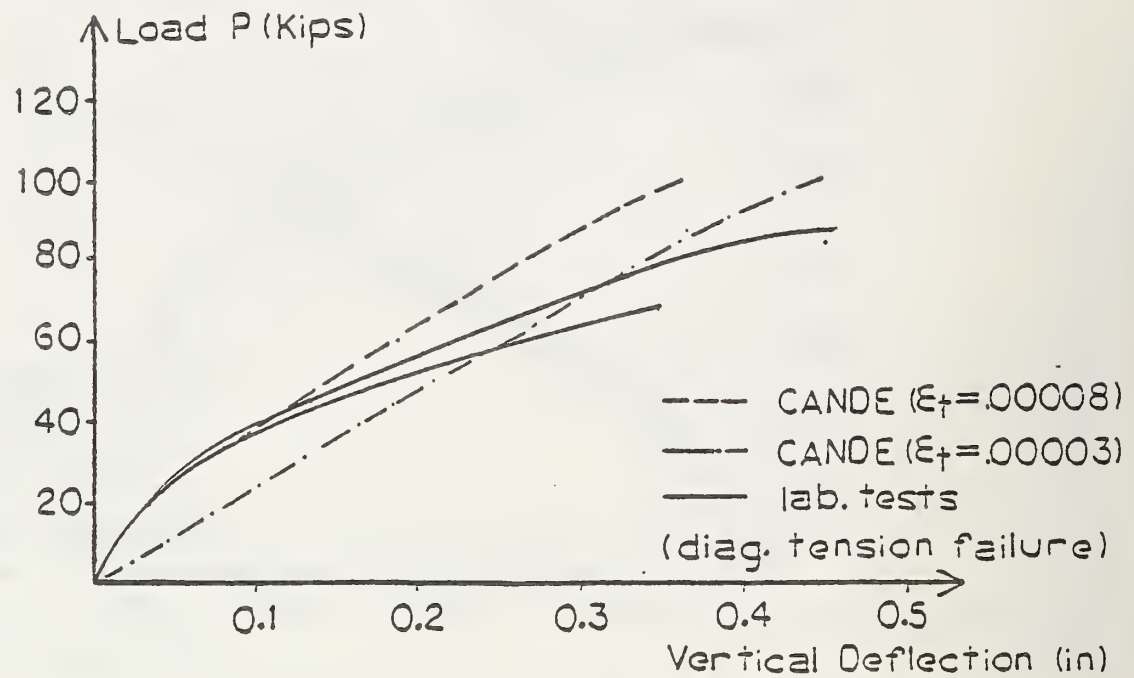


Figure 4.11 - Vertical Load - Vertical Deflection of Pipe D.

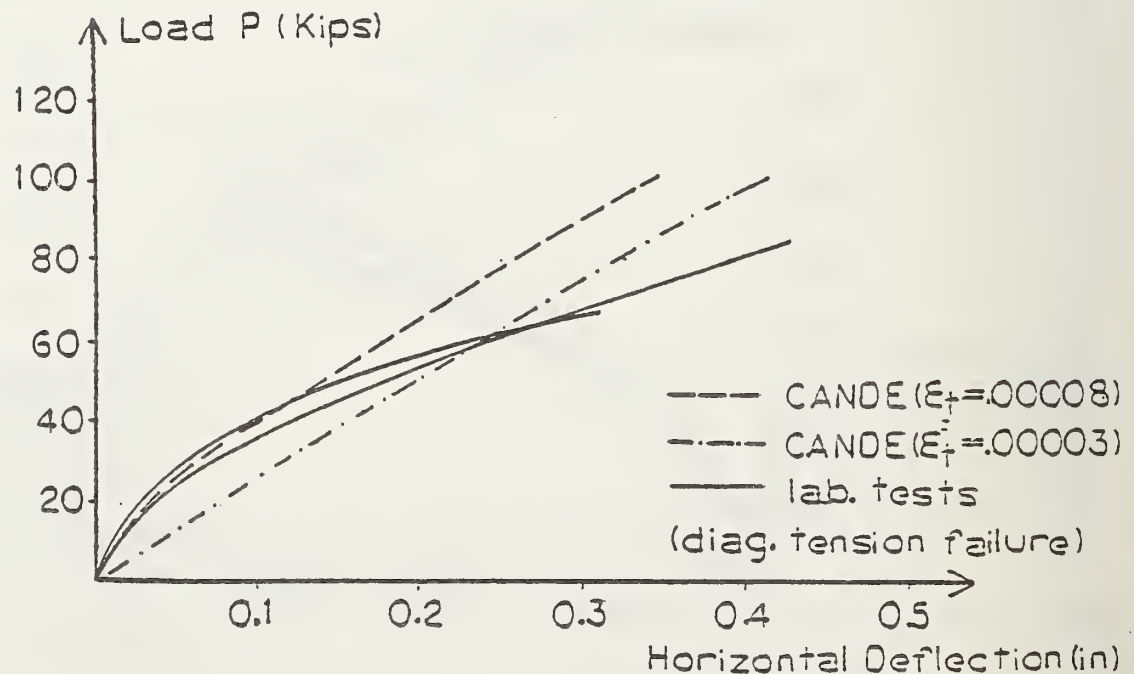


Figure 4.12 - Vertical Load - Horizontal Deflection of Pipe D.

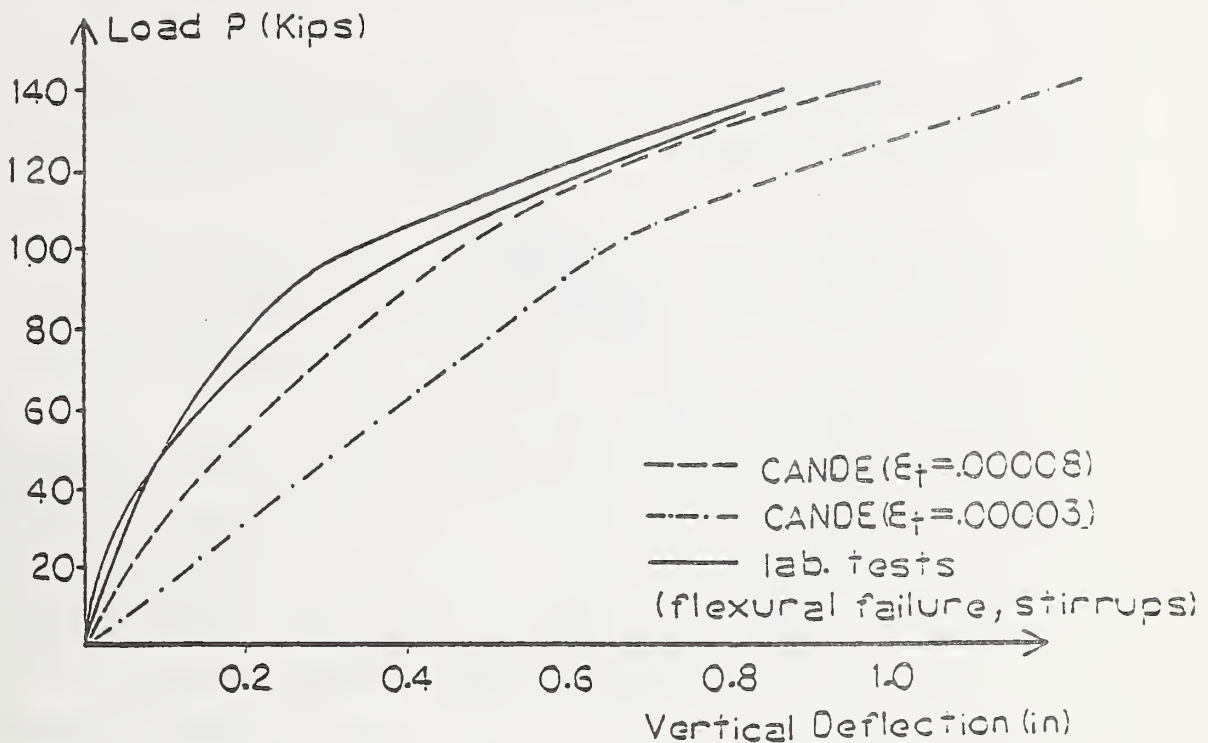


Figure 4.13 - Vertical Load - Vertical Deflection of Pipe Q.

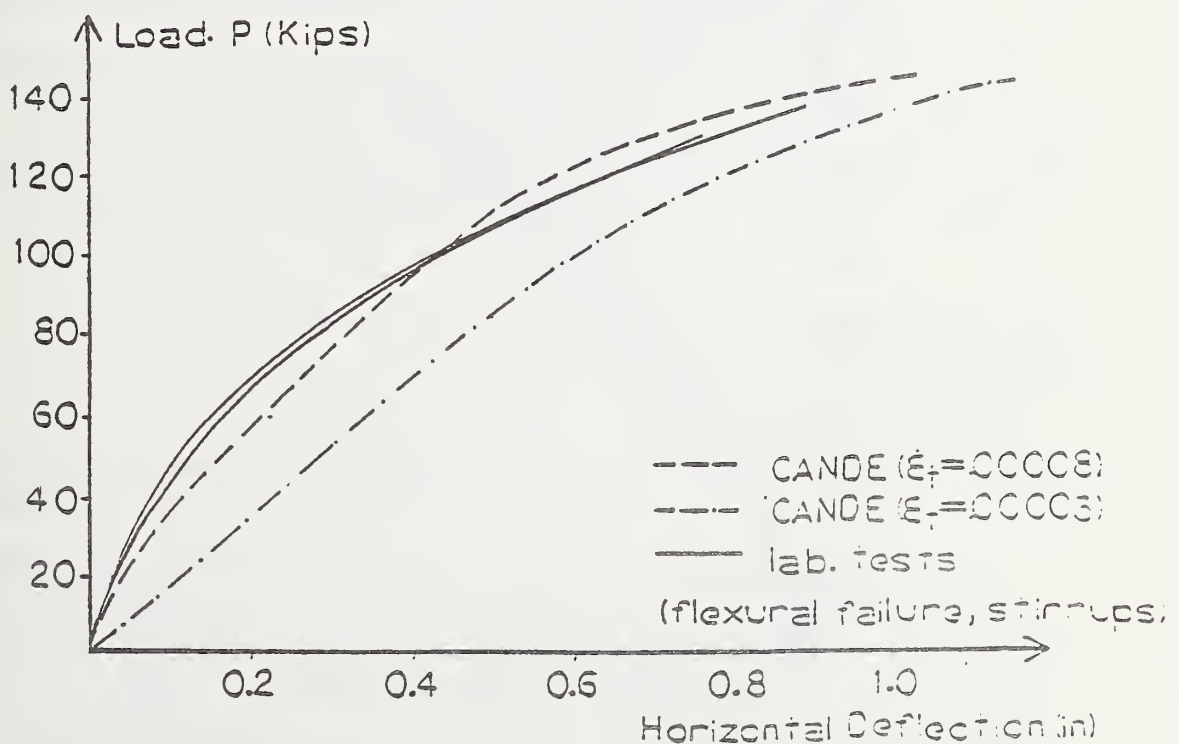


Figure 4.14 - Vertical Load - Horizontal Deflection of Pipe Q.

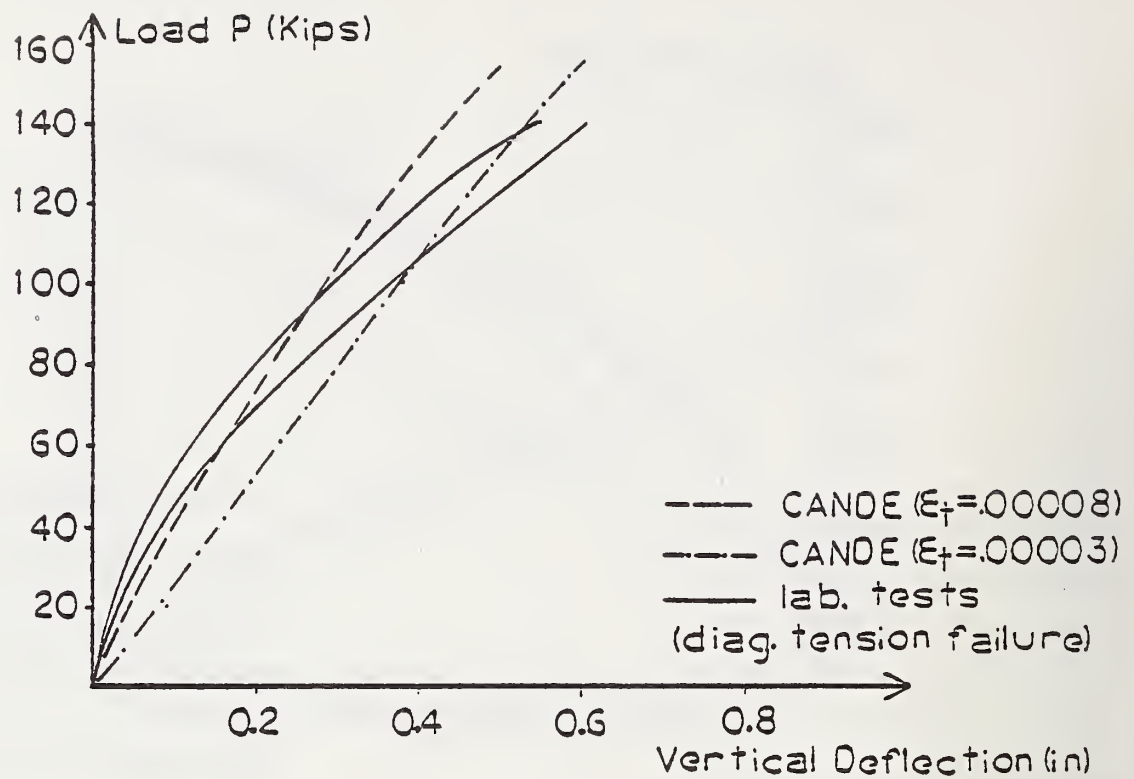


Figure 4.15 - Vertical Load - Vertical Deflection of Pipe P.

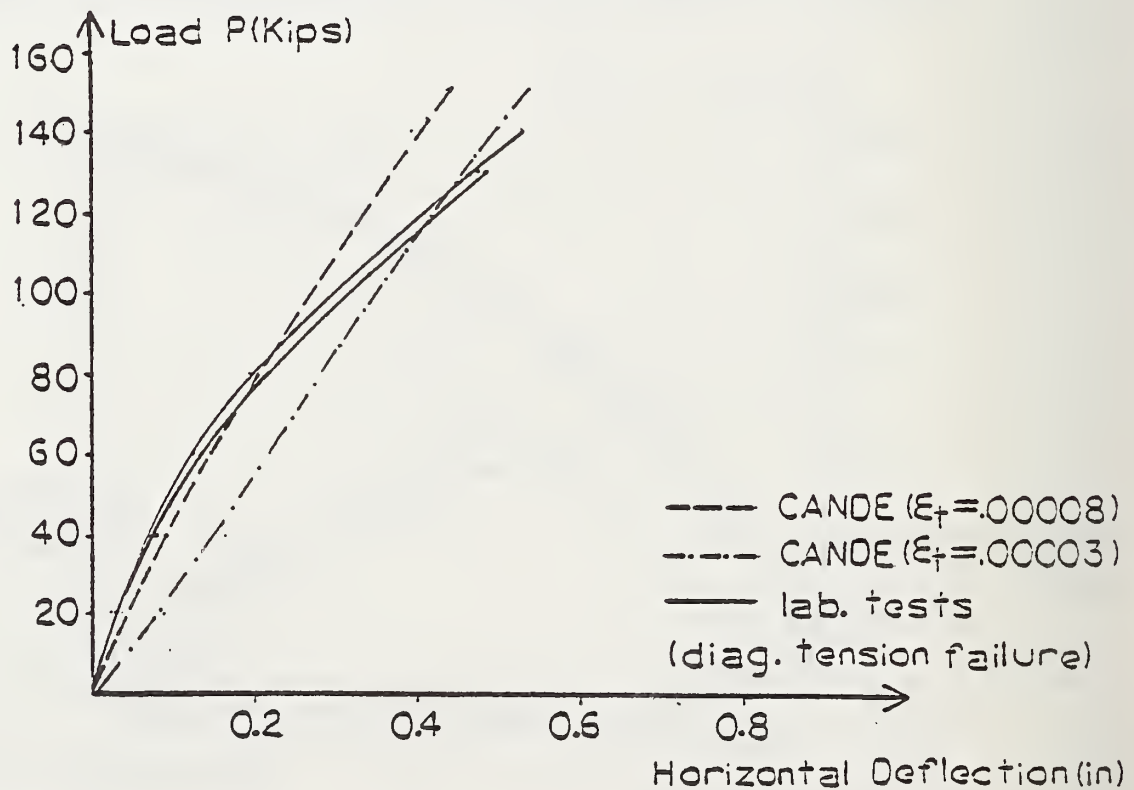


Figure 4.16 - Vertical Load - Horizontal Deflection of Pipe P.

measured values. This is to be expected since the CANDE model does not account for reduced stiffness due to diagonal cracking as shear failure develops.

For design service loads, say 0 to 2/3 ultimate, the predicted curves with $\epsilon_t = 0.00008$ correlate more closely with measured data than predicted curves with $\epsilon_t = 0.00003$.

Cracking Load. The cracking load in three-edge bearing is defined here as the applied load on the test pipe at which a 0.01 inch crack-width occurs extending over a foot in length. The so-called D-load for 0.01 inch cracking (D_{01}) is the above cracking load per foot of pipe length divided by the inside pipe diameter. ASTM C76-66T describes five strength classes of reinforced concrete pipe in terms of D_{01} .

Table 4.3 shows D_{01} values; as measured from the experiments, as predicted from CANDE, and as specified from ASTM C76 for comparable steel areas. The CANDE predictions (which employ the Gergely-Lutz formula in Chapter 3), are for the case $\epsilon_t = 0.00008$ which better represents the experimental data. Comparing CANDE predictions with test results, good agreement is observed overall. The worst case occurs for the medium size pipe with heavy reinforcement (pipe D) where the CANDE prediction is 30% higher than measured. If ϵ_t is reduced, the CANDE predictions for D_{01} are also reduced.

In view of the random nature of cracking and the inherent approximations in the Gergely-Lutz formula the CANDE predictions are considered very reasonable. As a point of interest, the predicted steel stress was approximately 50 ksi (345,000 kPa) for all pipes when the Gergely-Lutz formula predicted 0.01 inch cracking.

The ASTM D_{01} values are shown only for reference and indicate bracketing values for the steel areas used in the experimental tests.

Ultimate Loads. Of the seven pipe types considered in this study, three failed in flexure and four in shear. Two of the pipes failing in flexure had stirrup reinforcement to prevent shear failure (diagonal cracking) at an early load. The modes of failure predicted by CANDE

TABLE 4.3 - Comparison of D-load at 0.01" Crack
Between the Test, ASTM and CANDE Results

PIPES	D-Load (0.01" Crack)			
	TEST	TEST (average)	ASTM (range)	CANDE
(a) J 1 2	1190	1220	1350*	1145
	1250			
(b) K 1 2	1810	1810	1350 - 2000	1771
	-			
(b) B 1 2 3 4	1040	1396	1350*	1400
	1250			
	1460			
	1835			
(c) G 1 2 3	2000	1780	1350 - 2000	2130
	1670			
	1670			
(d) D 1 2	2292	2234	2000 - 3000	2972
	2175			
(e) Q 1 2	1650	1635	1350*	1216
	1620			
P 1 2	2540	2260	1350 - 2000	2490
	1980			

* The asterisk implies the D_{01} value is less than the minimum ASTM rating (1350).

agreed with observed failure modes when stirrup reinforcement was taken into account.

Table 4.4 shows the comparison between test results and CANDE predictions for the applied load at ultimate flexural failure. CANDE predictions are in excellent agreement with test data. Predicted ultimate loads in flexure occur when the slopes of the load-deflection curves become flat, indicating a collapse mechanism has formed.

Table 4.5 shows the load comparison for shear failures. Here, three CANDE predictions are shown based on three empirical formulas to estimate ultimate shear stress; (1) ACI formula for straight members (Chapter 3), (b) Theoretical Modification of Committee 326 for pipes (16), and (c) MIT Correlation Test formula for pipes (16). When the maximum shear stress predicted by CANDE reaches the value of these empirical formulas, shear failure is predicted (assuming no stirrup reinforcement). Of the three predictions, the standard ACI formula correlates best with experimental data (except for pipe B).

Summarizing this chapter, we conclude the beam-rod element is performing very well and is capable of predicting the structural responses of concrete pipe throughout the entire loading history.

Table 4.4. - Flexural Failure of Circular Pipes

PIPES	LOAD ** (kips)	LOAD (kips) (average)	LOAD (kips) (CANDE)
J 1	41.6	41.5	40.8
2	41.2		
* G 1	106.0	106.0	115.2
2	106.0		
3	106.0		
* Q 1	152.2	152.2	144.0
2	152.2		

* with stirrups

** test load on 4 foot pipe lengths

1 kip = 4.48 kN

Table 4.5. - Shear Failure Loads

PIPES	TEST LOAD (kips)		CANDE LOAD (kips)		
	each	average	(a) *	(b)	(c)
K 1	59.0	59.6	56.3	45.6	52.8
2	60.2				
B 1	62.4	63.0	73.3	60.0	67.2
2	64.2				
3	64.0				
4	61.5				
D 1	65.2	76.2	78.5	72.0	91.2
2	87.2				
P 1	142.8	147.0	154.2	129.6	165.6
2	151.2				

*

$$(a) v_c = 2.0 \sqrt{f'_c} \quad (\text{Standard ACI})$$

$$(b) v_c = 1.6 \sqrt{f'_c} + 64 A_{si} / D_i \quad (\text{Committee 326})$$

$$(c) v_c = 1.53 \sqrt{f'_c} + 320 A_{si} / D_i \quad (\text{MIT Correlation})$$

CHAPTER 5

EVALUATION OF REINFORCED CONCRETE MODEL FOR BOX CULVERTS LOADED IN FOUR-EDGE BEARING

Like the previous chapter, this chapter continues to examine the validity of CANDE's reinforced concrete, beam-rod element. Here, we compare CANDE results with experimental data for box culverts tested in four-edge bearing. The results to be compared include the load for 0.01 inch cracking and ultimate load. The experimental data did not include load-deformation histories, consequently these cannot be compared. For reference, the comparisons also include the SGH analytical predictions (12) based on an elastic analysis discussed in Chapter 2.

5.1 EXPERIMENTAL TEST

The experimental results used for the comparison belong to a test program (13,14) where out-of-ground reinforced concrete box culverts with welded wire fabric were loaded up to failure. The loading was applied as shown in Figure 5.1 using a 4-edge bearing testing apparatus. The material properties of concrete were determined using cylinder tests and core tests for each kind of box, and the mechanical properties of the reinforcement were determined by tensile tests (19). Three span sizes of box were tested, small, medium and large with three levels of reinforcement in each size, low, medium and high. Thus, nine types of boxes were tested with two repeated tests per box type.

Tables 5.1 and 5.2 together with Figure 5.1 show the measured geometries and material strengths for each test box where repeated boxes are labelled A and B. Note that the core tests for f'_c are generally higher than cylinder tests for f'_c and the ultimate steel stress is 10 to 20% higher than initial yield stress.

The test program was performed to verify the SGH analysis/design method (12) which in turn was used to develop the ASTM standard designs for reinforced concrete box culverts (21).

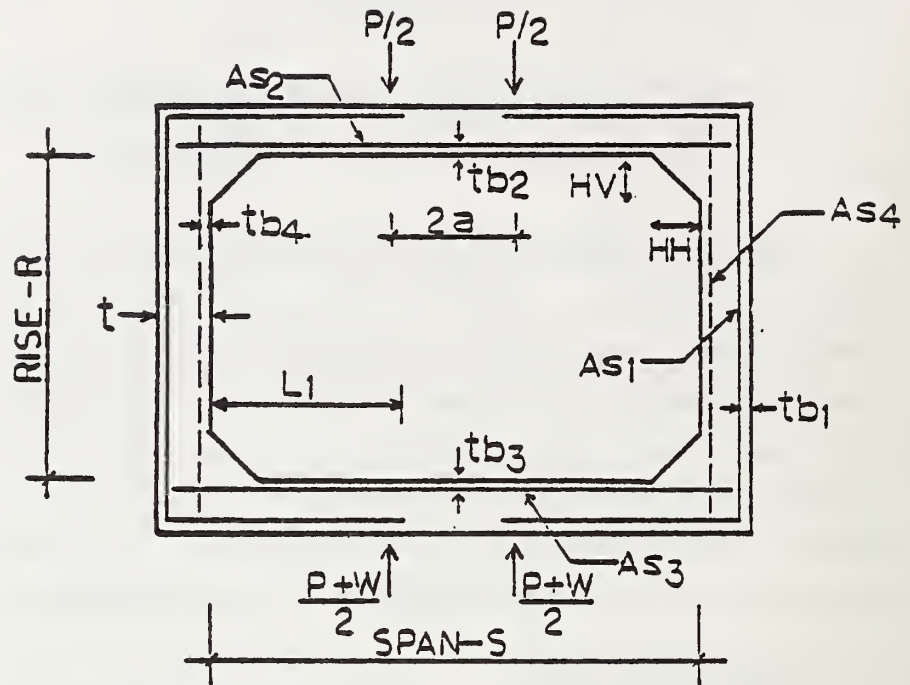


Figure 5.1 - Typical Cross Section of Concrete Box Culvert.

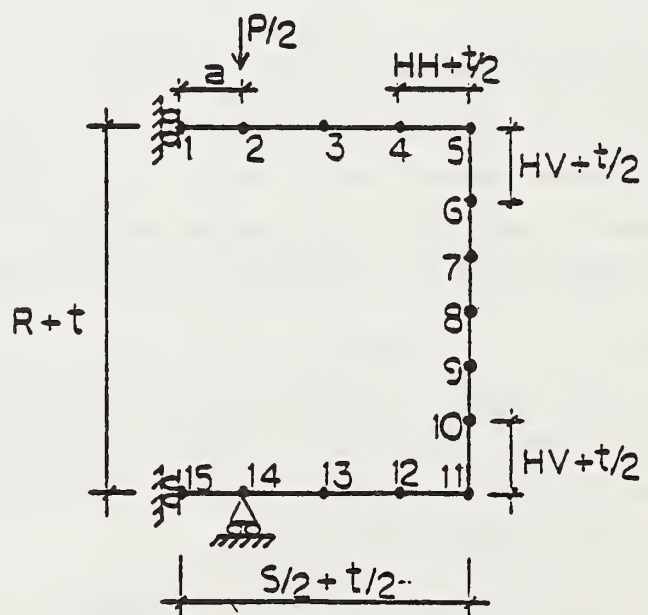


Figure 5.2 - Finite Element Model of Concrete Box Culvert.

TABLE 5.1 Geometric Characteristics of Test Box Culverts

BOXES **		SPAN S(in)	RISE R(in)	HH, HV (in)	t_2 (in)	t_3 (in)	t_{b2} (in)	t_{b3} (in)	a (in)
8*4-8	A	96	48	8	8.125	8.125	1.376	1.251	12
	B	96	48	8	8.250	8.000	1.126	1.251	12
8*4-2	A	96	48	8	8.188	8.251	1.526	1.214	12
	B	96	48	8	8.253	8.188	1.278	1.401	12
8*4-18	A	96	48	8	8.250	8.251	1.229	1.354	12
	B	96	48	8	8.250	8.126	1.416	1.229	12
6*4-10	A	72	48	7	7.313	7.251	1.053	1.303	9
	B	72	48	7	7.313	7.313	1.240	1.240	9
6*4-2	A	72	48	7	7.375	7.438	1.068	1.006	9
	B	72	48	7	7.375	7.438	1.443	1.006	9
6*4-22	A	72	48	7	7.313	7.375	1.086	1.148	9
	B	72	48	7	7.438	7.375	1.523	1.148	9
4*4-4	A	48	48	5	5.187	5.375	1.353	1.103	6
	B	48	48	5	5.188	5.250	1.385	1.353	6
4*4-18	A	48	48	5	5.188	5.188	1.237	0.862	6
	B	48	48	5	5.313	5.188	1.112	1.175	6
4*4-2	A	48	48	5	5.563	5.188	1.756	1.381	6
	B	48	48	5	5.376	5.250	1.694	1.173	6

t_2, t_3 = thickness of top and bottom slabs respectively

** Boxes are identified according to Reference (14): i.e., span(ft)*rise(ft) - design earth cover (ft) for interstate live load.

1 in = 2.54 cm

TABLE 5.2 Reinforcement and Material Properties
of the Box Culverts

BOXES		A_{s1} (in ² /in)	A_{s2} (in ² /in)	A_{s3} (in ² /in)	S_ℓ (in)	f'_c (psi) cylinder	f'_c (psi) cores	f_y^* (ksi)	f_{su}^* (ksi)
8*4-8	A	.02492	.02492	.02492	2	4934	12510	72.3	83.65
	B					4757	5515		
8*4-2	A	.04325	.03550	.03550	2	5288	4475	82.0	89.58
	B					4952	5425		
8*4-18	A	.04325	.04325	.04325	2	5111	5285	80.5	94.95
	B					5430	5855		
6*4-10	A	.01450	.02075	.02075	2	6296	7060	85.9	94.40
	B					5022	7460		
6*4-2	A	.03550	.03475	.02675	2	5624	6680	85.8	99.43
	B					5589	6965		
6*4-22	A	.02358	.03442	.03442	2	5553	5960	86.2	95.16
	B					5341	7190		
4*4-4	A	.01117	.01117	.01117	3	5518	6030	78.5	95.80
	B					7534	6670		
4*4-18	A	.01117	.01967	.01967	2	7428	7000	77.3	90.93
	B					7729	6635		
4*4-2	A	.01600	.02692	.02692	2	5872	5715	82.0	92.73
	B					6155	6430		

*This value is an average of the three reinforcements

S_ℓ = spacing of longitudinal wires

NOTE: A_{s4} steel not used

1 in = 2.54 cm

1 psi = 6.895 kPa

5.2 CANDE MODEL

Figure 5.2 shows the finite element model for a typical box culvert test. Because of symmetry only half the box is modeled with 14 beam-rod elements. The element pattern shown was found to be sufficiently accurate with regard to element lengths. The reaction support (shown at node 14) is modeled with a triangular element rather than a boundary condition in order to avoid imposing a moment constraint (a quirk of CANDE).

Each element cross section is assigned the concrete thickness, the steel area, and steel area locations as actually reported from the experiments (Tables 5.1 and 5.2). Haunches at the box corners are modeled with two corner elements whose thicknesses are increased by one-half the haunch dimensions.

For concrete material properties, f'_c is taken from the core tests (Table 5.2, except first box) as this is generally more representative of each test box, than cylinder tests. The cracking strain is assumed as $\epsilon_t = 0.0001$ for all box tests based on observing typical concrete test results. Other concrete parameters are assigned standard values (Table 3.1).

Steel "yield" stress for the elastic-perfectly plastic model is taken as the ultimate stress reported in the last column of Table 5.2 for each box. Ultimate steel stress, rather than initial yield stress is assumed because this better approximates ultimate load capacity. Other steel parameters are assigned standard values (Table 3.2). Within each test box the steel stress-strain properties for A_{s1} , A_{s2} , and A_{s3} are assumed identical.

5.3 COMPARISON OF MODELS WITH EXPERIMENTS

In the following comparisons for cracking load and ultimate load (flexure and shear), the "load" refers to the total applied load P per foot length of test pipe (see Figure 5.1). Each repeated experimental test is also repeated analytically with the associated variations in geometry and material properties.

Cracking Load. Table 5.3 shows a comparison between test data and CANDE predictions for the load producing a 0.01 inch crack. These cracks occur near the centerline on the inside surfaces of the top or bottom box slabs. The table specifies "top" or "bottom" indicating which slab the 0.01-inch crack was first observed, and the CANDE prediction corresponds to that location. Also shown in Table 5.3, are the SGH predictions for cracking loads to serve as a reference.

Overall it is observed the CANDE predictions are very good and are statistically better than the SGH predictions as shown at the bottom of Table 5.3. A graphical comparison of the data is shown in Figure 5.3 from where it is seen that CANDE cracking load predictions are slightly lower in the average (conservative) than the test data, but only on the order of 5 to 10%.

As previously discussed, CANDE predictions are semi-empirical and employ the Gergely-Lutz crackwidth formula. Although not reported here, the ACI crackwidth formula (4) was tried with CANDE but not found satisfactory in this study.

Ultimate Loads. In loading the 9 pairs of boxes (18 tests) to ultimate, 10 tests failed in flexure and 8 tests failed in shear (diagonal cracking). Two pairs of boxes produced a failure of each kind. Modes of failure predicted by CANDE agreed with observed failure modes.

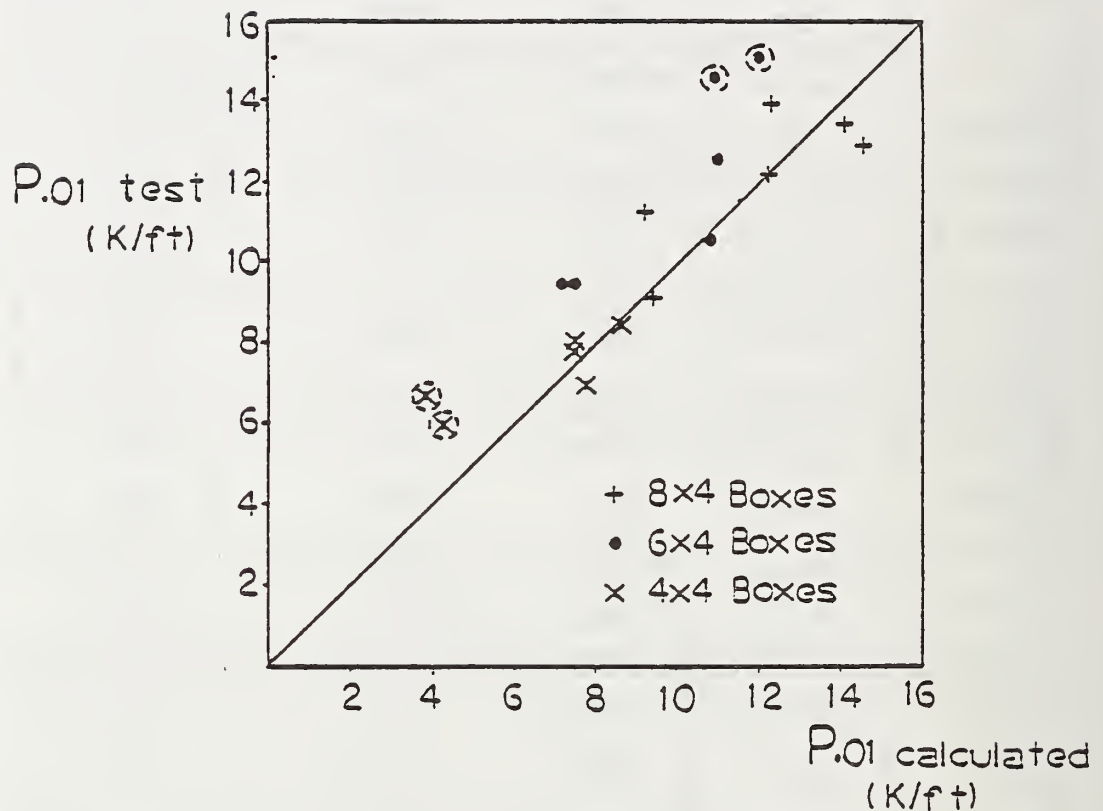
Table 5.4 shows the comparison of the ultimate load for flexural failure between CANDE prediction, the test results, and the SGH analytical results. The values calculated by CANDE are in very good agreement with test results, and are slightly better than the SGH analytical results. Figure 5.4 shows graphically the comparison between CANDE and the test results for ultimate load at flexural failure. CANDE's overall results correlate excellently with the test results, with a \pm 6% error range.

Table 5.5 shows the comparison of the ultimate load for shear failure (diagonal cracking) between CANDE prediction, the test results,

TABLE 5.3 -- Comparison of CANDE Results with Test and
SGH Results for 0.01 inch Cracking Load

BOXES		P _{.01} (1b/ft)		
		TEST	CALCULATED	
			SGH Report (14)	CANDE
8*4-8	A	Top	9250	7840
	B	Top	11300	9430
8*4-2	A	Bottom	14000	10950
	B	Top	12300	12360
8*4-18	A	Top	13000	15650
	B	Bottom	13500	13442
6*4-10	A	Bottom	9500	5830
	B	Bottom	9500	6220
6*4-2	A	Bottom	14500	10640
	B	Bottom	10500	10650
6*4-22	A	Bottom	15000	12510
	B	Top	12500	11090
4*4-4	A	Bottom	6700	2740
	B	Top	6000	2700
4*4-18	A	Bottom	7000	7770
	B	Top	8000	7090
4*4-2	A	Bottom	7800	6940
	B	Bottom	8500	8380
P _{.01} test P _{.01} calc.		Average	1.29	1.10
		Standard Deviation	0.43	0.24
		Coefficient of Variation	34%	21%

1 lb/ft = 14.6 N/m



$$\frac{\sum P.01 \text{ (test)}}{\sum P.01 \text{ (calculated)}} = 1.1063$$

$$\frac{\sum P.01^* \text{ (test)}}{\sum P.01 \text{ (calculated)}} = 1.0475$$

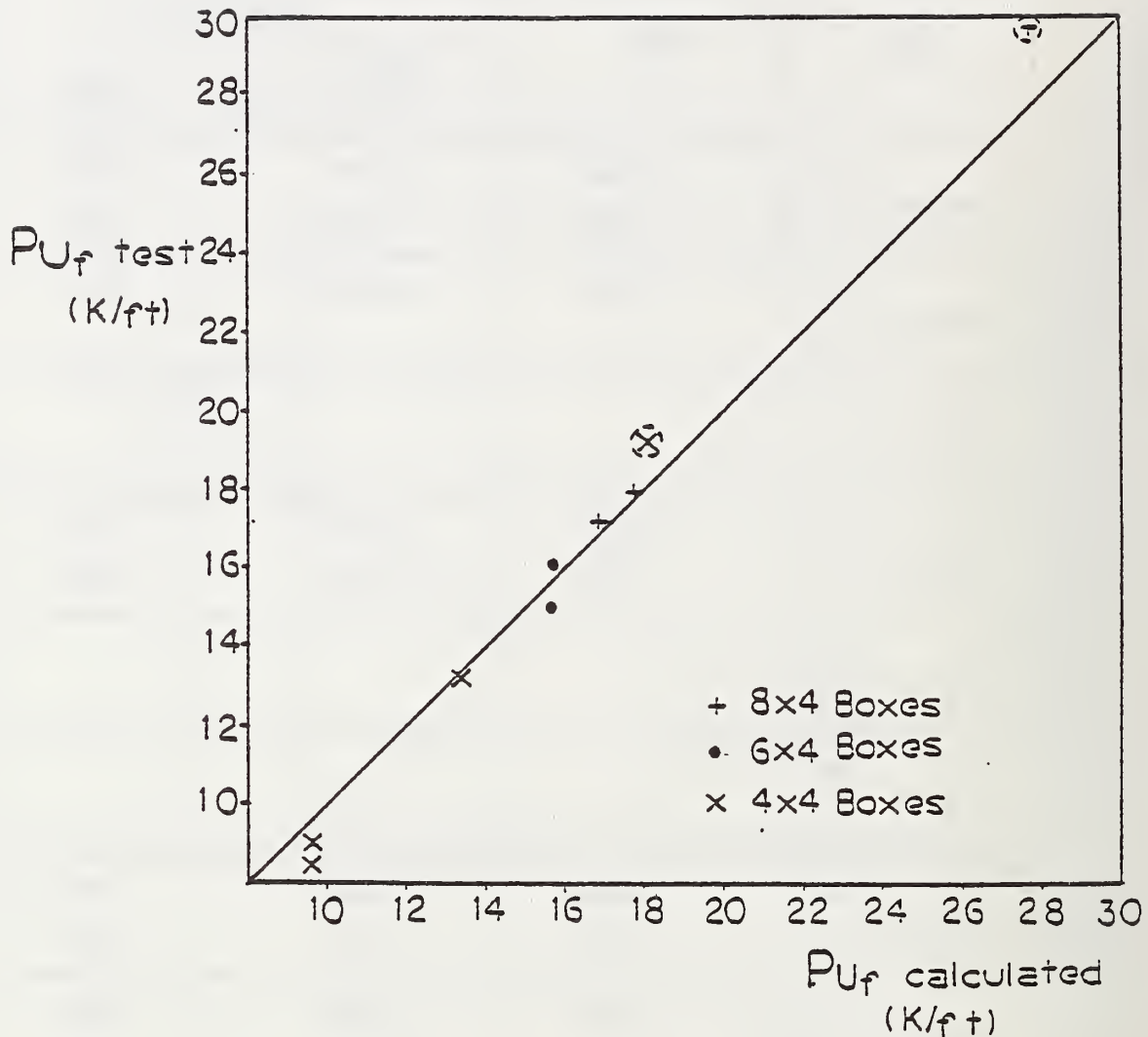
* Excluding \odot

Figure 5.3 - Comparison of Test and Calculated 0.01 inch Crack Load.

TABLE 5.4 - Comparison of CANDE Ultimate Load with Test and
SGH Ultimate Loads for Flexural Failure

BOXES		P_{uf} (lb/ft)		
		TEST	CALCULATED	
			SGH Report (14)	CANDE
8*4-8	A	17860	16050	17700
	B	17230	15780	16800
8*4-2	A	29690	28200	27600
	B			
8*4-18	A			
	B			
6*4-10	A	16100	15380	15600
	B	15000	15390	15600
6*4-2	A			
	B			
6*4-22	A			
	B			
4*4-4	A	8980	9800	9600
	B	8440	9011	9600
4*4-18	A	13150	12680	13200
	B	13170	12730	13200
4*4-2	A			
	B	19300	18510	18000
P_{uf} test		Average	1.03	1.01
		Standard Derivation	0.06	0.06
		Coefficient of Variation	6%	5.8%

1 lb/ft = 14.6 N/m



$$\frac{\sum P_{U_f} (\text{test})}{\sum P_{U_f} (\text{calculated})} = 1.0129$$

$$\frac{\sum P_{U_f}^* (\text{test})}{\sum P_{U_f} (\text{calculated})} = .9897$$

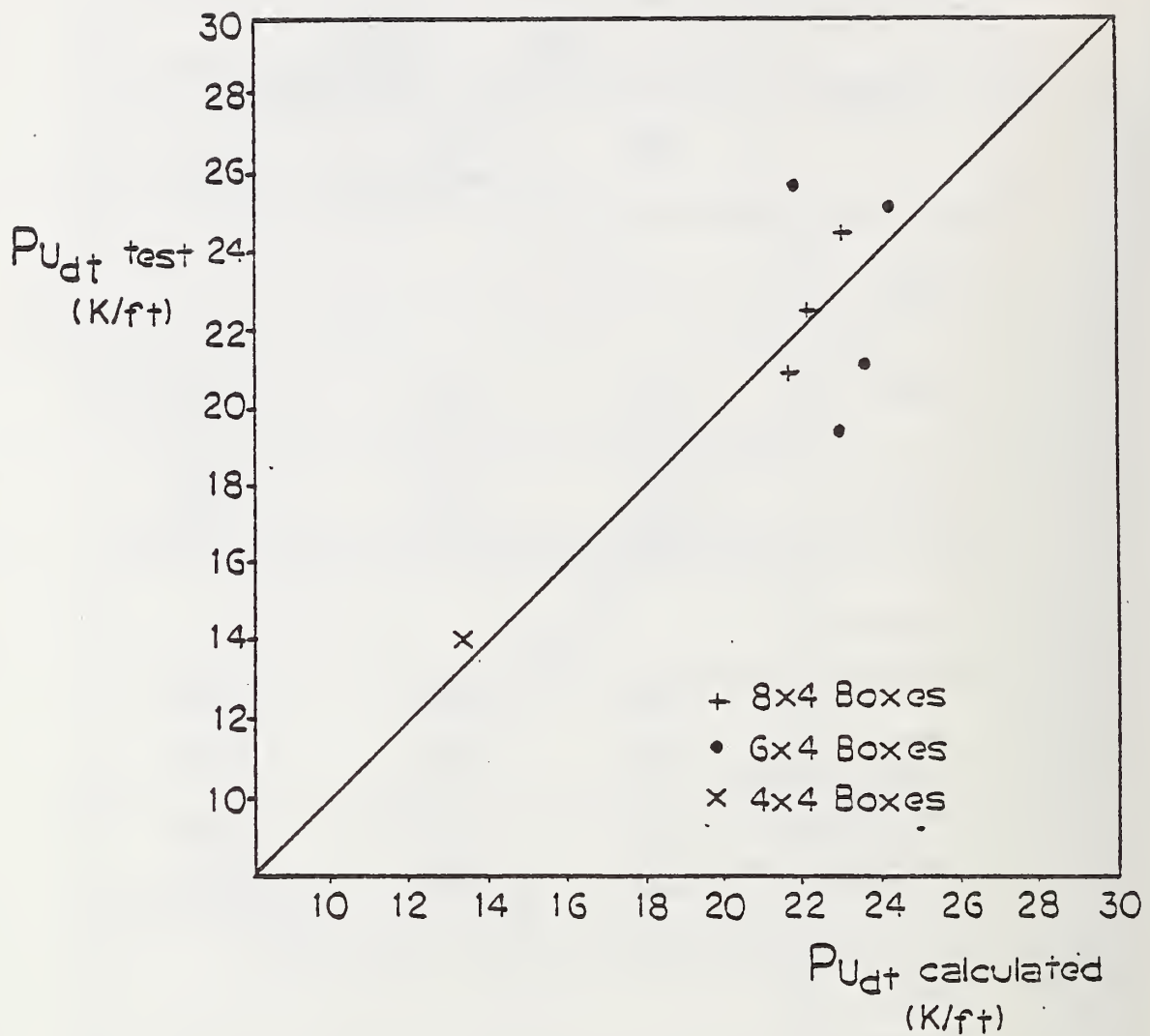
* Excluding 0

Figure 5.4 - Comparison of Test and Calculated Ultimate Flexural Load.

TABLE 5.5 - Comparison of CANDE Ultimate Load with Test
and SGH Ultimate Loads for Shear Failure

BOXES		$P_{u_{dt}}$ (1b/ft)		
		TEST	CALCULATED	
			SGH Report(14)	CANDE
8*4-8	A			
	B			
8*4-2	A			
	B	22520	21520	22000
8*4-18	A	20890	21590	21600
	B	24490	22860	23000
6*4-10	A			
	B			
6*4-2	A	19400	23420	22800
	B	25250	23950	24000
6*4-22	A	25680	21260	21600
	B	21150	23530	23400
4*4-4	A			
	B			
4*4-18	A			
	B			
4*4-2	A	14080	12790	13200
	B			
$\frac{P_{u_{dt}} \text{ test}}{P_{u_{dt}} \text{ calc.}}$		Average	1.02	1.01
		Standard Deviation	0.12	0.10
		Coefficient of Variation	12%	10%

1 lb/ft = 14.6 N/m



$$\frac{P_{Udt} \text{ (test)}}{P_{Udt} \text{ (calculated)}} = 1.0108$$

Figure 5.5 - Comparison of Test and Calculated Ultimate Diagonal Tension Load.

and the SGH analytical results. The values obtained from CANDE are assuming that the maximum shear stress resisted by the concrete is $2.0 \sqrt{f'_c}$. Once again the values obtained from CANDE are very close to the test results and are a better prediction than the analytical results of SGH. The test results are compared graphically with CANDE results in Figure 5.5, from where we can observe that the amount of error from CANDE is in the range of $\pm 10\%$, a very good correlation for practical purposes.

The performance of the beam-rod element used in the CANDE program to model reinforced concrete box culverts has been shown to perform very well in out-of-ground loading. Subsequent studies will consider the box culvert buried, subjected to soil loads as well as live loads. The empirical formulas for crack prediction and shear resistance used in CANDE will be the same ones used in this chapter, where their performance was found satisfactory.

CHAPTER 6

DEVELOPMENT OF LEVEL 2 BOX MESH

The reinforced concrete box culvert model is now considered for its actual function as a conduit buried in soil. Accordingly, both the soil and the box form the structural system, hereafter called box-soil structure. The soil plays a dual role; on the beneficial side it adds substantial stiffness to the box-soil structures, on the detrimental side it transits gravity and applied loads to the box during the installation process.

To determine loads acting on the box requires a complete model of the box-soil structure simulating the entire installation process. In this chapter a general finite element model of the box-soil structure is presented with the intent of developing an automated finite element mesh subroutine suitable for simulating the vast majority of box-soil installations encountered in practice. This is called the level 2 box option of CANDE.

To develop an automated finite element mesh requires some limiting assumptions and specifications of a variety of parameters describing the box-soil system. Overall assumptions are symmetry about the vertical centerline and plane strain geometry and loading. Adjustable system parameters include; box dimensions (span and rise), soil boundary dimensions (width from centerline, depth below box, and height of cover above box), soil zones (in situ soil, fill soil, and bedding soil) and installation type (embankment or trench). These parameters along with the question of mesh refinement are discussed in the following.

6.1 PARAMETERS TO DEFINE THE MODELS

The depth and width of the entire soil zone are specified in terms of the particular box dimensions being analyzed. The box culvert

is idealized with beam elements located along the middle line of the walls, so the nominal box span used in our model is equal to the inside span of the box plus its thickness. Likewise for the nominal rise of the box. Defining R_1 as half the nominal span and R_2 as half the nominal rise, as shown in Figure 6.1, the soil depth below the box is set at $3R_2$, and the soil width is set at $4R_1$ from the box sides. These soil boundaries are adjudged to be outside the zone of soil-structure interaction based on previous studies (1).

The height of cover (see Figure 6.1) is an input parameter denoting the final fill height above the box. However, the height of the mesh over the top of the box is limited to $3R_2$ or the specified height of soil cover, whichever is less. For cover heights greater than $3R_2$ equivalent loading is used as discussed subsequently.

Other geometry parameters that need to be defined are the trench depth and trench width as shown in Figure 6.1. If the mesh model is intended to represent an embankment installation, the trench width is $4R_1$ so that only fill soil exists on the sides and in situ soil is leveled with bottom of the box.

The material zones are in situ soil, bedding and fill soil, where each zone can be assigned the same or different soil mechanical properties. In addition to R_1 and R_2 , the box culvert geometry is defined with the side, bottom and top slabs thicknesses, and haunch dimensions as shown in Figure 6.2. The amount of steel reinforcement around the box is defined by steel areas A_{S1} , A_{S2} , A_{S3} and A_{S4} along with a common cover thickness as shown in Figure 6.3.

So far only the parameters of the box-soil systems and the general dimensions have been discussed, nothing has been said about the finite element mesh itself or the sequence of loading. The example shown in Figure 6.4 will be used to explain the mesh arrangement. All the dimensions and height of soil cover are shown. A trench configuration is used with three zones of soil for the system. The values of R_1 and R_2 give the overall size of the mesh as previously discussed (see

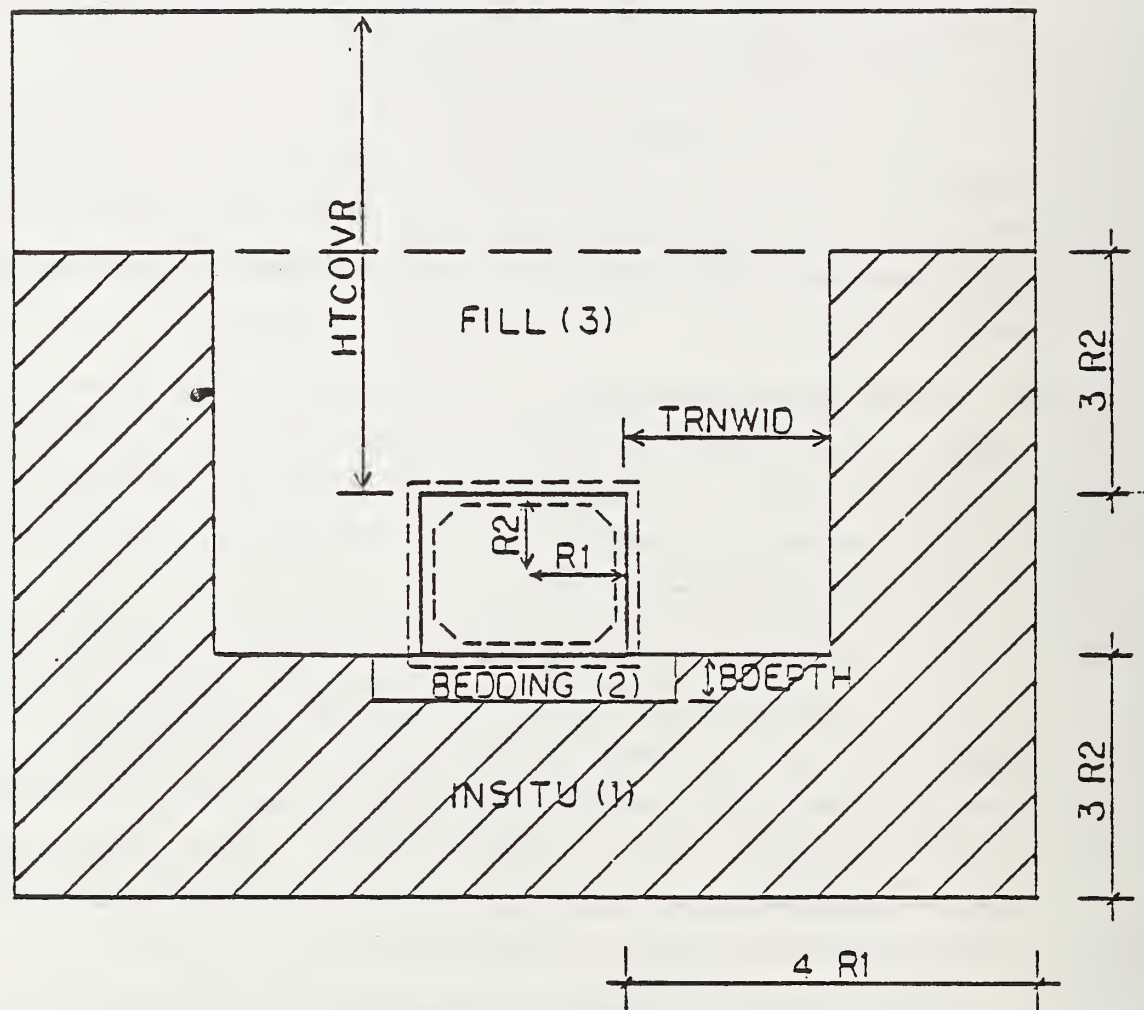


Figure 6.1 - Parameters to Define Buried Concrete Box Culvert.

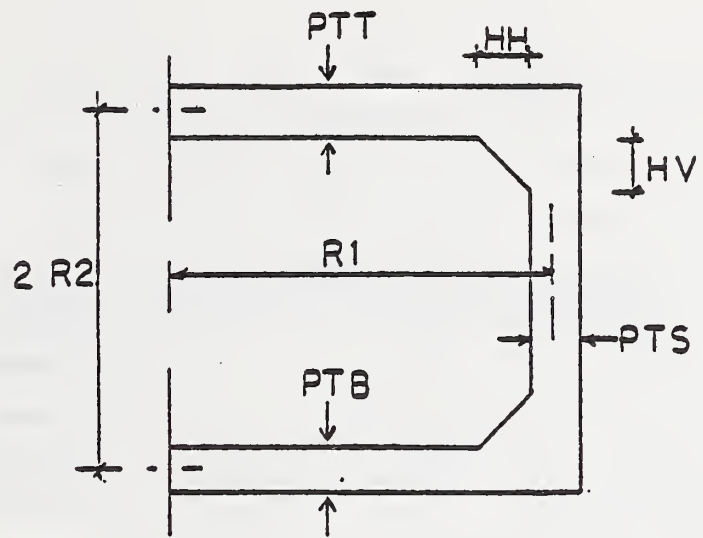


Figure 6.2 - Parameters to Define the Geometry of the Box Culvert.

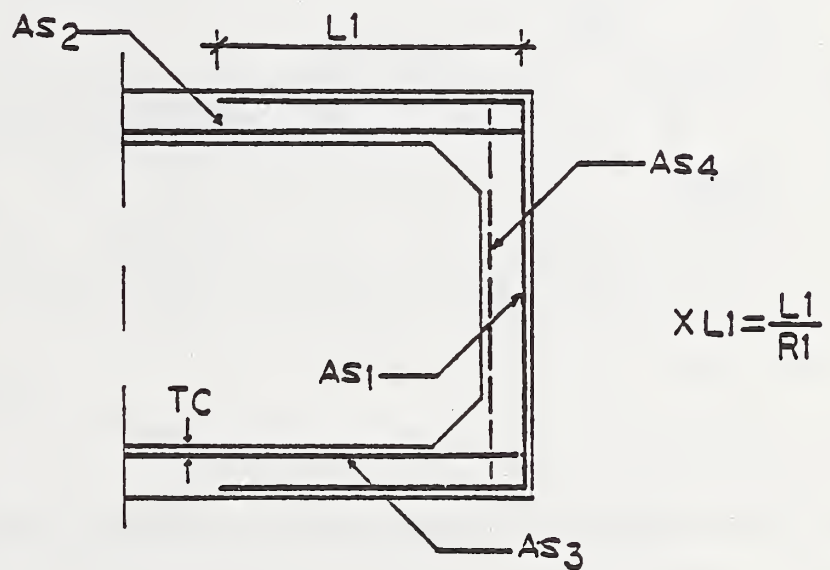


Figure 6.3 - Parameters to Define the Reinforcement of the Box Culvert.

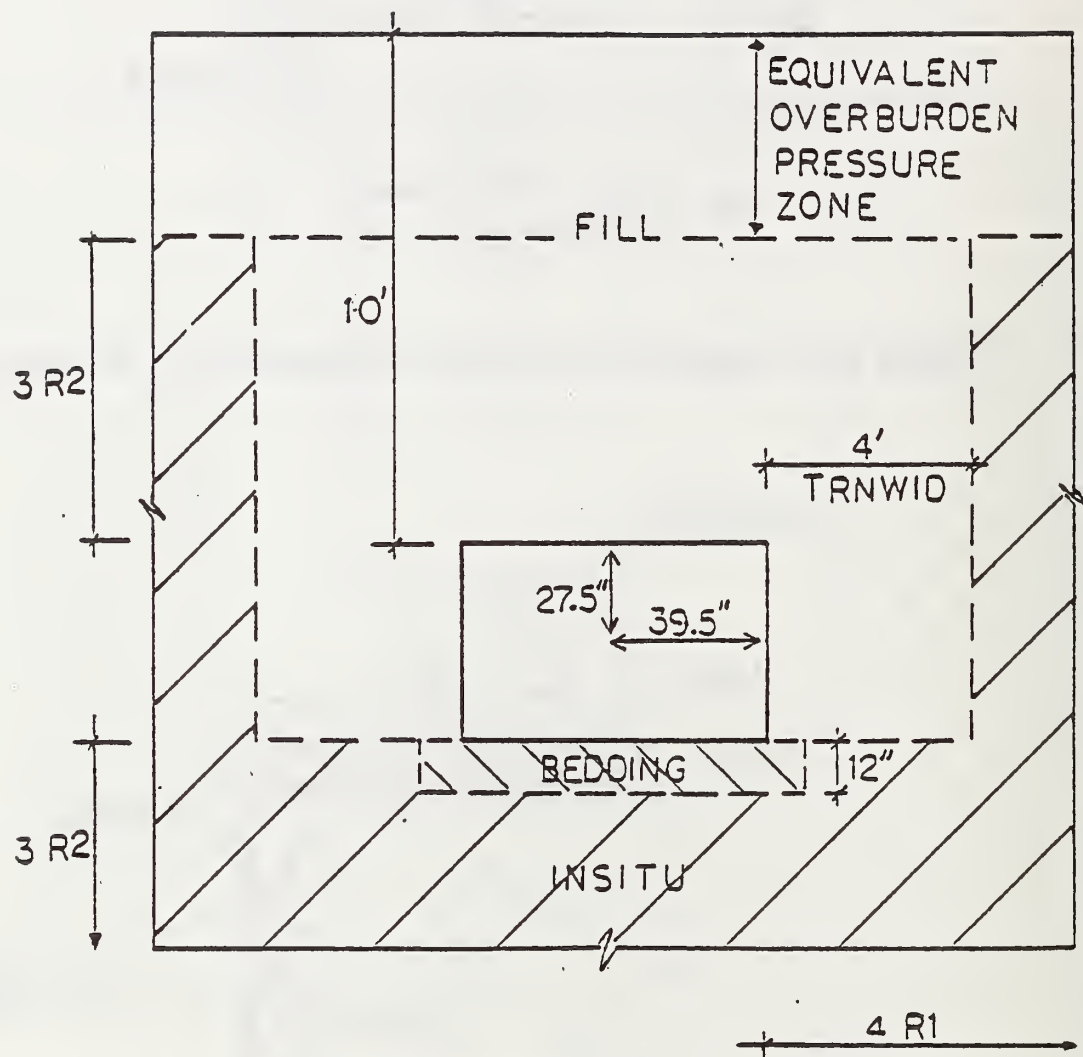


Figure 6.4 - Example of Box Culvert to Define a Mesh.

Figure 6.1). The finite element mesh configuration for the example is shown in Figure 6.5, where by symmetry only half of the box-soil system is modeled. The same figure shows the soil elements and the nodal points of the mesh. The number of layers of soil elements on top of the box can decrease if the height cover of soil is less than $3R_2$, but will never be less than two rows. The soil elements near the box are smaller, so that a more refined mesh around the box can provide a better behavior of the box-soil model where the stress gradients are known to be highest. The soil elements are four node, nonconforming quadrilaterals with excellent performance characteristics (1). The coordinates of the nodes are all related to R_1 and R_2 and, if desired, can be changed using the extended level 2 option (see Appendix B).

The loading sequence, called incremental construction (1,2), simulates the actual installation process of placing soil layers in a series of lifts. Figure 6.6 shows the construction increment numbers of element groups entering sequentially into the system. The initial system (first construction increment) includes all in situ soil, bedding, and the box loaded with its own body weight. Subsequent increments, numbers 2 through 9, are gravity loaded layers of fill soil. For specified heights of soil cover less than $3R_2$, the mesh over the top of the box is assigned proportionally less soil layers. If the height of soil cover is greater than $3R_2$, the load due to the soil over $3R_2$ is applied as equivalent overburden pressure increments. This load sequence is applied after the ninth soil layer using $n-9$ additional load increments, where n is the total number of construction increments specified in the input.

The box-soil mesh described here is generated automatically using the CANBOX subroutine to generate all the necessary data required to define the finite element mesh of the system. CANBOX subroutine parameters, options and mesh size are discussed with more detail in Appendix B.

6.2 ASSUMPTIONS AND LIMITATIONS

When using this automatic mesh generation, there are some assumptions involved that should be remembered.

NODAL NUMBERS

157	158	159	150	151	152	153	154	155	156	157
146	147	148	149	150	151	152	153	154	155	156
135	138	137	138	139	140	141	142	143	144	145
124	125	125	127	129	129	130	131	132	133	134
113	114	115	116	117	119	118	120	121	122	123
102	103	104	105	106	107	108	109	110	111	112
95	96			97		98		99		101
88	89			90		91		92		94
81	82			93		54		85		87
74	75			76		77		78		80
67	68			69		70		71		73
58	57	58	59	60	61	52	53	54	65	66
45	46	47	49	49	50	51	52	53	54	55
34	35	36	37	38	39	40	41	42	43	44
23	24	25	25	27	28	29	30	31	32	33
12	13	14	15	16	17	18	19	20	21	22
1	2	3	4	5	5	7	8	9	10	11

Figure 6.5 - Undeformed Grid with Nodal Points.

INCREMENT NUMBERS

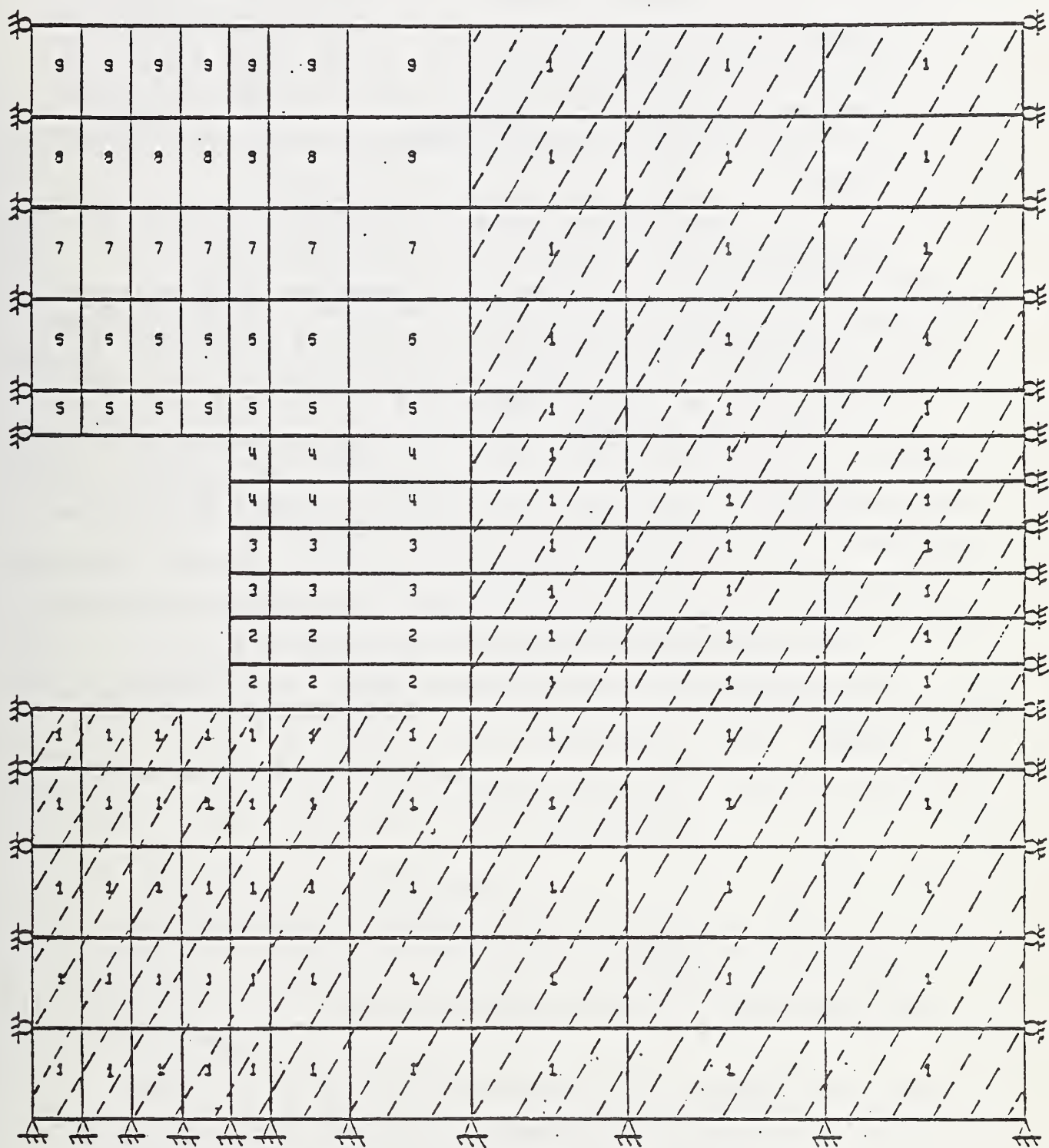


Figure 6.6 - Load Increment Pattern for the Layers of Soil.

a) To simplify the mesh, we are assuming symmetry about the vertical axis so only half of the box-soil system is analyzed. This assumption implies that only symmetric loading can be applied to the box when using concentrated loads on top of the mesh. For most of the cases a symmetric loading arrangement satisfies the loading conditions.

b) Three different zones of soil can be specified within the soil mesh; fill soil, bedding soil, and in situ soil.

c) When a trench condition is specified, the in situ soil forming the trench extrados goes all the way up to the top of the mesh, whereas for the embankment condition, the in situ soil remains at the level of the bottom slab of the box culvert.

d) For the concrete box culvert, the thickness of the wall is constant along a particular side but may vary between sides. However, the concrete cover of the reinforcement is the same for all sides.

Many of the above assumptions can be removed by use of extended level 2 option (see Appendix B) which allows selective modification of the automated mesh discussed above. Virtually all limitations can be removed by use of level 3 option wherein the user defines his own mesh (1,2).

CHAPTER 7

EVALUATION OF CANDE BOX-SOIL SYSTEM

In the previous chapters the reinforced concrete beam-rod element was evaluated with experimental data for out-of-ground structures from which we concluded that the beam-rod element itself performs satisfactorily. In this chapter we examine the performance of the reinforced concrete model as a buried box culvert, where the soil-box structure is modeled with the level 2 box finite element idealization described in the previous chapter. Using this structural system the loads acting on the box are not prespecified, but rather are determined from the finite element solution of the box-soil system. Thus, the performance of the box culvert model depends, in part, on the responses of the soil system.

To evaluate the CANDE box-soil model we first consider a parameter sensitivity study to assess the influence of soil stiffness and installation type on the structural behavior of a typical box culvert. Secondly, we compare the CANDE predictions with full scale field test data (24), providing a direct validation of the box-soil model.

7.1 SENSITIVITY OF SOIL PARAMETERS

In this section the influence of soil parameters on the structural performance of a particular box section is examined. Soil parameters considered include; elastic properties and type of installation (trench or embankment).

The particular box section (hereafter called standard box) used to examine sensitivity of the soil parameters was obtained from the ASTM Standards (21) for box sections under earth dead load conditions. An intermediate size box with medium reinforcement was chosen to be representative for this study. Specifically, the standard box has 8 feet (2.4 m)

span, 6 feet (1.8 m) rise and 8 inches (20.3 cm) wall thicknesses (8*6-8) with a specified design earth cover of 10 feet (3.05 m). The material properties for the standard box culvert are:

f'_c	= 5000 psi (34500 kPa)	(unconfined compressive stress of concrete)
ϵ_t	= 0.0001	(maximum tensile strain of concrete)
f_y	= 65000 psi (448000 kPa)	(yield stress of reinforcement)
γ_c	= 150 pcf (23.5 kN/m ³)	(unit weight of concrete)
E_c	= 4286.8 ksi (29550 MPa)	(concrete Young's modulus)
ν_c	= 0.017	(concrete Poisson's ratio)
E_s	= 29000 ksi (200000 MPa)	(steel Young's modulus)
ν_s	= 0.30	(steel Poisson's ratio)

and

TC	= 1.25 inch (3.18 cm)	(concrete cover)
S_ℓ	= 2.0 inch (5.08 cm)	(spacing longitudinal reinforcement)

The characteristics of the 8*6-8 box cross section are shown in Table 7.1, where the nomenclature is referred to the typical cross section shown in Figure 7.1.

For the purposes of this study, elastic soil properties are assumed in a range covering stiff, medium and soft soils, where their parameters are Young's modulus and Poisson's ratio. Table 7.2 summarizes the properties of the in situ, bedding and fill soil for the soft, medium and stiff soil model. The fill soil weight density is assumed 120 pcf (18.8 kN/m³) for all types so that only stiffness is varied. Bedding and in situ soil zones are not assigned a weight density since they form the initial configuration.

Installation type. For the first study the influence of installation type on the standard box is considered for a trench condition versus

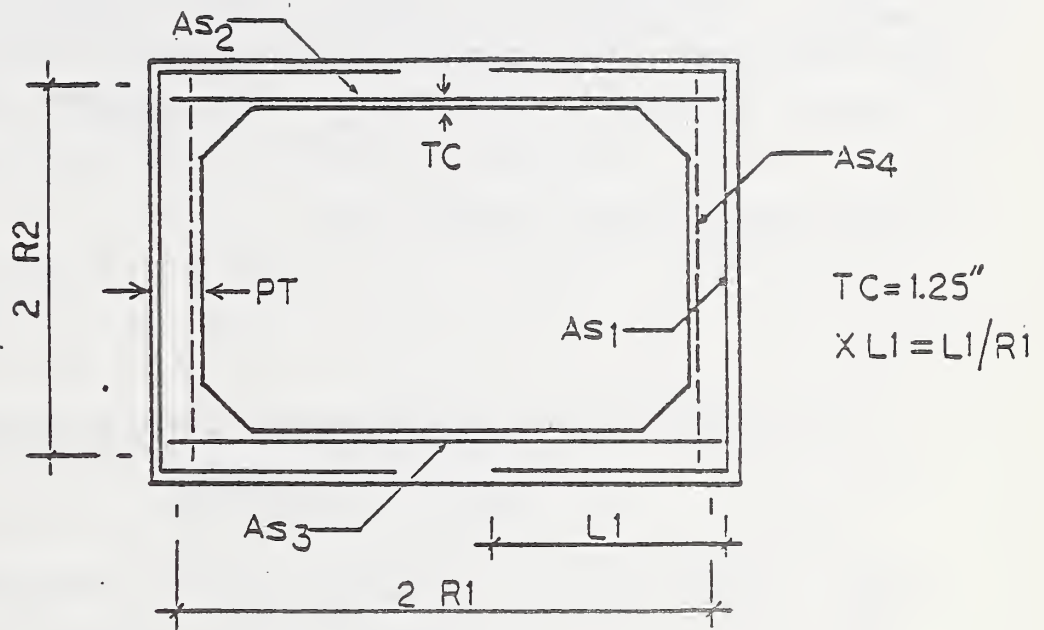


Figure 7.1 - Typical Cross Section and Parameters to Define a Concrete Box Culvert.

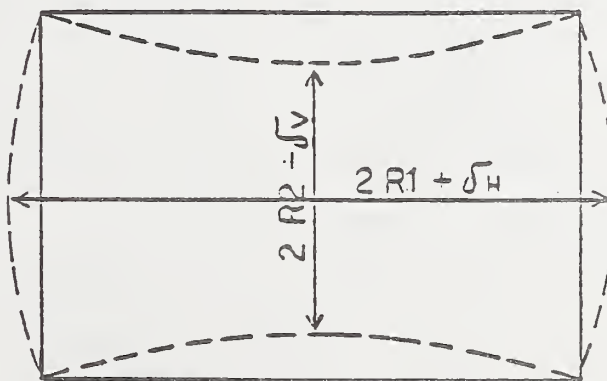


Figure 7.2 - Definition of Vertical Deflection δ_v and Horizontal Deflection δ_H .

TABLE 7.1 Characteristics of Standard Box Culvert
Used in Sensitivity Study

Box (ft*ft-in)	ASTM Design Earth Cover (ft)	A_{s1} (in ² /in)	A_{s2} (in ² /in)	A_{s3} (in ² /in)	A_{s4} (in ² /in)	XL1	PT (in)
8*6-8	10.0 [*]	0.01667	0.02417	0.02583	0.01583	0.50	8.0

^{*}From Table 3 of ASTM Standards (21).

TABLE 7.2 Properties of the Linear Soil Models
Used in CANDE Solution

Type of Soil [*]		Young's Modulus (psi)	Poisson's Ratio
SOFT	Insitu (1)	333	0.33
	Bedding (2)	666	0.33
	Fill (3)	333	0.33
MEDIUM	Insitu (1)	2000	0.33
	Bedding (2)	4000	0.33
	Fill (3)	2000	0.33
STIFF	Insitu (1)	3333	0.33
	Bedding (2)	6666	0.33
	Fill (3)	3333	0.33

^{*}Unit weight is 120pcf for fill soil

$$1 \text{ ft} = 0.3048 \text{ m}$$

$$1 \text{ in} = 2.54 \text{ cm}$$

$$1 \text{ psi} = 6.895 \text{ kPa}$$

$$1 \text{ pcf} = 157.1 \text{ N/m}^3$$

an embankment condition. The trench width beyond the box sides is taken as 2.0 feet (0.61 m) (narrow trench) and soil properties for both installation types are assigned medium stiffness values (see Table 7.2). In both cases, the box was loaded up to 28 feet (8.53 m) of soil cover above the box. Figure 7.2 shows the definition of vertical and horizontal relative displacements used in subsequent discussions.

Figure 7.3 shows the fill height versus vertical displacement history of the box, from where it's observed that the embankment configuration produces slightly greater vertical deflections in the box. Figure 7.4 shows the bending moment diagrams and shear force diagrams in the box at 28 feet of soil cover for both installation types. The embankment condition gives greater bending moments and shear forces acting in the box, which conforms to the greater deflections previously observed.

From this comparison it was concluded that the embankment condition produces slightly greater loading conditions on the box so that in all subsequent studies presented herein only the embankment condition will be considered.

Soil Stiffness. The effect of elastic soil stiffness is investigated using the same standard box (8*6-8) with an embankment soil configuration, where the properties of the soil are varied to idealize a soft, medium and stiff soil as defined in Table 7.2. With these values a range of variation is covered so the effect of each can be observed. Figure 7.5 shows the load versus vertical deflection history of the box for the three classes of soil stiffness, where the box is loaded up to failure for each case. The failures for the box culverts are defined by exceeding ultimate shear capacity (V_u) or by the formation of plastic hinge mechanisms from excessive moments and thrust (M_u). In this study shear failure occurs before plastic hinging in the standard box (8*6-8) for all the three types of soil. Failure occurs first for the soft condition, whereas for the medium and stiff soil conditions failure occurs at a greater height of soil cover. Note that when ultimate bending failure (M_u) occurs, the deflections do not show a flat slope (increase without bounds) as

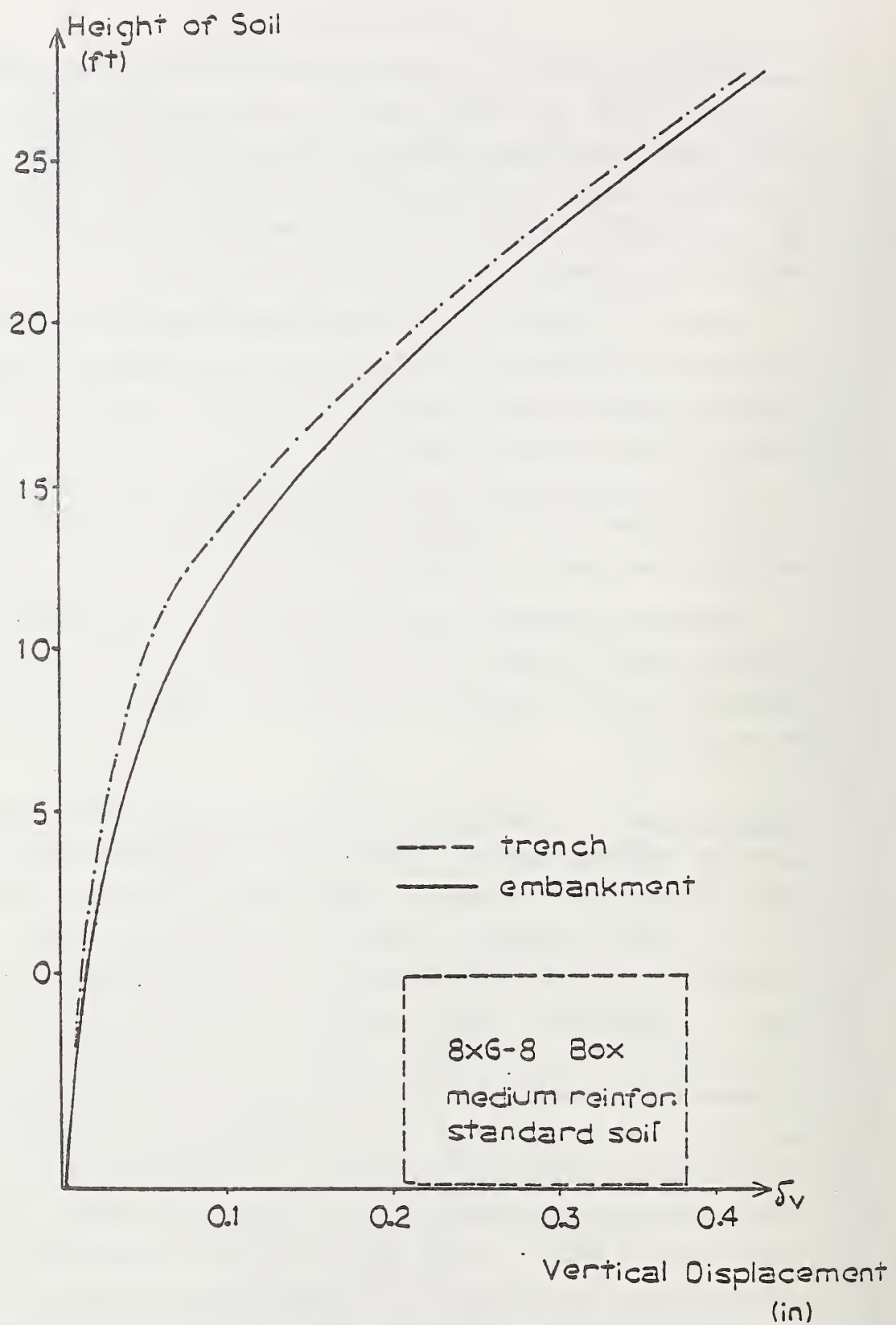
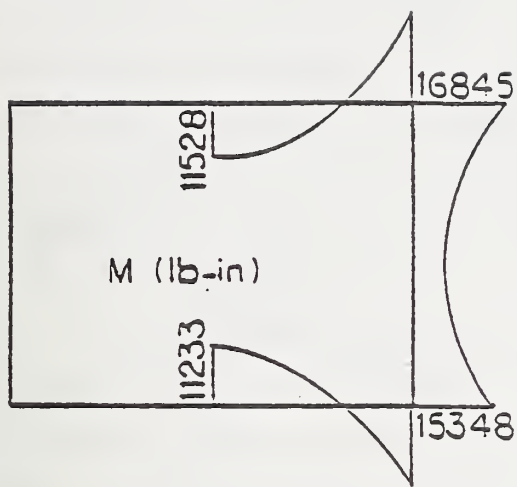
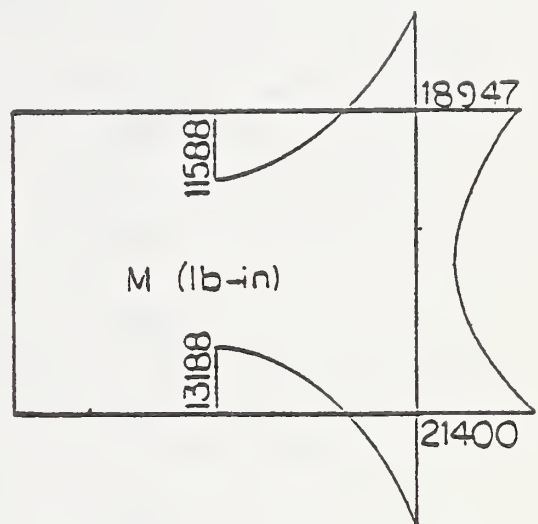


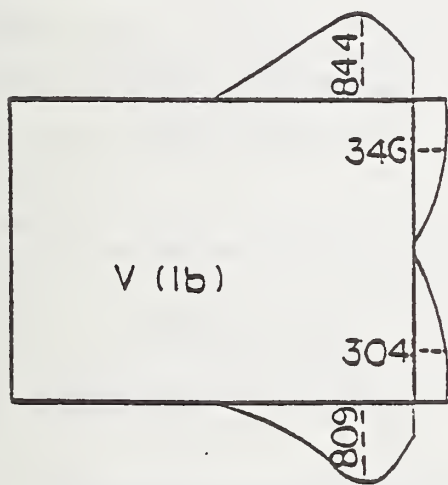
Figure 7.3 - Height of Soil Over the Top of the Box - Vertical Deflection for Trench and Embankment Situations.



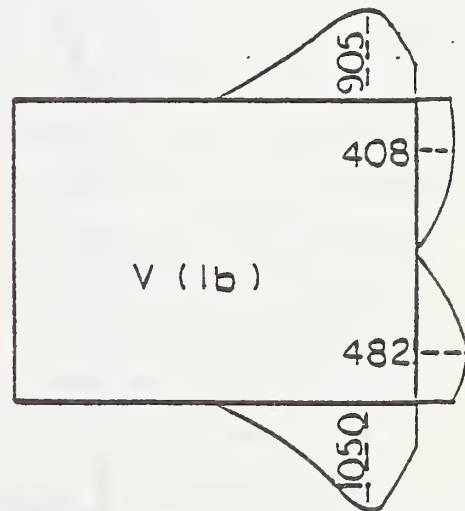
(a) Bending Moment diagram
for trench = 2.0 ft.



(b) Bending Moment diagram
for embankment



(c) Shear Force diagram
for trench = 2.0 ft.



(d) Shear Force diagram
for embankment

Figure 7.4 - Bending Moment Diagrams and Shear Force Diagrams of 8x6 Box Culvert with 28 ft of Soil Cover for Trench = 2.0 ft and Embankment Conditions.

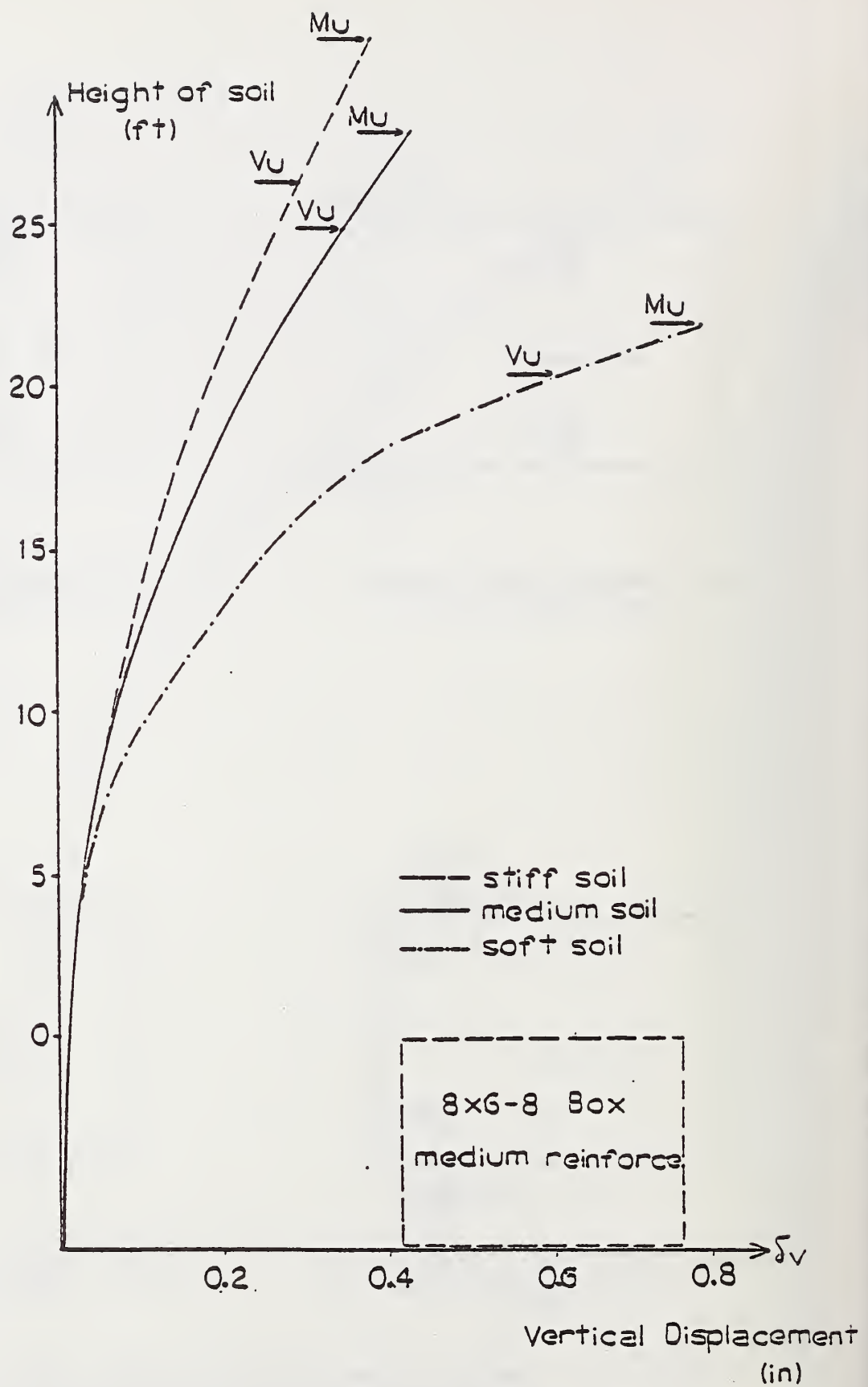


Figure 7.5 - Height of Soil Over the Top of the Box - Vertical Deflection for Three Kinds of Soil.

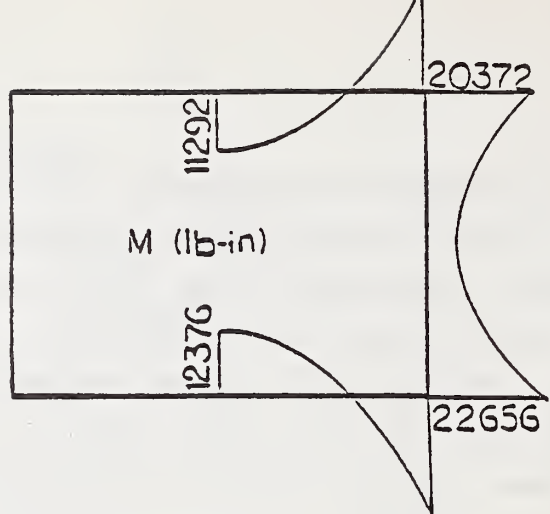
they did in previous studies with out-of-ground culverts with applied loads. This is because the soil stiffness is now controlling deflections at ultimate. Accordingly, the slope of the deflection curves at ultimate is in near proportion to soil stiffness. From Figure 7.5 it is evident that the soft soil condition is restricted to smaller cover heights to reach ultimate than the stiffer soils. Thus, the medium and stiff soil conditions are more favorable for the box behavior.

Figure 7.6 shows the bending moment diagrams for the box at bending failure (presuming stirrups) for the three types of soil conditions. It is observed that even when the failure occurs at different heights of soil cover, the maximum moments are similar as would be expected for ultimate moments. From this comparison it is evident that the type of soil is an important factor for analysis and design of a box culvert.

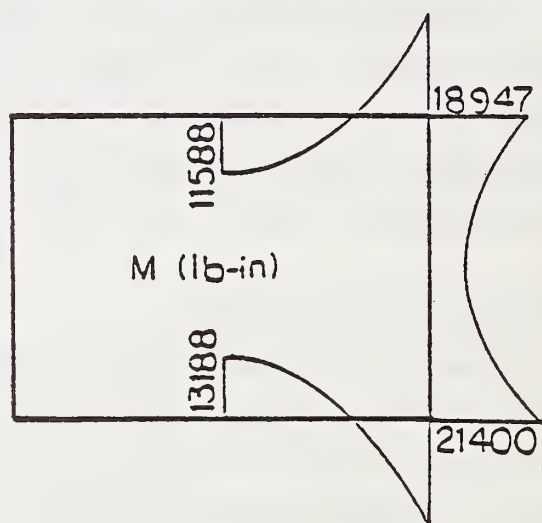
7.2 COMPARISON WITH TEST DATA

To validate the box-soil model, CANDE results are compared with test data from a full scale field installation. Test data on buried box culverts is very limited. However, recent research reports from the Department of Transportation, Lexington, Kentucky (23,24,25) have supplied some test data. From these reports, data was obtained for a box culvert in Clark County, Kentucky, designed as an embankment with a yielding foundation within a bedrock formation (24). Instrumentation on the box included normal pressure gages and a few strain gages on reinforcement steel which were reported not to function properly, thus only normal pressure comparisons are used for this study. The box is identified as Station 123+95 in the report (24) and its cross section as modeled by CANDE is shown in Figure 7.7 along with reinforcement areas.

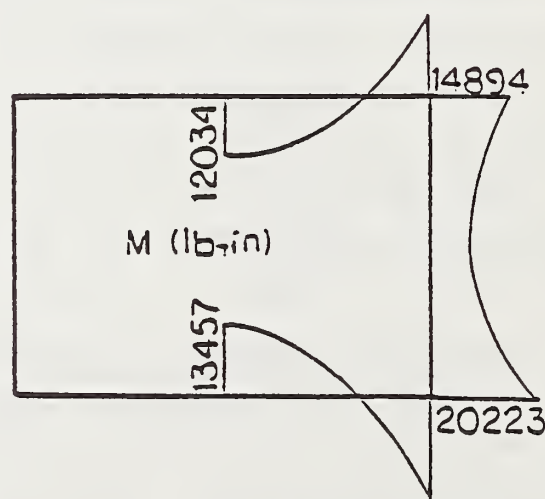
The level 2 box embankment condition is used for the model with three zones of soil that are assumed linear with the properties shown in Table 7.3. The in situ soil is bedrock so a large value is assumed for its modulus of elasticity. Table 7.4 shows the material properties used in CANDE to model the box culvert. The concrete and steel strengths used in CANDE were obtained from data presented in a report (25) and the



(a) Stiff soil and 31 ft of soil cover



(b) Medium soil and 28 ft of soil cover



(c) Soft soil and 22 ft of soil cover

Figure 7.6 - Bending Moment Diagram of 8x6 Box Culvert at Bending Failure Using Three Different Kinds of Soil.

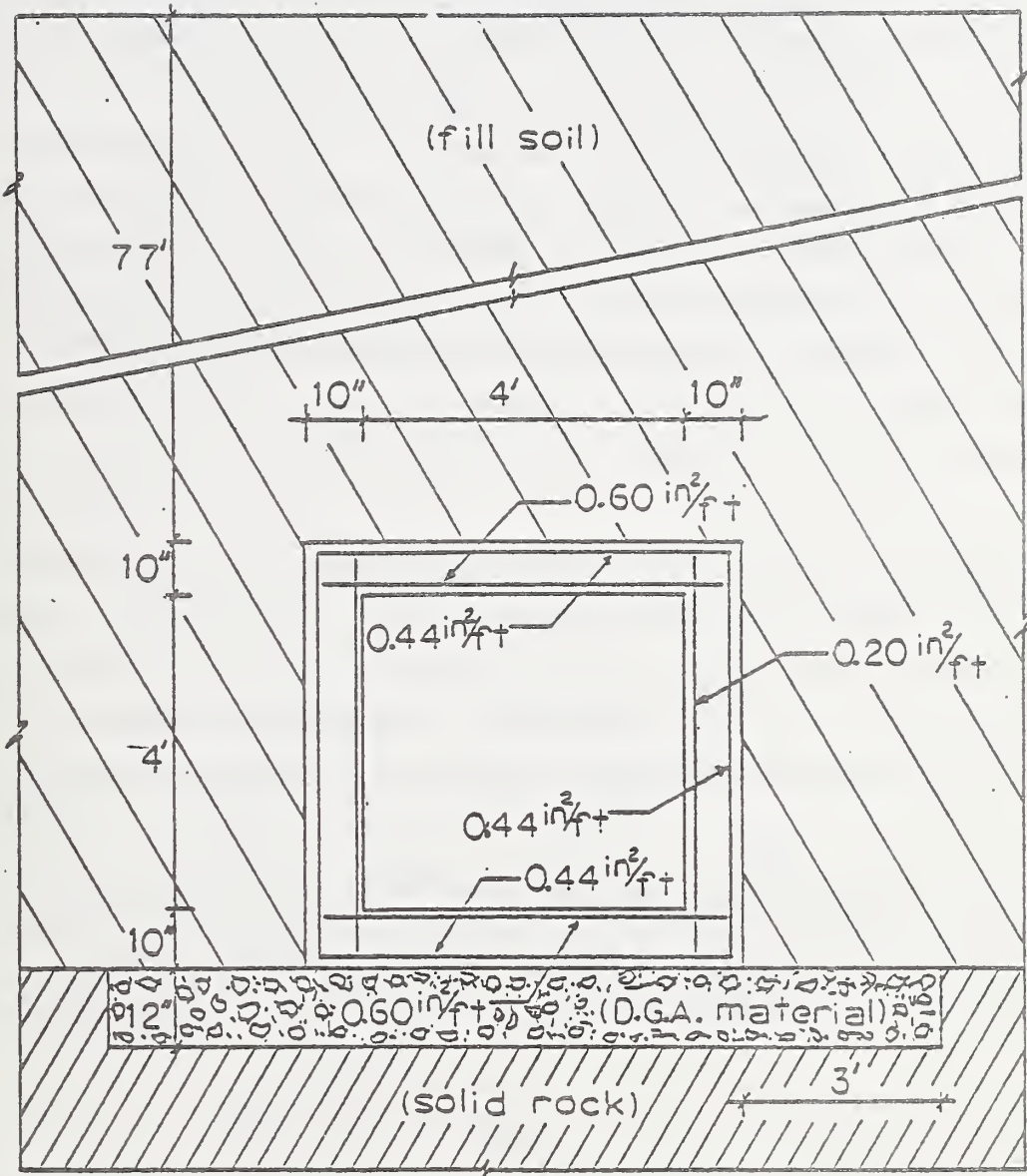


Figure 7.7 Cross Section of Buried Test Box Culvert (Station 123+95).

TABLE 7.3 - Linear Soil Properties for Test

Box Culverts

SOIL	Young's Modulus (psi)	Poisson's Ratio
INSITU (rock)	100000	0.25
BEDDING	4000	0.25
FILL	2000	0.25

Note: soil weight density of 138pcf for fill soil

TABLE 7.4 - Box Culvert Properties

BOX	f'_c (psi)	γ_c (pcf)	f_y (psi)	ϵ_t
Station 123+95	4500	150	60000	.0001

$$1 \text{ psi} = 6.895 \text{ kPa}$$

$$1 \text{ pcf} = 157.1 \text{ N/m}^3$$

other properties are assigned standard values (Tables 3.1 and 3.2).

The box is loaded up to 77 feet (23.5 m) of soil cover using small load increments thereby obtaining a history of the box-soil system performance. However, the only information that can be used for comparison is the pressure distribution on the box which was experimentally measured at two heights of fill soil, 21.6 feet (6.58 m) and 77 feet (23.5 m).

To measure the pressure around the box, eight Carlson earth pressure cells were installed, two on each side of the box. Figure 7.8 shows the CANDE pressure distribution around the box at the two fill heights of soil, along with the measured test data. CANDE predictions of the pressure is very close to the measured value for the top and bottom slabs. The measured pressure on the sidewalls is different for the right wall and the left wall, and CANDE prediction is closer to the values measured for the right wall.

From CANDE, some interesting observations are, when loaded up to the maximum 77 feet (23.5 m) of soil cover, the bottom corner steel started to yield for the last load increment. Also, the 0.01 inch (0.0254 cm) crack first developed with 60 feet (18.3 m) of soil cover. These observations suggest an economical design was achieved with no conservatism.

After this last study it can be said that the reinforced concrete beam element to model the box culverts and the box-soil system appear to give reasonably good predictions of the behavior and performance of buried box culverts.

----- fill height 21.6' } CANDE-normal pressure
 _____ fill height 77' }
 • instant value ($H=21.6'$) }
 • lapsed time value ($H=77'$) } test-normal pressure

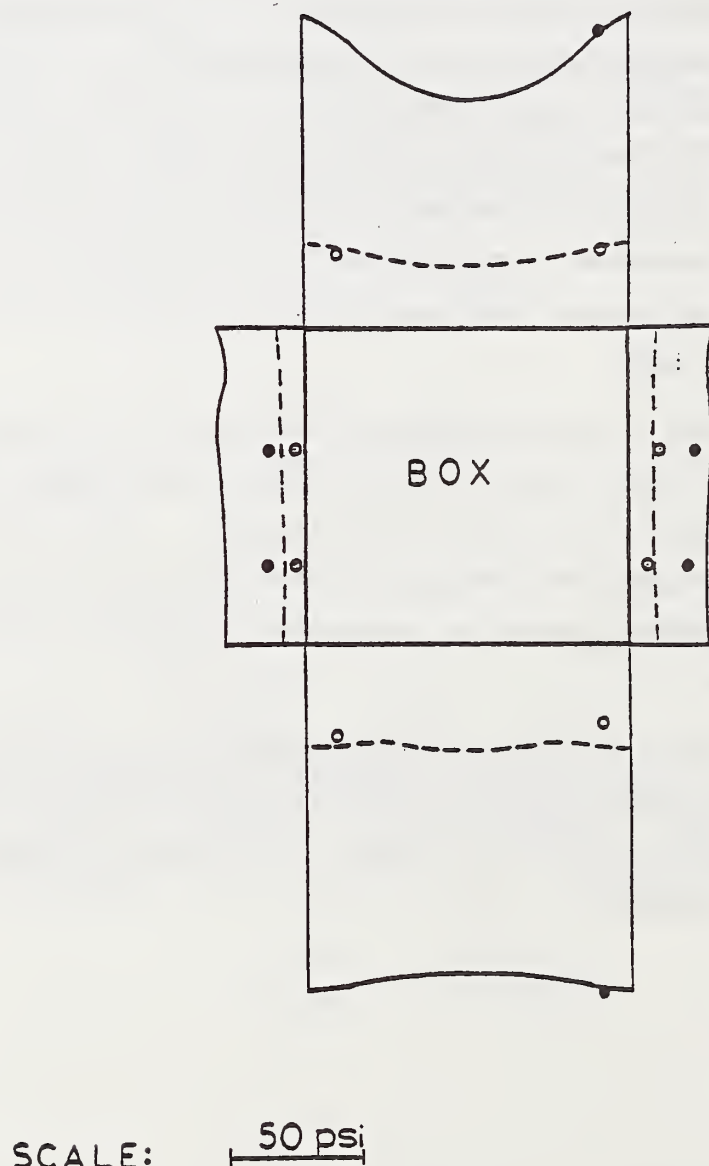


Figure 7.8 - Comparison of Test Data with CANDE Prediction of Pressure Over the Box Culvert.

CHAPTER 8

EVALUATION OF ASTM C-789 DESIGN TABLES WITH CANDE

In the previous chapter, CANDE's reinforced concrete beam-rod element has been developed and compared with experimental data for both in ground and out-of-ground culverts. Overall, very good correlation was observed for all aspects of structural performance, including; load-deformation curves, cracking loads, ultimate loads, and soil pressures, thereby lending a measure of confidence and validity to the CANDE model.

In this chapter the objective is to cross-evaluate CANDE with ASTM-C789 design tables for buried box culverts (21). As discussed in Chapter 2, the ASTM design tables are based on an elastic method of standard analysis together with the ultimate method of reinforced concrete design (12). However, the magnitude and distribution of loads acting on the box are assumed, as opposed to determining loads with soil-structure interaction models like CANDE. In Chapter 5 it was shown that CANDE predictions for out-of-ground box culverts loaded in bearing correlated very closely with the analytical predictions subsequently used to develop the ASTM design tables (14). Thus for buried boxes, it may be presumed that comparisons between CANDE and ASTM design tables will be influenced primarily by the modeling of soil and soil-structure interaction as opposed to the modeling of the box.

The comparisons reported herein are divided into two main sections; (1) dead loading due to soil weight only (ASTM C789, Table 3), and (2) dead loading due to soil weight plus HS20 live loading conditions (ASTM C789, Table 1).

8.1 BOX SECTION STUDIES FOR DEAD LOAD

Table 3 of ASTM C789 lists the design earth cover (allowable fill height) for each standard box size as a function of the steel reinforce-

ment areas A_{S1} , A_{S2} , A_{S3} , and A_{S4} . For this study, a subset of these standard boxes were selected covering the typical range of box spans, rise/span ratios and amounts of steel reinforcement. These subsets are shown in Tables 8.1a and 8.1b.

Table 8.1a represents the typical range of box spans; large (10 foot span), intermediate (8 foot span) and small (4 foot span) where the span/rise ratio is an intermediate range 1.3 to 1.7. For each box, three levels of steel area (low, medium, and high) are listed and correspond to increased levels of design earth cover. In a similar manner, Table 8.1b identifies three standard boxes with span/rise ratios ranging from 1.0 to 2.0 and a common box span of 8 feet (2.44 m). Taken together, Tables 8.1a and 8.1b cover the typical range of the standard ASTM box designs. Note that the intermediate box 8*6-8 (span*rise-inches wall thickness) is common to both tables. Thus, there is a total of 5 different box sizes with three levels of reinforcement, providing 15 different box sections for comparative analysis.

Comparison Objectives and CANDE Model. For each of the ASTM box sections defined above, CANDE predictions are compared with ASTM assumptions for (a) soil load distribution on box at design earth cover, and (b) soil load distribution on box at failure cover heights. In addition, the consistency of ASTM designs are evaluated with CANDE with regard to 0.01 inch cracking load and failure load.

In order to make these comparisons, the parameters of the CANDE model are defined as consistently as possible with ASTM assumptions. The concrete properties assumed for each box are:

f'_c = 5000 psi (345000 kPa)	compressive strength
ϵ_t = 0.0001 in/in	cracking tensile strain
γ_c = 150 lbs/ft ³ (23.5 kN/m ³)	weight density

The remaining concrete parameters are taken as the standard values in Table 3.1.

TABLE 8.1 Reinforcement of Concrete Box Culverts Under Earth
Dead Load Conditions (ASTM Table 3) Used for Comparison

(a) Span/Rise Approximately 1.5, Span = large, intermediate and small

BOX	ASTM Design Earth Cover (ft)	Reinf.	A_{s1} (in ² /in)	A_{s2} (in ² /in)	A_{s3} (in ² /in)	A_{s4} (in ² /in)
10*6-10	6	Low	.02000	.02000	.02000	.02000
	10	Medium	.02333	.02833	.03000	.02000
	14	High	.03250	.03833	.04000	.02000
8*6-8	6	Low	.01583	.01583	.01667	.01583
	10	Medium	.01667	.02417	.02583	.01583
	14	High	.02333	.03333	.03500	.01583
4*3-5	10	Low	.01000	.01000	.01083	.01000
	14	Medium	.01000	.01417	.01000	.01000
	18	High	.01167	.01833	.01833	.01000

(b) Intermediate Span, Span/Rise from 1.0 to 2.0

BOX	ASTM Design Earth Cover (ft)	Reinf.	A_{s1} (in ² /in)	A_{s2} (in ² /in)	A_{s3} (in ² /in)	A_{s4} (in ² /in)
8*4-8	6	Low	.01583	.01583	.01583	.01583
	10	Medium	.02000	.02166	.02250	.01583
	14	High	.02833	.02917	.03000	.01583
8*6-8	6	Low	.01583	.01583	.01667	.01583
	10	Medium	.01667	.02417	.02583	.01583
	14	High	.02333	.03333	.03500	.01583
8*8-8	5	Low	.01583	.01583	.01667	.01583
	8	Medium	.01583	.02167	.02333	.01583
	12	High	.01750	.03083	.03333	.01583

1 ft = 0.3048 m

1 in = 2.54 cm

Assumed steel properties are:

f_y = 65000 psi (448000 kPa) yield stress
 E_s = 29000 ksi (200000 MPa) Young's modulus

and

T_c = 1.25 in (3.18 cm) concrete cover to steel center
 s_ℓ = 2.00 in (5.08 cm) longitudinal spacing for crack prediction

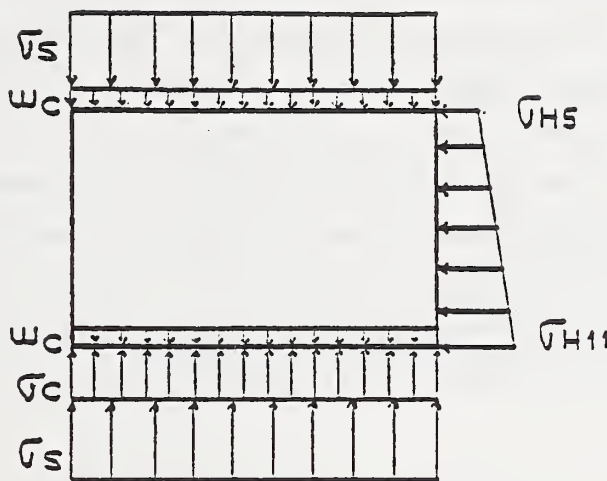
An example of the CANDE input parameters for 8x6 box is given in Appendix C.

Since the ASTM approach does not consider soil stiffness, the CANDE solutions use two soil conditions, soft and stiff, for the analysis of each box, thereby bracketing the practical range of soil stiffness. Soil moduli values for soft and stiff conditions are given in previous chapter in Table 7.2. For both conditions, soil density is taken as 120pcf (18.8 kN/m^3).

All CANDE solutions are obtained using the new level 2 box generation scheme for an embankment installation. Nine construction increments of soil are used to bring the soil height up to the ASTM design cover height to facilitate the comparison of loading distributions assumed by ASTM with those predicted by CANDE. Thereafter, additional soil layers are added until flexural failure is observed. During this loading sequence, the cover height causing initial 0.01 inch cracking is determined along with the cover height causing shear failure, providing shear failure occurs before flexural failure.

Load Distribution Comparisons at Design Cover Height. The ASTM assumed load pattern due to soil pressure and box weight are shown in Figure 8.1. Vertical soil pressures are assumed uniform and proportional to cover height. Lateral pressures are assumed to vary linearly, dependent on the coefficient of lateral earth pressure generally assumed to be 0.5. No shear traction on the box sides is assumed in the ASTM pattern.

Figure 8.2 illustrates the nature of a typical load distribution predicted by CANDE resulting from soil loading and box weight. Vertical soil pressures are not uniform, lower in the middle where bending deformation is greatest. Lateral pressure along the box increases with depth



$$\sigma_s = \gamma_s \times H$$

$$\sigma_c = W/(S+2t)$$

$$w_c = \gamma_c \times t$$

$$\sigma_{hs} = 0.5(\sigma_s)$$

$$\sigma_{hi} = \sigma_{hs} + 0.5\gamma_s(R+t)$$

W = Total Weight of Box

S = Span of Box

R = Rise of Box

H = Height of Soil from Top of Box

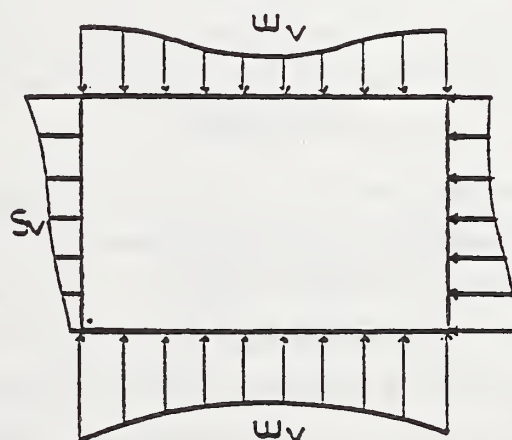
γ_c = Unit Weight of Concrete

γ_s = Unit Weight of Soil

t = Thickness of Box

α = Coefficient for Lateral Pressure

Figure 8.1 Loading of a Box Culvert Due to Soil According to ASTM Norms.



w_v = Normal Load in the Vertical Direction

w_h = Normal Load in the Horizontal Direction

s_v = Shear Load Over the Walls

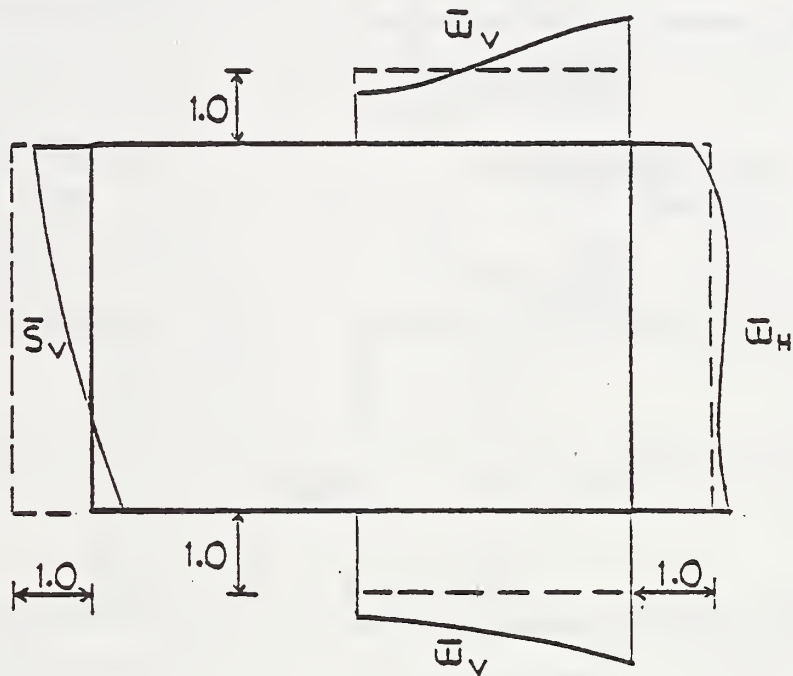
Figure 8.2 Typical Load Pattern Due to Soil Load Obtained from CANDE.

but not linearly. This applies to both sides of the box but is only illustrated on the right side in Figure 8.2. In addition to the normal pressures, significant shear traction develops over the side walls acting mostly downward. This is illustrated on the left side of the box. Shear traction on the top and bottom slabs is also present but is not significant and is not shown. Shear traction on the side walls can amount to 50% of the net downward force which must be equilibrated by the pressure along the bottom slab. This is an effect not considered in the ASTM load pattern and should be kept in mind in the subsequent comparisons.

In order to compare ASTM and CANDE load distributions at design earth cover, normalized plots are constructed by dividing the CANDE predictions by the ASTM assumption at each point around the box. This is clarified in Figure 8.3 where the dashed lines represent normalized values of unity, and the solid lines represent the ratio of CANDE prediction to ASTM assumption. Shear traction is arbitrarily normalized by dividing the CANDE prediction for shear traction by the ASTM assumption for normal pressure on the top slab. Due to symmetry, both sides on the box experience identical loading distributions. Normalized plots for lateral soil pressure are shown on the right side of the box, while normalized plots for shear traction are shown on the left.

With the above understanding, Figures 8.4 through 8.8 show the normalized load distributions for each box in Table 8.1a,b. Each figure shows six normalized plots per box representing the three levels of reinforcement and the two soil conditions.

In general, CANDE predictions for the normal pressure on the top and bottom slabs are not uniform, increasing from the center of the slab to the corner of the box. Normal pressure at the center of the top slab are very close to ASTM assumption and increases to a range of 20% to 30% greater than the ASTM assumption near the corner, depending on the soil conditions and level of reinforcement. CANDE predictions for the normal pressure on the bottom slab is significantly higher for soft soil than stiff soil. This is because soft soil generates greater shear

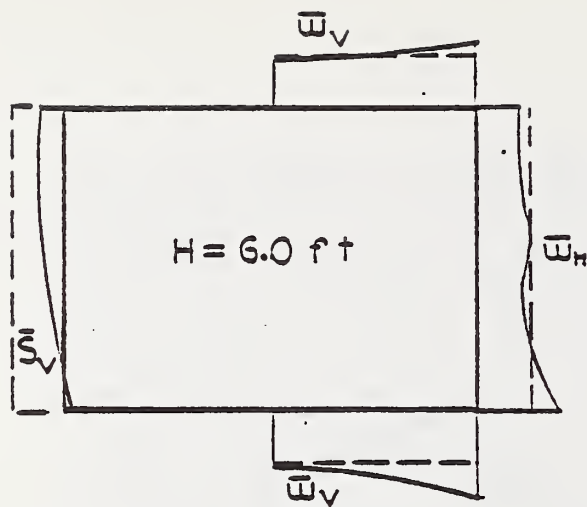


$$\bar{W}_v = w_v / (\bar{v}_s + w_c)$$

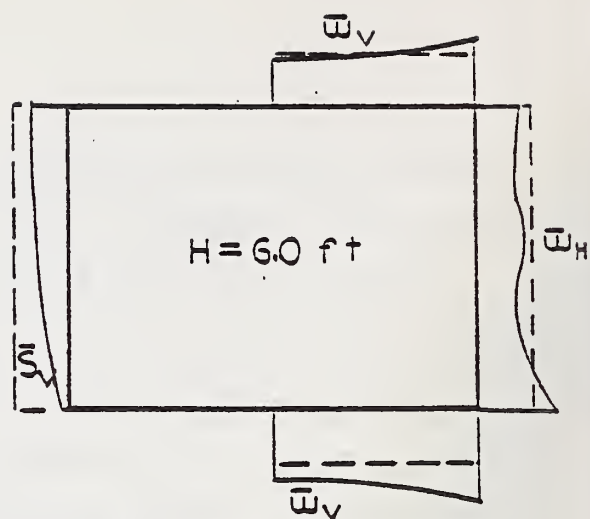
$$\bar{W}_H = w_H / \bar{v}_H$$

$$\bar{S}_v = s_v / \bar{v}_s$$

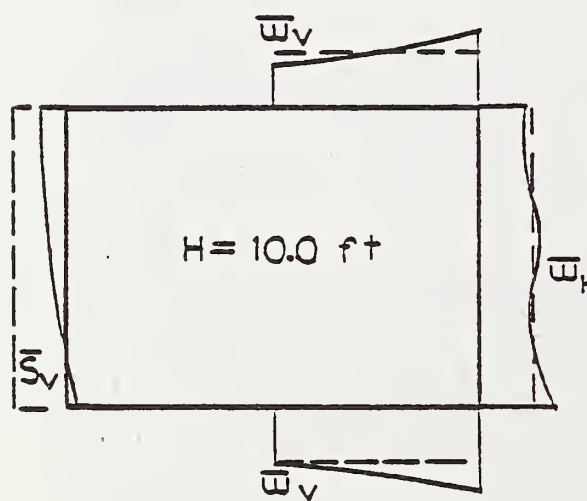
Figure 8.3 - Explanation of the Plots for Normalized Normal Pressure and Shear Forces Acting on the Box (CANDE Prediction/ASTM Assumption).



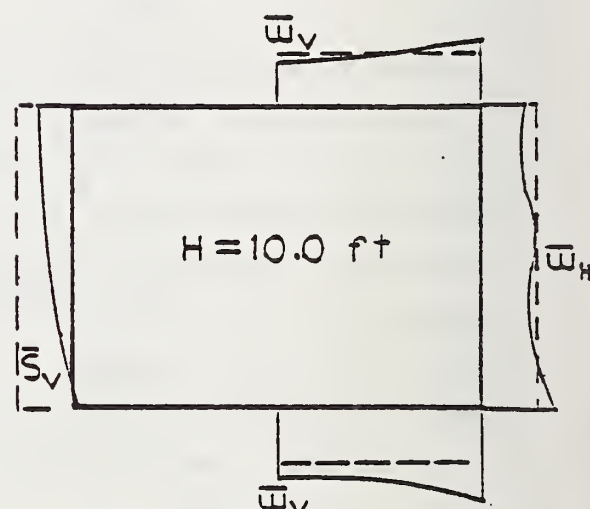
(a) Low reinforced and stiff soil



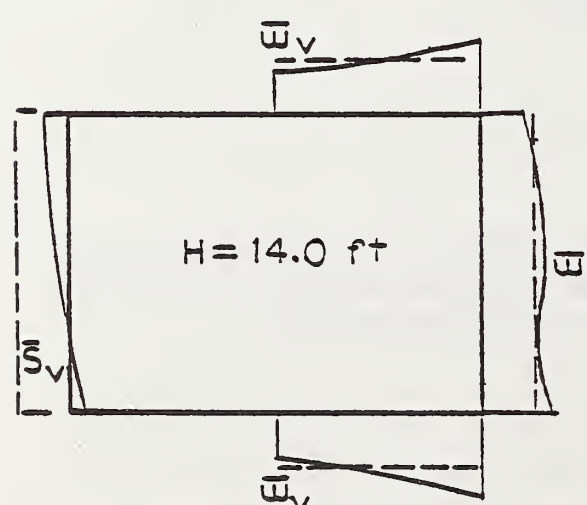
(b) Low reinforced and soft soil



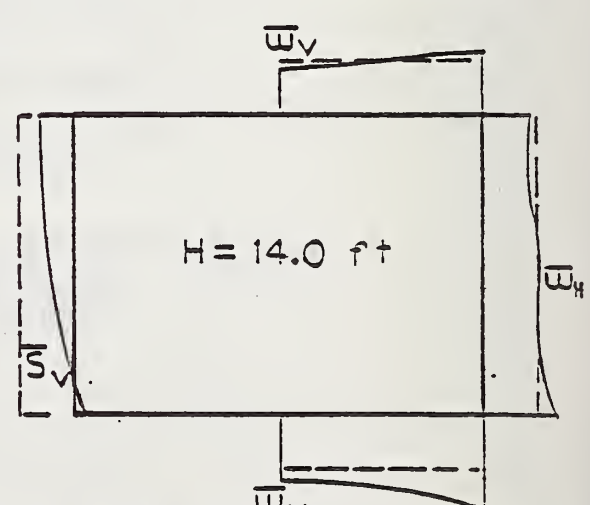
(c) Medium reinforced and stiff soil



(d) Medium reinforced and soft soil

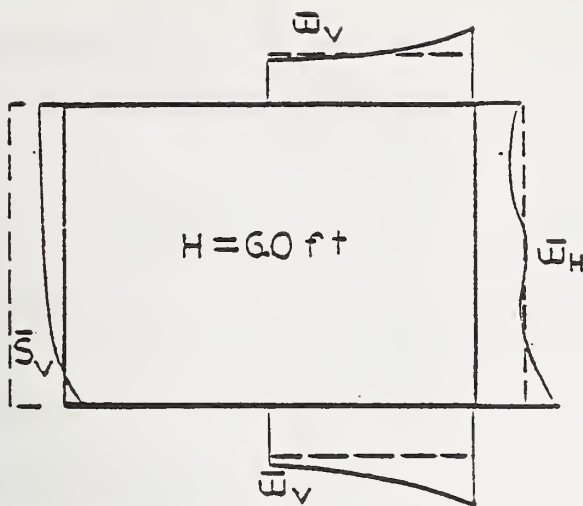


(e) High reinforced and stiff soil

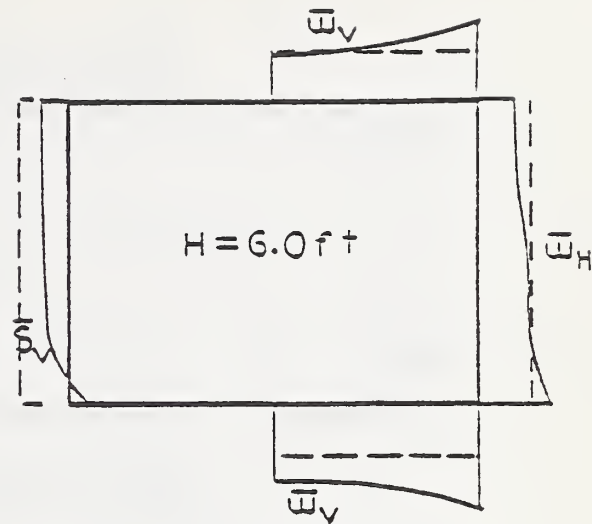


(f) High reinforced and soft soil

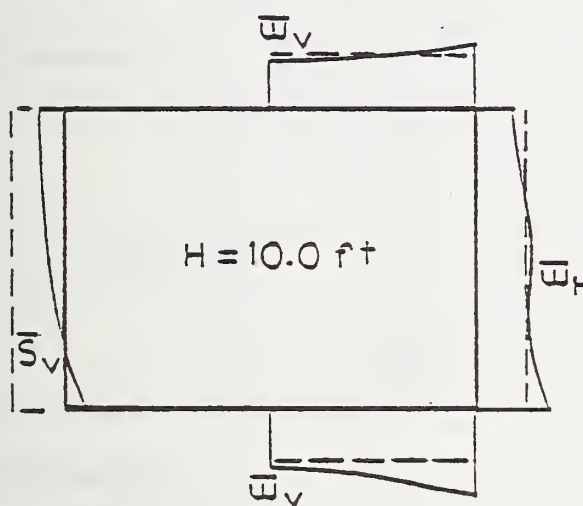
Figure 8.4 - Normalized Plots for Normal Pressure and Shear Acting on a 10x6 Box \dagger ASTM Height of Soil



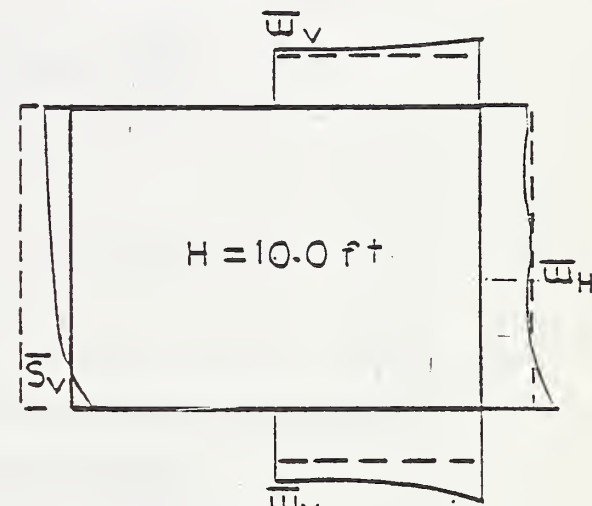
(a) Low reinforced and stiff soil



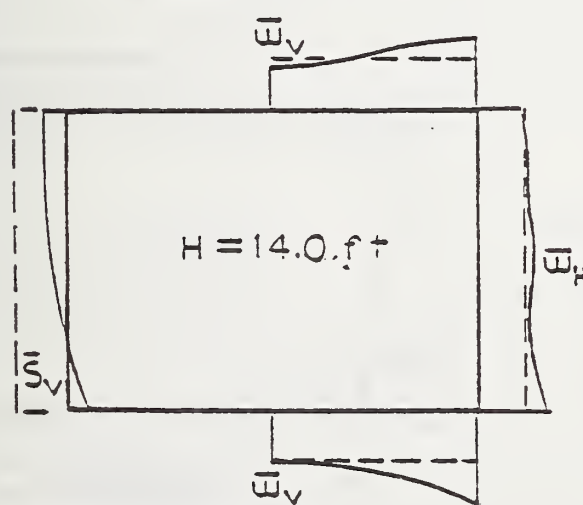
(b) Low reinforced and soft soil



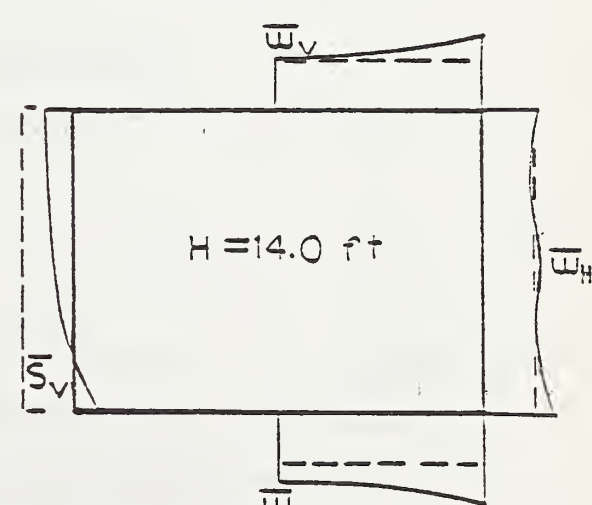
(c) Medium reinforced and stiff soil



(d) Medium reinforced and soft soil

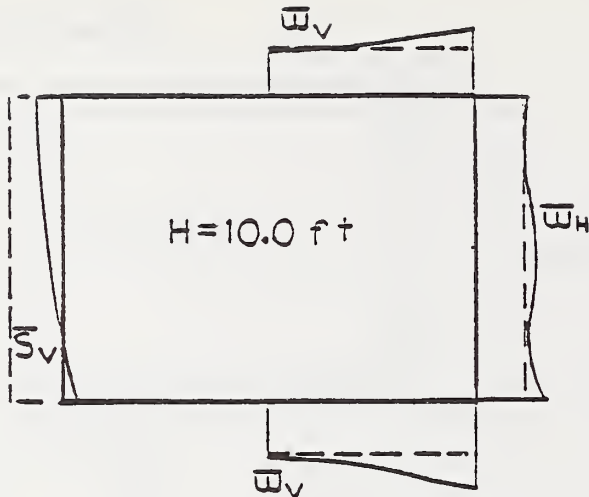


(e) High reinforced and stiff soil

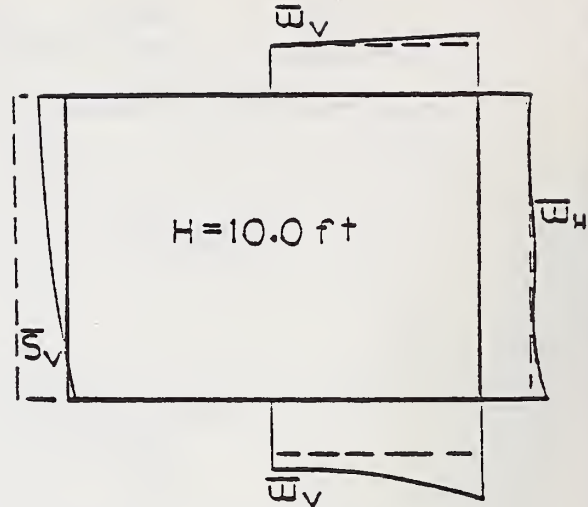


(f) High reinforced and soft soil

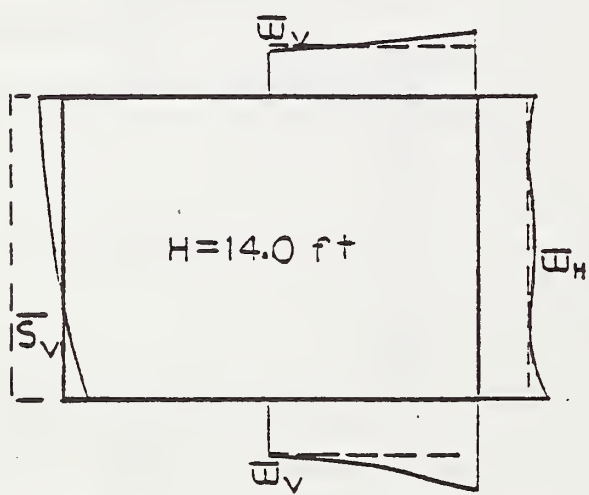
Figure 8.5 - Normalized Plots for Normal Pressure and Shear Acting on a 8x6 Box at ASTM Height of Soil.



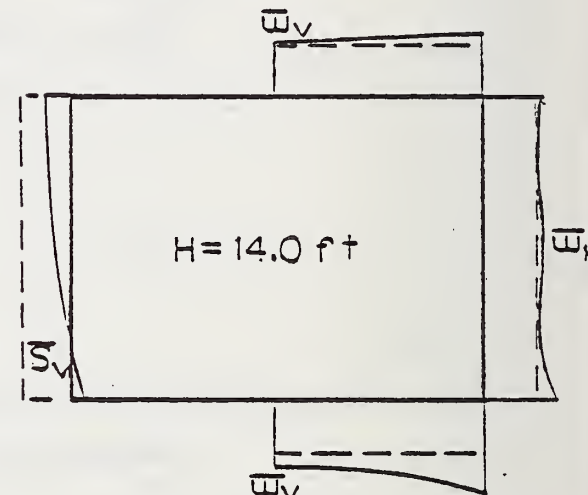
(a) Low reinforced and stiff soil



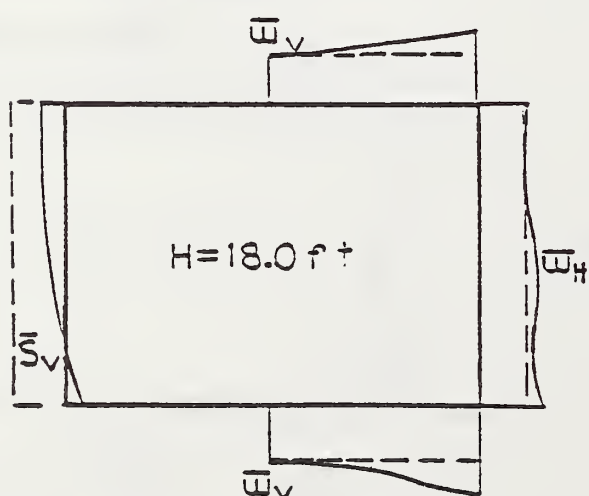
(b) Low reinforced and soft soil



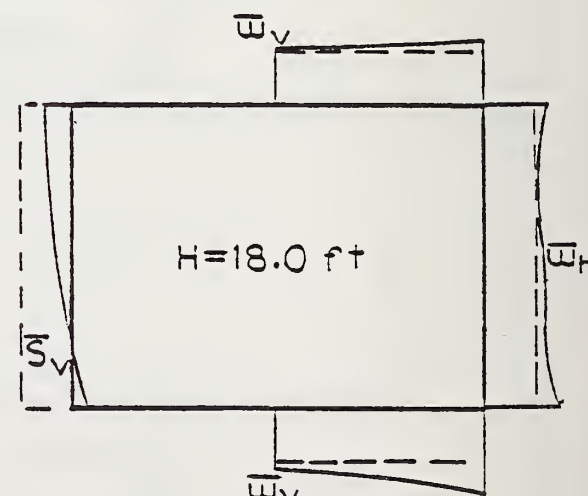
(c) Medium reinforced and stiff soil



(d) Medium reinforced and soft soil

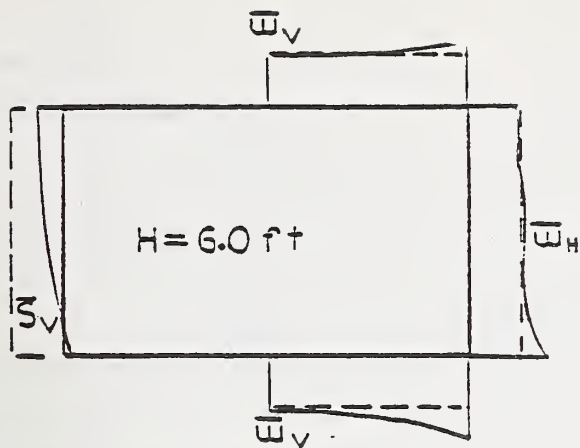


(e) High reinforced and stiff soil

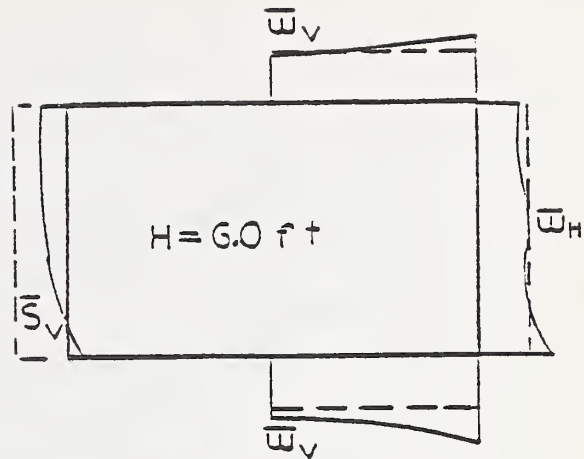


(f) High reinforced and soft soil

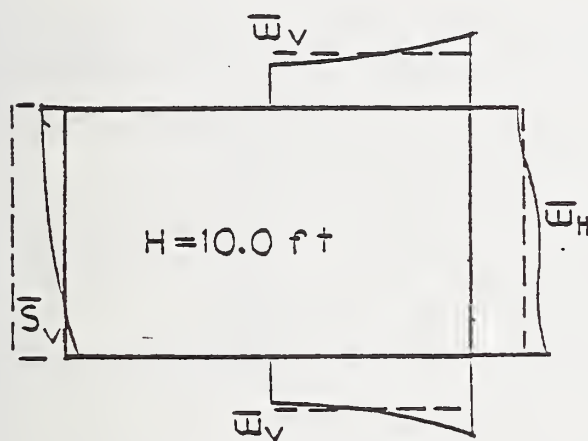
Figure 8.6 - Normalized Plots for Normal Pressure and Shear Acting on a 4x3 Box at ASTM Height of Soil.



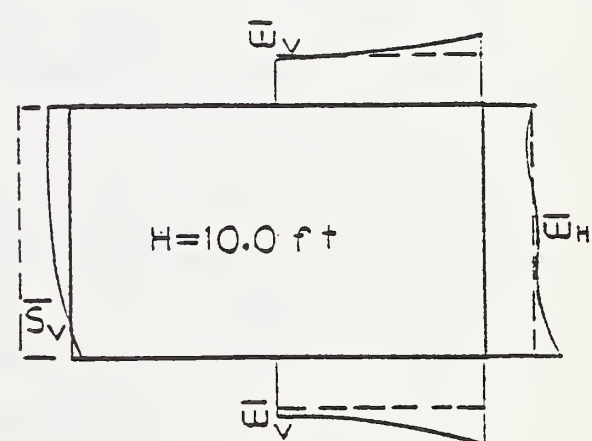
(a) Low reinforced and stiff soil



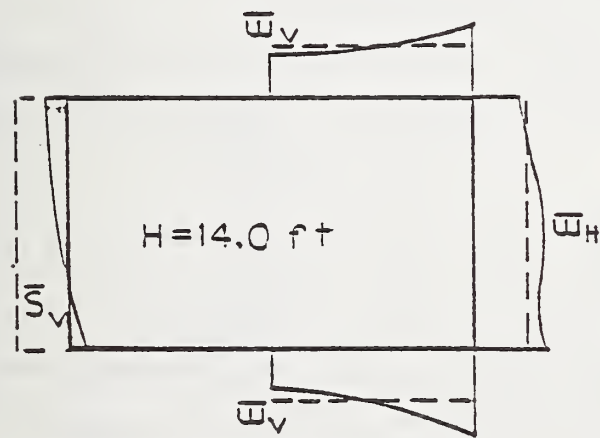
(b) Low reinforced and soft soil



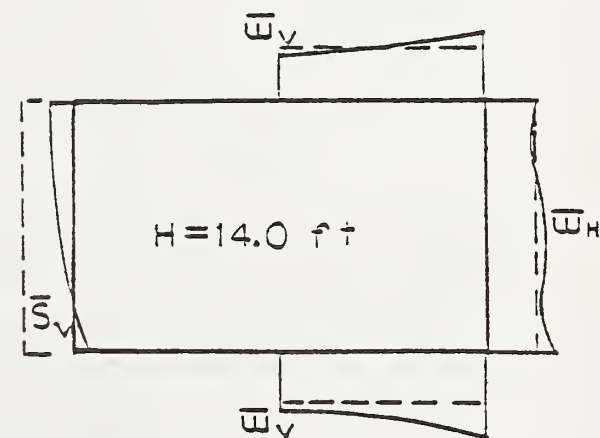
(c) Medium reinforced and stiff soil



(d) Medium reinforced and soft soil

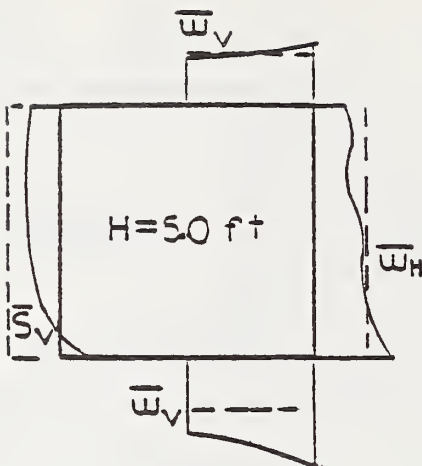


(e) High reinforced and stiff soil

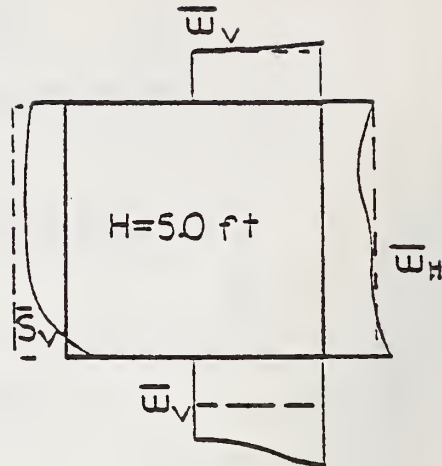


(f) High reinforced and soft soil

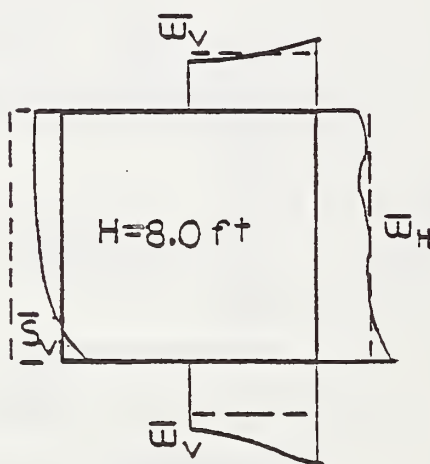
Figure 8.7 - Normalized Plots for Normal Pressure and Shear Acting on a 8x4 Box at ASTM Height of Soil.



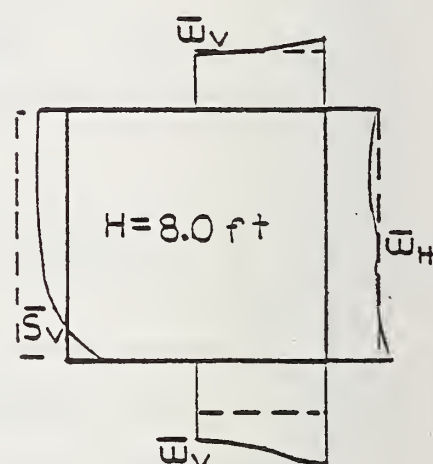
(a) Low reinforced and stiff soil



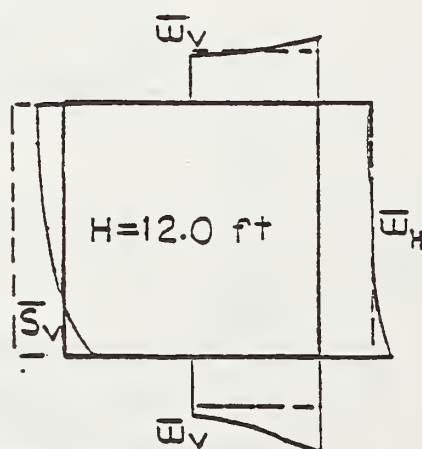
(b) Low reinforced and soft soil



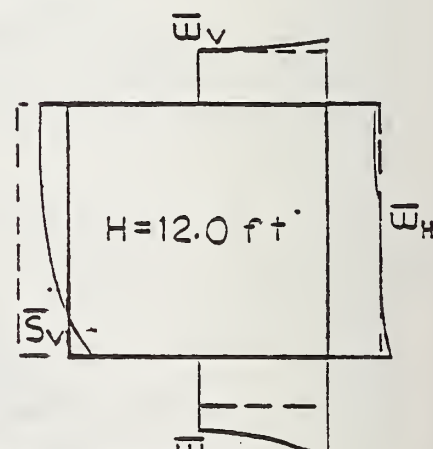
(c) Medium reinforced and stiff soil



(d) Medium reinforced and soft soil



(e) High reinforced and stiff soil



(f) High reinforced and soft soil

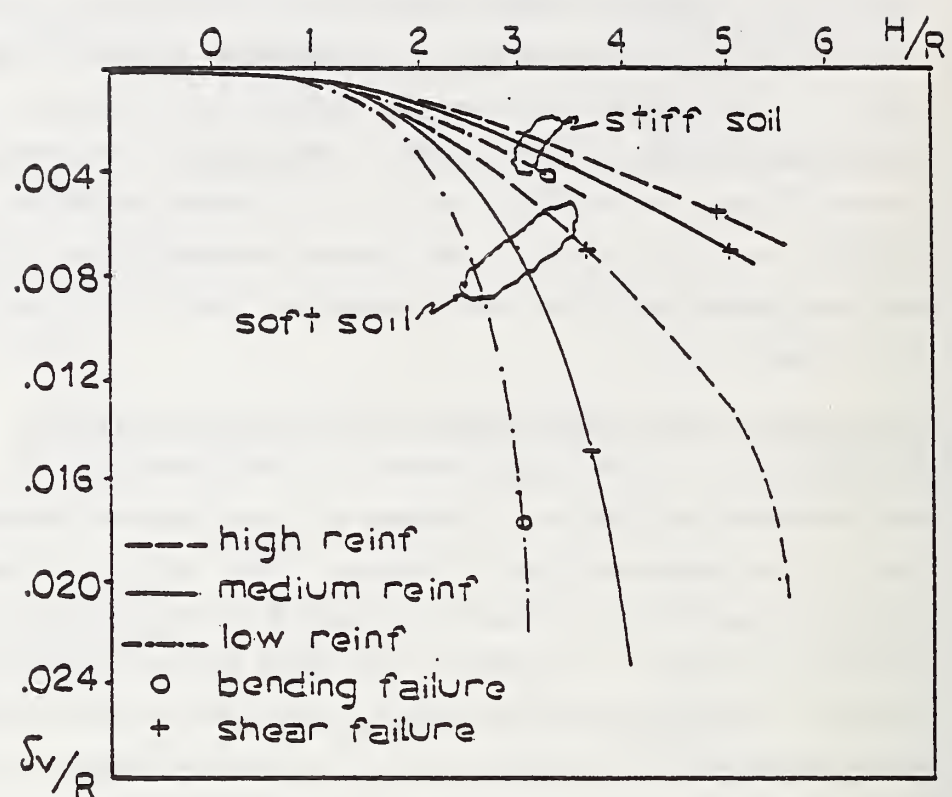
Figure 8.8 - Normalized Plots for Normal Pressure and Shear Acting on a 8x8 Box at ASTM Height of Soil.

forces over the side walls producing a greater downward force. For the stiff soil condition CANDE predictions are similar to ASTM assumption at the center of the bottom slab and increases to about 60% to 70% greater than the ASTM assumption near the corner. For the soft soil condition CANDE predictions are about 20% to 40% greater than the ASTM assumption at the center of the bottom slab and increases to about 70% to 100% greater near the corners. The lateral pressure from CANDE predictions are not linear like the ASTM assumption, but in general the magnitudes are close.

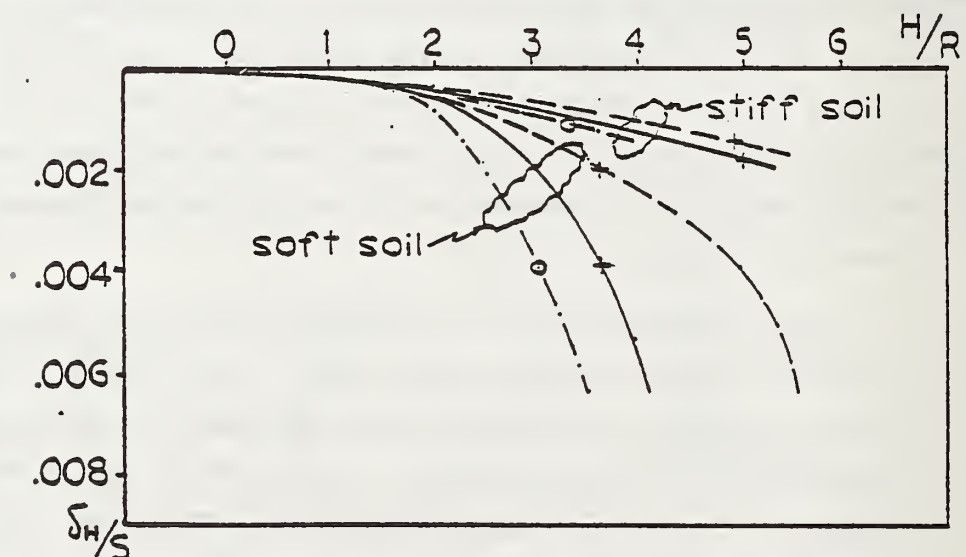
Load Distribution Comparisons at Failure Cover Heights. To further this study, each box was loaded beyond the ASTM design earth cover to failure for both soil conditions. Figures 8.9 to 8.13 show load-deflection histories of all the boxes analyzed to failure. For each box shown, the type of failure that first occurred is indicated at the height of soil cover where failure occurred. As expected, the boxes buried under soft soil conditions exhibit greater deflections during their load history and fail prior to the identical box analyzed in stiff soil conditions.

For fill heights at failure, normalized load-distribution plots (CANDE prediction divided by the ASTM assumption) are constructed in the same manner as previously described and are shown in Figures 8.14 to 8.18. Note, the magnitude of the ASTM load distributions are linearly related to cover height but retain the same shape for all fill heights. Load distributions from CANDE change both in magnitude and in shape during loading as a consequence of soil-structure interaction and changing stiffness of the box.

The normalized plots at failure show the same general trends as the normalized plots at design earth cover. Now, however, the normal pressure distributions on the top and bottom slab tend to increase more rapidly, beginning with relatively smaller magnitudes at the slab centers and increasing to relatively higher magnitudes at the slab corners. This is attributed to the reduction of slab bending stiffness as failure develops, i.e., a greater portion of the soil load is shifted to the stiffer corners where the side walls serve as thrust columns.

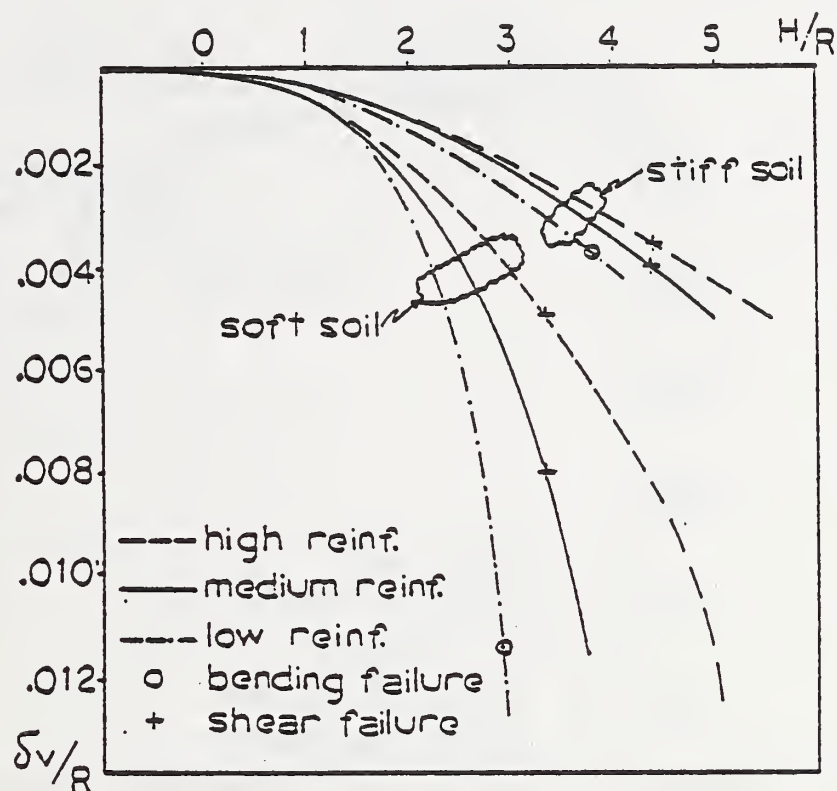


(a) Vertical deflection/rise vs. fill height/rise.

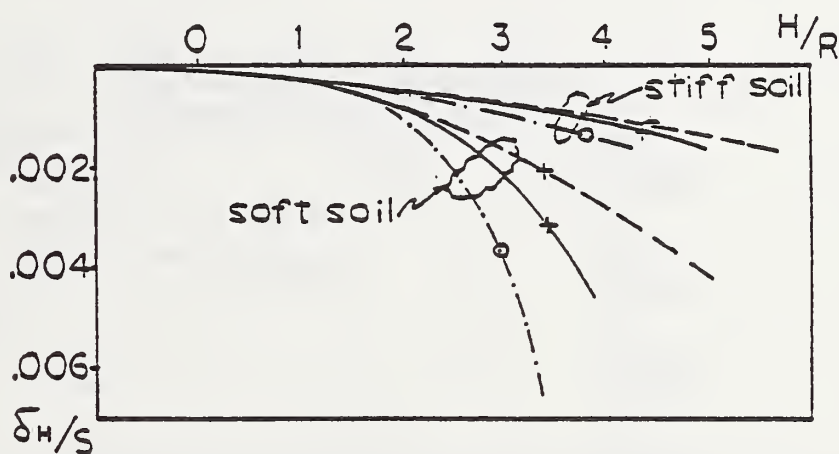


(b) Horizontal deflection/span vs. fill height/rise.

Figure 8.9 - Height of Soil - Deflection for 10×6 Box with Soil Loads.

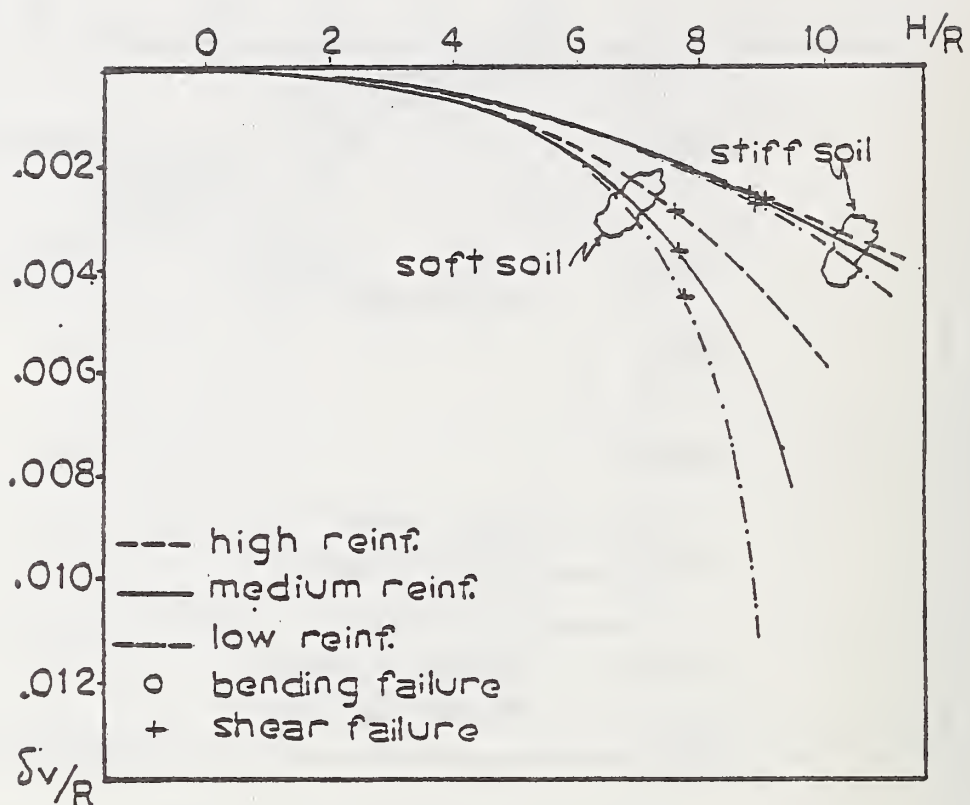


(a) Vertical deflection/rise vs. fill height/rise.

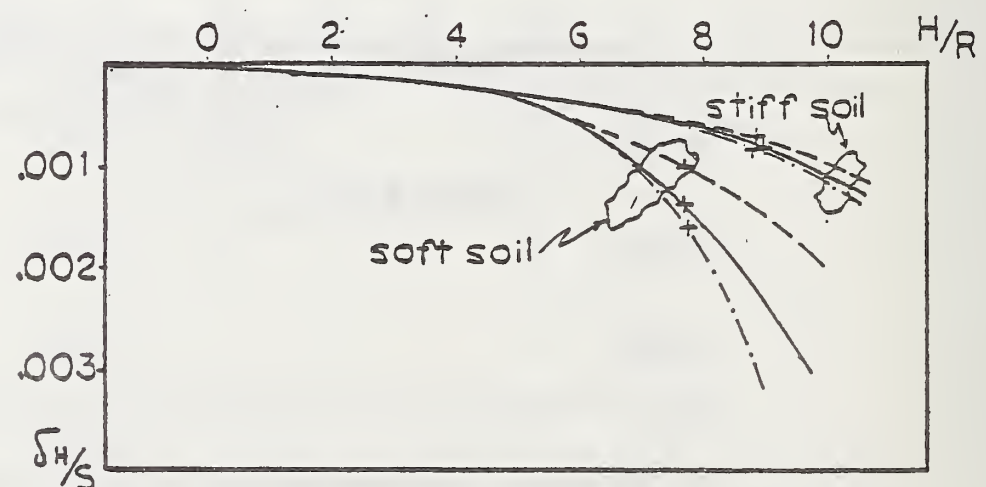


(b) Horizontal deflection/span vs. fill height/rise.

Figure 8.10 - Height of Soil - Deflection for 8x6 Box with Soil Loads.

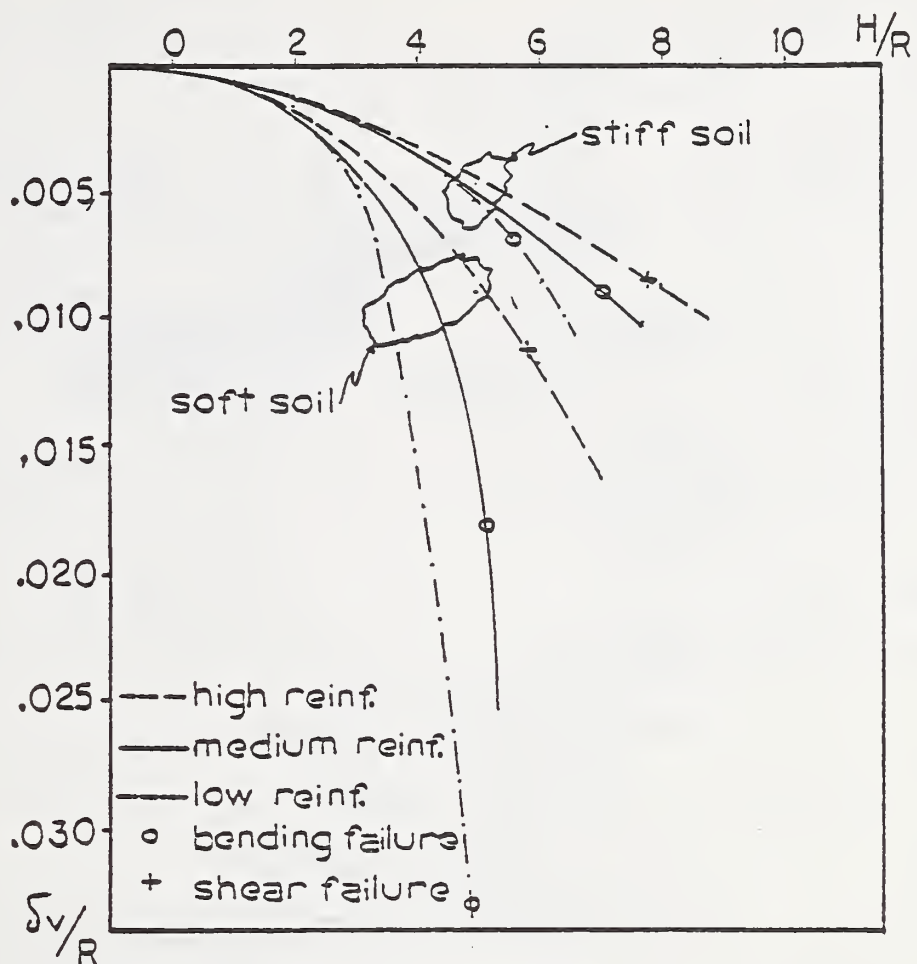


(a) Vertical deflection/rise vs. fill height/rise.

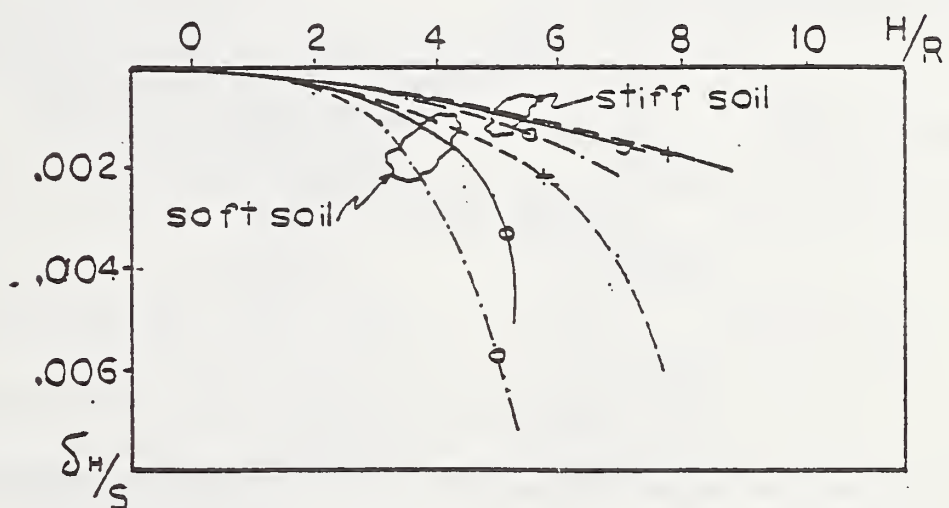


(b) Horizontal deflection/span vs. fill height/rise.

Figure 8.11 - Height of Soil - Deflection for 4×3 Box with Soil Loads.

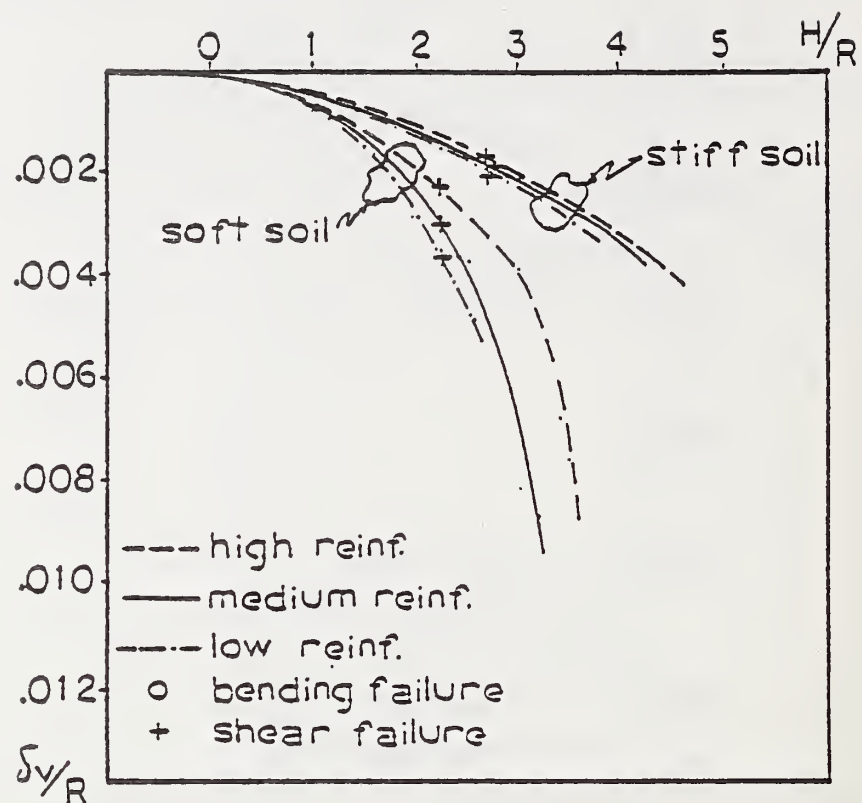


(a) Vertical deflection/rise vs. fill height/rise.

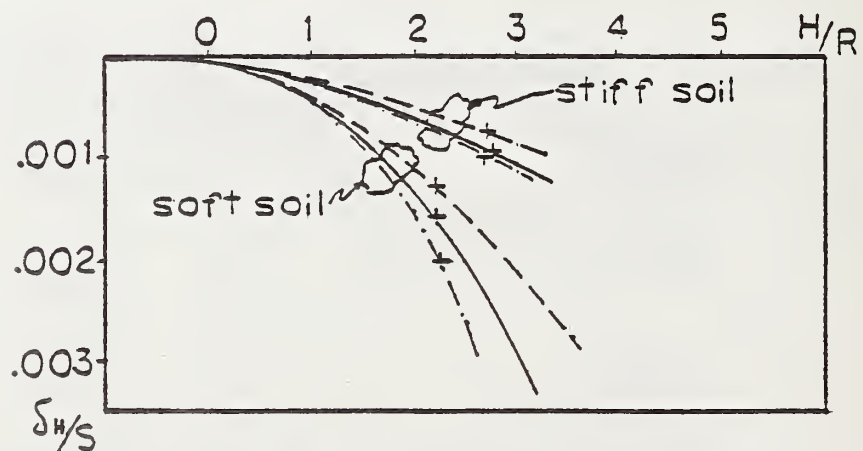


(b) Horizontal deflection/span vs. fill height/rise.

Figure 8.12 - Height of Soil - Deflection for 8x4 Box with Soil Loads.

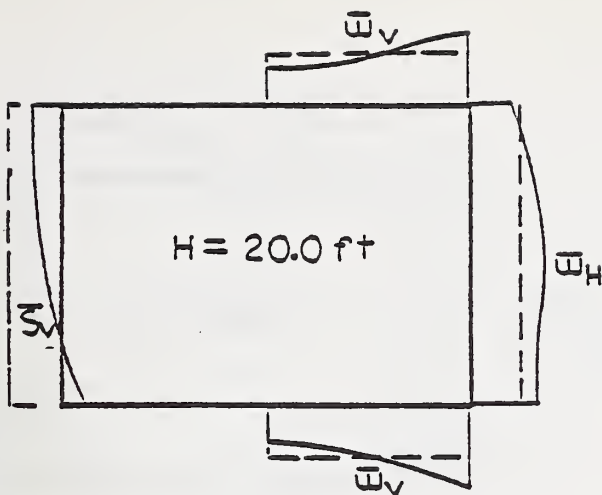


(a) Vertical deflection/rise vs. fill height/rise.

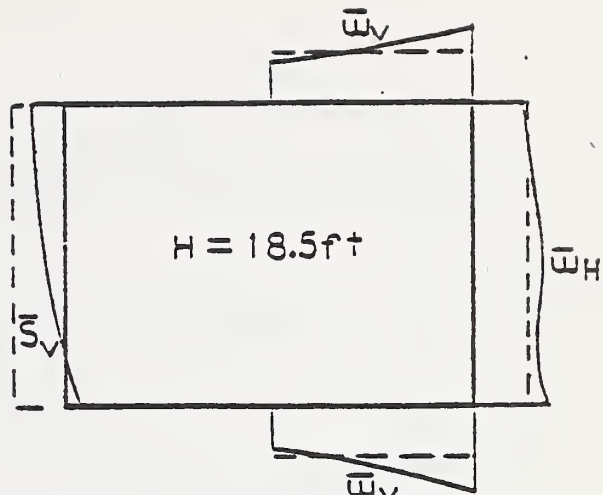


(b) Horizontal deflection/span vs. fill height/rise.

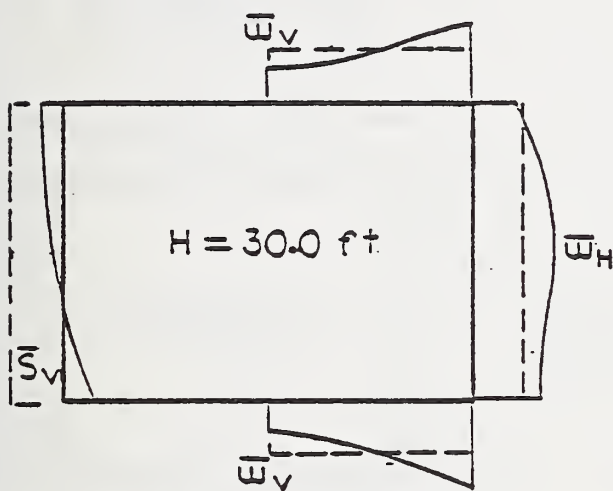
Figure 8.13 - Height of Soil - Deflection for 8x8 Box with Soil Loads.



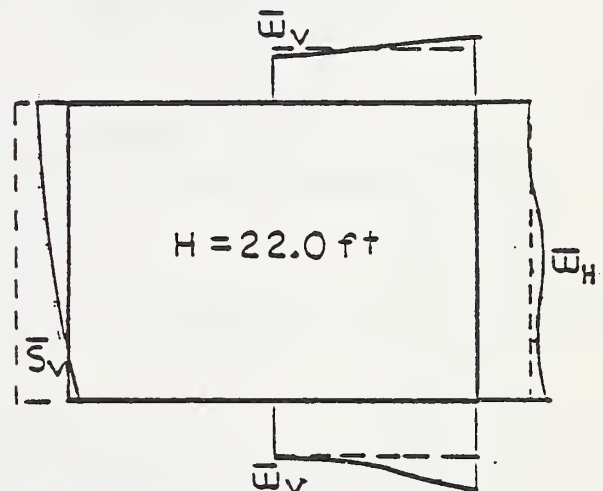
(a) Low reinforced and stiff soil



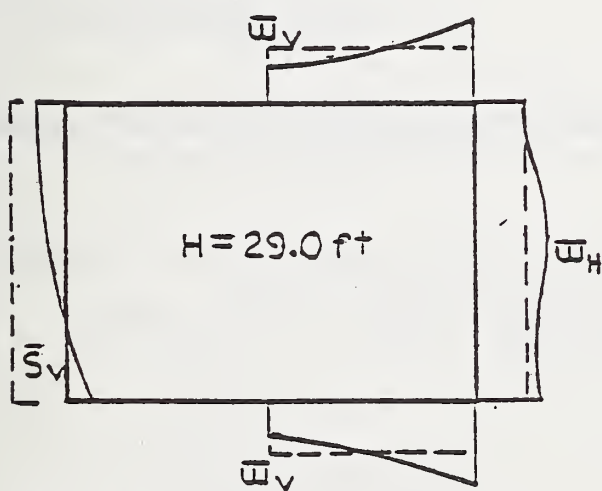
(b) Low reinforced and soft soil



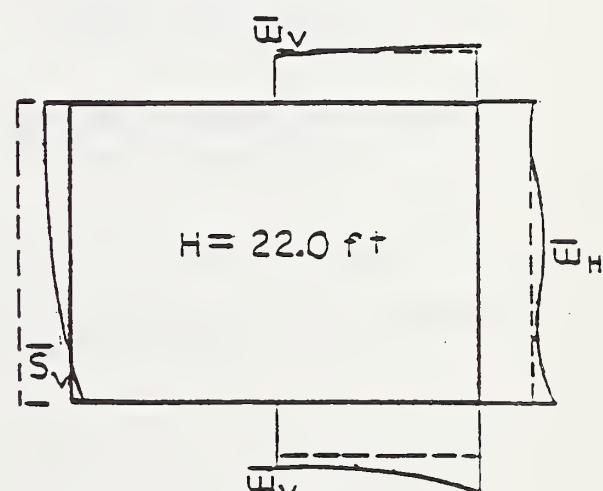
(c) Medium reinforced and stiff soil



(d) Medium reinforced and soft soil

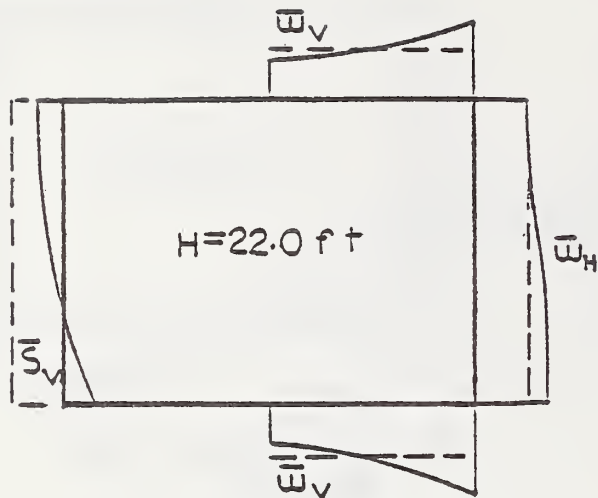


(e) High reinforced and stiff soil

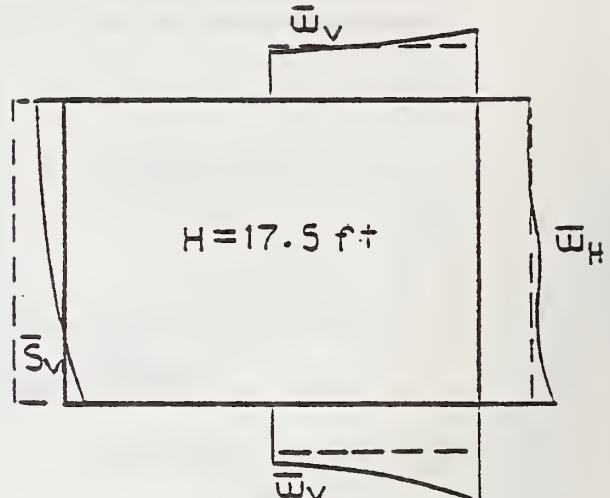


(f) High reinforced and soft soil

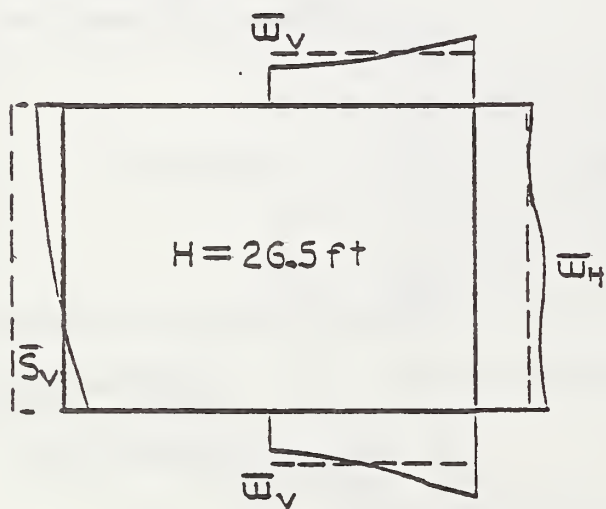
Figure 8.14 - Normalized Plots for Normal Pressure and Shear Acting on a 10x6 Box at Failure Load.



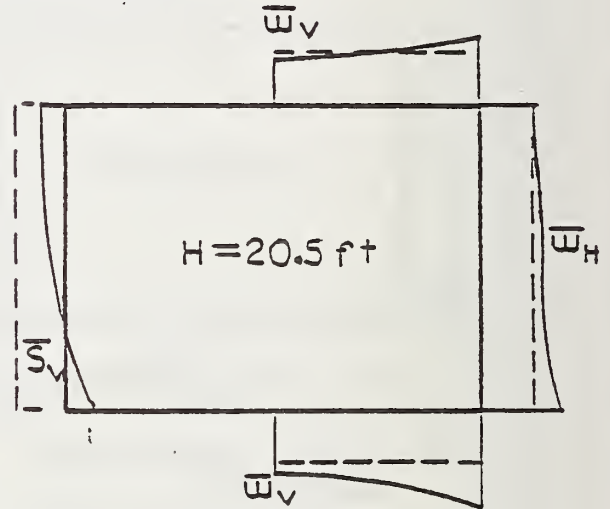
(a) Low reinforced and stiff soil



(b) Low reinforced and soft soil



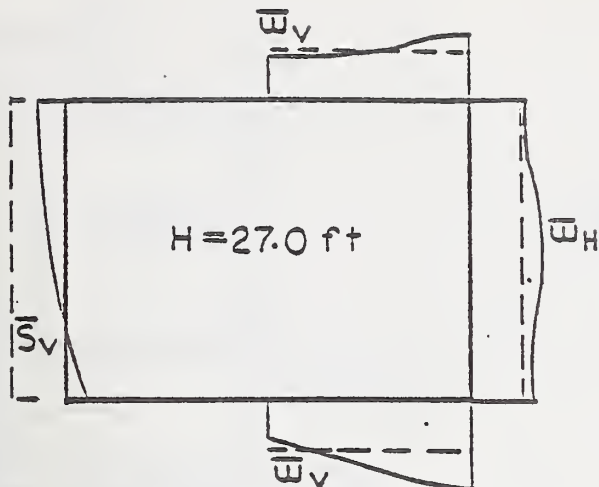
(c) Medium reinforced and stiff soil



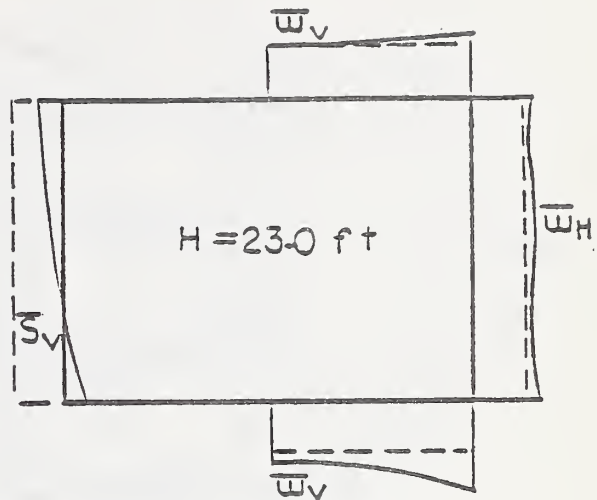
(d) Medium reinforced and soft soil

Note: The 8x6 box with high reinforcement has plots similar to the medium reinforced, where the failure is due to shear.

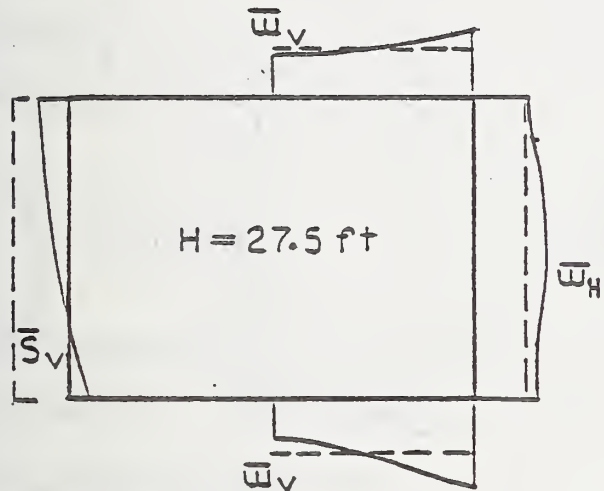
Figure 8.15 - Normalized Plots for Normal Pressure and Shear Acting on a 8x6 Box at Failure Load.



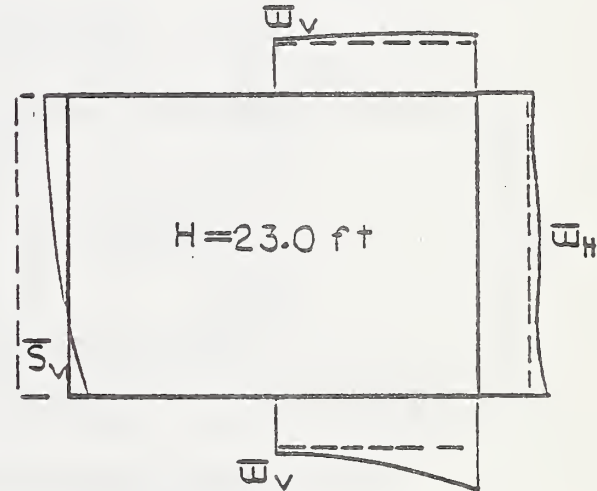
(a) Low reinforced and stiff soil



(b) Low reinforced and soft soil



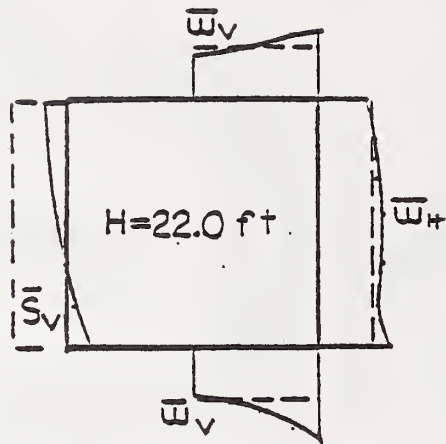
(c) Medium reinforced and stiff soil



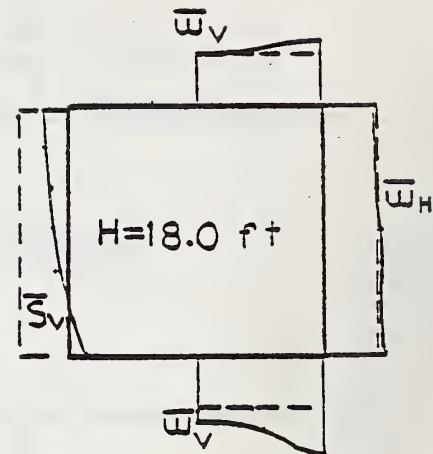
(d) Medium reinforced and soft soil

Note: The 4x3 box with high reinforcement has plots similar to the medium reinforced, where the failure is due to shear.

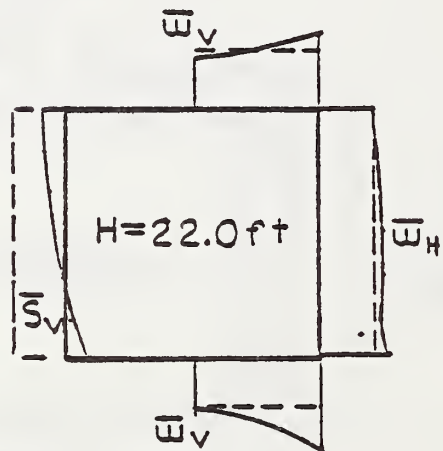
Figure 8.16 - Normalized Plots for Normal Pressure and Shear Acting on a 4x3 Box at Failure Load.



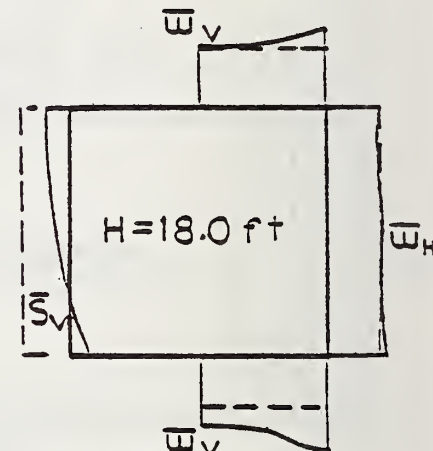
(a) Low reinforced and stiff soil



(b) Low reinforced and soft soil



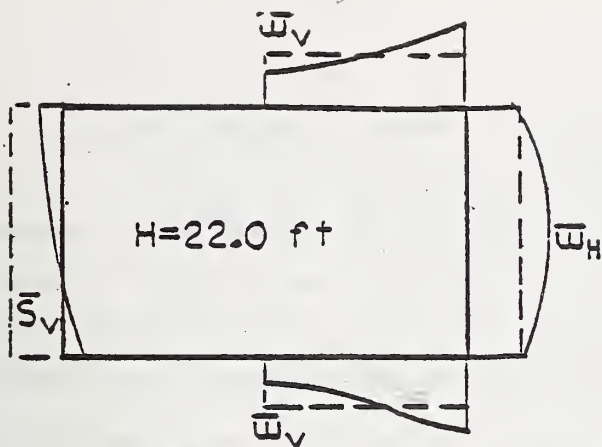
(c) Medium reinforced and stiff soil



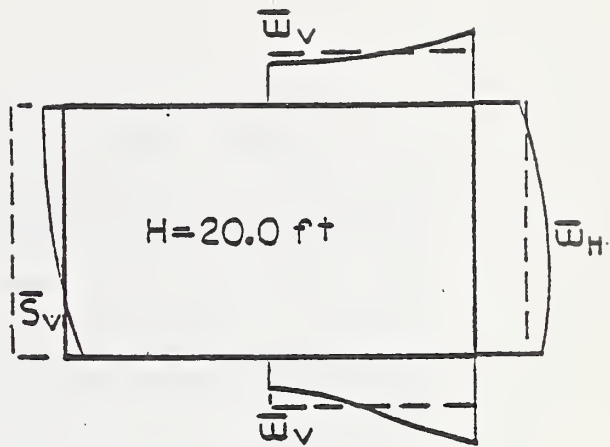
(d) Medium reinforced and soft soil

Note: The 8x8 box with high reinforcement has plots similar to the medium reinforced, where the failure is due to shear.

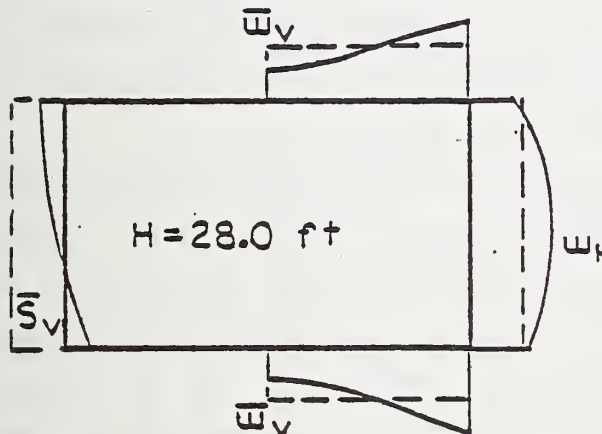
Figure 8.17 - Normalized Plots for Normal Pressure and Shear Acting on a 8x8 Box at Failure Load.



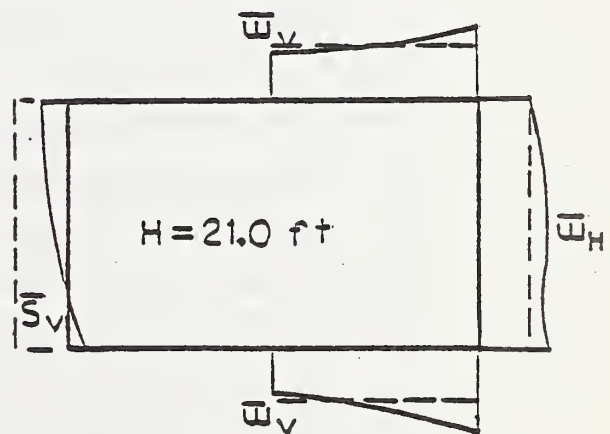
(a) Low reinforced and stiff soil



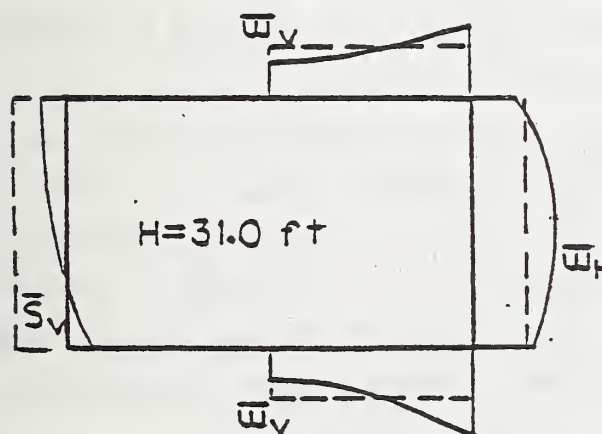
(b) Low reinforced and soft soil



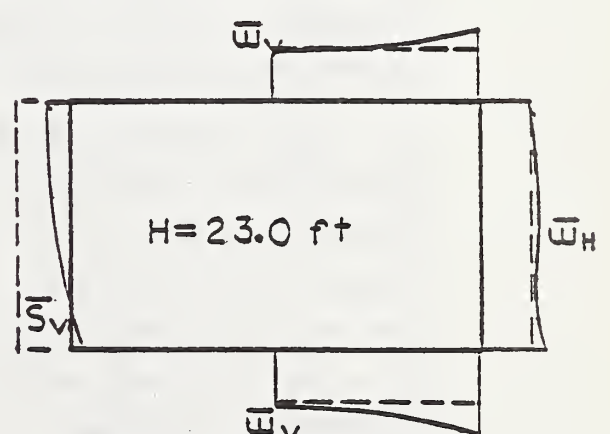
(c) Medium reinforced and stiff soil



(d) Most reinforced and soft soil



(e) High reinforced and stiff soil



(f) High reinforced and soft soil

Figure 8.18 - Normalized Plots for Normal Pressure and Shear Acting on a 8x4 Box at Failure Load.

Lateral pressure on the side wall tend to be greater than ASTM predictions, particularly in the center region where outward deflections mobilize passive soil resistance. Side wall shear traction is maximum at the top walls acting in the downward direction. Near the bottom, shear traction reverses sign, but the net effect is a significant downward force, an effect not considered in the ASTM assumed load pattern.

Cracking and Failure Loads Comparisons. The CANDE prediction for the fill height producing 0.01 inch cracking is shown in Tables 8.2 and 8.3 (second column from end) corresponding to the boxes defined in Tables 8.1a and 8.1b for both soft and stiff soil conditions. For each box size it is observed that the cracking load (fill height) increases with the level of reinforcement. Also for identical box cross sections, the cracking load increases with soil stiffness.

To check if the ASTM design earth covers are conservative compared to predicted fill heights at which 0.01 inch cracking occurs, a fill-height ratio (CANDE prediction/ASTM design cover) is shown in the last columns. This ratio should be more than 1.0 for conservative designs. For stiff soils, the cracking load ratio varies from 1.06 to 2.02 implying the ASTM design covers are conservative. For soft soils, the ratio varies from 0.75 to 1.44 implying some designs may not be conservative. Boxes with low reinforcement tend to be more conservative than with high reinforcement. As a general conclusion, the ASTM boxes are moderately conservative with respect to 0.01 inch cracking at design earth cover providing good quality soil is used.

Also shown in Tables 8.2 and 8.3 are the CANDE predictions for fill height at failure as controlled by flexure or shear. In most cases shear failure occurs prior to flexure failure except for some lightly reinforced boxes. Identical boxes fail at lower fill heights in soft soil than in stiff soil. Both shear and flexure failure heights are reduced in soft soils, but flexure failure heights are reduced by a greater precentage.

A "failure load ratio" is defined here by dividing the predicted failure height (as controlled by shear or flexure) by the ASTM design

TABLE 8.2 - Comparison Between ASTM Load and CANDE Results

BOXES		DESIGN COVER (ft)	SOIL	CANDE			CANDE			CANDE		
				SHEAR FAILURE H (ft)	H/H ASTM (SHEAR F)	BENDING FAILURE H (ft)	H/H ASTM (BEND F)	H FAILURE (ft)	H/H ASTM (FAILURE)	H FAILURE (ft)	H/H ASTM (FAILURE)	CANDE
Low Reinf.	6.0	STIFF	—	—	20.0	3.3	20.0	3.3	6.0	10.0	1.67	
Medium Reinf.	10.0	STIFF	SOFT	—	18.5	3.1	18.5	3.1	6.0	8.0	1.33	
High Reinf.	14.0	STIFF	SOFT	30.0	3.0	31.0	3.1	30.0	3.0	10.0	13.0	1.30
		STIFF	SOFT	24.0	2.4	22.0	2.2	22.0	2.2	10.0	9.0	0.90
Low Reinf.	6.0	STIFF	SOFT	29.0	2.1	38.5	2.8	29.0	2.1	14.0	21.5	1.54
Medium Reinf.	10.0	STIFF	SOFT	22.0	1.6	31.0	2.2	22.0	1.6	14.0	15.5	1.11
High Reinf.	14.0	STIFF	SOFT	—	—	22.0	3.7	22.0	3.7	6.0	10.0	1.67
		STIFF	SOFT	—	—	17.5	2.9	17.5	2.9	6.0	8.0	1.33
Low Reinf.	10.0	STIFF	SOFT	26.5	2.7	31.0	3.1	26.5	2.7	10.0	12.0	1.20
Medium Reinf.	14.0	STIFF	SOFT	20.5	2.1	22.0	2.2	20.5	2.1	10.0	8.0	0.80
High Reinf.	18.0	STIFF	SOFT	26.0	1.9	40.0	2.9	26.0	1.9	14.0	16.0	1.14
		STIFF	SOFT	20.0	1.4	30.0	2.1	20.0	1.4	14.0	12.5	0.89
Low Reinf.	10.0	STIFF	SOFT	27.0	2.7	35.0	3.5	27.0	2.7	10.0	14.5	1.45
Medium Reinf.	14.0	STIFF	SOFT	23.0	2.3	23.0	2.3	23.0	2.3	10.0	12.0	1.20
High Reinf.	18.0	STIFF	SOFT	27.0	1.5	46.0	2.6	27.0	1.5	18.0	19.0	1.06
		STIFF	SOFT	23.0	1.3	36.0	2.0	23.0	1.3	18.0	19.0	1.06

TABLE 8.3 - Comparison Between ASTM Load and CANDE Results

ROWS	DESIGN COVER (ft)	SOIL	CANDE			CANDE		
			SHEAR FAILURE H (ft)	H/H ASTM (SHEAR F)	BENDING FAILURE H (ft)	H/H ASTM (BEND F)	H FAILURE (ft)	H/H ASTM (FAILURE)
2.0	6.0	STIFF	-	-	22.0	3.7	22.0	3.7
		SOFT	-	-	20.0	3.3	20.0	3.3
Medium Reinf.	10.0	STIFF	34.0	3.4	38.0	2.8	28.0	2.8
		SOFT	-	-	21.0	2.1	21.0	2.1
High Reinf.	14.0	STIFF	31.0	2.2	40.0	2.9	31.0	2.2
		SOFT	23.0	1.6	26.0	1.9	23.0	1.6
8*4-8	Low Reinf.	STIFF	-	-	22.0	3.7	22.0	3.7
		SOFT	-	-	17.5	2.9	17.5	2.9
8*6-8	Medium Reinf.	STIFF	26.5	2.7	31.0	3.1	26.5	2.7
		SOFT	20.5	2.1	22.0	2.2	20.5	2.1
8*8-8	High Reinf.	STIFF	26.0	1.9	40.0	2.9	26.0	1.9
		SOFT	20.0	1.4	30.0	2.1	20.0	1.4
1.0	Low Reinf.	STIFF	22.0	4.4	23.5	4.7	22.0	4.4
		SOFT	18.0	3.6	20.0	4.0	18.0	3.6
8*8-8	Medium Reinf.	STIFF	22.0	2.8	27.0	3.4	22.0	2.8
		SOFT	18.0	2.3	23.0	2.9	18.0	2.3
8*8-8	High Reinf.	STIFF	22.0	1.8	32.0	2.7	22.0	1.8
		SOFT	18.0	1.5	27.0	2.3	18.0	1.5

earth cover and is tabulated in the center column of the tables. Presumably, the ASTM designs are based on a load factor of 1.5 times the design earth load. Thus, the failure load ratio defined above should be at least 1.5 to achieve the intended ultimate capacity. For stiff soils, the ratio varies from 1.5 to 4.4, whereas for soft soils, the ratio varies from 1.3 to 3.6. For a given soil condition and box size, the ratios are higher for low reinforcement than for high reinforcement. Overall, it is concluded that the ASTM box designs are conservative with respect to the 1.5 load factor criterion when good quality soil is used, but less so for the high reinforcement than low reinforcement. In other words, the ASTM design earth cover specified for a box with low reinforcement is more conservative than the specified earth cover for the identical box with high reinforcement.

8.2 BOX SECTION STUDIES WITH LIVE LOADS

In this section the effect of live loads on shallowly buried boxes are investigated and compared with ASTM C789 design tables.

The ASTM Specifications consider two types of live load in their box culvert design tables, HS-20 truck loads (ASTM Table 1) and interstate truck loads (ASTM Table 2). Due to the small difference between these design tables, only the HS-20 live loads are considered in this study. Figure 8.19 shows the HS-20 truck axle loads along with an "equivalent" transverse strip load $P = 222 \text{ lb/in}$ (389 N/cm) used as a reference plane strain loading in the CANDE analysis. The strip load P represents the static weight of the middle axle tire loads distributed by the axle length as shown in the Figure.

The box-soil system analyzed in CANDE is an embankment installation using the Level 2 box automatic mesh generation along with the extended level 2 option for defining the live loads. As before, two types of soil, stiff and soft (see Table 7.2), are used for each box culvert. Figure 8.20 shows a typical box culvert cross section, where the live load P representing the HS-20 truck's middle axle is applied over the center of the box culvert. The other axles are well away from the box culverts con-

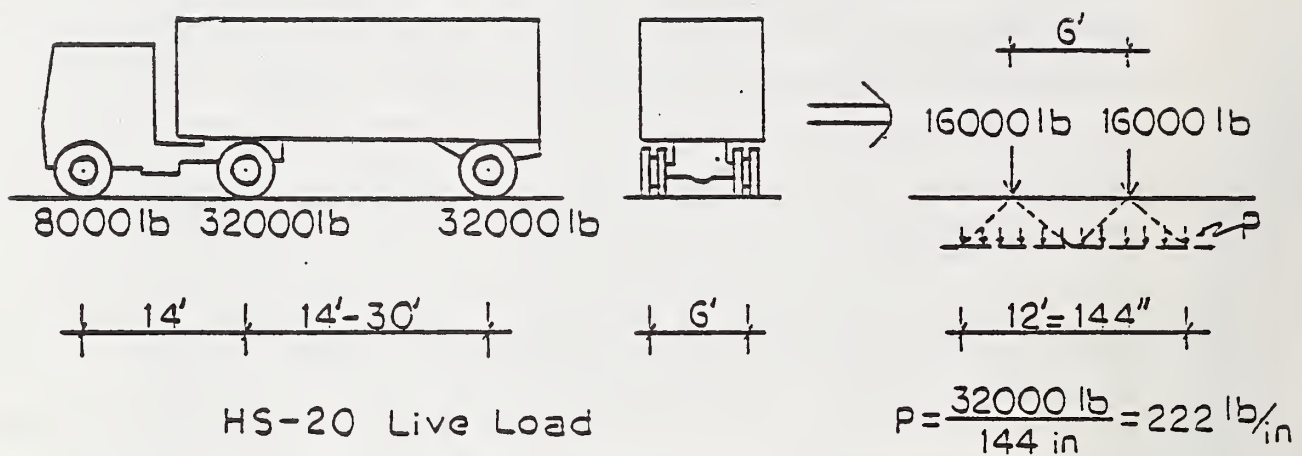


Figure 8.19 - HS-20 Truck Live Load and Equivalent Plane Strain Strip Load.

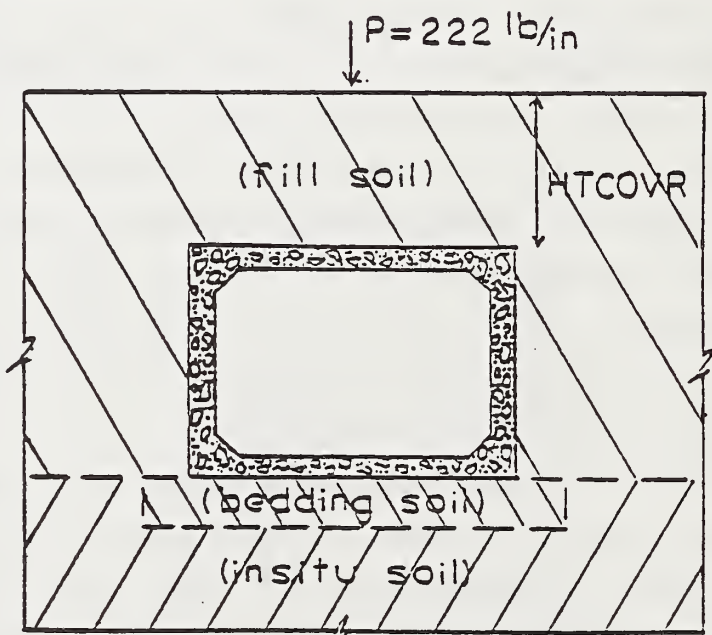


Figure 8.20 - Typical Box Culvert Cross Section Used for Live Load Comparison Study.

sidered herein and have negligible influence on the box deformations.

To study the effect of live load at shallow soil cover, a set of five boxes representing a range of sizes and span/rise ratios were selected from ASTM Table 1. Each of these boxes has as a minimum allowable fill height of 2.0 feet (0.61 m) to disperse the concentrated live load. Table 8.4 lists these boxes and the ASTM steel reinforcement areas specified for the common minimum soil cover. For the CANDE analysis each box was incrementally loaded with soil layers up to 2.0 feet cover height. Next, the live load P was applied and then incrementally increased to a value P^* at which a 0.01 inch crack occurred in the box culvert. This was repeated for each of the five boxes using stiff and soft soil conditions.

By forming the load ratio P^*/P , the ASTM designs can be evaluated on the basis of 0.01 inch cracking design criterion. Table 8.5 shows the results of this study. Note that the load ratios are high but fairly uniform, ranging from 4.0 to 4.7 including both soil conditions. Thus, it is concluded that ASTM designs at 2.0 ft cover heights tend to be overly conservative even if impact loads are added to the HS-20 loading (ASTM recommends impact loads up to 20%).

Studies similar to the above indicated that the influence of live loads is negligible compared to dead loads for fill heights greater than eight feet.

Table 8.4 Reinforcement of Box Culverts with Minimum
Soil Cover and HS-20 Live Load (ASTM Table 1)

BOX	ASTM H _{soil} (ft)	A _{S1} (in ² /in)	A _{S2} (in ² /in)	A _{S3} (in ² /in)	A _{S4} (in ² /in)
4*3-5	2.0	.01750	.02250	.02000	.01000
8*6-8	2.0	.02583	.03833	.02917	.01583
10*6-10	2.0	.02917	.03833	.02833	.02000
8*8-8	2.0	.02167	.04250	.03333	.01583
8*4-8	2.0	.03083	.03333	.02417	.01583

Table 8.5 Live Load Performance Factor for Box Culverts
with Minimal Soil Cover and HS-20 Live Load

BOX	ASTM H _{soil} (ft)	HS-20 P (lb/in)	Type of Soil	P [*] (lb/in)	P [*] /P
4*3-5	2.0	222	STIFF	1046	4.71
			SOFT	942	4.24
8*6-8	2.0	222	STIFF	1006	4.51
			SOFT	942	4.24
10*6-10	2.0	222	STIFF	1030	4.64
			SOFT	930	4.19
8*4-8	2.0	222	STIFF	1022	4.60
			SOFT	892	4.02
8*8-8	2.0	222	STIFF	926	4.17
			SOFT	880	3.96

*Result obtained from CANDE

1 ft = 0.3048 m

1 lb/in = 1.22 N/m

CHAPTER 9

SOIL MODELS

Soil models originally incorporated into the CANDE-1976 program included: (a) linear elastic (isotropic or orthotropic); (b) incremental elastic, wherein elastic moduli are dependent on current fill height (overburden dependent); and (c) variable modulus model using a modified version of the Hardin soil model. The latter model employs a variable shear modulus and Poisson's ratio which are dependent on maximum shear strain and hydrostatic pressure (1).

The purpose of this chapter is to discuss the implementation of a new soil model into the CANDE program, called here the Duncan soil model, and to present standard parameters for characterizing this model. The Duncan soil model has had a substantial history of development and application over the last decade (26, 27, 28, 29 and associated references). It is a variable modulus model such that increments of stress are related to increments of strain by the isotropic form of Hooke's law wherein the elastic parameters are dependent on the stress state. For plane strain, this incremental relationship may be written as:

$$\begin{bmatrix} \Delta\sigma_x \\ \Delta\sigma_y \\ \Delta\tau \end{bmatrix} = \begin{bmatrix} C_{11} & C_{12} & 0 \\ C_{12} & C_{22} & 0 \\ 0 & 0 & C_{33} \end{bmatrix} \begin{bmatrix} \Delta\epsilon_x \\ \Delta\epsilon_y \\ \Delta\gamma \end{bmatrix} \quad 9.1$$

where

$$\begin{aligned} \Delta\sigma_x, \Delta\sigma_y &= \text{normal stress increments} \\ \Delta\tau &= \text{shear stress increments} \\ \Delta\epsilon_x, \Delta\epsilon_y &= \text{normal strain increments} \\ \Delta\gamma &= \text{shear strain increments} \\ C_{ij} &= \text{constitutive matrix components (variable)} \end{aligned}$$

In accordance with Hooke's law (isotropic form), the matrix components C_{ij} are all defined with any two elastic parameters. Table 9.1

Table 9.1 Elastic Equivalents for
Isotropic Plane Strain

Matrix Component	(E, ν)	(E, B)
$C_{11} = C_{22}$	$\frac{E(1-\nu)}{(1+\nu)(1-2\nu)}$	$\frac{3B(3B+E)}{9B-E}$
C_{12}	$\frac{E\nu}{(1+\nu)(1-2\nu)}$	$\frac{3B(3B-E)}{9B-E}$
C_{33}	$\frac{E}{2(1+\nu)}$	$\frac{3BE}{9B-E}$

shows this relationship for the elastic parameters pertinent to this study: Young's modulus and Poisson's ratio (E, ν) and Young's modulus and bulk modulus (E, B). If (E, ν) or (E, B) are described as a function of stress, characterizing the nonlinear behavior of soil, then the matrix components C_{ij} are also defined and infer tangent relationships between stress and strain increments.

9.1 DUNCAN MODEL REPRESENTATION OF ELASTIC PARAMETERS

Initially, Duncan and his colleagues characterized soil behavior with a variable tangent Young's modulus E_t and a constant Poisson's ratio where E_t employed the so-called hyperbolic stress-strain model (27). Subsequently, a variable Poisson's ratio formulation was introduced to better represent the volume change behavior observed in triaxial soil tests (26,28). Recently, a tangent bulk modulus formulation was introduced to replace the variable Poisson's ratio (29).

The last model, which employs tangent Young's modulus and tangent bulk modulus formulations, is adopted for this study and incorporation into CANDE. An extensive evaluation of the variable Poisson ratio formulation was undertaken during the course of this study and was found to behave erratically in some cases (30). Consequently, it was not incorporated into the CANDE program.

Development details of the Duncan model are well documented elsewhere (29). The final expressions for tangent Young's modulus and bulk modulus as a function maximum and minimum principle stresses for loading conditions are given here.

The tangent Young's modulus expression is:

$$E_t = K P_a \left(\frac{\sigma_3}{P_a} \right) \left[1 - \frac{R_f (1 - \sin\phi) (\sigma_1 - \sigma_3)}{2 c \cos\phi + 2 \sigma_3 \sin\phi} \right]^2 \quad 9.2$$

where σ_3 = minimum principle stress (compression positive).

σ_1 = maximum principle stress (compression positive).

P_a = atmospheric pressure (for dimensionless convenience).

K = modulus number, nondimensional

n = modulus exponent, typical range -1.0 to 1.0.
 R_f = failure ratio, typical range 0.5 to 0.9.
 c = cohesion intercept, units same as P_a .
 ϕ_o = friction angle, radians
 $\Delta\phi$ = reduction in ϕ for 10-fold increase in σ_3 .
(i.e., $\phi = \phi_o - \Delta\phi \log_{10} \left(\frac{\sigma_3}{P_a} \right)$)

The tangent bulk modulus expression is a function of minimum compressive stress given by:

$$B_t = K_b P_a \left(\frac{\sigma_3}{P_a} \right)^m \quad 9.3$$

where K_b = bulk modulus number, dimensionless.

m = bulk modulus exponent, typical range 0.0 to 1.0.

In Equations 9.2 to 9.3, there are a total of eight parameters to define a particular soil in loading: K , n , R_f , c , ϕ_o , and $\Delta\phi$ to define E_t ; and K_b and m to define B_t . Established methods for determining these parameters from conventional triaxial tests have been reported by Duncan and his colleagues (28,29). In the last section of this chapter, conservative estimates of these parameters are given for various soil types and degree of compaction.

The behavioral characteristics and limitations of the Duncan soil model (Equations 9.2 and 9.3) are enumerated below along with the programming strategy used in the Duncan finite element program called SSTIPN.

- (1) As σ_3 increases (e.g. confining pressure in a triaxial test) E_t and B_t becomes stiffer (assuming m and n are greater than zero). However, as maximum shear stress increases (i.e. $(\sigma_1 - \sigma_3)/2$), E_t becomes weaker, but B_t remains constant. Such behavior is typical of triaxial tests on which the model was developed.
- (2) Shear failure is said to occur when E_t approaches zero. That is, the bracketed term in Equation 9.2 approaches zero as

$\sigma_1 - \sigma_3$ increases. If a significant portion of the soil mass fails in shear, the results may no longer be reliable because the model is not applicable for soil instability. To avoid numerical problems, the SSTIPN algorithm arbitrarily limits the minimum value of the bracketed term in Equation 9.2 to $1 - .95 R_f$. Thus, E_t does not actually become zero in shear failure.

- (3) Tension failure is said to occur when σ_3 becomes tensile. In such cases the soil stiffness breaks down and cannot carry load. To cope with this problem, the SSTIPN algorithm computes a small value for bulk modulus from Equation 9.3 by specifying $\sigma_3/P_a = 0.1$ whenever σ_3 is tensile. For the second elastic parameter, Poisson's ratio is arbitrarily assigned the value 0.495 and Equation 9.2 is ignored. This results in equivalent Young's modulus whose value is approximately 3% of the bulk modulus.
- (4) In addition to the special treatment for shear and tension failures, the SSTIPN algorithm sets limits on B_t as predicted from Equation 9.3 dependent on the value of E_t from Equation 9.2. Specifically, $B_t = E_t/3.0$, if B_t is less than this value, and, $B_t = 34.0 E_t$, if B_t is greater than this value. These limits correspond to maintaining the equivalent Poisson's ratio within the range 0.0 to 0.495.
- (5) For each load step (e.g. construction increment), the SSTIPN algorithm utilizes two iterations to determine B_t and E_t as defined above. For the first iteration, the stresses existing in the element at the end of the previous load step are used to estimate B_t and E_t to obtain approximate stress increments. The second iteration repeats this solution wherein B_t and E_t are now determined by adding one-half of the stress increments determined in the first iteration to the previous stress state. Upon completion of the second iteration, the stresses are accumulated and printed out, and the next load step is considered. No convergence check is made.

(6) When an element first enters the system, the "existing" stress state used to determine B_t and E_t for the first iteration is determined in a special manner depending on whether the element is part of the initial system (e.g. pre-existing foundation) or part of a new construction increment. For the case of elements belonging to the initial system, existing stresses are defined by the user (input), or if the foundation is composed of horizontal rows, initial stresses can be automatically approximated by overburden pressure and a lateral coefficient.

Elements belonging to a new construction increment do not have an existing stress state prior to entering the system. However in order to evaluate E_t and B_t for the first iteration, the SSTIPN algorithm estimates initial stresses based on element height, soil density, assumed Poisson's ratio, and humped surface angle.

(7) According to published reports (28,29), "unloading" of the Duncan soil model is accomplished by replacing the tangent Young's modulus function (Equation 9.2) with an unloading expression; $E_u = K_u P_a \left(\frac{\sigma_3}{P}\right)^n$, where K_u is an unloading modulus number whose value is greater than K .

Although this is relatively easy to program, there are serious theoretical objections to this description of unloading. Presumably, the criterion for unloading (i.e. switching from E_t to E_u) is by observing a decrease in maximum shear stress irrespective of σ_3 . Such a criterion may be sufficient for load paths where σ_3 is constant (e.g. triaxial test), however for more general load paths, serious violations of the continuity principle can occur, i.e., two arbitrarily close load paths should not result in dramatically different stress-strain responses.

For this reason, the unloading function is not incorporated into the CANDE program. Further research on unloading is warranted.

9.2 CANDE SOLUTION STRATEGY FOR DUNCAN MODEL

The CANDE algorithm for the Duncan soil model is contained in a new subroutine called DUNCAN. Here the representation of E_t and B_t (Equations 9.2 and 9.3), shear failure, and tension failure are treated in a similar fashion to the SSTIPN algorithm discussed in the previous section. However, there are some significant differences in the CANDE solution strategy with regard to (a) number of iterations, (b) averaging E_t and B_t over a load step, and (c) treatment of elements entering the system for the first time. These differences are discussed below.

Iterations. As previously explained, the SSTIPN algorithm uses two iterations per load step for all loading schedules. Preliminary studies during this research indicated that using just two iterations can lead to serious error in predicting E_t and B_t even when load increments are relatively small (e.g. one layer of elements per construction increment).

To deal with this problem, the CANDE algorithm allows the maximum number of iterations to be specified by the user. During the iteration process, the current estimate of E_t for each element is compared percentage-wise with the previous estimate of E_t . If two succeeding estimates of E_t converge within a specified error tolerance for all elements, the iteration process is terminated and algorithm advances to the next load step. Should convergence not be achieved after the specified maximum number of iterations, a warning message is printed out prior to advancing to the next load step.

Note, the convergence check is only considered for E_t , not B_t . However, it may be presumed that B_t converges more rapidly than E_t since the former is only a function σ_3 , whereas the latter is a more sensitive function dependent on σ_1 and σ_3 .

Averaging E_t and B_t . Equations 9.2 and 9.3 are tangent moduli expressions for E_t and B_t for a particular principle stress state σ_1 and σ_3 . As a load increment is applied, the stress state changes, inferring changes in E_t and B_t . In order to adequately represent the effects of these changes in Equation 9.1, E_t and B_t should represent "average" values over the load step. This, of course, is the purpose of iteration.

One way of obtaining average values is to evaluate E_t and B_t based on the average stress state during the load step as is done in the SSTIPN algorithm. Alternatively, one may average E_t at the beginning of the load step with E_t at the end of the load step. Likewise for B_t . Specifically, this may be written as:

$$E_{avg} = (1-r)E_1 + rE_2 \quad 9.4$$

$$B_{avg} = (1-r)B_1 + rB_2 \quad 9.5$$

where $E_1, B_1 = E_t, B_t$ at start-of-load-step (known)

$E_2, B_2 = E_t, B_t$ at end-of-load-step (iteratively determined)

r = averaging ratio, (generally $r = 1/2$)

For reasons to be subsequently discussed, the CANDE algorithm employs the averaging scheme given by Equations 9.4 and 9.5. Comparison studies between the stress averaging scheme and the moduli averaging scheme were found to give nearly identical results for $r = 1/2$.

The averaging ratio r is treated as a material input parameter in the CANDE program. Generally $r = 1/2$, however for pre-existing soil zones, $r = 1$ permits proper calculation of pre-existing stresses as discussed next.

Entering Elements. Soil elements enter the structural system in one of two categories. The first category applies to pre-existing or in-situ soil elements in which an initial stress state exists but is unknown. Elements entering in this category are part of the initial configuration and belong to the first construction increment.

The second category applies to fill soil elements, i.e., soil layers added to the system in a predefined construction schedule. Here, the initial stress state is non-existent prior to entry into the system. Both categories present special starting problems for the iteration procedures because the initial stress state is unknown or undefined.

If pre-existing soil zones are to be characterized by the Duncan soil model, the initial stress state can be determined iteratively by

assuming the pre-existing soil zone is a construction increment loaded with its own body weight (and, if desired, a consolidation pressure). Here the averaging ratio should be set to 1.0, so that, E_{avg} and B_{avg} are equal to the end-of-load-step values E_2 and B_2 , respectively, and correspond to the existing stress state. Beginning-of-load-step values E_1 and B_1 are initially set to 0.0 when an element enters the system. However when $r = 1$, they have no influence on the averaging process. After the first construction increment is complete, the program automatically sets the value of r to 1/2, so that, all subsequent moduli calculations represent load step averages.

Elements entering the system in the second category have no initial stiffness prior to loading so that $E_1 = B_1 = 0$. Accordingly, using $r = 1/2$ gives average moduli values equal to one-half of the end-of-load-step values, E_2 and B_2 .

To start the iteration process for entering elements of either category, some guess must be made for E_2 and B_2 in order to construct the first trial stiffness matrix. This is achieved by arbitrarily defining "dummy" principle stresses from which initial estimates of E_2 and B_2 are calculated. The dummy principle stresses have no effect on the final values of E_2 and B_2 , however they do influence the number of iterations for convergence. Once an element has entered the system, the initial guess for E_2 and B_2 for all subsequent load steps are equated to the last calculated values, thus dummy stresses are not required.

Cande Algorithm. Figure 9.1 is a flow chart of the CANDE algorithm illustrating the solution strategy previously described. Some of the limit bounds are defined differently than in the SSTIPN algorithm. For example, the maximum equivalent Poisson ratio, ν_{max} , is set at 0.48 rather than 0.495 in order to avoid unreasonably high values of C_{11} in Equation 9.1. Also, the shear failure factor (1-D) is assigned a lower limit of 0.05, rather than 1-0.95 R_f in order to provide a greater reduction of stiffness in shear failure.

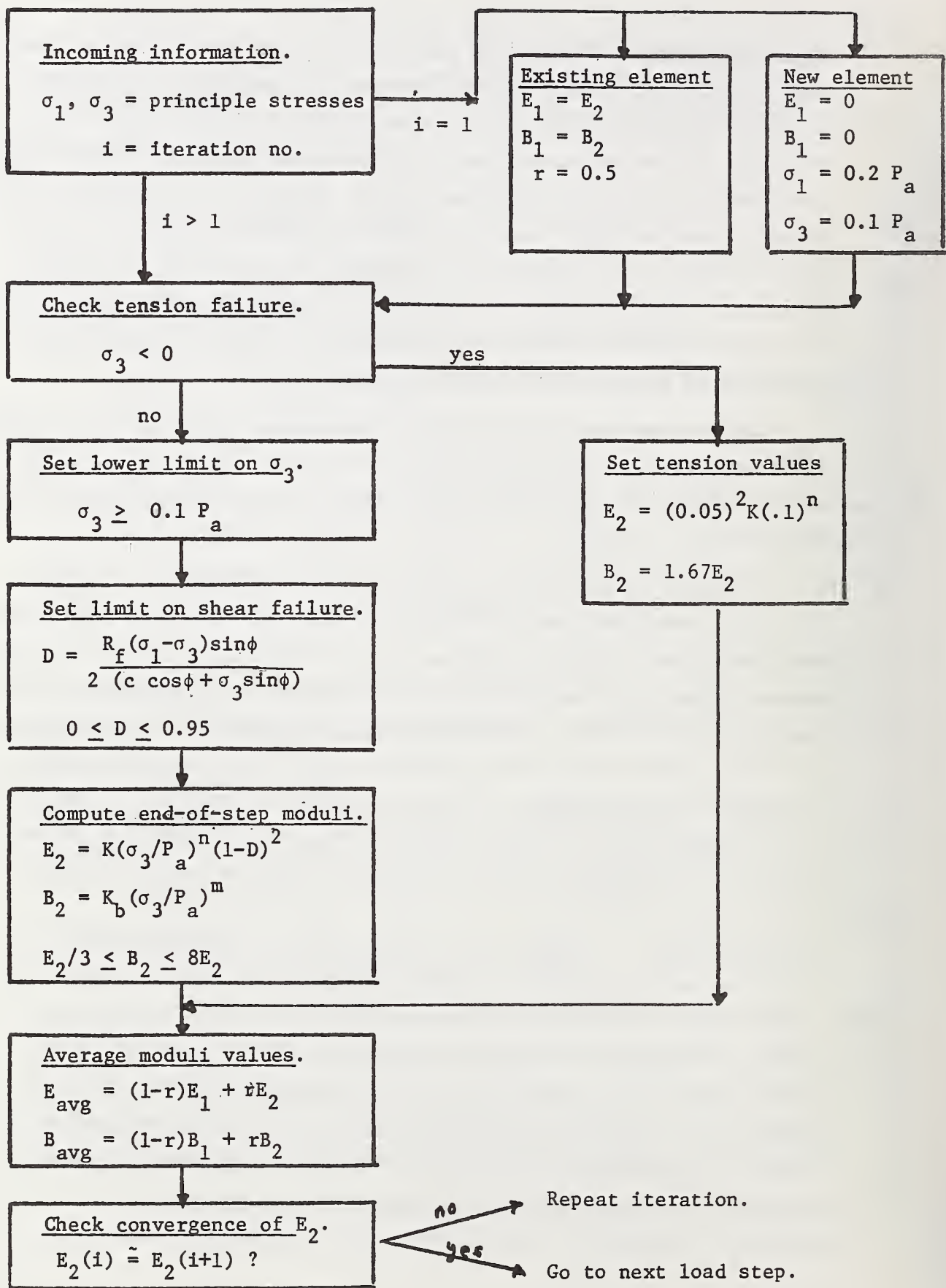


Figure 9.1 CANDE Algorithm for Duncan Soil Model.

Two additional features of the CANDE algorithm not shown in Figure 9.1 are; (1) an under relaxation scheme to improve the rate of convergence for E_2 , and (2) a constant Poisson ratio option which replaces the tangent bulk modulus formulation.

The under relaxation scheme comes into play after the second iteration wherein each estimate of E_2 is a weighted average of the current estimate and the previous estimate. This feature takes advantage of the observation that E_2 generally converges in an oscillatory manner.

When the constant Poisson ratio option is exercised, all references to the bulk modulus formulation are bypassed. Otherwise, the algorithm is essentially the same.

9.3 STANDARD HYPERBOLIC PARAMETERS

Whenever possible, the hyperbolic parameters characterizing the Duncan soil model should be determined directly from triaxial tests using established curve-fitting procedures (28,29). In many instances, however, triaxial data may be unavailable, and so, it is convenient to establish "standard" parameter values for various types of soil and degrees of compaction. Table 9.2 (abstracted from Reference 29) provides parameter values for four soil classifications, each with three levels of compaction. These "standard" values are conservative in the sense that they are typical of lower values of strength and moduli observed from numerous triaxial tests for each soil type. An independent study (30) to establish standard parameters for E_t utilizing the same data base is in good agreement with Table 9.2.

For convenience, the hyperbolic parameters in Table 9.2 are stored in CANDE and may be used by simply identifying soil type and level of compaction.

The behavior of the Duncan soil model for simulated uniaxial strain and triaxial loading tests is shown in Figures 9.2 through 9.5 for the standard parameters in Table 9.2. Specifically, Figure 9.2a shows axial stress vs. axial strain in confined compression for three compaction levels of coarse aggregates. The slope of these curves is the tangent

TABLE 9.2 Standard Hyperbolic Parameters

Unified Classification	RC Stand. AASHTO	γ_m kip/ft ³	ϕ_o deg	$\Delta\phi$ deg	C kip/ft ²	K	n	R _f	K _b	m
Coarse Aggregates GW, GP SW, SP	105	0.150	42	9	0	600	0.4	0.7	175	0.2
	95	0.140	36	5	0	300	0.4	0.7	75	0.2
	90	0.135	33	3	0	200	0.4	0.7	50	0.2
Silty Sand SM	100	0.135	36	8	0	600	0.25	0.7	450	0.0
	90	0.125	32	4	0	300	0.25	0.7	250	0.0
	85	0.120	30	2	0	150	0.25	0.7	150	0.0
Silty Clayey Sand SM-SC	100	0.135	33	0	0.5	400	0.6	0.7	200	0.5
	90	0.125	33	0	0.3	150	0.6	0.7	75	0.5
	85	0.120	33	0	0.2	100	0.6	0.7	50	0.5
Silty Clay CL	100	0.135	30	0	0.4	150	0.45	0.7	140	0.2
	90	0.125	30	0	0.2	90	0.45	0.7	80	0.2
	85	0.120	30	0	0.1	60	0.45	0.7	50	0.2

RC = Relative compaction
 γ_m = Weight density

$$\begin{aligned} \text{kip/ft}^3 &= 157.1 \text{ kN/m}^3 \\ \text{kip/ft}^2 &= 47.9 \text{ kN/m}^2 \end{aligned}$$

confined modulus (i.e. C_{11} in Equation 9.1) and are observed to increase with axial stress and compaction level. Figure 9.2b shows the behavior of the same soil models in triaxial loading. Here, the slope of the curve is the tangent Young's modulus E_t and are observed to decrease with shear stress and increase with compaction level as expected.

The remaining three pairs of figures illustrate the same trends for other soil types. The silty-sand soil type (Figures 9.3a,b) have the largest stiffness values (slopes) in confined compression, while the silty-clay (Figures 9.5a,b) have the lowest.

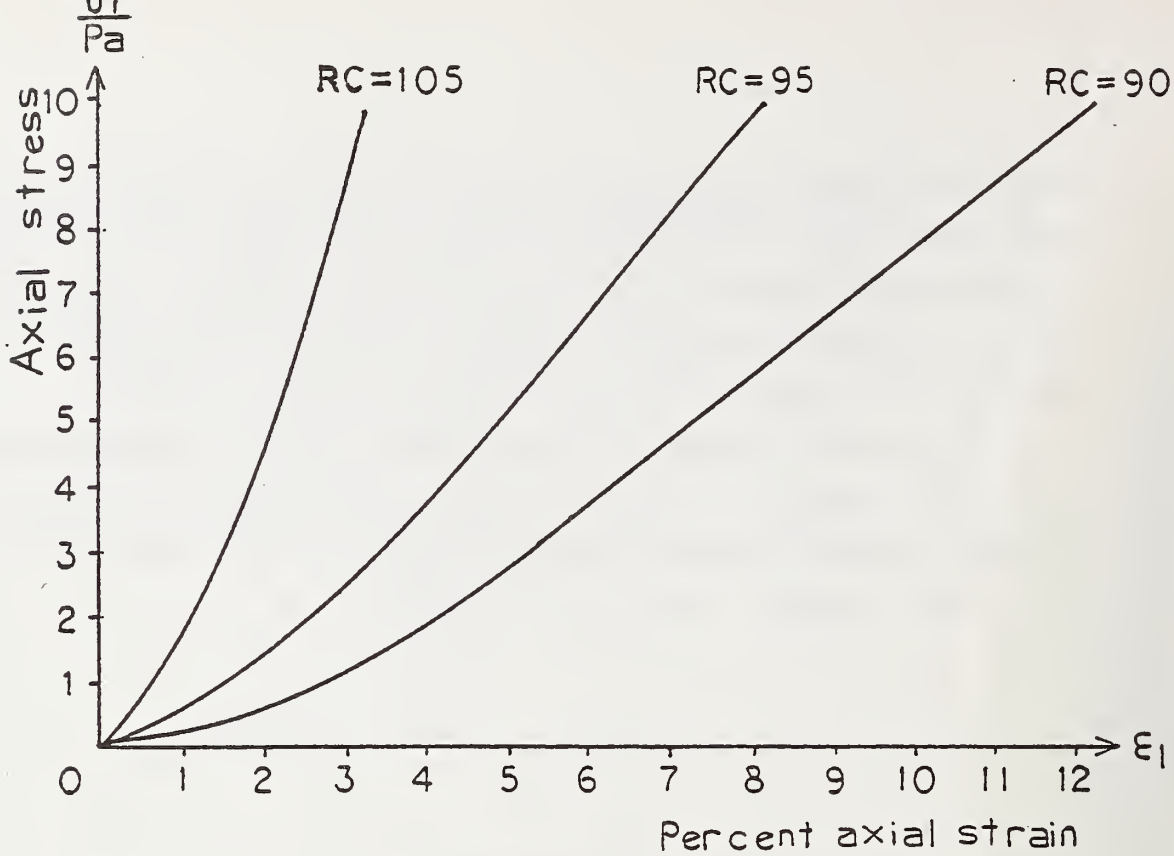


Figure 9.2a. Coarse Aggregates, Uniaxial Behavior

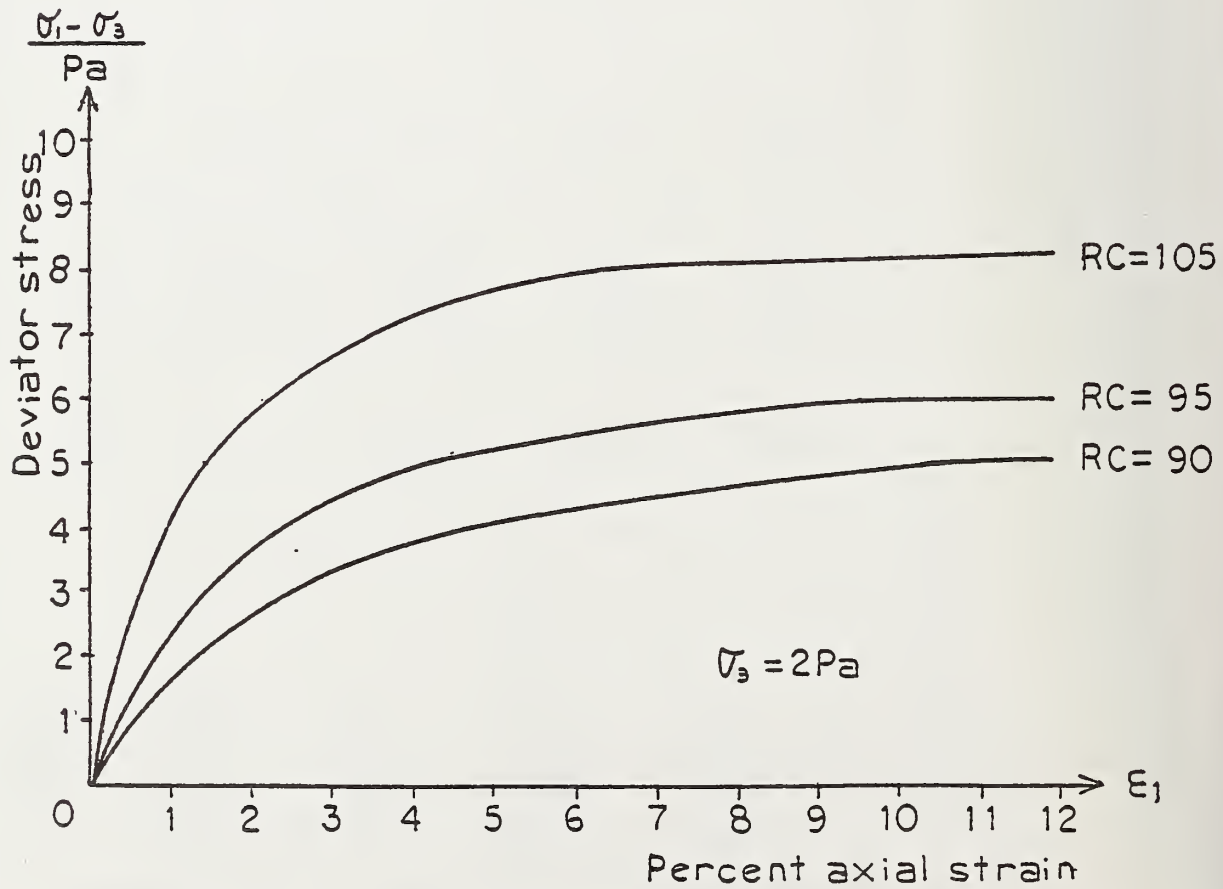


Figure 9.2b. Coarse Aggregates, Triaxial Behavior

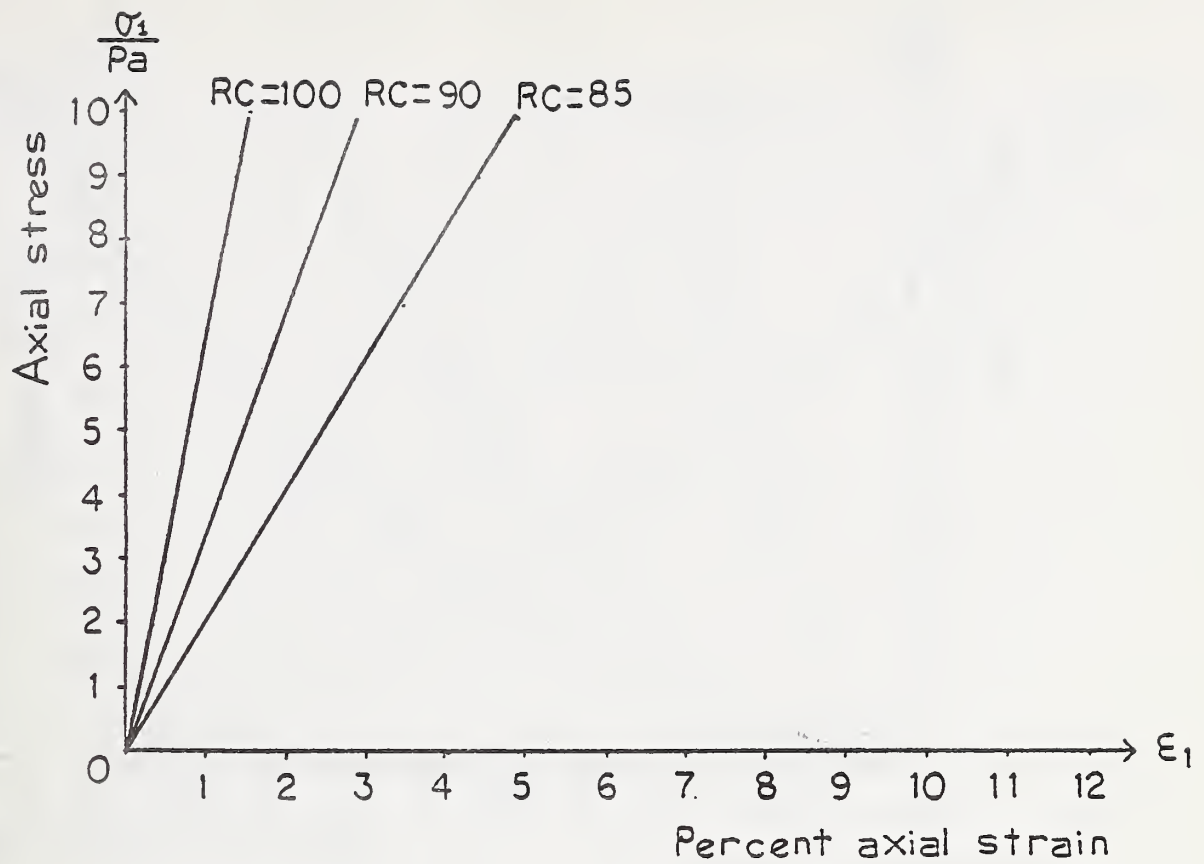


Figure 9.3a Silty Sand, Uniaxial Behavior

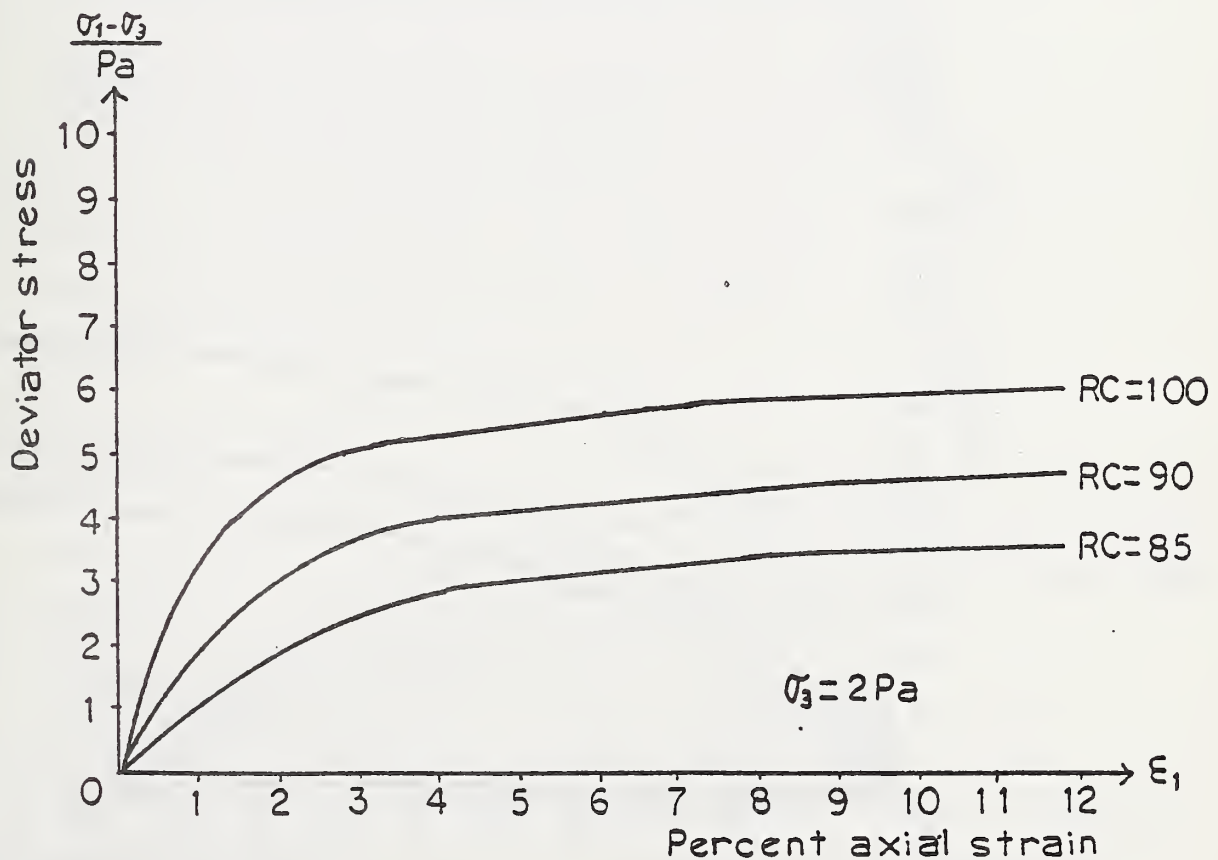


Figure 9.3b Silty Sand, Triaxial Behavior

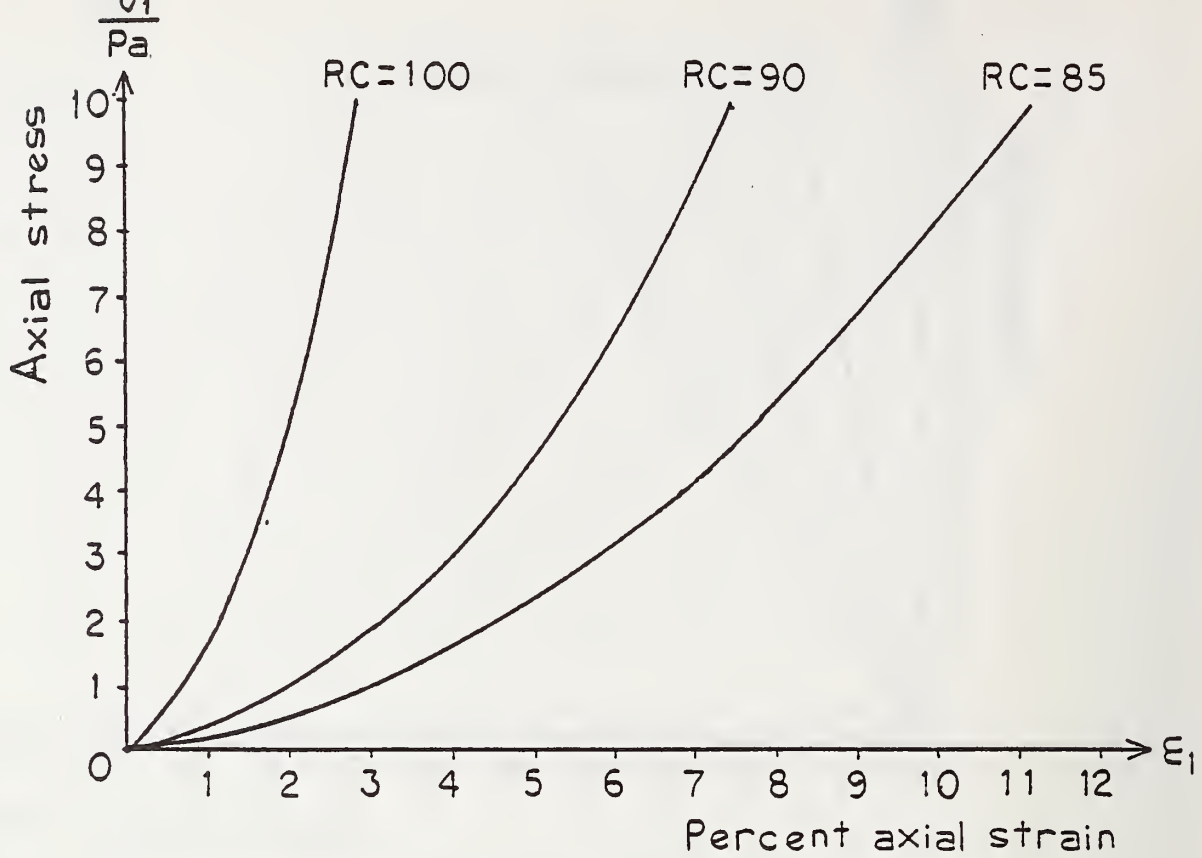


Figure 9.4a. Silty Clayey Sand, Uniaxial Behavior

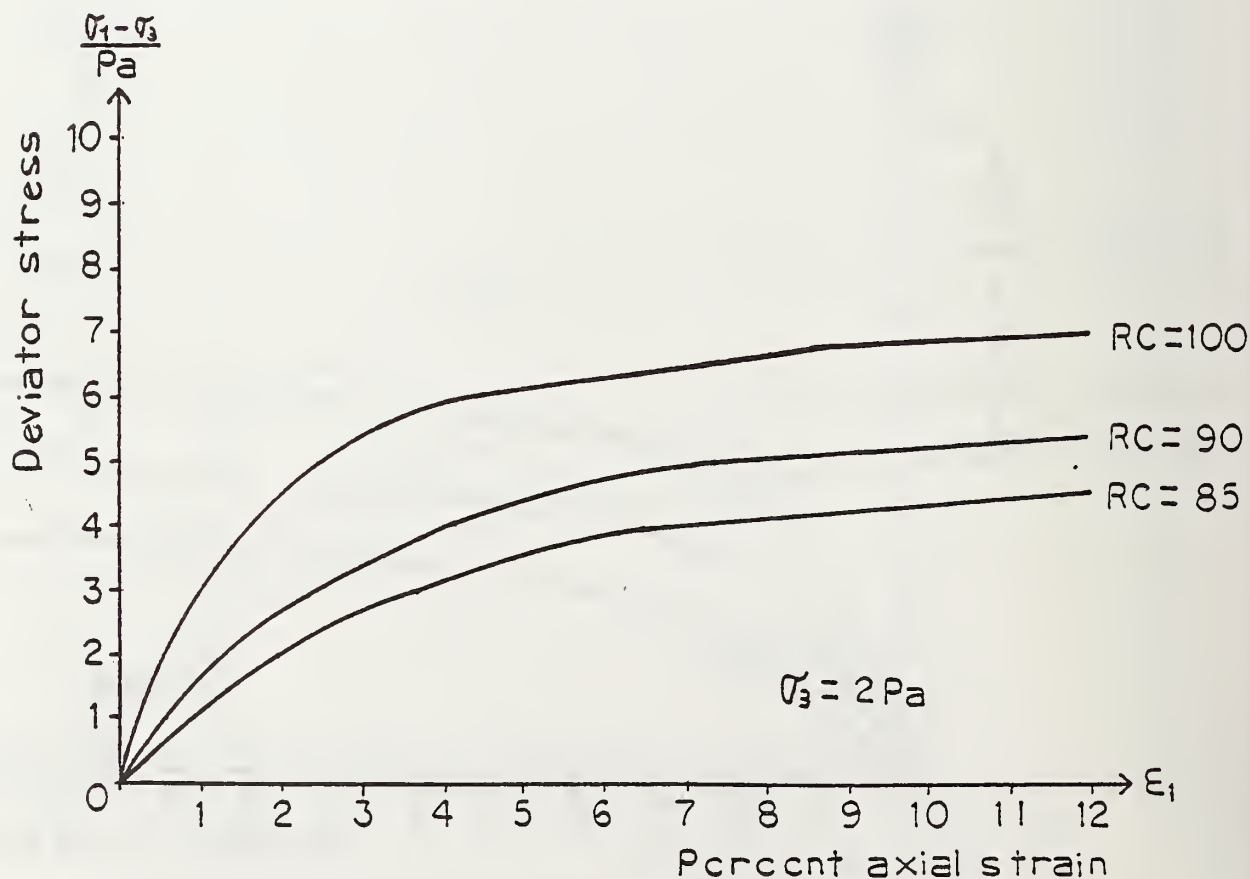


Figure 9.4b. Silty Clayey Sand, Triaxial Behavior

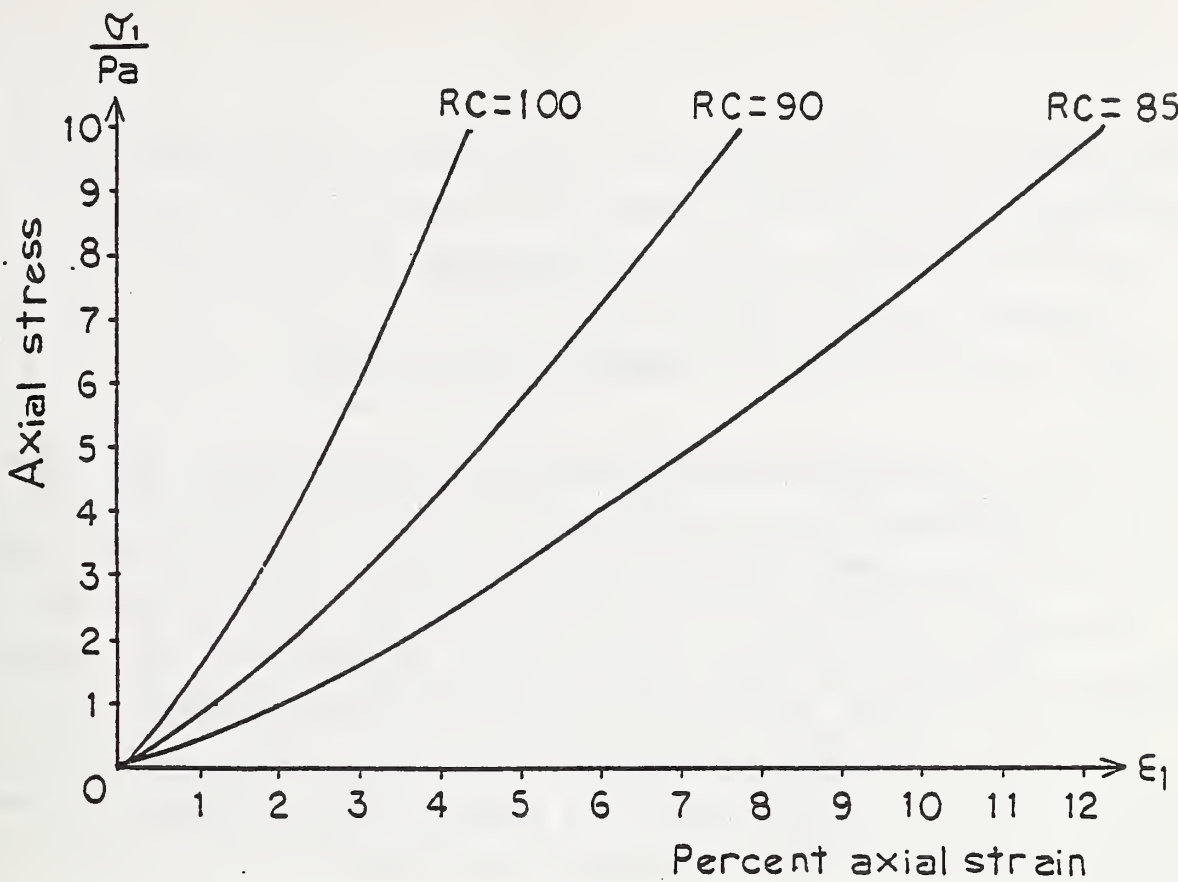


Figure 9.5a. Silty Clay, Uniaxial Behavior

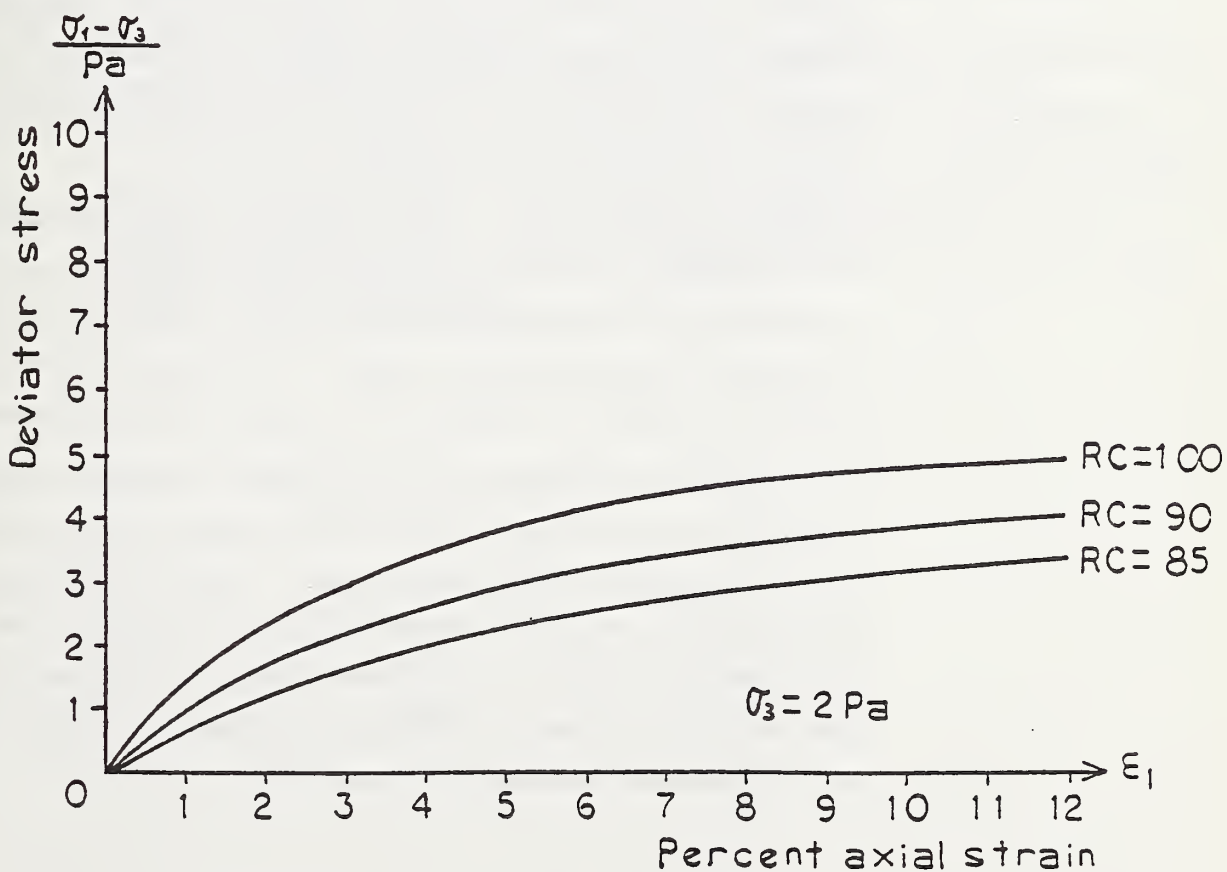


Figure 9.5b. Silty Clay, Triaxial Behavior

CHAPTER 10

SUMMARY AND CONCLUSIONS

This report presented a step by step development for the structural analysis of buried, precast reinforced concrete box culverts using the finite element method to model the soil-box system. Model predictions were validated with measured data from both in-ground and out-of-ground experimental tests. A user oriented soil-box model with automated finite element mesh generation is operational in the CANDE-1980 computer program and is referred to as "level 2 box" option. Also operational in CANDE-1980 is the Duncan soil model with simplified input options for standard types of soil. Specific findings and conclusions from this work are listed below.

1. Load-deformation curve predictions for reinforced concrete culverts are sensitive to the cracking strain parameter ϵ_t . However at ultimate flexural capacity, the maximum stresses of concrete f'_c and steel f_y are the controlling parameters with regard to the reinforced concrete model.
2. CANDE predictions are in good agreement with experimental data from reinforced concrete pipes in three-edge bearing. Better correlation for load-deformation curves was observed for pipes failing by flexure than by shear. Predicted ultimate loads, whether in shear or flexure, are within 10% of measured values.
3. The measured cracking load and ultimate load for reinforced concrete box culverts tested in four-edge bearing show good correlation with CANDE predictions. Predicted cracking loads averaged 10% lower and ultimate loads averaged 1% lower than experimental results. Predictions from the SGH design/analysis approach are similar to CANDE predictions but showed slightly more deviation from experimental data.

4. Measured soil pressures from a full scale buried box installation are in good agreement with CANDE predictions at both intermediate and final burial depths. Vertical soil pressures on top and bottom slabs were in very close agreement, whereas measured lateral pressures on the sides at full burial depth were somewhat lower than predicted.
5. Assumed soil load distributions on buried boxes used in the development of ASTM C789 design tables were compared with predicted soil load distributions determined from CANDE resulting in the following observations. (a) Vertical soil pressure on the top and bottom slabs are not uniform as assumed but increases monotonically from the centerline to the corners. (b) Shear traction on the sidewalls produces a significant downward force that must be equilibrated by an upward pressure on the bottom slab. (c) Soil stiffness is an important parameter for determining soil load distributions and magnitudes. The latter two effects are not presently taken into account in the ASTM loading assumptions.
6. Based on CANDE predictions, the design earth covers specified in ASTM C789 design tables are generally conservative providing good quality backfill soil is assumed. However, specified earth covers for boxes with high levels of reinforcement tend to be less conservative than specified earth covers for boxes with low levels of reinforcement.

APPENDIX A

DETAILS OF REINFORCED CONCRETE MODEL

The reinforced concrete beam-rod model presented in Chapter 3 is discussed in further detail in this appendix. This model replaces the original CANDE concrete pipe type and can be used with solution levels 1, 2 or 3. Subroutine CONMAT is the heart of the new reinforced concrete model wherein concrete cracking, loading to ultimate and unloading is simulated. For purposes of this appendix, it is presumed the reader is familiar with basic assumptions and general solution strategy presented in Chapter 3. Here attention is focused on programming details.

I. VARIABLES USED

To calculate the initial and load dependent mechanical properties of the reinforced concrete sections, parameters describing the material behavior of concrete and steel have to be defined. Some of these parameters are primary (defined by input) while others are secondary (derived from primary). The main purpose of these parameters is to define an idealized stress-strain diagram for concrete and for the steel reinforcement (see Figure A.1, A.2). The following parameters are primary input data for the material properties, where, in parentheses, are the default values used in CANDE.

ϵ_t = concrete strain at tensile cracking (0.000 in/in)

ϵ_y = concrete strain at elastic limit (0.5 f'_c/E_1)

ϵ'_c = concrete strain at f'_c (0.002 in/in)

f'_c = unconfined compressive strength of concrete (4000 psi)

E_1 = Young's modulus for linear concrete ($33\sqrt{f'_c}(\gamma_c)^{1.5}$)

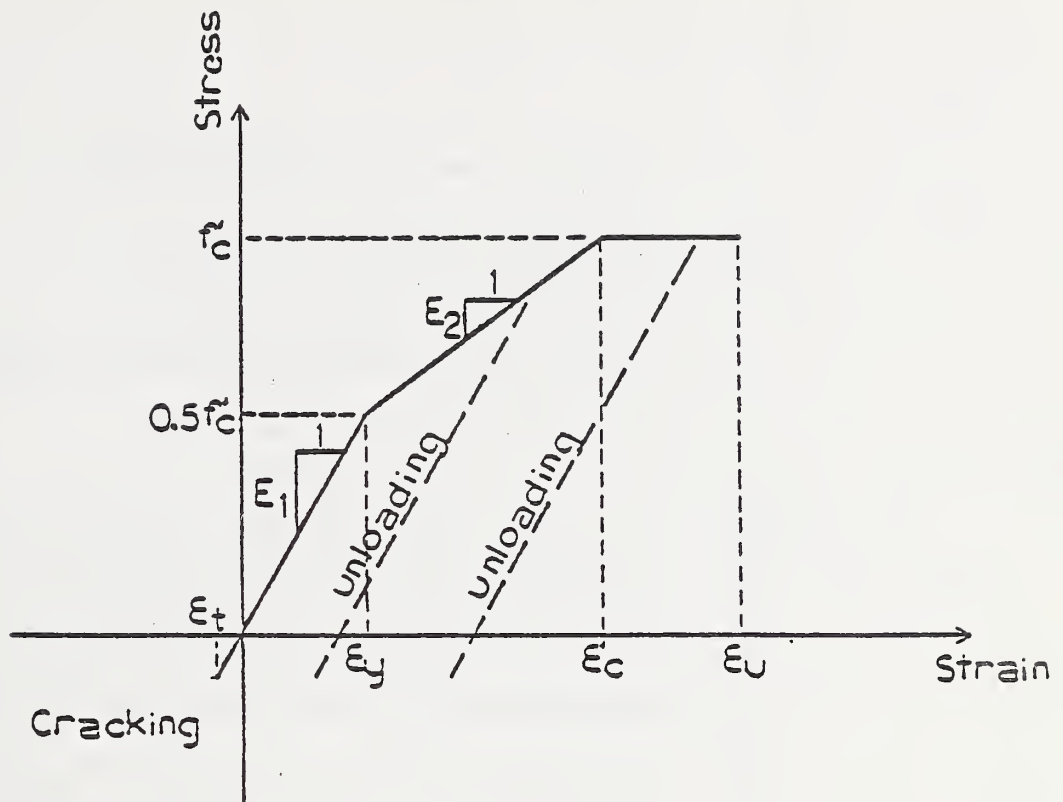


Figure A.1 - Idealized Concrete Stress-Strain Diagram.

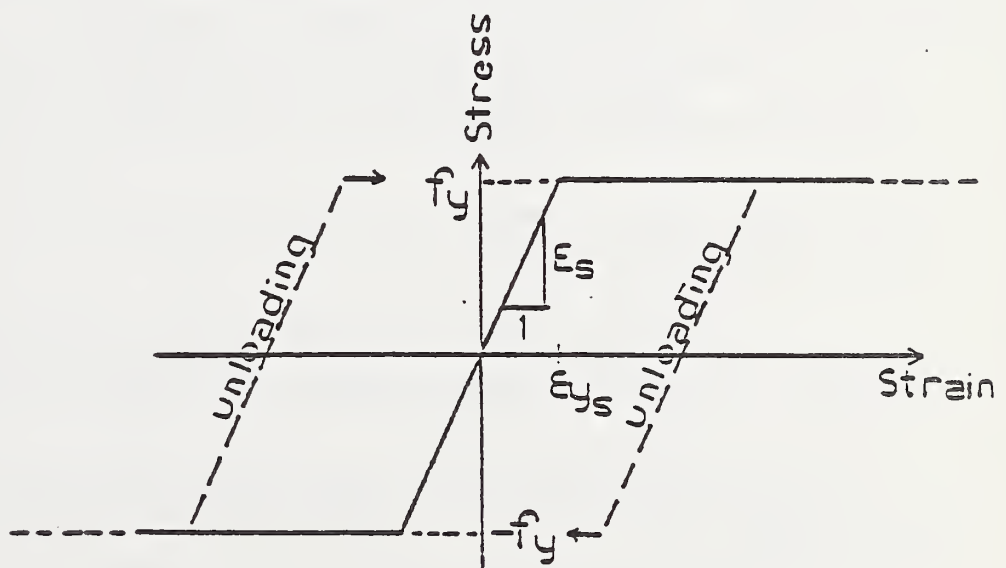


Figure A.2 - Idealized Steel Stress-Strain Diagram.

ν_c = Poisson's ratio for concrete (0.17)
 γ_c = unit weight of concrete (150 pcf)
 f_y = yield stress of steel (40000 psi)
 E_o = Young's modulus of steel (29×10^6 psi)
 ν_s = Poisson's ratio of steel (0.30)

The following are secondary parameters derived from primary data:

E_c = confined elastic modulus of concrete ($E_1 / (1 - \nu_c^2)$)
 ν_c = shear strength of concrete ($2\sqrt{f'_c}$ psi)
 f_t = maximum tensile stress of concrete ($\epsilon_t \times E_1$)
 f_{yc} = concrete stress at elastic limit ($\epsilon_y \times E_1$)
 E_s = confined elastic modulus of steel ($E_o / (1 - \nu_s^2)$)
 n = concrete-to-steel modulus ratio (E_c / E_s)

In addition, the analysis mode requires (see Figure A.4):

h = wall thickness of concrete (in)
 A_{s_i} = area of inner reinforcement per unit length of pipe
 (in^2/in)
 A_{s_o} = area of outer reinforcement per unit length of pipe
 (in^2/in)
 c_i = concrete cover on inner reinforcement (1.25 in)
 c_o = concrete cover on outer reinforcement (1.25 in)

Using these parameters the initial uncracked section properties are defined as:

Effective axial stiffness:

$$EA^* = E_c (h + (n-1) A_{s_i} + (n-1) A_{s_o})$$

Neutral axis of bending:

$$\bar{y} = E_c \frac{\left(\frac{h^2}{2} + A_{s_i}(n-1)c_i + A_{s_o}(n-1)(h-c_o)\right)}{EA^*}$$

Effective bending stiffness:

$$EI^* = E_c \left[\frac{h^3}{12} + \left(\frac{h}{2} - \bar{y}\right)^2 h + (n-1) (A_{s_i}(c_i - \bar{y})^2 + A_{s_o}(h - c_o - \bar{y})^2) \right]$$

The above section properties EA^* , \bar{y} and EI^* are for the uncracked cross section of 1 inch width with no loading. Now that the initial stiffnesses of the beam-rod sections are defined, the beam-rod elements are ready to be analyzed for the first load increment.

II. PROCEDURE TO CALCULATE THE SECTION PROPERTIES

Using the initial section properties above, the structural system is solved for the first load increment resulting in trial solutions for thrust and moment increments within each element. Due to the non-linearity of the materials, the initially assumed section properties are modified and another trial solution is obtained. This iterative solution technique, which considers the average stress state during the increment to find effective section properties, is repeated until convergence within the load step is achieved.

CONMAT subroutine evaluates EA^* , \bar{y} , and EI^* for each element until all elements converge as the system advances from load step $i-1$ to load step i . The procedure used for each load step is as follows:

- a) For each element an increment of moment and thrust is obtained from the general solution process. If a section initially cracks or extends its crack, the stresses in the newly cracked region are zero, thus, the pre-existing stresses prior to cracking must be redistributed. This redistribution can be achieved with corrections to the thrust and moment increment (called here thrust and moment redistribution). In our approach this correction is made after the inner loop convergences, so that, initially, moment and thrust redistribution is zero (see step h

for redistribution).

b) Assuming the section properties EA^* , \bar{y} , and EI^* from the converged solution at load increment $i-1$ and using the increment of moment and thrust, a linear strain distribution for the section is calculated (see Figure A.3).

$$\epsilon_i = \epsilon_{i-1} + \frac{\Delta N}{EA^*} + \frac{\Delta M}{EI^*} (y - \bar{y})$$

where

ϵ_{i-1} = strain distribution from converged solution at load increment $i-1$

ΔN = increment of thrust + (thrust redistribution, last iteration)

ΔM = increment of moment + (moment redistribution, last iteration)

y = spatial coordinate from section bottom.

This linear strain distribution ϵ_i is the first tentative solution of the iterative procedure.

For computational convenience, the section stiffness properties of EA^* and EI^* (defined in Chapter 3) are divided by the confined-elastic concrete modulus E_c^* , so that we may define A^* and I^* as:

$$A^* = EA^*/E_c^*$$

$$I^* = EI^*/E_c^*$$

Or more explicitly, to obtain section properties the following integrals must be evaluated (see Figure A.4):

$$A^* = \int_0^h FE(y) dy + WSI (n-1) A_{si} + (WSO)(n-1) A_{so}$$

$$\bar{y} = \frac{\int_0^h FE(y) y dy + WSI (n-1) y_{ti} A_{si} + WSO (n-1) y_{to} A_{so}}{A^*}$$

$$I^* = \int_0^h FE(y) (\bar{y} - y)^2 dy + WSI (n-1) (y_{ti} - \bar{y})^2 A_{si} + WSO (n-1) (y_{to} - \bar{y})^2 A_{so}$$

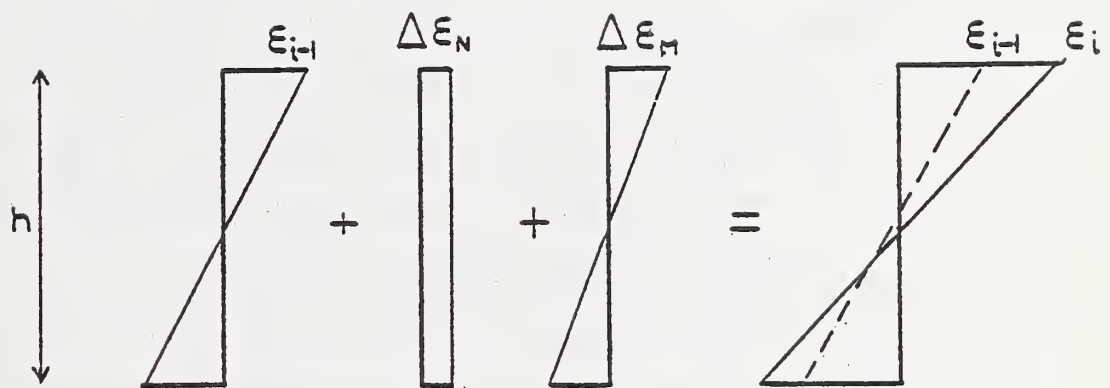


Figure A.3 - Strain Distribution at Load Increment i .

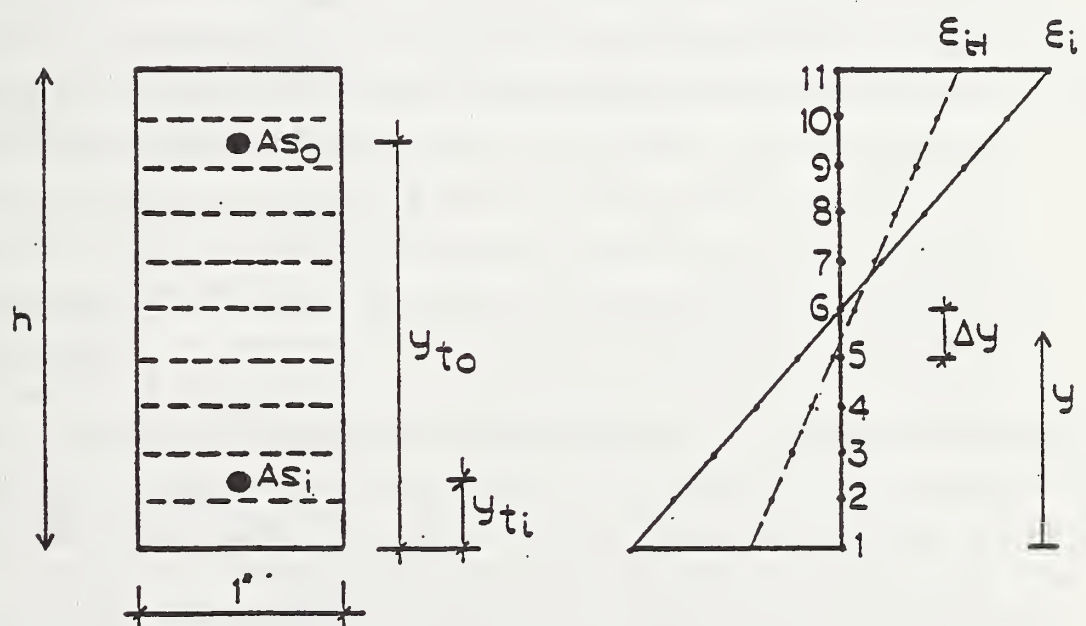


Figure A.4 - Integration Points of the Cross Section.

where:

$$FE(y) = E'_c/E_c \quad (\text{modulus reduction ratio for concrete})$$

$$WSI = E'_s/E_s \quad (\text{for inner reinforcement reduction})$$

$$WSO = E'_s/E_s \quad (\text{for outer reinforcement reduction})$$

E'_c = tangent modulus of concrete

E'_s = tangent modulus of steel

Using the above formulas and the strain distribution, ϵ_i , the new properties EA^* , y^* and EI^* are calculated. From the formulas it is observed that the concrete part of the section requires an integration of $FE(y)$ to evaluate its properties, where the function $FE(y)$ is not smooth. Thus, Simpson's integration is performed for the concrete section using eleven points along its depth (see Figure A.4).

c) The concrete is analyzed first using the strain distribution ϵ_{i-1} and ϵ_i . The integration points are analyzed one at a time, dependent, in part, on the value $FE(y)$. The first step is to update the record for the maximum stress-strain occurrence of each point during its loading history. Specifically, the converged strain distribution of load step $i-1$ and the maximum strain-stress values of the point computed in previous steps are used to identify if there are new maximum values to be saved. If the strain of the point at load step $i-1$ is less than any previous maximum strain, no change is made in the history vector. If the strain of the point at load step $i-1$ is greater than the maximum strain, a new maximum was reached for that point at load step $i-1$. Using the new maximum strain, the new maximum stress is computed using the old maximum stress-strain value located along the basic stress-strain diagram (see Figure A.1). The value of the maximum stress-strain of the point is saved and subsequently used to define the unloading and reloading path of the stress-strain diagram at load step i .

d) A comparison of the strain ϵ_i with ϵ_{i-1} for the integration point indicates if the point is loading or unloading. If the point is unloading ($|\epsilon| < |\epsilon_{i-1}|$) the stress σ_i of the point can be calculated

knowing that the unloading is elastic,

$$\sigma_i = \sigma_{\max} + (\epsilon_i - \epsilon_{\max}) E_c$$

where $(\sigma_{\max}, \epsilon_{\max})$ = maximum stress-strain value

ϵ_i = strain of the point at load step i

If the point was not previously cracked and σ_i doesn't reach the concrete tensile strength then $FE(y) = 1.0$, if the point was previously cracked and σ_i is in compression then $FE(y) = 1.0$. Otherwise $FE(y)$ is 0.0 (see Figure A.5).

If the point is loaded, it can be initial loading or reloading. Using the previous strain-stress values $(\epsilon_{i-1}, \sigma_{i-1})$ and the maximum strain-stress of the point $(\epsilon_{\max}, \sigma_{\max})$, the loading or reloading cases are identified. If the previous values are equal to the maximum it means initial loading, otherwise it means reloading. Once the case is defined and the values of $(\epsilon_{i-1}, \sigma_{i-1})$ and $(\epsilon_{\max}, \sigma_{\max})$ are known, the case falls in one of the possible point histories presented in Figure A.5. Knowing in what case the point is, the stress value σ_i of the point for load step i is evaluated. Now that the stress-strain value (σ_i, ϵ_i) is defined. E'_c is determined by the slope between $(\epsilon_{i-1}, \sigma_{i-1})$ and (ϵ_i, σ_i) . Thus $FE(y)$ for each point is:

$$FE(y) = \frac{(\sigma_i - \sigma_{i-1})}{(\epsilon_i - \epsilon_{i-1})/E_c}$$

This procedure is executed until $FE(y)$ is defined for the eleven integration points.

e) In the previous step (d), when the value of $FE(y)$ is determined for each integration point, at the same time, it is possible to determine what points are cracked or uncracked. With this data and doing a linear interpolation of stresses between the points of crack and no crack, the crack depth of the section is calculated. This calculated crack depth is printed out. Note crack depth is completely different than crack width discussed in Chapter 3.

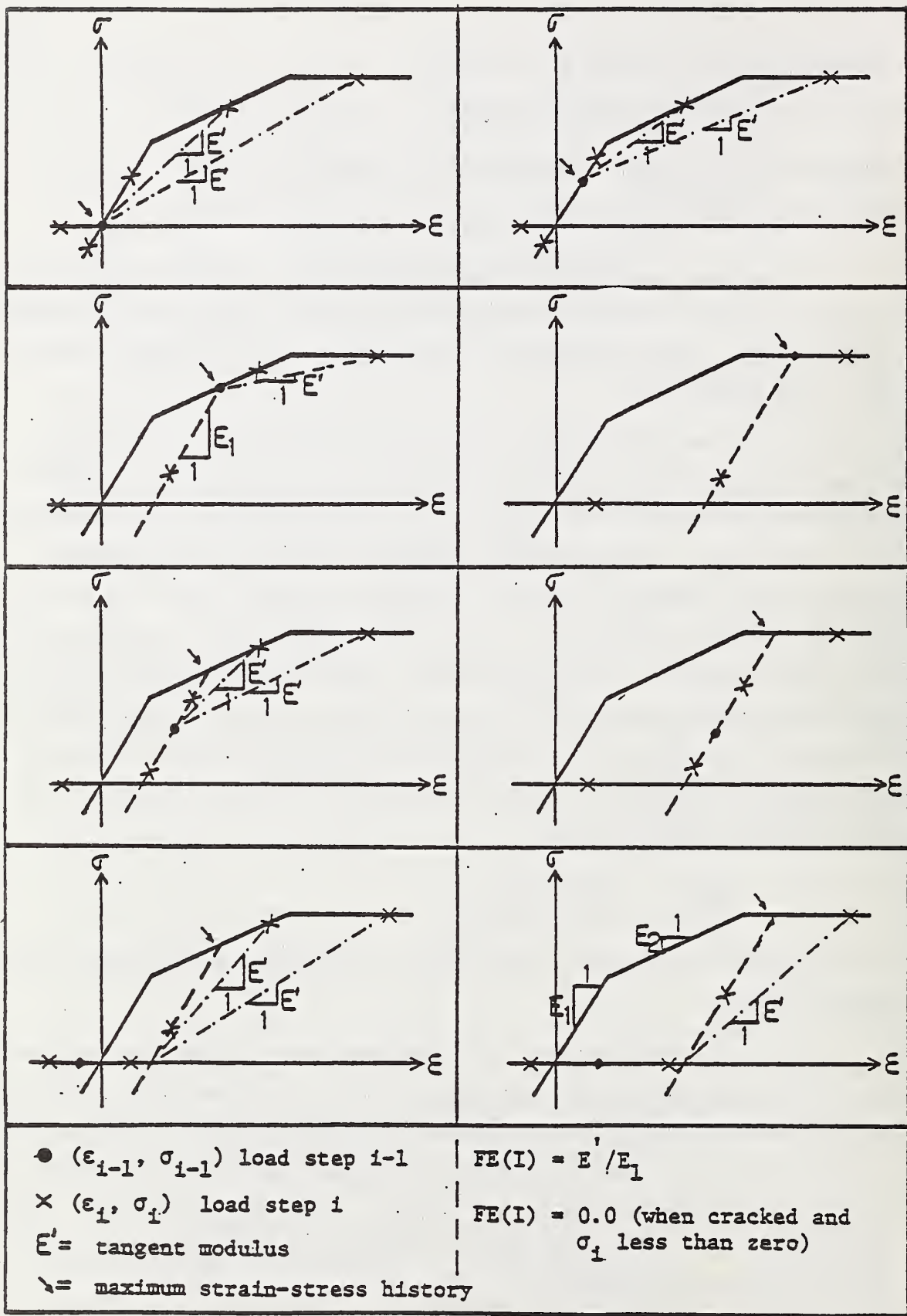


Figure A.5 - Modulus Function for all Possible Concrete Strain Histories at a Point in the Beam Cross Section.

f) Knowing the cross section strain distribution ϵ_{i-1} , ϵ_i and the location of the reinforcement in the cross section, the strains of the inner and outer reinforcement are calculated for load step $i-1$ and i . Using the stress-strain values at load step $i-1$ and the strain value at load step i for the reinforcement, the value of the stress at load step i is calculated for elastic loading or unloading as:

$$\sigma_i = \sigma_{i-1} + (\epsilon_i - \epsilon_{i-1}) E_s$$

For plastic loading we have:

$$\sigma_i = f_y \quad (\text{steel yielding stress})$$

This procedure applies to both inner and outer reinforcement. Using their stress-strain values, the factors WSI and WSO for the inner and outer reinforcement are calculated respectively as follows:

$$\begin{aligned} WSI &= \frac{(\sigma_i - \sigma_{i-1})}{(\epsilon_i - \epsilon_{i-1}) E_s} \quad (\text{stress-strain values for the inner reinforcement}) \\ WSO &= \frac{(\sigma_i - \sigma_{i-1})}{(\epsilon_i - \epsilon_{i-1}) E_s} \quad (\text{stress-strain values for the outer reinforcement}) \end{aligned}$$

All the possible cases of strain histories for the steel reinforcement are shown in Figure A.6.

g) With the preceding developments, the section properties defined in step b are evaluated with the aid of eleven point Simpson integration as follows:

$$\begin{aligned} A^* &= \text{SUM1} + \text{SI} + \text{SO} \\ -y &= (\text{SUM2} + y_i \text{ SI} + y_o \text{ SO})/A^* \\ I^* &= \bar{y}^2 \text{ SUM1} - 2\bar{y} \text{ SUM2} + \text{SUM3} + (y_i - \bar{y})^2 \text{ SI} + (y_o - \bar{y})^2 \text{ SO} \end{aligned}$$

In the above, SUM1, SUM2, and SUM3 represent the concrete contributions and are the numerical integrations of the integrands $FE(y)$, $yFE(y)$ and $y^2FE(y)$, respectively, i.e.,

$$\text{SUM1} = \frac{\Delta y}{3} (FE(1) + 4FE(2) + 2FE(3) + \dots + FE(11))$$

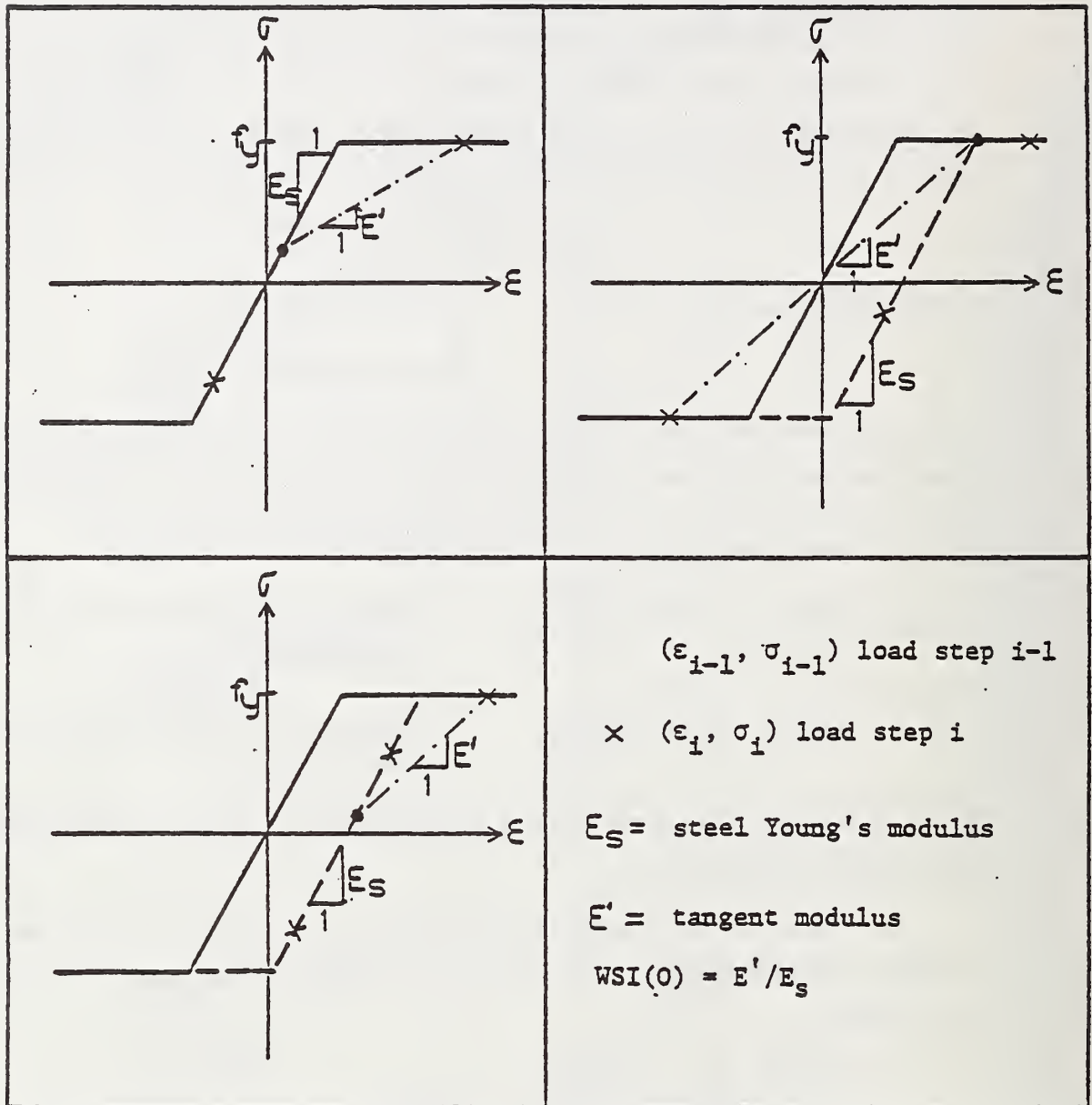


Figure A.6 - Modulus Function for all Possible Steel Strain Histories at a Point in the Beam Cross Section.

$$\text{SUM2} = \frac{\Delta y}{3} (\text{FE}(1)y_1 + 4\text{FE}(2)y_2 + 2\text{FE}(3)y_3 + \dots + \text{FE}(11)y_{11})$$

$$\text{SUM3} = \frac{\Delta y}{3} (\text{FE}(1)y_1^2 + 4\text{FE}(2)y_2^2 + 2\text{FE}(3)y_3^2 + \dots + \text{FE}(11)y_{11}^2)$$

Steel contributions SI and SO are associated with inner and outer reinforcement and are given by:

$$SI = WSI(n-1)A_{si}$$

$$SO = WSO(n-1)A_{so}$$

If either or both reinforcements are located in a cracked zone, the value of "n" is used instead of "n-1". That is, n-1 accounts for the reinforcement hole in uncracked concrete.

These values of A^* , \bar{y} and I^* are compared with the assumed values at step (b). The value A^* is used to check convergence. If the convergence is not reached, a new set of strains ϵ_i are evaluated at step (b) using the new A^* , \bar{y} , I^* . The entire procedure is repeated until successive values of A^* , \bar{y} , and I^* converge or after four iterations (inner loop), then the program goes to the next step h.

h) Now that new values of A^* , \bar{y} and I^* are known for the cross section at load step i (however, convergence of ΔM and ΔN are not yet assured), a modified set of strain-stress values (ϵ_i, σ_i) for each point in the cross section is computed to account for stress redistribution due to cracking. These values are compared with the strain-stress value $(\epsilon_{i-1}, \sigma_{i-1})$. If for some point the stress σ_i implies that the point is cracked and was not previously cracked, it means that the stress σ_{i-1} must be redistributed to the remaining uncracked concrete and reinforcement. The procedure adopted in the program is to evaluate an equivalent moment and thrust to be redistributed due to the cracking of those points at load step i, where:

$$\Delta N_R = \Sigma \Delta y \cdot \sigma_{i-1} \quad (\text{thrust redistribution})$$

$$\Delta M_R = \Sigma \Delta y \cdot \sigma_{i-1} (\bar{y} - y) \quad (\text{moment redistribution})$$

After the moment and thrust redistribution is complete the program is ready to go to step (a) and do the same procedure for the next element (node).

i) All elements of the reinforced concrete structure are analyzed and the values of A^* , \bar{y} , I^* , ΔN_R and ΔM_R are calculated for each one. If the values of A^* and \bar{y} obtained for every element converge with the ones obtained in the previous iteration and ΔN_R , ΔM_R are zero for all the nodes, the trial solution has converged. Otherwise, the system is solved again using the values of A^* , \bar{y} and I^* from the last iteration. This is called "inner loop" iteration. Once the inner loop converges, the section properties, EA^* , \bar{y} , EI^* , are used to get another solution to the entire soil-structure system. This gives new values for ΔM and ΔN to repeat the inner loop. Successive solutions for ΔM and ΔN is called outer loop iteration.

Outer loop iteration is repeated until a convergence is reached between successive solutions for ΔM and ΔN . If convergence is not reached after six trial response solutions, the program assumes the last one as an approximate solution and advances to next load step.

APPENDIX B

CANDE-1980: USER MANUAL SUPPLEMENT

The following user's guide is a supplement to the 1976 "CANDE USER MANUAL" (2). This supplement provides input instructions for the new options on reinforced concrete box culverts and Duncan soil model described in the main body of this report.

The original 1976 manual is still the principal reference source and may be used without reference to this supplement if the new options are not desired. Taken together, the original and new options form the program called CANDE-1980. Input instructions for CANDE-1980 follows the same pattern as the original program, composed of three main sections (A, B, and C) as shown in Figure B.1, where new options are marked with an asterisk.

Section A is the master control input (card 1A) and is unchanged from the original program. Section B (cards 1B to 3B) includes a new input option for modeling reinforced "concrete box" culverts in addition to the original pipe types. The "concrete box" culvert type is only operative in the analysis mode and cannot be used with solution level 1. Section C (card sets C and D) includes the new "level 2 box" finite element generation scheme discussed in Chapter 6 along with the new Duncan soil model option presented in Chapter 9.

The supplemental input instructions to be given here provide a complete set of data input for the subset of options shown in Figure B.2. Thus, these instructions are self contained for "level 2 box" solutions with any soil model. For extended level 2 and level 3 options, however, the 1976 user manual must also be used where noted.

Formatted input instructions for Sections A, B, and C are presented in order, followed by explanatory comments and illustrations. Example input-output data is given in the next appendix.

SECTION A - MASTER CONTROL: CARD 1A

- Execution mode = design or analysis
- Culvert (pipe) type = steel, etc.
- Solution Level = 1,2, or 3 (option, level 2-extended)

SECTION B - CULVERT TYPE INPUT: CARDS 1B up to 3B

Steel	Aluminum	Concrete Pipe	Plastic	Basic	Concrete* box
1B, 2B	1B, 2B	1B, 2B, 3B	1B, 2B	1B, 2B	1B, 2B, 3B

SECTION C - SOLUTION LEVEL INPUT: CARDS C1 up to C7

Level-1	Level-2 pipe	Level-2 box*	Level-2 extended	Level-3
1C, 2C	1C, 2C, 3C	1C, 2C	4C to 7C	1C to 5C

End

SOIL MODELS: CARDS D1 up to D4

Elastic	Ortho Elastic	Duncan* model	Over-Burden	Hardin model	Interface
1D, 2D	1D, 2D	1D to 4D	1D, 2D	1D, 2D	1D, 2D

End

* New CANDE Options.

FIGURE B.1 General Input Flow for CANDE-1980

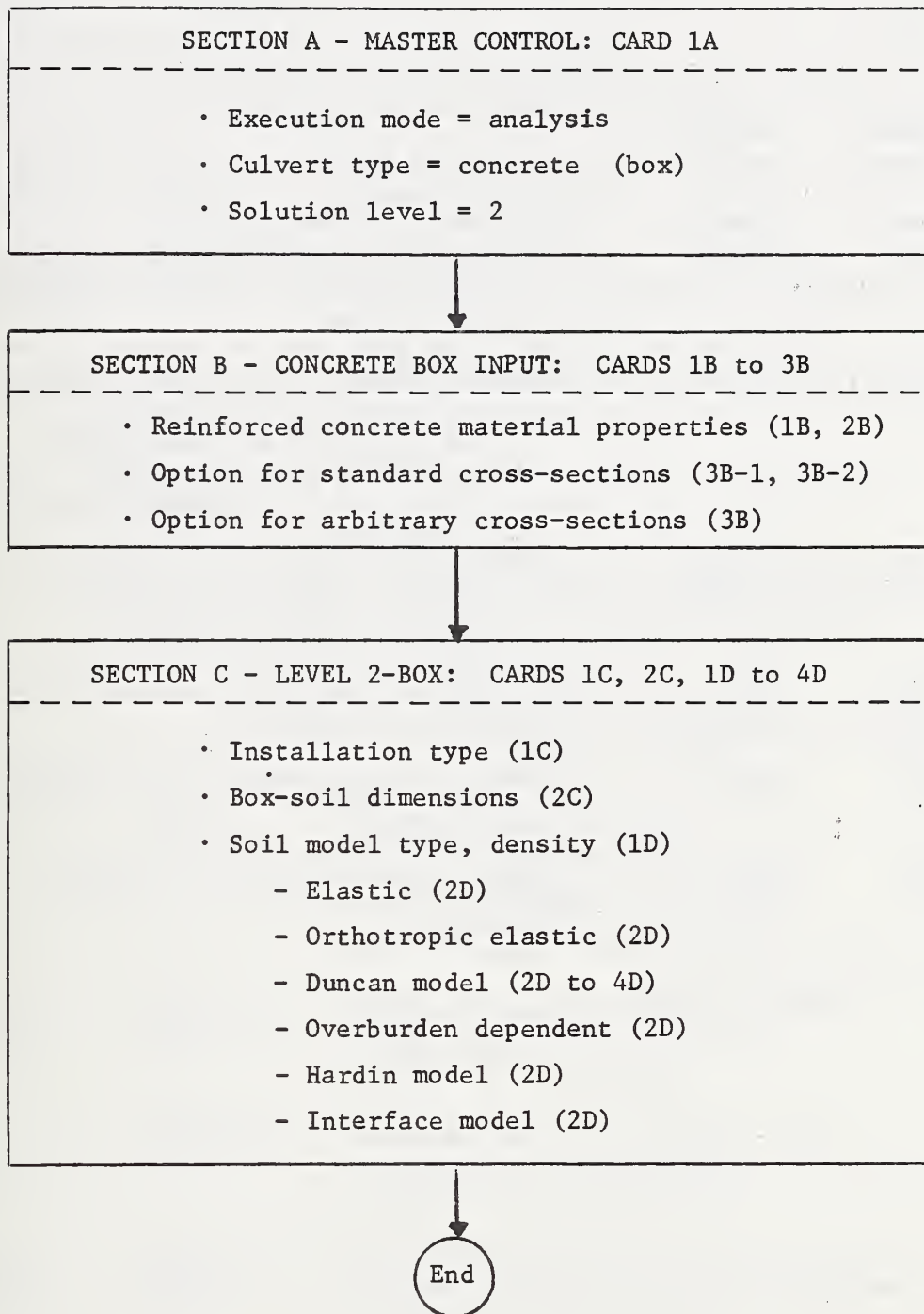


FIGURE B.2 Specific input flow for level-2 box culverts described in supplemental user's manual.

SECTION A - MASTER CONTROL CARD

Input

Card 1A. Master control card (one card per problem):

Columns (format)	Variable (units)	Entry Description	Notes
01-06 (A4,2X)	XMODE (word)	Word defining program mode, = ANALYS, denotes analysis problem = STOP, program terminates, last card in deck	(1)
08-08 (I1)	LEVEL	Defines solution level to be used = 2, denotes finite element solution with automated mesh = 3, denotes finite element solution with user-defined mesh	(2)
10-15 (A4,2X)	PTYPE (word)	Defines pipe material to be used, = CONCRE, denotes reinforced concrete (pipe or box)	(3)
17-76 (15A4)	HED (words)	User defined heading of problem to be printed with output	
77-78 (I2)	NPMAT	Number of pipe elements; only required when LEVEL = 3	
79-80 (I2)	NPPT	Number of pipe nodes; only required when LEVEL = 3	

*** GO TO SECTION B ***

SECTION B - BOX CULVERT

Reinforced Concrete Input (Cards 1B, 2B, 3B)

Card 1B. Material properties of reinforced concrete.

Columns (format)	Variable (units)	Entry Description	Notes
01-10 (F10.0)	PDIA (in.)	Any negative value. This signals program that is working with box culverts	(4)
11-20 (F10.0)	PT (in.)	Nominal concrete wall thickness. This value is used whenever wall thickness is not specified on Card 3B	(5)
22-25 (A4)	RSHAPE (word)	Control word to, select manner of input for cross section properties on Card 3B <ul style="list-style-type: none"> = ARBI, implies section properties at each node along connected sequence will be specified by user (arbitrary) = STD, implies simplified property input will be allowed in conjunction with Level 2 box mesh 	(6)
26-30 (I5)	NONLIN	Degree of nonlinearity, <ul style="list-style-type: none"> = 1, concrete cracking only = 2, also include nonlinear compression of concrete = 3, also include steel yielding 	(7)
31-40 (F10.0)	STNMAT (1) in/in.	Concrete strain at which tensile cracking occurs (positive), Default = 0.0 in/in.	(8)
41-50 (F10.0)	STNMAT (2) in./in.	Concrete strain at elastic limit in compression (positive) Default = 1/2 PFPC/PCE (see next card)	
51-60 (F10.0)	STNMAT (3) in/in.	Concrete strain at initial compressive strength, f'_c (positive), Default = 0.002 in/in.	

Card 2B. Concrete and steel properties:

Columns (format)	Variable (units)	Entry Description	Notes
01-10 (F10.0)	PFPC (psi)	Compressive strength of concrete, f'_c , Default = 4,000 psi	(8)
11-20 (F10.0)	PCE (psi)	Young's modulus of concrete in elastic range, Default = $33(\text{density})^{3/2} (f'_c)^{1/2}$	
21-30 (F10.0)	PNU	Poisson ratio of concrete, Default = 0.17	
31-40 (F10.0)	PDEN (pcf)	Unit weight of concrete (density) Default = 0.0 for body weight; however, Default = 150 pcf for modulus calculation	
41-50 (F10.0)	PFSY (psi)	Yield stress of reinforcing steel, Default = 40,000 psi	(9)
51-60 (F10.0)	PSE (psi)	Young's modulus of steel Default = 29×10^6 psi	
61-70 (F10.0)	PSNU	Poisson's ratio of steel, Default = 0.3	
71-80 (F10.0)	SL (in.)	Spacing of reinforcement Default = 2.0 in.	(10)

Card 3B. For RSHAPE = STD (only), two cards are required.
Only for Level 2 Box.

Card 3B-1. Concrete Box-wall dimensions

Columns	Variable	Entry Description	(Notes)
01-10 (F10.0)	PTT (in.)	Thickness of top slab Default = PT	(11)
11-20 (F10.0)	PTS (in.)	Thickness of side slab Default = PT	
21-30 (F10.0)	PTB (in.)	Thickness of bottom slab Default = PT	
31-40 (F10.0)	HH (in.)	Horizontal haunch dimension	(12)
41-50 (F10.0)	HV (in.)	Vertical haunch dimension	

Card 3B-2. Steel reinforcement dimensions

Columns	Variable	Entry Description	(Notes)
01-10 (F10.0)	AS1 (in. ² /in.)	Outer steel area, side wall	(13)
11-20 (F10.0)	AS2 (in. ² /in.)	Inner steel area, top slab	
21-30 (F10.0)	AS3 (in. ² /in.)	Inner steel area, bottom slab	
31-40 (F10.0)	AS4 (in. ² /in.)	Inner steel area, side wall	
41-50 (F10.0)	XL1	Length ratio of AS1 steel along top (bottom) slab	
51-60 (F10.0)	TC (in.)	Uniform thickness of cover to all steel centers Default = 1.25 in.	

*** GO TO SECTION C ***

Card 3B. For RSHAPE = ARBI (only) repeat this card for number of pipe nodes (NPPT*). This card may be used for Level 2 or Level 3.

Columns (format)	Variable (units)	Entry Description	Notes
01-10 (F10.0)	ASI (in. ² /in.)	Area of inner steel reinforcement	(14)
11-20 (F10.0)	ASO (in. ² /in.)	Area of outer steel reinforcement	
21-30 (F10.0)	TBI (in.)	Thickness of concrete cover to center of inner steel Default = 1.25 in.	
31-40 (F10.0)	TBO (in.)	Thickness of concrete cover to center of outer steel Default = 1.25 in.	
41-50 (F10.0)	PTV (in.)	Thickness of concrete Default = PT	

* In Level 2 solution NPPT = 15

*** GO TO SECTION C ***

SECTION C - SOLUTION LEVEL DESCRIPTION

Level 2 Input (Cards 1C, 2C, 1D, 2D)

Card 1C. Define mesh type, title, and special options:

Columns (format)	Variable (units)	Entry Description	Notes
01-04 (A4)	WORD	Name to identify type of automatic mesh = EMBA, embankment mesh = TREN, trench mesh	(15)
05-72 (17A4)	TITLE	User description of mesh to be printed with output	
73-76 (A4)	WORD1	Command to permit user to selectively modify the automatic mesh, = MOD, mesh will be modified ≠ MOD, mesh will not be modified (left, justified)	(16)

For level 3 input, see Section C in 1976 manual.

Card 2C. Define print options and mesh parameters:

Columns (format)	Variable (units)	Entry Description	Notes
01-05 (I5)	IPLOT	Signal to create a plot data tape on unit 10 = 0, no data tape created = 1, create data tape	
06-10 (I5)	IWRT	Signal to print out soil response for all elements, = 0, no soil response printed out = 1, print out soil response	
11-15 (I5)	MGENPR	Code to control amount of print out of mesh data, = 1, minimal printout; just control data = 2, above, plus node and element input data = 3, above, plus generated mesh data = 4, maximal printout of input data Default = 3	
16-20 (I5)	NINC	Number of construction increments, = -1, combine all lifts into one monolith = 0, used for data check only; all data is read but not executed = N, number of construction increments to be executed, N = 1 to 20	(17)
21-30 (F10.0)	R1 (in.)	Distance from center of the box to center of side wall	(18)
31-40 (F10.0)	R2 (in.)	Half of the distance from center of top slab to center of bottom slab.	
41-50 (F10.0)	HTCOVR (ft.)	Height of soil cover over the top of the box	(19)
51-60 (F10.0)	DENSTY (pcf)	Density of soil above truncated mesh to be used as equivalent overburden pressure	

continued

Card 2C. continued

Columns (format)	Variable (units)	Entry Description	Notes
61-70 (F10.0)	TRWID (ft.)	Width of trench; only required for WORD = TREN	(20)
71-80 (F10.0)	BDEPTH (in.)	Depth of bedding material Default = 12 in.	(21)

For extended level 2 option (WORD1=MOD), insert cards 4C to 7C here prior to card set D (See note 16). Otherwise, go directly to card set D.

Soil Data Cards:

Card 1D. Material identifier card (repeat D cards for each material)

Columns (format)	Variable (units)	Entry Description	Notes
01-01 (A1)	LIMIT	Last material card-set indicator; = 0, read another set of material definitions = L, this is the last material input	
02-05 (I4)	I	Material zone identification number for level 2 box use: = 1, for in-situ soil zones = 2, for bedding zones = 3, for fill soil zones	(22)
06-10 (I5)	ITYP	Selection of material model to be associated with material zone I, = 1, linear elastic (isotropic) = 2, linear elastic (orthotropic) = 3, Duncan soil model = 4, overburden dependent model = 5, Hardin soil model = 6, frictional interface (not operative with Level 2 box)	(23)
11-20 (F10.0)	DEN(I) (pcf)	Density of material I used to compute gravity loads; not applicable for ITYP = 6.	
21-40 (5A4)	MATNAM (words)	For ITYP = 3,4, or 5, MATNAM is used to select soil subgroup models as shown in Table B.1 on the next page. In all cases, MATNAM is printed out with the data but has no control for ITYP = 1, 2 or 6.	(24)

Go to card 2D corresponding to ITYP.

TABLE B.1. Soil models controlled by MATNAM (Card 1D)

MATNAM*	Soil Model Description
ITYP = 3, Duncan soil model, Chapter 9, Table 9.2	
CA105	coarse aggregate, relative compaction 105%
CA95	coarse aggregate, relative compaction 95%
CA90	coarse aggregate, relative compaction 90%
SM100	silty sand, relative compaction 100%
SM90	silty sand, relative compaction 90%
SM85	silty sand, relative compaction 85%
SC100	silty clayey sand, relative compaction 100%
SC90	silty clayey sand, relative compaction 90%
SC85	silty clayey sand, relative compaction 85%
CL100	clay, relative compaction 100%
CL90	clay, relative compaction 90%
CL85	clay, relative compaction 85%
USER	Parameters supplied by user
ITYP = 4, Overburden Dependent, 1976 CANDE manual, pg. 39	
GGOOD	granular soil, good compaction
GFAIR	granular soil, fair compaction
MGOOD	mixed soil, good compaction
MFAIR	mixed soil, fair compaction
CGOOD	cohesive soil, good compaction
CFAIR	cohesive soil, fair compaction
USER	parameters supplied by user
ITYP = 5, Hardin soil model, 1976 CANDE manual	
GRAN	granular soil, specified void ratio
MIXED	mixed soil, specified void ratio
COHE	cohesive soil, specified void ratio
TRIA	parameters specified by user (triaxial test)

* MATNAM must be left justified (i.e. start in column 21).
 Defaults are: MATNAM = USER for ITYP = 3 and 4, or
 MATNAM = MIXED for ITYP = 5.

Card 2D. ITYP = 1, linear elastic:

Columns (format)	Variable (units)	Entry Description	Notes
01-10 (F10.0)	E (psi)	Young's modulus of material I	(25)
11-20 (F10.0)	GNU	Poisson's ratio of material I	

Card 2D, ITYP = 2, orthotropic, linear elastic:

Columns (format)	Variable (units)	Entry Description	Notes
01-10 (F10.0)	CP(1,1) (psi)	Constitutive parameter at matrix position (1,1)	(26)
11-20 (F10.0)	CP(1,2) (psi)	Constitutive parameter at matrix position (1,2)	
21-30 (F10.0)	CP(2,2) (psi)	Constitutive parameter at matrix position (2,2)	
31-40 (F10.0)	CP(3,3) (psi)	Constitutive parameter at matrix position (3,3)	
41-50 (F10.0)	THETA (deg)	Angle of the material axis with respect to the global x-axis	

Card 2D, ITYP = 3, Duncan soil model

Columns (format)	Variable (units)	Entry Description	Notes
01-05 (I5)	NON	Maximum number of iterations Default = 5	(27)
06-15	RATIO	Moduli averaging ratio Default = 0.5	(28)

Go to cards 3D and 4D if MATNAM = USER. Otherwise input is complete for Duncan model.

Card 3D, Hyperbolic parameter for tangent Young's modulus

Columns (format)	Variable (units)	Entry Description	Notes
01-10 (F10.0)	C (psi)	Cohesion intercept	(29)
11-20 (F10.0)	PHIO (radians)	Initial friction angle	
21-30 (F10.0)	DPHI (radians)	Reduction in friction angle for a 10-fold increase in confining pressure	
31-40 (F10.0)	ZK	Modulus number, K	
41-50 (F10.0)	ZN	Modulus exponent, N	
51-60 (F10.0)	RF	Failure ratio, R_f	

Card 4D, Hyperbolic parameters for tangent bulk modulus, or constant Poisson ratio option.

Columns (format)	Variable (units)	Entry Description	Notes
01-10 (F10.0)	BK	Bulk modulus number, K_b	(30)
11-20 (F10.0)	BM	Bulk modulus number, M	
21-30 (F10.0)	VT	Poisson's ratio. If a nonzero value is entered, the bulk modulus is not used. Instead, the specified constant VT is used.	

Card 2D, * ITYP = 4 (MATNAM = USER), Overburden dependent model, user defined table, repeat Card 2D as needed to define input table, last card is blank to terminate reading.

Columns (format)	Variable (units)	Entry Description	Notes
01-10 (F10.0)	H(N) (psi)	Overburden pressure for table entry N	(31)
11-20 (F10.0)	E(N) (psi)	Young's secant modulus for table entry N	
21-30 (F10.0)	GNV(N)	Poisson's ratio table entry N	

* Note, Card 2D is not required if MATNAT is other than USER since overburden dependent tables are stored in CANDE for specified categories of soil.

Card 2D. ITYP = 5, and MATNAM = GRAN, MIXE, or COHE; Extended-Hardin model for three soil classifications:

Columns (format)	Variable (units)	Entry Description	Notes
01-10 (F10.0)	XNUMIN	Poisson's ratio at low shear strain Default = 0.10	(32)
11-20 (F10.0)	XNUMAX	Poisson's ratio at high shear strain Default = 0.49	
21-30 (F10.0)	XQ	Shape parameter q for Poisson's ratio function Default = 0.26	
31-40 (F10.0)	VOIDR	Void ratio of soil, range 0.1 to 3.0	
41-50 (F10.0)	SAT	Ratio of saturation, range 0.0 to 1.0	
51-60 (F10.0)	PI	Plasticity-index/100, range 0.0 to 1.0	
61-65	NON	Maximum iterations per load step; Default = 5	

Card 2D. ITYP = 5, and MATNAM = TRIA; Extended-Hardin model for triaxial data input

Columns (format)	Variable (units)	Entry Description
01-30	-----	Same as card above (XNUMIN, XNUMAX, XQ)
31-40 (F10.0)	S1	Hardin parameter used to calculate maximum shear modulus
41-50 (F10.0)	C1	Hardin parameter used to calculate reference shear strain
51-60 (F10.0)	A	Hardin parameter used to calculate hyperbolic shear strain
61-65 (I5)	NON	Maximum iterations per load step Default = 5

Card 2D. ITYP = 6, interface property definition

Columns (format)	Variable (units)	Entry Description	Notes
01-10 (F10.0)	ANGLE (deg)	Angle from x-axis to normal of interface	(33)
11-20 (F10.0)	FCOEF	Coefficient of friction	
21-30 (F10.0)	TENSIL (lb/in)	Tensile breaking force of contact nodes	

* * * End of input * * *

COMMENTARY NOTES

- (1) Each problem begins with the command ANALYSIS. The DESIGN option is not available for box culverts. The program will continue to execute problem data sets back-to-back until the command STOP is encountered.
- (2) Setting LEVEL=2 signals the program that the automatic mesh generation feature will be used. "Level 2 box" is distinguished from "Level 2 pipe" by a subsequent instruction in Section B. Setting LEVEL=3 allows description of arbitrary reinforced concrete structures and loading conditions. LEVEL=1 is not operable for box culverts.
- (3) By setting PTYPE = CONCRE, the reinforced concrete beam-rod element is used to model the culvert (for other pipe types see 1976 manual).
- (4) Setting PDIA = -1.0 signals the program that Section B input data is for a concrete box as opposed to a concrete pipe. Also, if LEVEL = 2, it subsequently signals the program to read Section C input for "level 2 box" instead of "level 2 pipe".
- (5) Defining the default concrete wall thickness, PT, is simply for convenience in limiting input data on subsequent cards.
- (6) RSHAPE controls the two options for defining section properties around the box. Setting RSHAPE = STD allows simplified input for standard ASTM box sections and can only be used with LEVEL = 2. Setting RSHAPE = ARBI allows the user to arbitrarily define section properties at each node around the box and may be used with LEVEL = 2 or 3.
- (7) Generally set NONLIN = 3 for all problems. Other options are primarily for behavior studies.
- (8) Figure B.3 illustrates the concrete material parameters representing the concrete stress-strain behavior. Generally, the default options provide reasonable parameter values except for cracking strain

STNMAT(1) and compressive strength PFPC which are conservative. Cracking strain values up to 0.0001 were used for box culverts studied in this report.

- (9) Figure B.4 illustrates the reinforcement material parameters representing the steel stress-strain behavior. Default options provide reasonable parameter values except for steel yield stress which is conservative. Standard ASTM box section reinforcement assumes 65,000 psi yield strength.
- (10) The spacing parameter is used only for crackwidth predictions in the Gergely-Lutz formula (see Chapter 3). The default value was used in this study.
- (11) For the RSHAPE = STD option, refer to Figure B.5 for illustration of standard box section parameters. If the top, side and bottom slabs are the same thickness, these input variables can be skipped and the default value PT, input on Card 1B, will be used.
- (12) Haunch dimensions are used by CANDE to increase the wall thickness at corner nodes by a simple averaging process and are shown on the printed output. Generally, HH = HV = PT.
- (13) Steel placement is illustrated in Figure B.5 and corresponds to standard ASTM box designs. All reinforcement steel areas are to be defined per inch of length in the longitudinal direction. Concrete cover to all steel centers is specified with the parameters TC. If variable TC values are desired use RSHAPE = ARBI.
- (14) For the RSHAPE = ARBI option, refer to Figure B.6 for illustration of parameters. In the level 2 option, the section properties are defined individually at the 15 points (nodes) shown in the figure. For level 3 solutions, the section properties are defined at the culvert nodes (NPPT) established by the user.
- (15) The embankment and trench configurations are illustrated in Figure B.7 and B.8. Each is composed of three soil zones; in situ, bedding, and fill.

- (16) By setting WORD1 = MOD, the level 2 mesh can be selectively modified by using the extended level 2 option. Modifications include; defining new soil zones and shapes and specifying live loads. When this option is exercised, additional data cards C4 to C7 are inserted after card C2. Card C3 does exist for level 2 box input. Input instructions for cards C4 to C7 are in the 1976 user manual and the finite element mesh topology for level 2 box is shown in Figure B.11 to B.14.
- (17) Construction increments for the trench and embankment installations are shown in Figures B.9 and B.10. In both cases, the first construction increment contains the box culvert and in situ soil. Increments 2,3,4 are each composed of two rows of elements uniformly spaced along the sides of the box. Increments 5 to 9 are composed of one element row, increment 5 is 1/3 R2 thick, and increments 6 to 9 are 2/3 R2 thick. For deep fill heights, subsequent increments are formed with equivalent overburden pressure (see note 19). The special case of NINC = -1 combines all increments into one (not recommended).
- (18) R1 and R2 define the box size and control the overall dimensions of the mesh as shown in Figure B.11.
- (19) HTCOVR is the distance from the middle of the top slab to the final soil surface. If HTCOVR is specified greater than 3R2, the mesh top boundary is truncated at the 3R2 level, and the remaining soil load is applied as equivalent increments of overburden pressure (i.e. DENSTY * (HTCOVR - 3R2)/(NINC - 9)). If HTCOVR is specified less than 3R2, the horizontal mesh line closest to HTCOVR is moved to the specified height, but with the condition that at least two layers of soil exist over the top of the box.
- (20) TRNWID defines the trench width from the middle of the box sidewall to the in situ soil as shown in Figure B.7. The vertical mesh line (Figure B.11) closest to the specified position is moved to this position to form the trench wall boundary. Minimum value

for TRNWID is 0.1 R1. If TRNWID is greater than 4R1 an embankment installation is obtained.

- (21) BDEPTH defines the depth of bedding below the bottom slab. The bedding zone is composed of one layer of elements and is kept within the depth limits (1/10) R2 to (2/3)R2. The bedding width extends one element beyond the box side.
- (22) For level 2 box, three sets of D cards are to be input corresponding to the predefined soil zones: I = 1, 2, and 3 implying in situ, bedding, and fill, respectively. For level 3, I corresponds to material number of element defined by user.
- (23) Any soil model (ITYP = 1, 2, 3, 4 or 5) may be assigned to any soil zone. Choice of a soil model is dependent on the problem objective, availability of actual soil data, and user's preference. Suggestions for soil model applications are given in subsequent notes.
- (24) The MATNAM subcategories provide a simplified data input option for ITYP = 3, 4, and 5 wherein the soil model parameters for standard types of soil are stored in the CANDE program. Alternatively, by setting MATNAM = USER (or MATNAM = TRIA for ITYPE = 5) model parameters may be defined by the user.
- (25) The linear elastic model (ITYP = 1) is useful for parameter studies and bracketing solutions with soft and stiff moduli values. See Chapter 7 (Table 7.2) for typical moduli values. It is generally reasonable to model in situ soil with the elastic model.
- (26) Orthotropic models can be used to simulate reinforced earth (see Reference 31).
- (27) If the maximum number of iterations (NON) for convergence is exceeded, the program advances to the next load step. If NON is specified as a negative value, iteration values and convergence checks are printed out.
- (28) Generally set RATIO = 0.5. If Duncan model is used for pre-existing soil zones (e.g. bedding and in situ), set RATIO = 1.0. The Duncan

model is probably best suited for characterizing fill soil. See Chapter 9 (Table 9.2) for hyperbolic parameters corresponding to standard soil types stored in the program.

- (29) For MATNAM = USER, the tangent Young's modulus hyperbolic parameters are input by the user (usually determined from triaxial tests, see Reference 29).
- (30) For MATNAM = USER, the tangent bulk modulus hyperbolic parameters may be specified. Or, as an alternative, a constant Poisson's ratio may be specified. The latter option is the original version of the Duncan soil model, still preferred by some investigators.
- (31) Moduli values for the overburden dependent model correspond to secant relations from confined compression tests. Thus, this model provides reasonable representation of soil behavior in zones where deformation is primarily vertical. For this reason, the model is better suited for rigid culvert installations than flexible culvert installations. If MATNAM is other than USER, the table entries are automatically supplied by CANDE. Table values are listed in the 1976 user manual, page 39.
- (32) The Hardin model is discussed in detail in the 1976 CANDE manual. This option is best utilized in conjunction with triaxial test data.
- (33) See the CANDE 1976 manual.

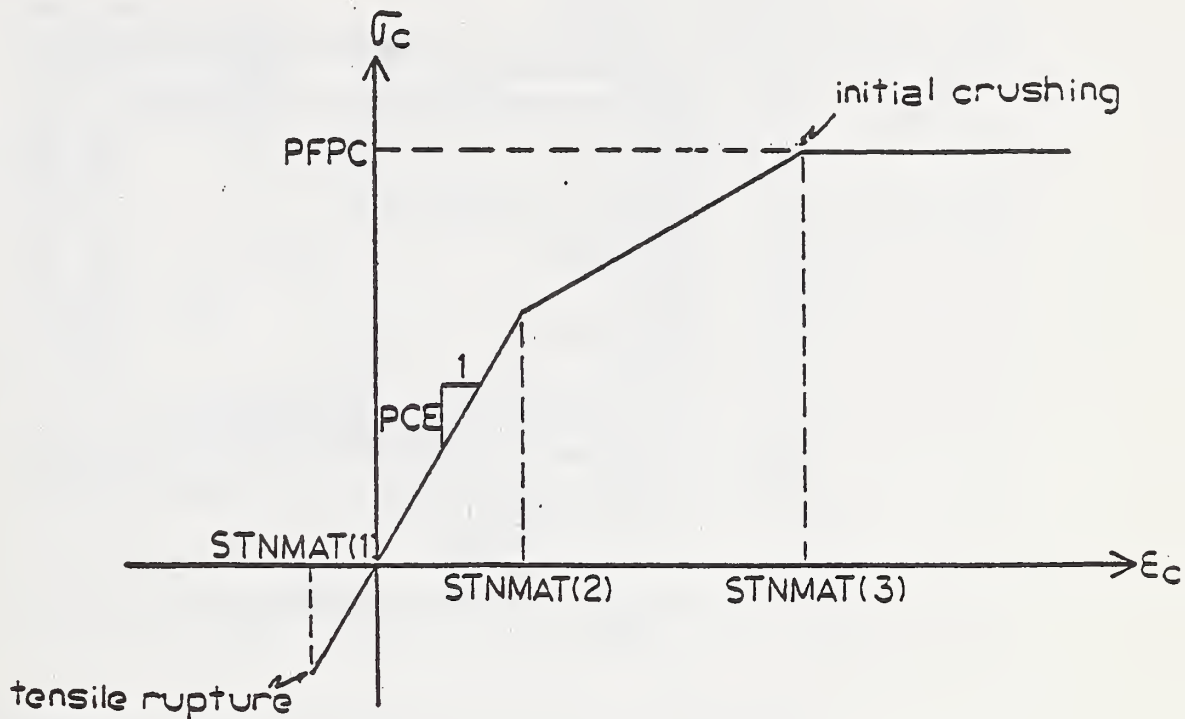


Figure B.3 - Idealized Stress-Strain Diagram of Concrete.

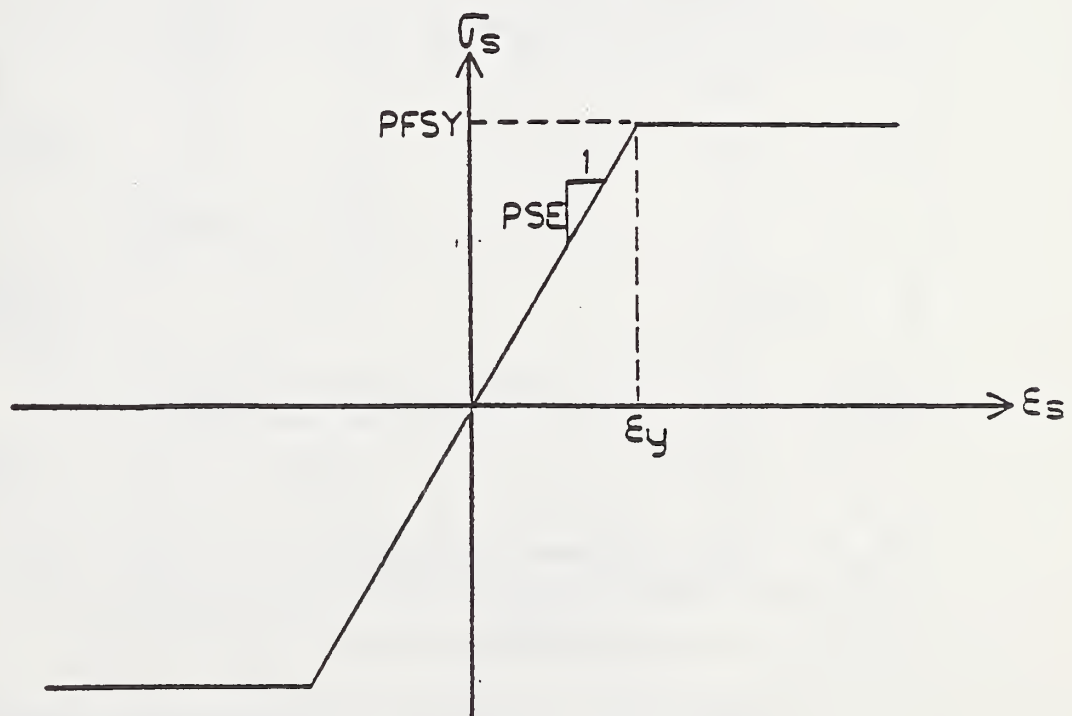


Figure B.4 - Idealized Stress-Strain Diagram of Steel.

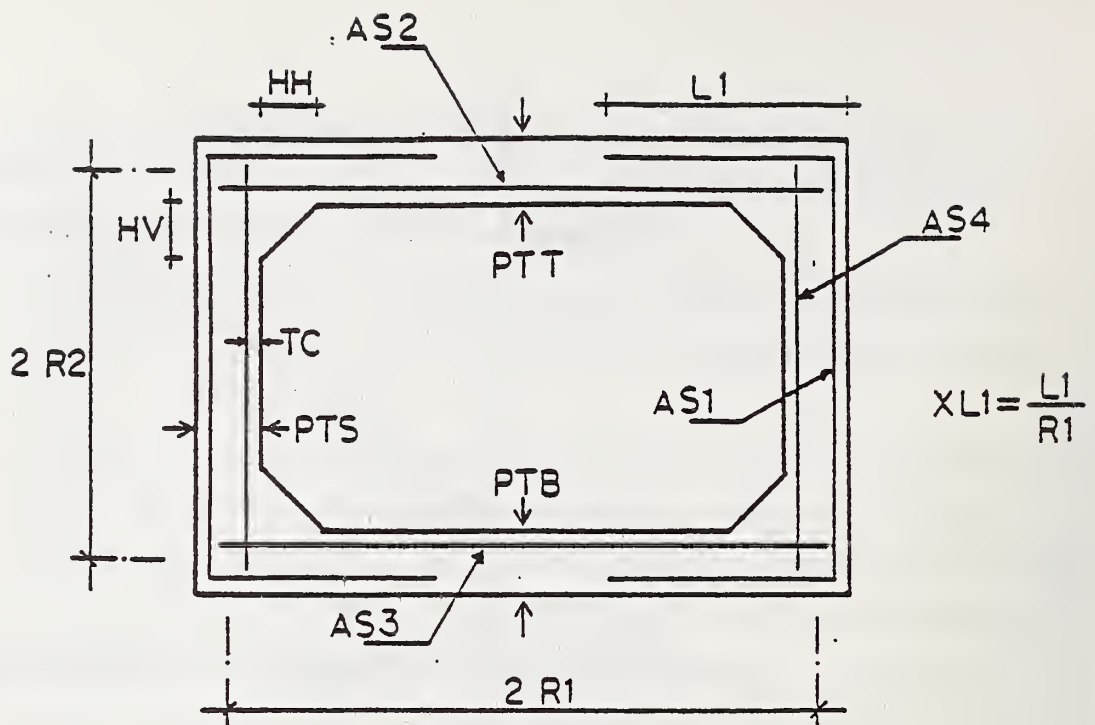


Figure B.5 - Box Culverts Parameters for RSHAPE = STD and Level 2 Solution.

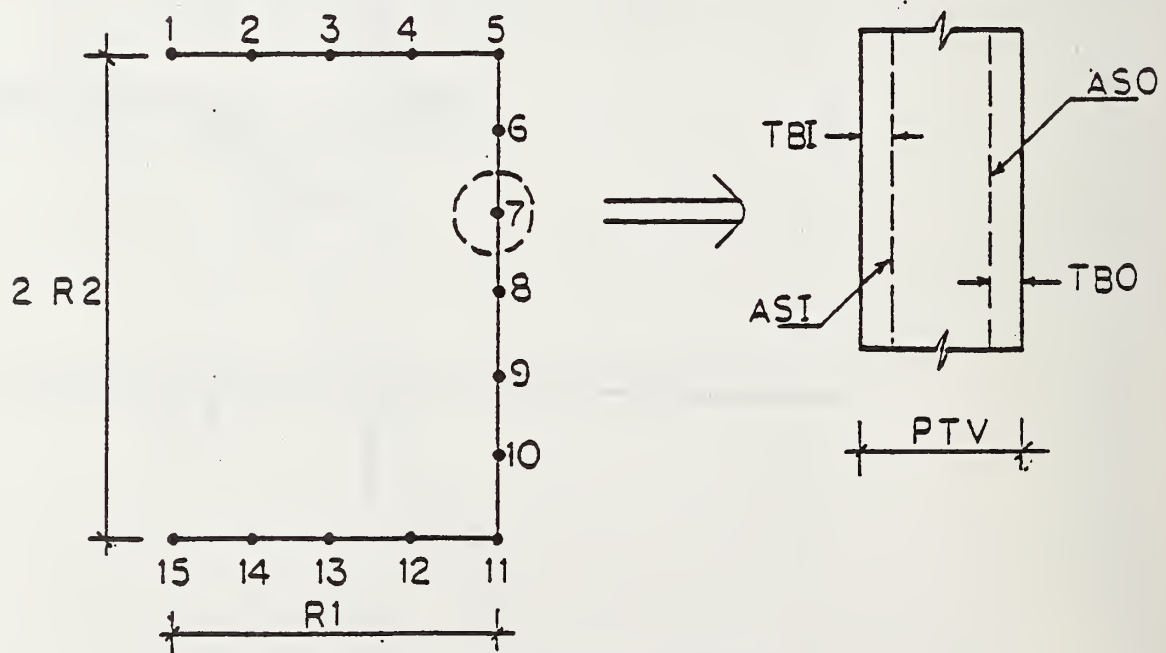


Figure B.6 - Box Culvert Generated Mesh (Level 2), and Properties Definition (Level 2 or 3).

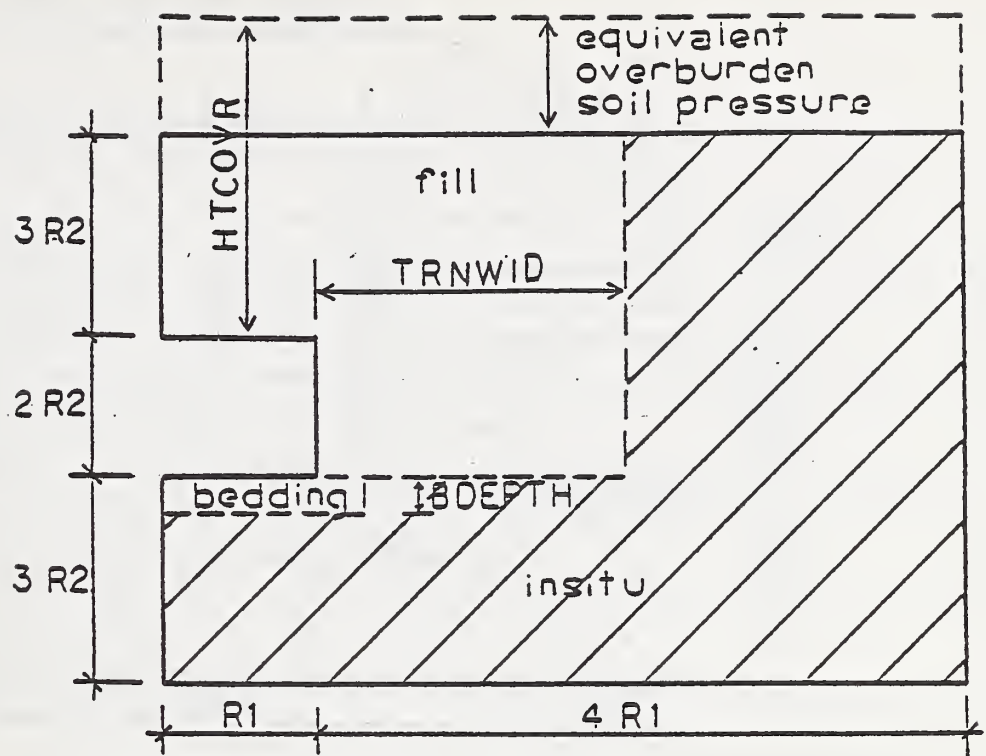


Figure B.7 - Trench Soil Installation.

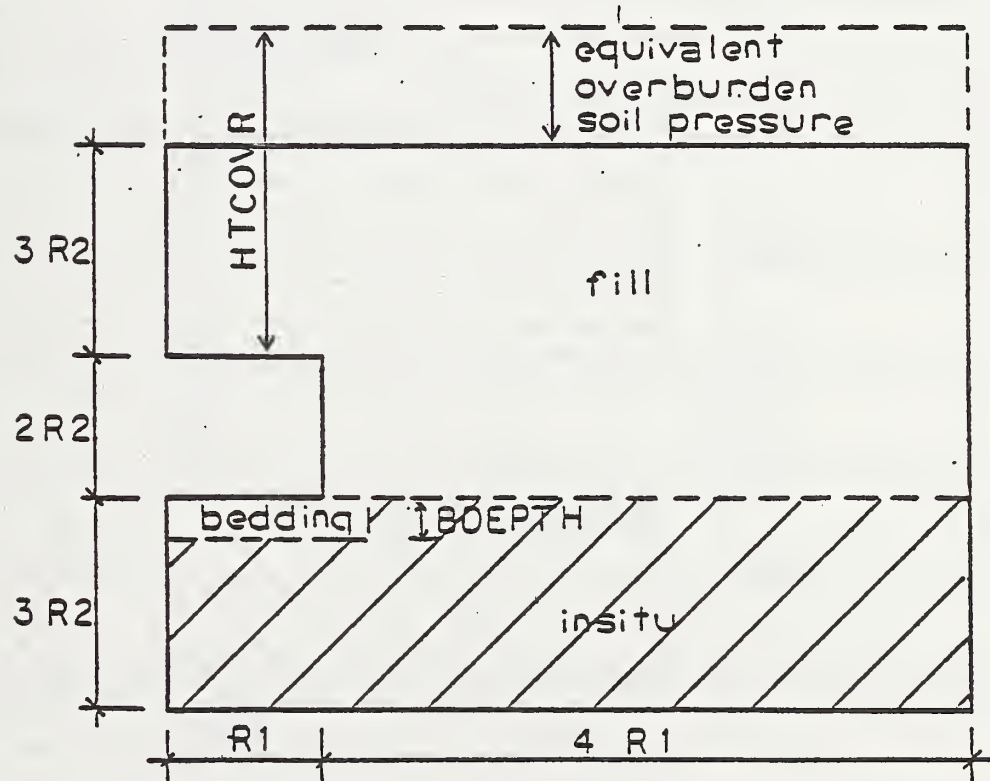


Figure B.8 - Embankment Soil Installation.

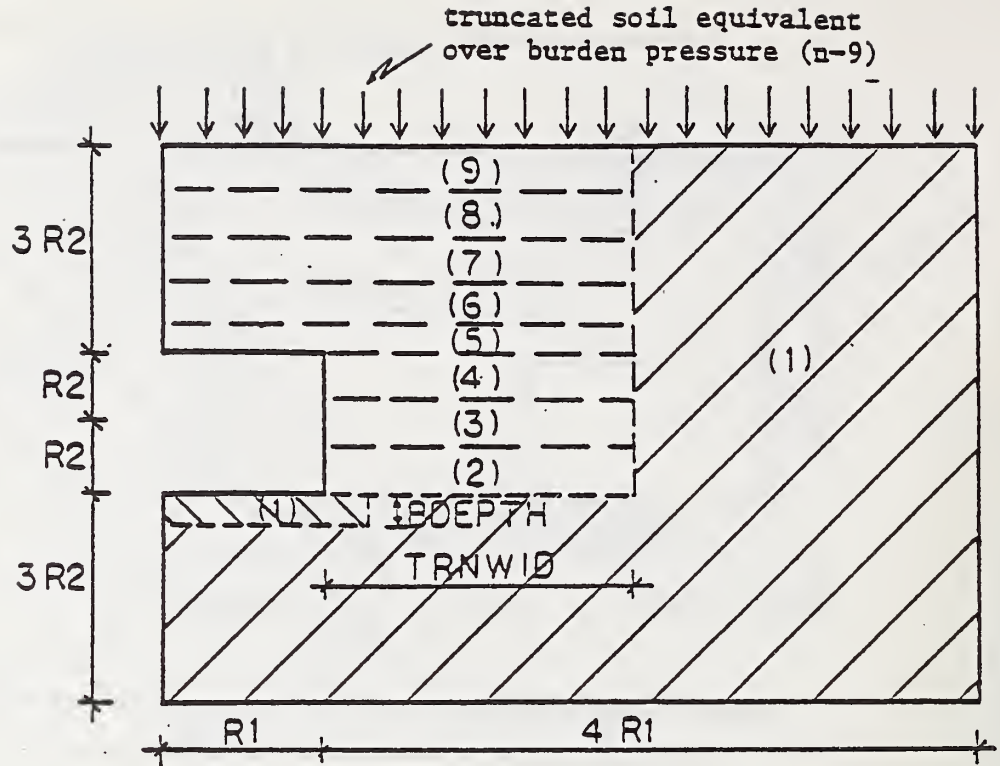


Figure B.9 - Soil Layers and Construction Increment when they are Applied for Trench Soil Installation.

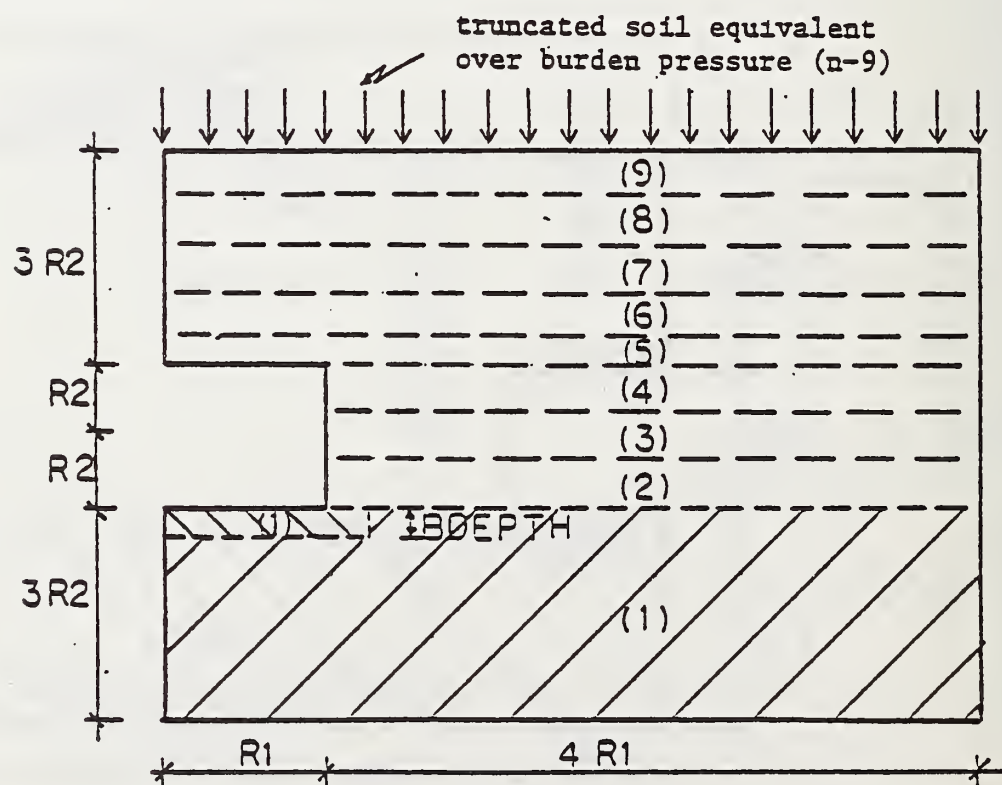


Figure B.10 - Soil Layers and Construction Increment when they are Applied for Embankment Soil Installation.

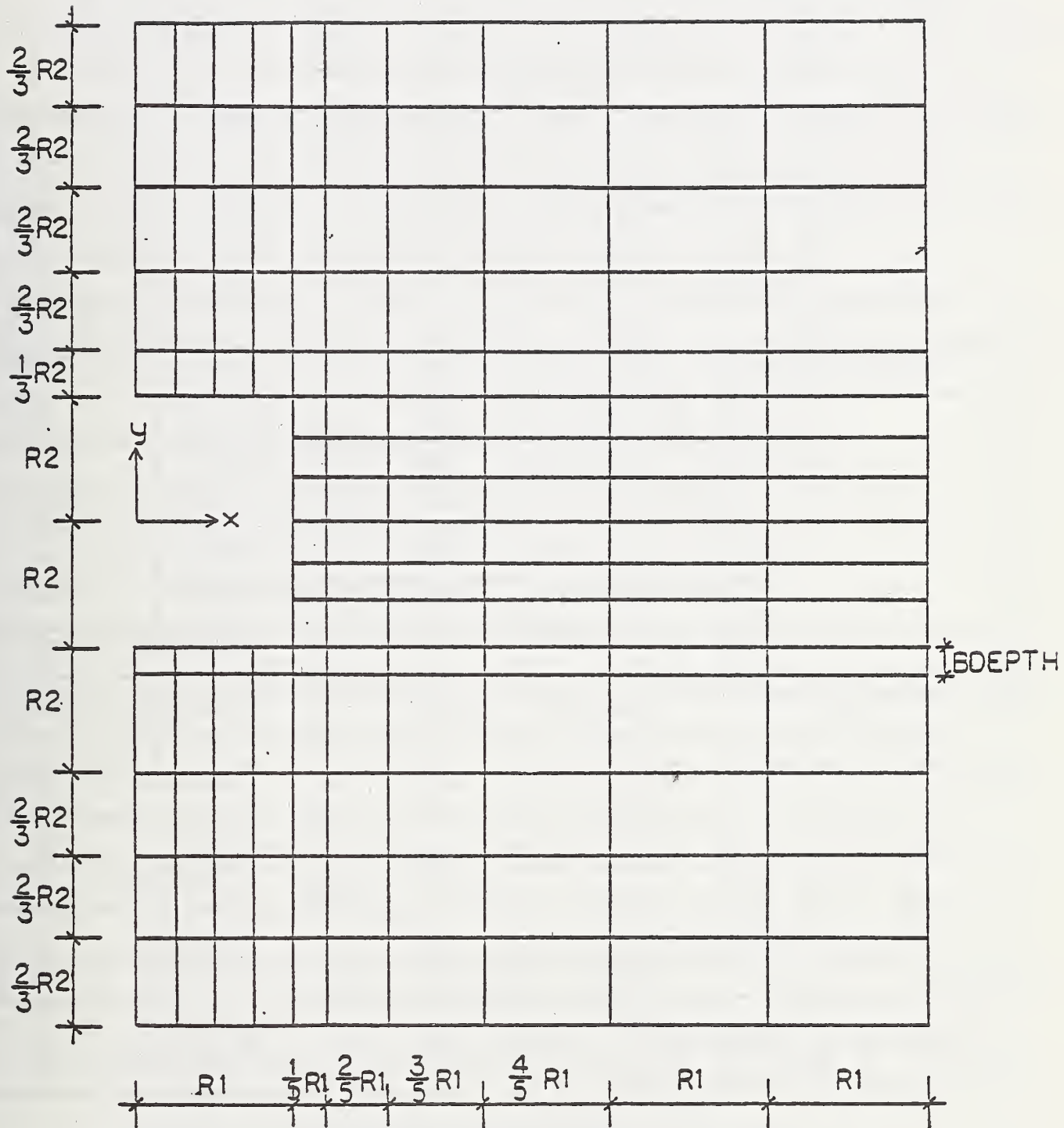


Figure B.11 - Geometry of the Soil Undeformed Grid Configuration.

ELEMENT NUMBERS

14	142	143	144	145	146	147	148	149	150
13	132	133	134	135	136	137	138	139	140
12	122	123	124	125	126	127	128	129	130
11	112	113	114	115	116	117	118	119	120
10	102	103	104	105	106	107	108	109	110
	95	96		97		98		99	100
	99	90		91		92		93	94
	83	84		85		86		87	88
	77	78		79		80		81	82
	71	72		73		74		75	76
	55	56		57		58		59	60
55	56	57	58	59	50	51	52	53	54
45	46	47	48	49	50	51	52	53	54
35	36	37	38	39	40	41	42	43	44
25	26	27	28	29	30	31	32	33	34
15	16	17	18	19	20	21	22	23	24

Figure B.12 - Soil Mesh Elements Number.

NOVAL NUMBERS

157	153	159	150	151	152	153	154	155	156	157
146	147	148	149	150	151	152	153	154	155	155
135	135	137	138	139	140	141	142	143	144	145
124	125	125	127	129	129	130	131	132	133	134
113	114	115	115	117	119	119	120	121	122	123
102	103	104	105	106	107	109	109	110	111	112
				95	95	97	99	99	100	101
				99	99	90	91	92	93	94
				81	82	83	84	85	85	87
				74	75	75	77	79	79	90
				57	58	59	70	71	72	73
55	57	53	59	60	51	52	53	54	55	55
45	46	47	49	49	50	51	52	53	54	55
34	35	36	37	39	39	40	41	42	43	44
23	24	25	26	27	29	29	30	31	32	33
12	13	14	15	15	17	19	19	20	21	22
1	2	3	4	5	5	7	8	9	10	11

Figure B.13 - Soil Mesh Nodal Numbers.

INCREMENT NUMBERS

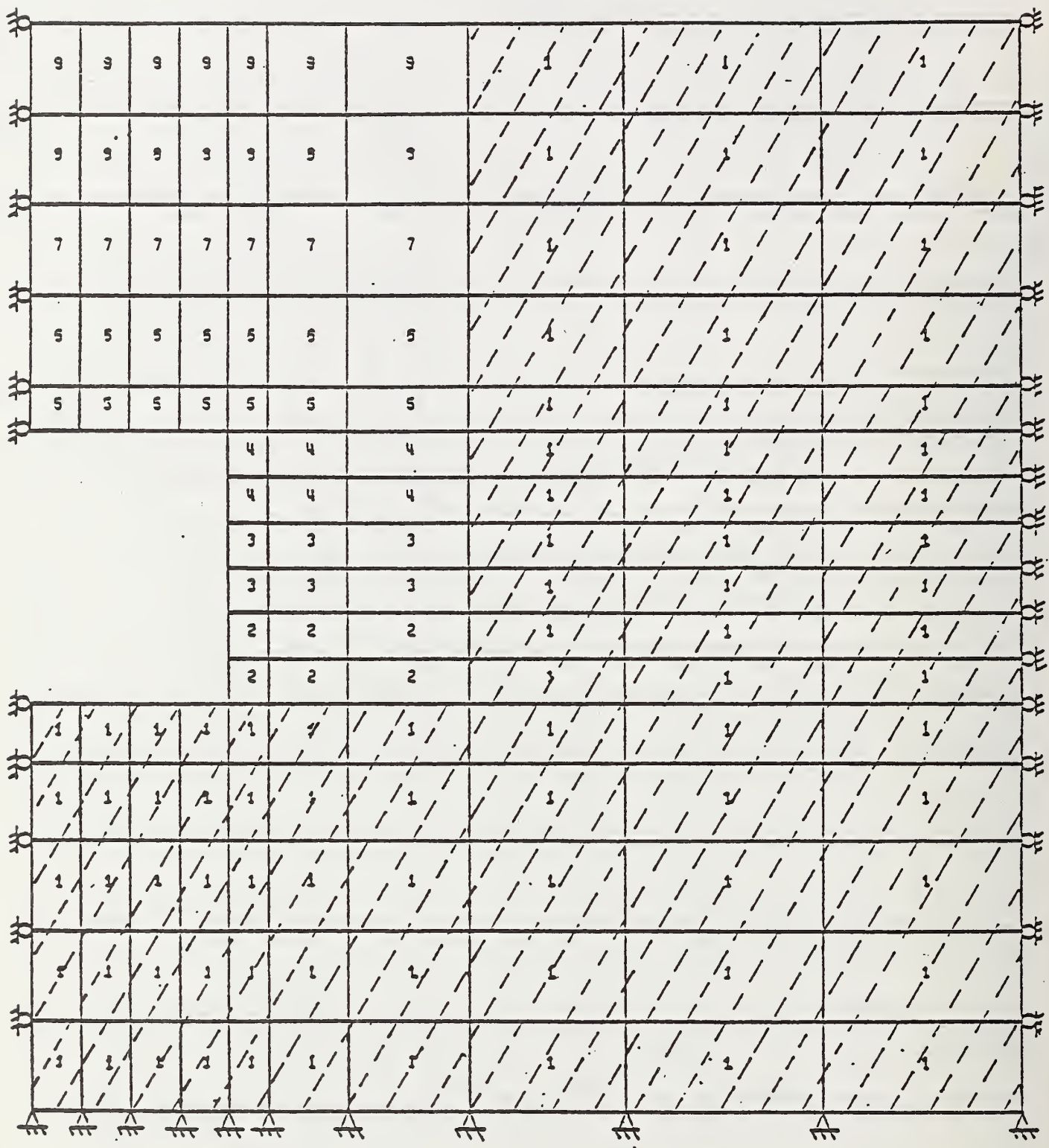


Figure B.14 - Soil Layers Incremental Loading for Trench Installation and Mesh Boundary Conditions.

APPENDIX C

SAMPLE OF INPUT DATA AND OUTPUT

The three sample problems presented here cover the three solution levels available when analyzing a reinforced concrete box culvert, that is: level 2 box, extended level 2, and level 3. The three samples correspond to box culverts analyzed during the process of this work.

Table D.1 gives a brief description of the box type, solution level, installation type, and some special comments of the sample problems. Each problem is presented in the following format: (1) a listing of all the input cards, and (2) selected CANDE output for the box responses. The soil responses are not presented.

TABLE C.1 Example Problems for Analysis of Reinforced
Concrete Box Culverts

Problem No.	Solution Level	Soil Installation	Special Comments
1	2	Embankment	8*6-8 Box Culvert ASTM H = 10 ft. stiff linear soil soil dead load only automatic mesh generation
2	2 Extended	Embankment	8*6-8 Box Culvert ASTM H = 2 ft. stiff linear soil soil plus twice HS-20 L.L. automatic mesh generation
3	3	N	6*4-2 Box Culvert out-of ground loading user's input mesh

Problem 1 - Input

CARD TYPE 1...X...10....X...20....X...30....X...40....X...50....X...60....X...70....X...80

CARD 1A ANALYS 2 CONCRE BOX CULVERT 8*6-8 (MEDIUM REINFORCED - H=10 FT)

CARD 1B -1.0 8.0 STD 3 0.0001

CARD 2B 5000.0 150.0 65000.0

CARD 3B-1 8.0 8.0 8.0 8.0 8.0

CARD 3B-2 .01667 .02417 .02583 .01583 0.50

CARD 1C EMBA EMBANKMENT - STIFF SOIL

CARD 2C 0 1 3 9 52.00 40.00 10.00 120.00 12.00

CARD 1D 1 1 0.0 INSITU-SOIL

CARD 2D 3333.0 0.33

CARD 1D 2 1 0.0 BEDDING-SOIL

CARD 2D 6666.0 0.33

CARD 1D L 3 1 120.0 FILL-SOIL

CARD 2D 3333.0 0.33

STOP

Problem 1 - Output

*** PROBLEM NUMBER 1 ***

BOX CULVERT.8*6-8 (MEDIUM REINFORCED - H=10 FT)

EXECUTION MODEANAL

SOLUTION LEVELF.E.AUTO

CULVERT TYPE CONCRETE

***NEGATIVE PIPE DIAMETER IMPLIES NEW CANOE OPTION FOR VARIABLE CONCRETE THICKNESS. ***

***OPTION IS RESTRICTED TO ANALYSIS ONLY WITH LEVEL 2-BOX, OR LEVEL 3. ***

PIPE PROPERTIES ARE AS FOLLOWS ...
(UNITS ARE INCH-POUND SYSTEM)

NOMINAL PIPE DIAMETER	-1.0000
CONCRETE COMPRESSIVE STRENGTH	5000.0000
CONCRETE ELASTIC MODULUS	4286826.00
CONCRETE POISSON RATIO	0.1700
DENSITY OF PIPE (PCF)	150.0000
STEEL YIELD STRENGTH	65000.0000
STEEL ELASTIC MODULUS	29000000.0
STEEL POISSON RATIO	0.3000
NONLINEAR CODE (1,2,OR 3)	3
CONC. CRACKING STRAIN (1,2,3)	0.000100
CONC. YIELDING STRAIN (2,3)	0.000566
CONC. CRUSHING STRAIN (2,3)	0.002000
STEEL YIELDING STRAIN (3)	0.002040
SPACING LONGITUDINAL REINFORCEMENT	2.00

Problem 1 - Output (continued)

NODE #	STEEL AREAS (IN2)		STEEL COVERS (IN)		THICKNESS (IN)	
	V	ASI (IN)	ASU (IN)	TBI (IN)	TBO (IN)	PTV (IN)
1		0.0242	0.0	1.2500	1.2500	8.0000
2		0.0242	0.0	1.2500	1.2500	8.0000
3		0.0242	0.0167	1.2500	1.2500	8.0000
4		0.0242	0.0167	1.2500	1.2500	8.0000
5		0.0200	0.0167	1.2500	1.2500	15.0000
6		0.0158	0.0167	1.2500	1.2500	8.0000
7		0.0158	0.0167	1.2500	1.2500	8.0000
8		0.0158	0.0167	1.2500	1.2500	8.0000
9		0.0158	0.0167	1.2500	1.2500	8.0000
10		0.0158	0.0167	1.2500	1.2500	8.0000
11		0.0208	0.0167	1.2500	1.2500	16.0000
12		0.0258	0.0167	1.2500	1.2500	8.0000
13		0.0258	0.0167	1.2500	1.2500	8.0000
14		0.0258	0.0	1.2500	1.2500	8.0000
15		0.0258	0.0	1.2500	1.2500	8.0000

* * BEGIN GENERATION OF CANNED MESH * *

THE DATA TO BE RUN IS ENTITLED

EMBANKMENT - STIFF SOIL

TYPE OF MESH ----- EMBANKMENT
 PLOTTING DATA SAVED ----- 0
 PRINT SOIL RESPONSES ----- 1
 PRINT CONTROL FOR PREP OUTPUT ----- 3
 NUMBER OF CONSTRUCTION INCREMENTS ----- 9
 SPAN OF BOX ----- 104.00
 HEIGHT OF BOX ----- 80.00
 SOIL ABOVE TOP OF BOX (FT) ----- 10.00
 MESH HEIGHT ABOVE TOP OF BOX (FT) ----- 10.00
 SOIL DENSITY ABOVE MESH (PCF) ----- 120.00

IDENTIFICATION OF MATERIAL ZONE WITH MATERIAL NUMBER

MATERIAL-ZONE MATERIAL NO.

INSITU	1
BEDDING	2
FILL	3

Problem 1 - Output (continued)

* * BEGIN PREP OF FINITE ELEMENT INPUT * *

THE DATA TO BE RUN IS ENTITLED

EMBANKMENT - STIFF SOIL

NUMBER OF CONSTRUCTION INCREMENTS-----	9
PRINT CONTROL FOR PREP OUTPUT-----	3
INPUT DATA CHECK-----	0
PLOT TAPE GENERATION-----	0
ENTIRE FINITE ELEMENT RESULTS OUTPUT---	1
THE NUMBER OF NODES IS-----	167
THE NUMBER OF ELEMENTS IS-----	150
THE NUMBER OF BOUNDARY CONDITIONS IS---	200

MATERIAL CHARACTERIZATION FOR SOILS.

PROPERTIES FOR MATERIAL 1 ***** INSITU-SOIL

DENSITY = 0.0

YOUNGS MODULUS= 0.3333E+04
POISONS RATIO= 0.3300E+00
CONFINED MOD.= 0.4938E+04
LATERAL COEFF.= 0.4925E+00

PROPERTIES FOR MATERIAL 2 ***** BEDDING-SOIL

DENSITY = 0.0

YOUNGS MODULUS= 0.6666E+04
POISONS RATIO= 0.3300E+00
CONFINED MOD.= 0.9877E+04
LATERAL COEFF.= 0.4925E+00

PROPERTIES FOR MATERIAL 3 ***** FILL-SOIL

DENSITY = 0.12000E+03

YOUNGS MODULUS= 0.3333E+04
POISONS RATIO= 0.3300E+00
CONFINED MOD.= 0.4938E+04
LATERAL COEFF.= 0.4925E+00

Problem 1 - Output (continued)

STRUCTURAL RESPONSE OF CULVERT FOR LOAD INCREMENT 9

COORDINATES, DISPLACEMENTS AND CRACK DEPTHS ARE IN INCHES
 PRESSURES ARE IN LB/IN**2
 MOMENTS ARE IN IN.*LB/IN.
 THRUST AND SHEAR ARE IN LB/IN.

NPPT	X-COORD. Y-COORD.	X-DISP. Y-DISP.	N-PRES. S-PRES.	MOMENT THRUST	SHEAR CRACK DEPTH
1	0.0 40.00	0.0 -0.36327E+00	-0.82428E+01 0.0	0.55599E+04 -0.11517E+03	0.0 0.60566E+01
2	13.00 40.00	-0.48848E-04 -0.36062E+00	-0.85117E+01 -0.16894E+00	0.48633E+04 -0.11626E+03	0.10890E+03 0.0
3	26.00 40.00	-0.90817E-04 -0.35366E+00	-0.91547E+01 -0.37016E+00	0.27284E+04 -0.11977E+03	0.22374E+03 0.0
4	39.00 40.00	-0.13419E-03 -0.34457E+00	-0.10687E+02 -0.12311E+00	-0.94880E+03 -0.12297E+03	0.35271E+03 0.0
5	52.00 40.00	-0.16387E-03 -0.33563E+00	-0.93348E+01 -0.10699E+02	-0.64476E+04 -0.36492E+03	0.14262E+03 0.0
6	52.00 26.67	0.79563E-02 -0.33548E+00	-0.44441E+01 -0.45603E+01	-0.46375E+04 -0.63646E+03	-0.10731E+03 0.0
7	52.00 13.33	0.13600E-01 -0.33524E+00	-0.50773E+01 -0.39506E+01	-0.36019E+04 -0.69321E+03	-0.43829E+02 0.0
8	52.00 0.0	0.15840E-01 -0.33498E+00	-0.62997E+01 -0.28920E+01	-0.34689E+04 -0.73882E+03	0.32017E+02 0.0
9	52.00 -13.33	0.14765E-01 -0.33470E+00	-0.65201E+01 -0.21085E+01	-0.44556E+04 -0.77216E+03	0.11748E+03 0.0
10	52.00 -26.67	0.91028E-02 -0.33438E+00	-0.70390E+01 -0.84638E+00	-0.66014E+04 -0.79186E+03	0.20788E+03 0.60218E+01
11	52.00 -40.00	-0.44758E-03 -0.33417E+00	-0.15362E+02 0.93181E+01	-0.10001E+05 -0.56033E+03	-0.16154E+03 0.0
12	39.00 -40.00	-0.37012E-03 -0.32325E+00	-0.14983E+02 0.55771E+00	-0.24900E+04 -0.31954E+03	-0.48049E+03 0.0
13	26.00 -40.00	-0.25810E-03 -0.31149E+00	-0.12640E+02 0.94244E+00	0.24882E+04 -0.30979E+03	-0.30094E+03 0.0
14	13.00 -40.00	-0.14314E-03 -0.30161E+00	-0.11427E+02 0.53084E+00	0.53298E+04 -0.30021E+03	-0.14451E+03 0.54325E+01
15	0.0 -40.00	0.0 -0.29753E+00	-0.10805E+02 0.0	0.62411E+04 -0.29676E+03	0.0 0.58268E+01

Problem 1 - Output (continued)

STRESSES IN CULVERT WALL (PSI) FOR LOAD INCREMENT 9

NPPT	ELLIP. OR INNER CAGE STEEL ¹	OUTER CAGE STEEL	CONCRETE COMPRESSION	SHEAR STRESS
1	0.34614E+05	0.0	-0.13187E+04	0.0
2	0.20485E+04	0.0	-0.46337E+03	0.16134E+02
3	0.13956E+04	-0.13196E+04	-0.25882E+03	0.33146E+02
4	-0.52378E+03	0.31524E+03	-0.98963E+02	0.52253E+02
5	-0.10500E+04	0.72864E+03	-0.16826E+03	0.96690E+01
6	-0.26324E+04	0.15131E+04	-0.49515E+03	-0.15897E+02
7	-0.22193E+04	0.10012E+04	-0.40881E+03	-0.64931E+01
8	-0.21999E+04	0.90183E+03	-0.40239E+03	0.47433E+01
9	-0.26704E+04	0.13131E+04	-0.49531E+03	0.17405E+02
10	-0.26859E+04	0.41673E+05	-0.17685E+04	0.30797E+02
11	-0.16246E+04	0.11323E+04	-0.26039E+03	-0.10952E+02
12	-0.13679E+04	0.82989E+03	-0.25867E+03	-0.71184E+02
13	0.82146E+03	-0.13772E+04	-0.25998E+03	-0.44584E+02
14	0.23769E+05	0.0	-0.13087E+04	-0.21408E+02
15	0.32348E+05	0.0	-0.14766E+04	0.0

STRAINS IN THE INNER AND OUTER FIBER OF THE CULVERT WALL
(ONLY STRAINS FOR COMPRESSION ZONES HAVE PHYSICAL MEANING)

NPPT	INNER STRAIN	OUTER STRAIN
1	0.13426E-02	-0.29872E-03
2	0.95622E-04	-0.10497E-03
3	0.51603E-04	-0.58631E-04
4	-0.22419E-04	0.15875E-04
5	-0.38117E-04	0.28032E-04
6	-0.11217E-03	0.77045E-04
7	-0.92608E-04	0.54384E-04
8	-0.91153E-04	0.50420E-04
9	-0.11220E-03	0.69614E-04
10	-0.40063E-03	0.16240E-02
11	-0.58987E-04	0.43540E-04
12	-0.58597E-04	0.41715E-04
13	0.41457E-04	-0.58895E-04
14	0.93886E-03	-0.29646E-03
15	0.12650E-02	-0.33450E-03

Problem 1 - Output (continued)

CALCULATED SAFETY FACTORS FOR LOAD INCREMENT	
STEEL YIELD STRESS / MAX. STEEL STRESS	1.560
CONCRETE STRENGTH / MAX. COMPRESSIVE STRESS	2.827
WALL SHEAR CAPACITY / MAX. SHEAR	1.987
PERFORMANCE FACTORS	
0.01 INCH / MAX. CRACK WIDTH	1.215

* * * * NORMAL EXIT FROM CANDE * * * *

Problem 2 - Input

CARD TYPE 1...X...10....X...20....X...30....X...40....X...50....X...60....X...70....X...80

CARD 1A ANALYS 2 CONCRE BOX CULVERT 8*6-8 - HS-20 LIVE LOAD (MINIMUM SOIL COVER)

CARD 1B -1.0 8.0 STD 3 0.0001

CARD 2B 5000.0 150.0 65000.0

CARD 3B-1 8.0 8.0 8.0 8.0 8.0

CARD 3B-2 .02583 .03833 .02917 .01583 0.65

CARD 1C EMBA EMBANKMENT - STIFF SOIL

CARD 2C 0 1 3 8 52.00 40.00 2.00 120.00 MOD 12.00

CARD 4C 2

CARD 7C 124 0 -60.0 7

CARD 7C 124 0 -51.1 8

CARD 1D 1 1 0.0 INSITU-SOIL

CARD 2D 3333.0 0.33

CARD 1D 2 1 0.0 BEDDING-SOIL

CARD 2D 6666.0 0.33

CARD 1D L 3 1 120.0 FILL-SOIL

CARD 2D 3333.0 0.33

STOP

Problem 2 - Output

*** PROBLEM NUMBER 1 ***

BOX CULVERT 8*6-8 - HS-20 LIVE LOAD (MINIMUM SOIL COVER)

EXECUTION MODEANAL

SOLUTION LEVELF.E.AUTO

CULVERT TYPE CONCRETE

***NEGATIVE PIPE DIAMETER IMPLIES NEW CANDE OPTION FOR VARIABLE CONCRETE THICKNESS. ***

***OPTION IS RESTRICTED TO ANALYSIS ONLY WITH LEVEL 2-BUX, OR LEVEL 3. ***

PIPE PROPERTIES ARE AS FOLLOWS ...
(UNITS ARE INCH-POUND SYSTEM)

NOMINAL PIPE DIAMETER	-1.0000
CONCRETE COMPRESSIVE STRENGTH	5000.0000
CONCRETE ELASTIC MODULUS	4286826.00
CONCRETE POISSON RATIO	0.1700
DENSITY OF PIPE (PCF)	150.0000
STEEL YIELD STRENGTH	65000.0000
STEEL ELASTIC MODULUS	29000000.0
STEEL POISSON RATIO	0.3000
NONLINEAR CODE (1,2,OR 3)	3
CONC. CRACKING STRAIN (1,2,3)	0.000100
CONC. YIELDING STRAIN (2,3)	0.000566
CONC. CRUSHING STRAIN (2,3)	0.002000
STEEL YIELDING STRAIN (3)	0.002040
SPACING LONGITUDINAL REINFORCEMENT	2.00

Problem 2 - Output (continued)

NODE #	STEEL AREAS (IN ²)		STEEL COVERS (IN)		THICKNESS (IN)
	N	ASI (IN)	ASU (IN)	TBI (IN)	
1		0.0383	0.0	1.2500	1.2500
2		0.0383	0.0	1.2500	1.2500
3		0.0383	0.0258	1.2500	1.2500
4		0.0303	0.0258	1.2500	1.2500
5		0.0271	0.0258	1.2500	1.2500
6		0.0158	0.0258	1.2500	1.2500
7		0.0158	0.0258	1.2500	1.2500
8		0.0158	0.0258	1.2500	1.2500
9		0.0158	0.0258	1.2500	1.2500
10		0.0158	0.0258	1.2500	1.2500
11		0.0225	0.0258	1.2500	1.2500
12		0.0292	0.0258	1.2500	1.2500
13		0.0292	0.0258	1.2500	1.2500
14		0.0292	0.0	1.2500	1.2500
15		0.0292	0.0	1.2500	1.2500

* * BEGIN GENERATION OF CANNED MESH * *

THE DATA TO BE RUN IS ENTITLED

EMBANKMENT - STIFF SOIL

TYPE OF MESH ----- EMBANKMENT
 PLOTTING DATA SAVED ----- 0
 PRINT SOIL RESPONSES ----- 1
 PRINT CONTROL FOR PREP OUTPUT ----- 3
 NUMBER OF CONSTRUCTION INCREMENTS ----- 8
 SPAN OF BOX ----- 104.00
 HEIGHT OF BOX ----- 80.00
 SOIL ABOVE TOP OF BOX (FT) ----- 2.00
 MESH HEIGHT ABOVE TOP OF BOX (FT) ----- 2.00
 SOIL DENSITY ABOVE MESH (PCF) ----- 120.00

IDENTIFICATION OF MATERIAL ZONE WITH MATERIAL NUMBER

MATERIAL-ZONE MATERIAL NO.

INSITU	1
BEDDING	2
FILL	3

Problem 2 - Output (continued)

*** BEGIN PREP OF FINITE ELEMENT INPUT ***

THE DATA TO BE RUN IS ENTITLED

EMBANKMENT - STIFF SOIL

NUMBER OF CONSTRUCTION INCREMENTS-----	8
PRINT CONTROL FOR PREP OUTPUT-----	3
INPUT DATA CHECK-----	0
PLOT TAPE GENERATION-----	0
ENTIRE FINITE ELEMENT RESULTS OUTPUT---	1
THE NUMBER OF NODES IS-----	134
THE NUMBER OF ELEMENTS IS-----	120
THE NUMBER OF BOUNDARY CONDITIONS IS---	200

* * * CHANGES TO STANDARD LEVEL 2 MESH * * *
* NUMBER OF NODES TO BE CHANGED ----- 0*
* NUMBER OF ELEMENTS TO BE CHANGED ----- 0*
* ADDITIONAL BOUNDARY CONDITIONS ----- 2*

***ADDITIONAL BOUNDARY CONDITIONS---FORCES = LBS . . . DISPLACEMENTS = INCHES . . .

BOUNDARY NODE	LOAD STEP	X-FORCE X-DISPLACEMENT	Y-FORCE Y-DISPLACEMENT	X-Y ROTATION DEGREES
124	7	F = 0.0	F = -0.6000E+02	3.7
124	8	F = 0.0	F = -0.5110E+02	0.2

Problem 2 - Output (continued)

MATERIAL CHARACTERIZATION FOR SOILS.

PROPERTIES FOR MATERIAL 1 ***** INSITU-SOIL

DENSITY = 0.0

YOUNGS MODULUS= 0.3333E+04
POISONS RATIO= 0.3300E+00
CONFINED MOD.= 0.4938E+04
LATERAL COEFF.= 0.4925E+00

PROPERTIES FOR MATERIAL 2 ***** BEDDING-SOIL

DENSITY = 0.0

YOUNGS MODULUS= 0.6666E+04
POISONS RATIO= 0.3300E+00
CONFINED MOD.= 0.9877E+04
LATERAL COEFF.= 0.4925E+00

PROPERTIES FOR MATERIAL 3 ***** FILL-SOIL

DENSITY = 0.12000E+03

YOUNGS MODULUS= 0.3333E+04
POISONS RATIO= 0.3300E+00
CONFINED MOD.= 0.4938E+04
LATERAL COEFF.= 0.4925E+00

-

Problem 2 - Output (continued)

STRUCTURAL RESPONSE OF CULVERT FOR LOAD INCREMENT 8

COORDINATES, DISPLACEMENTS AND CRACK DEPTHS ARE IN INCHES
 PRESSURES ARE IN LB/IN*2
 MOMENTS ARE IN IN.*LB/IN.
 THRUST AND SHEAR ARE IN LB/IN.

NPPT	X-COORD. Y-COORD.	X-DISP. Y-DISP.	N-PRES. S-PRES.	MOMENT THRUST	SHEAR CRACK DEPTH
1	0.0 40.00	0.0 -0.19304E+00	-0.82800E+01 0.0	0.40991E+04 0.25164E+02	0.0 0.0
2	13.00 40.00	0.89571E-05 -0.19143E+00	-0.65124E+01 -0.17414E+01	0.33993E+04 0.13845E+02	0.96151E+02 0.0
3	26.00 40.00	0.98505E-05 -0.18703E+00	-0.34548E+01 -0.19975E+01	0.15991E+04 -0.10453E+02	0.16094E+03 0.0
4	39.00 40.00	0.16997E-05 -0.18138E+00	-0.23285E+01 -0.42829E+00	-0.78224E+03 -0.26225E+02	0.19853E+03 0.0
5	52.00 40.00	-0.51747E-05 -0.17587E+00	-0.16976E+01 -0.33003E+01	-0.35617E+04 -0.14470E+03	0.85171E+02 0.0
6	52.00 26.67	0.50434E-02 -0.17581E+00	-0.97901E+00 -0.20297E+01	-0.29905E+04 -0.27393E+03	-0.36796E+02 0.0
7	52.00 13.33	0.84971E-02 -0.17571E+00	-0.11326E+01 -0.23598E+01	-0.25871E+04 -0.30319E+03	-0.22718E+02 0.0
8	52.00 0.0	0.95969E-02 -0.17559E+00	-0.22470E+01 -0.20561E+01	-0.23849E+04 -0.33263E+03	-0.18745E+00 0.0
9	52.00 -13.33	0.84966E-02 -0.17546E+00	-0.23406E+01 -0.20560E+01	-0.25821E+04 -0.36005E+03	0.30747E+02 0.0
10	52.00 -26.67	0.50164E-02 -0.17533E+00	-0.31713E+01 -0.15554E+01	-0.31953E+04 -0.38413E+03	0.67143E+02 0.0
11	52.00 -40.00	-0.16512E-03 -0.17523E+00	-0.79249E+01 0.32754E+01	-0.43750E+04 -0.26369E+03	-0.10125E+03 0.0
13	26.00 -40.00	-0.87913E-04 -0.16368E+00	-0.62716E+01 0.40764E+00	0.19106E+04 -0.12719E+03	-0.15253E+03 0.0
14	13.00 -40.00	-0.43730E-04 -0.15934E+00	-0.57943E+01 0.20350E+00	0.33603E+04 -0.12322E+03	-0.74104E+02 0.0
15	0.0 -40.00	0.0 -0.15774E+00	-0.56062E+01 0.0	0.38322E+04 -0.12190E+03	0.0 0.0

Problem 2 - Output (continued)

STRESSES IN CULVERT WALL (PSI) FOR LOAD INCREMENT 8

NPPT	ELLIP. OR INNER CAGE STEEL	OUTER CAGE STEEL	CONCRETE COMPRESSION	SHEAR STRESS
1	0.17847E+04	0.0	-0.37247E+03	0.0
2	0.14741E+04	0.0	-0.30974E+03	0.14245E+02
3	0.67317E+03	-0.70528E+03	-0.14109E+03	0.23843E+02
4	-0.35505E+03	0.31755E+03	-0.70357E+02	0.29412E+02
5	-0.54772E+03	0.42065E+03	-0.88291E+02	0.57743E+01
6	-0.15723E+04	0.10729E+04	-0.30107E+03	-0.54512E+01
7	-0.14181E+04	0.87080E+03	-0.26849E+03	-0.33656E+01
8	-0.13537E+04	0.75670E+03	-0.25395E+03	-0.27771E-01
9	-0.14655E+04	0.81929E+03	-0.27494E+03	0.45032E+01
10	-0.17599E+04	0.10670E+04	-0.33277E+03	0.99471E+01
11	-0.71466E+03	0.47993E+03	-0.11432E+03	-0.68642E+01
12	-0.37275E+03	0.14823E+03	-0.68036E+02	-0.35859E+02
13	0.72027E+03	-0.94374E+03	-0.18311E+03	-0.22597E+02
14	0.13637E+04	0.0	-0.32448E+03	-0.11978E+02
15	0.15715E+04	0.0	-0.36778E+03	0.0

STRAINS IN THE INNER AND OUTER FIBER OF THE CULVERT WALL
(ONLY STRAINS FOR COMPRESSION ZONES HAVE PHYSICAL MEANING)

NPPT	INNER STRAIN	OUTER STRAIN
1	0.81999E-04	-0.84375E-04
2	0.67815E-04	-0.70166E-04
3	0.30954E-04	-0.31962E-04
4	-0.15938E-04	0.14761E-04
5	-0.20001E-04	0.16013E-04
6	-0.68202E-04	0.52530E-04
7	-0.60822E-04	0.43649E-04
8	-0.57529E-04	0.38795E-04
9	-0.62283E-04	0.42004E-04
10	-0.75384E-04	0.53641E-04
11	-0.29897E-04	0.18531E-04
12	-0.15412E-04	0.83669E-05
13	0.34469E-04	-0.41481E-04
14	0.64327E-04	-0.73535E-04
15	0.73873E-04	-0.83314E-04

Problem 2 - Output (continued)

CALCULATED SAFETY FACTORS FOR LOAD INCREMENT	8
STEEL YIELD STRESS / MAX. STEEL STRESS	36.421
CONCRETE STRENGTH / MAX. COMPRESSIVE STRESS	13.424
WALL SHEAR CAPACITY / MAX. SHEAR	3.944
PERFORMANCE FACTORS	
0.01 INCH / MAX. CRACK WIDTH	9999.996

* * * * NORMAL EXIT FROM CANDE * * * *

Problem 3 - Input

CARD TYPE 1...X...10....X...20....X...30....X...40....X...50....X...60....X...70....X...80

CARD 1A ANALYS 3 CONCRE BOX CULVERT TEST (6*4-2) TEST-1 1415
 CARD 1B -1.0 7.0 ARBI 3 0.0001
 CARD 2B 6965.0 0.17 150.0 99430.0
 CARD 3B .03475 .00000 1.443 7.375
 CARD 3B .03475 .03550 1.443 7.375
 CARD 3B .03475 .03550 1.443 7.375
 CARD 3B .03475 .03550 1.443 7.375
 CARD 3B .01737 .03550 14.0
 CARD 3B .00000 .03550
 CARD 3B .01337 .03550 14.0
 CARD 3B .02675 .03550 1.006 7.438
 CARD 3B .02675 .03550 1.006 7.438
 CARD 3B .02675 .03550 1.006 7.438
 CARD 3B .02675 .00000 1.006 7.438
 CARD 1C PREP BOX CULVERT OUT-OF-GROUND STUDY (TEST 6*4-2)
 CARD 2C 10 3 0 0 1 17 15 14
 CARD 3C 1 0 0.0 27.5
 CARD 3C 2 0 9.0 27.5
 CARD 3C 3 0 19.0 27.5
 CARD 3C 4 0 29.0 27.5
 CARD 3C 5 0 39.5 27.5
 CARD 3C 6 0 39.5 17.0
 CARD 3C 7 0 39.5 8.5
 CARD 3C 8 0 39.5 0.0
 CARD 3C 9 0 39.5 -8.5
 CARD 3C 10 0 39.5 -17.0
 CARD 3C 11 0 39.5 -27.5
 CARD 3C 12 0 29.0 -27.5
 CARD 3C 13 0 19.0 -27.5
 CARD 3C 14 0 9.0 -27.5
 CARD 3C 15 0 0.0 -27.5
 CARD 3C 16 0 6.0 -33.5
 CARD 3C L 17 0 12.0 -33.5
 CARD 4C 1 2 1 0 0 1
 CARD 4C 2 3 2 0 0 2
 CARD 4C 3 4 3 0 0 3
 CARD 4C 4 5 4 0 0 4
 CARD 4C 5 6 5 0 0 5
 CARD 4C 6 7 6 0 0 6
 CARD 4C 7 8 7 0 0 7
 CARD 4C 8 9 8 0 0 8
 CARD 4C 9 10 9 0 0 9
 CARD 4C 10 11 10 0 0 10
 CARD 4C 11 12 11 0 0 11
 CARD 4C 12 13 12 0 0 12
 CARD 4C 13 14 13 0 0 13
 CARD 4C 14 15 14 0 0 14
 CARD 4C L 15 16 17 14 0 1

Problem 3 - Input (continued)

CARD TYPE 1....X....10....X....20....X....30....X....40....X....50....X....60....X....70....X....80

CARD 5C 1 1 0.0 1
CARD 5C 15 1 0.0 1
CARD 5C 16 1 0.0 1
CARD 5C 17 1 0.0 1
CARD 5C 2 0 -100.0 1
CARD 5C 2 0 -100.0 2
CARD 5C 2 0 -100.0 3
CARD 5C 2 0 -100.0 4
CARD 5C 2 0 -100.0 5
CARD 5C 2 0 -100.0 6
CARD 5C 2 0 -100.0 7
CARD 5C 2 0 -100.0 8
CARD 5C 2 0 -100.0 9
CARD 5C L 2 0 -100.0 10
CARD 1D L 1 1
CARD 2D 1.0E+11 0.0
STOP

Problem 3 - Output

*** PROBLEM NUMBER 1 ***

BOX CULVERT TEST (6*4-2) TEST-1

EXECUTION MODEANAL

SOLUTION LEVELF.E.USER

CULVERT TYPE CONCRETE

***NEGATIVE PIPE DIAMETER IMPLIES NEW CANOE OPTION FOR VARIABLE CONCRETE THICKNESS. ***

***OPTION IS RESTRICTED TO ANALYSIS ONLY WITH LEVEL 2-BOX, OR LEVEL 3. ***

PIPE PROPERTIES ARE AS FOLLOWS ...
(UNITS ARE INCH-POUND SYSTEM.)

NOMINAL PIPE DIAMETER	-1.0000
CONCRETE COMPRESSIVE STRENGTH	6965.00 00
CONCRETE ELASTIC MODULUS	5059544.00
CONCRETE POISSON RATIO	0.1700
DENSITY OF PIPE (PCF)	150.0000
STEEL YIELD STRENGTH	99430.0000
STEEL ELASTIC MODULUS	29000000.0
STEEL POISSON RATIO	0.3000
NONLINEAR CODE (1,2,OR 3)	3
CONC. CRACKING STRAIN (1,2,3)	0.000100
CONC. YIELDING STRAIN (2,3)	0.000668
CONC. CRUSHING STRAIN (2,3)	0.002000
STEEL YIELDING STRAIN (3)	0.003120
SPACING, LONGITUDINAL REINFORCEMENT	2.00

Problem 3 - Output (continued)

NODE #		STEEL AREA S (IN ²)		STEEL COVERS (IN)		THICKNESS (IN)
N	ASI (IN)	ASO (IN)	TBI (IN)	TDO (IN)	PTV (IN)	
1	0.0347	0.0	1.4430	1.2500	7.3750	
2	0.0347	0.0355	1.4430	1.2500	7.3750	
3	0.0347	0.0355	1.4430	1.2500	7.3750	
4	0.0347	0.0355	1.4430	1.2500	7.3750	
5	0.0174	0.0355	1.2500	1.2500	14.0000	
6	0.0	0.0355	1.2500	1.2500	7.0000	
7	0.0	0.0355	1.2500	1.2500	7.0000	
8	0.0	0.0355	1.2500	1.2500	7.0000	
9	0.0	0.0355	1.2500	1.2500	7.0000	
10	0.0	0.0355	1.2500	1.2500	7.0000	
11	0.0134	0.0355	1.2500	1.2500	14.0000	
12	0.0267	0.0355	1.0060	1.2500	7.4380	
13	0.0267	0.0355	1.0060	1.2500	7.4380	
14	0.0267	0.0355	1.0060	1.2500	7.4380	
15	0.0267	0.0	1.0060	1.2500	7.4380	

* * BEGIN PREP OF FINITE ELEMENT INPUT * *

THE DATA TO BE RUN IS ENTITLED

BOX CULVERT CUT-OF-GROUND STUDY (TEST 6*4-2)

NUMBER OF CONSTRUCTION INCREMENTS----- 10
 PRINT CONTROL FOR PREP OUTPUT----- 3
 INPUT DATA CHECK----- 0
 PLUT TAPE GENERATION----- 0
 ENTIRE FINITE ELEMENT RESULTS OUTPUT--- 1
 THE NUMBER OF NODES IS----- 17
 THE NUMBER OF ELEMENTS IS----- 15
 THE NUMBER OF BOUNDARY CONDITIONS IS--- 14

Problem 3 - Output (continued)

***BOUNDARY CONDITIONS...FORCES = LBS DISPLACEMENTS = INCHES...

BOUNDARY NODE	LOAD STEP	X-FORCE X-DISPLACEMENT	Y-FORCE Y-DISPLACEMENT	X-Y ROTATION DEGREES
1	1	D = 0.0	F = 0.0	0.0
15	1	D = 0.0	F = 0.0	0.0
16	1	F = 0.0	D = 0.0	0.0
17	1	F = 0.0	D = 0.0	0.0
2	1	F = 0.0	F = -0.1000E+03	0.0
2	2	F = 0.0	F = -0.1000E+03	0.0
2	3	F = 0.0	F = -0.1000E+03	0.0
2	4	F = 0.0	F = -0.1000E+03	0.0
2	5	F = 0.0	F = -0.1000E+03	0.0
2	6	F = 0.0	F = -0.1000E+03	0.0
2	7	F = 0.0	F = -0.1000E+03	0.0
2	8	F = 0.0	F = -0.1000E+03	0.0
2	9	F = 0.0	F = -0.1000E+03	0.0
2	10	F = 0.0	F = -0.1000E+03	0.0

Problem 3 - Output (continued)

STRUCTURAL RESPONSE OF CULVERT FOR LOAD INCREMENT 5

COORDINATES, DISPLACEMENTS AND CRACK DEPTHS ARE IN INCHES
 PRESSURES ARE IN LB/IN*2
 MOMENTS ARE IN IN.*LB/IN.
 THRUST AND SHEAR ARE IN LB/IN.

NPPT	X-COORD. Y-COORD.	X-DISP. Y-DISP.	N-PRES. S-PRES.	MOMENT THRUST	SHEAR CRACK DEPTH
1	0.0 27.50	0.0 -0.15773E+00	-0.64410E+00 0.0	0.91441E+04 0.13239E+02	0.0 0.56336E+01
2	9.00 27.50	0.21162E-05 -0.14942E+00	-0.53278E+02 -0.18070E-05	0.91178E+04 0.13239E+02	0.25597E+03 0.57301E+01
3	19.00 27.50	0.50681E-05 -0.12814E+00	-0.65051E+00 0.17166E-05	0.40270E+04 0.13239E+02	0.51229E+03 0.0
4	29.00 27.50	0.83627E-05 -0.10406E+00	-0.62088E+00 0.26052E-05	-0.11280E+04 0.13239E+02	0.51872E+03 0.0
5	39.50 27.50	0.10792E-04 -0.78849E-01	-0.46690E+00 -0.46118E+00	-0.66088E+04 -0.25778E+03	0.26759E+03 0.0
6	39.50 17.00	0.24313E-01 -0.78740E-01	0.34437E-02 -0.63980E+00	-0.67493E+04 -0.53184E+03	0.13265E+02 0.47313E+01
7	39.50 8.50	0.39382E-01 -0.78546E-01	0.29297E-02 -0.64936E+00	-0.68619E+04 -0.53763E+03	0.13236E+02 0.47405E+01
8	39.50 0.0	0.45814E-01 -0.78341E-01	0.51970E-03 -0.64522E+00	-0.69743E+04 -0.54314E+03	0.13221E+02 0.47867E+01
9	39.50 -8.50	0.42003E-01 -0.78109E-01	0.37887E-02 -0.64568E+00	-0.70867E+04 -0.54862E+03	0.13203E+02 0.47942E+01
10	39.50 -17.00	0.26661E-01 -0.77876E-01	-0.78634E-02 -0.64104E+00	-0.71989E+04 -0.55441E+03	0.13224E+02 0.48014E+01
11	39.50 -27.50	-0.90492E-05 -0.77757E-01	0.45906E+00 -0.45692E+00	-0.73280E+04 -0.28535E+03	-0.27550E+03 0.0
12	29.00 -27.50	-0.66193E-05 -0.50064E-01	0.64127E+00 0.19167E-04	-0.14131E+04 -0.13246E+02	-0.56754E+01 0.0
13	19.00 -27.50	-0.33335E-05 -0.23575E-01	0.64524E+00 -0.39101E-05	0.42963E+04 -0.13246E+02	-0.57406E+03 0.0
14	9.00 -27.50	-0.57829E-06 -0.11727E-07	-0.61072E+02 0.24769E-02	0.10070E+05 -0.13234E+02	-0.28719E+03 0.58606E+01
15	0.0 -27.50	0.0 0.92615E-02	0.64529E+00 0.0	0.10043E+05 -0.13222E+02	0.0 0.58531E+01

Problem 3 - Output (continued)

STRESSES IN CULVERT WALL (PSI) FOR LOAD INCREMENT 5

NPPT	ELLIP. OR INNER CAGE STEEL	OUTER CAGE STEEL	CONCRETE COMPRESSION	SHEAR STRESS
1	0.47231E+05	0.0	-0.24711E+04	0.0
2	0.48320E+05	-0.97052E+03	-0.23101E+04	0.42460E+02
3	0.15645E+04	-0.16679E+04	-0.41377E+03	0.84978E+02
4	-0.42373E+03	0.47940E+03	-0.11478E+03	0.86045E+02
5	-0.10902E+04	0.85525E+03	-0.21280E+03	0.20988E+02
6	0.0	0.27082E+05	-0.20249E+04	0.23067E+01
7	0.0	0.27558E+05	-0.20582E+04	0.23019E+01
8	0.0	0.29503E+05	-0.21715E+04	0.22994E+01
9	0.0	0.29974E+05	-0.22046E+04	0.22962E+01
10	0.0	0.30441E+05	-0.22376E+04	0.22999E+01
11	-0.12164E+04	0.95255E+03	-0.23742E+03	-0.21608E+02
12	-0.65296E+03	0.56926E+03	-0.14554E+03	-0.89944E+02
13	0.19400E+04	-0.17701E+04	-0.43570E+03	-0.90976E+02
14	0.62375E+05	-0.80526E+03	-0.26233E+04	-0.45513E+02
15	0.62147E+05	0.0	-0.26309E+04	0.0

STRAINS IN THE INNER AND OUTER FIBER OF THE CULVERT WALL
(ONLY STRAINS FOR COMPRESSION ZONES HAVE PHYSICAL MEANING)

NPPT	INNER STRAIN	OUTER STRAIN
1	0.15580E-02	-0.47430E-03
2	0.19930E-02	-0.44340E-03
3	0.80352E-04	-0.79416E-04
4	-0.22031E-04	0.22609E-04
5	-0.40844E-04	0.33473E-04
6	-0.38864E-03	0.11191E-02
7	-0.39504E-03	0.11386E-02
8	-0.41679E-03	0.12176E-02
9	-0.42314E-03	0.12370E-02
10	-0.42947E-03	0.12563E-02
11	-0.45569E-04	0.37288E-04
12	-0.27935E-04	0.27114E-04
13	0.83477E-04	-0.83626E-04
14	0.23422E-02	-0.50350E-03
15	0.23341E-02	-0.50496E-03

Problem 3 - Output (continued)

CALCULATED SAFETY FACTORS FOR LOAD INCREMENT 5	
STEEL YIELD STRESS / MAX. STEEL STRESS	1.594
CONCRETE STRENGTH / MAX. COMPRESSIVE STRESS	2.647
WALL SHEAR CAPACITY / MAX. SHEAR	1.835
PERFORMANCE FACTORS	
0.01 INCH / MAX. CRACK WIDTH	0.897

APPENDIX D

CANDE PROGRAM OVERLAY

This appendix provides job control language (JCL) for IBM computers in order to reduce core storage requirements (region size) for executing CANDE-1980. Instructions and examples are given for two FORTRAN IV compilers commonly supported at IBM installations; the G and the H-extended (HX) compilers.

For reference, a tree chart of the CANDE-1980 subroutines is shown in Table D.1 indicating the calling sequence of all subroutines. Subroutines CANBOX and DUNCAN are new subroutines added to the CANDE-1980 program, and subroutines CONMAT, CONCRE, and READM have been extensively modified from the CANDE-1976 program. Some minor changes have been made to other subroutines.

Table D.2 gives the JCL to compile an overlayed version of CANDE on the G compiler presuming the source program resides on a disk file created by standard TSO operations. Here, the overlay commands (ENTRY MAIN through INSERT BURNS) provide a simple overlay structure that may be used as a guide for overlaying CANDE on most computers.

In a similar manner, TABLE D.3 provides JCL for compiling an overlayed version of CANDE with the HX compiler. Here, the overlay structure is slightly different and takes advantage of special overlay options (i.e. OVERLAY C(REGION)) available at IBM installations. The overlay commands in Tables D.2 and D.3 may be interchanged, however the overlay structure in Table D.3 is more efficient on IBM.

Once a load module is created from either Table D.2 or D.3, the JCL to execute the program is shown in Table D.4. Efficiency comparisons of executing a typical problem (Example 1, Appendix C) are shown in Table D.4 for the G and HX compilers with and without overlay. These

examples were executed on the IBM 370/168 computer at the University of Notre Dame. It is observed that HX compiler with overlay provided the most efficient results in terms of core storage, execution time, and total cost.

TABLE D.1 - Subroutine Tree Structure for CANDE

TABLE D.2 - JCL to Create an Overlaid Version
of CANDE Using the G Compiler

```
//CNDEOVLY JOB (XX,XXXX,,15),IDNUMBER,NOTIFY=TSOID#,  
// REGION=256K,TIME=1  
//STEP1 EXEC FORTGCL,PARM.LKED='OVLY,MAP,XREF,LIST'  
//FORT.SYSLIN DD UNIT=DISK,DISP=(NEW,PASS),SPACE=(TRK,(10,5)),  
// DSN=&&LOADSET,DCB=BLKSIZE=80  
//FORT.SYSIN DD UNIT=DISK,VOL=SER=XXXXXX,DSN=TSOID#.CANDE.FORT,  
// DISP=SHR  
//LKED.SYSLMOD DD SPACE=(1024,(600,50,1),RLSE),DISP=(NEW,CATLG),  
// UNIT=DISK,VOL=SER=XXXXXX,DSN=TSOID#.CANDE.LOAD(CANDE)  
//LKED.SYSLIN DD UNIT=DISK,DSN=&&LOADSET,DISP=(OLD,DELETE)  
//LKED.SYSIN DD *  
ENTRY MAIN  
INSERT MAIN, PRHERO,RESOUT,PRINC,ESTAB  
INSERT STEEL,ALUMIN,EMOD  
INSERT HINGE,SETU,INVER  
INSERT CONCRE,CONMAT  
INSERT PLASTI,BASIC  
OVERLAY A  
INSERT PREP  
OVERLAY B  
INSERT CANBOX,CAN1,XCAN,XCAN2  
OVERLAY B  
INSERT GENNOD,SAVEG,GENEL,GENEND,AF,MODMSH,SAVED  
OVERLAY A  
INSERT HEROIC,CONVT,GEOM,RESPIP,REDUCI,BAKSUB,XFACES  
OVERLAY B  
INSERT READM,ANISP,DUNCAN,HARDIN,INTP1  
INSERT STIFNS,BEAMEL,STFSUB,STRESS,BEAMST  
OVERLAY A  
INSERT BURNS  
/*
```

Note: Overlay commands (ENTRY MAIN through INSERT BURNS)
start in column 2.

TABLE D.3 - JCL to Create an Overlaid Version of CANDE
Using the H Extended Compiler

```
//CNDEOVLY JOB (XX,XXXX,,15),IDNUMBER,NOTIFY=TSOID#,REGION=256K,  
// TIME=2  
//STEP1 EXEC FORTXCL,PARM.FORT='OPT(2)',PARM.LKED='OVLY,MAP,XREF,LIST'  
//FORT.SYSIN DD UNIT=DISK,VOL=SER=XXXXXX,DSN=TSOID#.CANDE.FORT,  
// DISP=SHR  
//LKED.SYSLMOD DD SPACE=(1024,(600,50,1),RLSE),DISP=(NEW,CATLG),  
// UNIT=DISK,VOL=SER=XXXXXX,DSN=TSOID#.CANDE.LOAD(CANDE)  
//LKED.SYSIN DD *  
ENTRY MAIN  
INSERT MAIN,PRHERO,RESOUT,PRINC,ESTAB  
OVERLAY A  
INSERT STEEL,ALUMIN,EMOD  
OVERLAY B  
INSERT HINGE,SETU,INVER  
OVERLAY A  
INSERT CONCRE,CONMAT  
OVERLAY A  
INSERT PLASTI,BASIC  
OVERLAY C(REGION)  
INSERT PREP  
OVERLAY D  
INSERT CANBOX,CAN1,XCAN,XCAN2  
OVERLAY D  
INSERT GENNOD,SAVEG,GENEL,GENEND,AF,MODMSH,SAVED  
OVERLAY C  
INSERT HEROIC,CONVT,GEOM,RESPIP,REDUCI,BAKSUB,XFACES  
OVERLAY D  
INSERT READM,ANISP,DUNCAN,HARDIN,INTP1  
INSERT STIFNS,BEAMEL,STFSUB,STRESS,BEAMST  
OVERLAY C  
INSERT BURNS  
/*
```

Note: Overlay commands start in column 2.

TABLE D.4 - JCL to run CANDE

```

//CANDERUN JOB (XX,XXXX,,10),IDNUMBER,NOTIFY=TSOID#,
//          REGION=256K,TIME=2
//STEP1    EXEC PGM=CANDE
//STEPLIB  DD UNIT=DISK,VOL=SER=XXXXXX,DISP=SHR,
//          DSN=TSOID#.CANDE.LOAD
//FT05F001 DD UNIT=DISK,VOL=SER=XXXXXX,DISP=SHR,
//          DSN=TSOID#.PROBNAME.DATA,
//          DCB=(RECFM=FB,LRECL=80,BLKSIZE=3120,BUFNO=1)
//FT06F001 DD SYSOUT=A
//FT10F001 DD UNIT=DISK,DSN=&&TEMPO,DISP=(NEW,DELETE),
//          SPACE=(TRK,(10,5)),DCB=(RECFM=VBS,BLKSIZE=8000,BUFNO=2)
//FT11F001 DD UNIT=DISK,DSN=&&TEMP1,DISP=(NEW,DELETE),
//          SPACE=(TRK,(10,5)),DCB=(RECFM=VBS,BLKSIZE=8000,BUFNO=2)
//FT12F001 DD UNIT=DISK,DSN=&&TEMP2,DISP=(NEW,DELETE),
//          SPACE=(TRK,(10,5)),DCB=(RECFM=VBS,BLKSIZE=8000,BUFNO=2)
//FT13F001 DD UNIT=DISK,DSN=&&TEMP3,DISP=(NEW,DELETE),
//          SPACE=(TRK,(10,5)),DCB=(RECFM=VBS,BLKSIZE=8000,BUFNO=2)
//FT30F001 DD UNIT=DISK,DSN=&&TEMP5,DISP=(NEW,DELETE),
//          SPACE=(TRK,(10,5)),DCB=(RECFM=VBS,BLKSIZE=8000,BUFNO=2)

```

TABLE D.5 - Efficiency comparisons of executing CANDE

Compiler & Overlay	Region size (K bytes)	Central Processor time (min:sec)	Disk time (sec)	Total cost (dollars)
G No-overlay	380	1:43	35.0	\$9.62
G Overlay	320	1:44	35.0	\$9.34
HX No-overlay	348	1:03	35.0	\$6.45
HX Overlay	264	1:04	35.0	\$6.14

REFERENCES

1. Katona, M.G., et al., "CANDE - A Modern Approach for the Structural Design and Analysis of Buried Culverts," Report No. FHWA-RD-77-5, Federal Highway Administration, Washington, D.C., October 1976.
2. Katona, M.G. and Smith, J.M., "CANDE User Manual," Report No. FHWA-RD-77-6, Federal Highway Administration, Washington, D.C., October 1976.
3. Katona, M.G. and Smith, J.M., "CANDE System Manual," Report No. FHWA-RD-77-7, Federal Highway Administration, Washington, D.C., October 1976.
4. Building Code Requirements for Reinforced Concrete, American Concrete Institute, ACI 318-77, 1977, Detroit.
5. Commentary on Building Code Requirements for Reinforced Concrete, American Concrete Institute, ACI 318-77, 1977, Detroit.
6. Vittes, Pedro D., "Finite Element Analysis of Reinforced Concrete Box Culvert," Master's Thesis, Dept. of Civil Eng., Univ. of Notre Dame, May, 1980.
7. Wang, C.K. and Salmon, D.G., Reinforced Concrete Design, Intext Educational Publishers, Second Edition.
8. Sozen, M.A. and Gamble, W.L., "Strength and Cracking Characteristics of Beams with #14 and #18 Bars Spliced with Mechanical Splices," American Concrete Institute Journal, Detroit, December 1969, pp. 949-956.
9. Berwanger, C., "Effect of Axial Load on the Moment-Curvature Relationships of Reinforced Concrete Member," SP-50-11, American Concrete Institute, Detroit 1975, pp. 263-288.
10. Gergely, P. and Lutz, L.A., "Maximum Crack Width in Reinforced Concrete Flexural Members," SP-20, American Concrete Institute, Detroit 1968, pp. 87-117.
11. Lloyd, J.P., Rejali, H.M. and Kesler, C.E., "Crack Control in One-Way Slabs Reinforced with Deformed Welded Wire Fabric," American Concrete Institute Journal, Detroit, May 1969, pp. 366-376.
12. LaTona, R.W. and Heger, F.J., "Computerized Design of Precast Reinforced Concrete Box Culverts," Highway Research Record, Number 443, pp. 40-51.
13. Boring, M.R., Heger, F.J. and Bealey, M., "Test Programs for Evaluating Design Method and Standard Designs for Precast Concrete Box Culverts with Welded Wire Fabric Reinforcing," Transportation Research Record 518, pp. 49-63.

14. Simpson Gumpertz and Heger Inc., "Report of Test Programs for Evaluation of Design Method and Standard Designs for Precast Concrete Box Culverts with Welded Wire Fabric Reinforcing," submitted to American Concrete Pipe Association, July 1973.
15. Heger, F.J. and Saba, B.K., "The Structural Behavior of Precast Concrete Pipe Reinforced with Welded Wire Fabric," Progress Report No. 2, Project No. 1-7734, Cambridge, Massachusetts, July 1961.
16. Heger, F.J., "A Theory for the Structural Behavior of Reinforced Concrete Pipe," Thesis submitted to the Department of Civil Engineering, Massachusetts Institute of Technology, January 1962.
17. Heger, F.J., "Structural Behavior of Circular Reinforced Concrete Pipe-Development of Theory," Journal of the American Concrete Institute, November 1963, pp. 1567-1613.
18. American Society for Testing Materials, "Standard Specification for Reinforced Concrete Culvert, Storm Drain, and Sewer Pipe," (ASTM Designation C76-70), 1970.
19. Breton, J.M., "Precast Box Culvert Project - Fabric Materials Test," Report to Frank Smith - Gifford Hill Pipe Company, April 1973.
20. American Society for Testing Materials, "Standard Specifications for Welded Wire Fabric for Concrete Reinforcement," (ASTM Designations A185-73), 1973.
21. American Society for Testing Materials, "Standard Specification for Precast Reinforced Concrete Box Sections for Culverts, Storm Drains, and Sewers," (ASTM Designation C789-76), 1976.
22. American Association of State Highway and Transportation Officials, "Interim Specification for Precast Reinforced Concrete Box Sections for Culverts, Storm Drains and Sewers," (AASHTO Designation: M 259-76I), 1976.
23. Girdler, H.F., "Loads on Box Culverts Under High Embankments," Research Report 386, Department of Transportation, Division of Research, Lexington, Kentucky, April 1974.
24. Russ, R.L., "Loads on Box Culverts under High Embankments: Positive Projection, without Imperfect Trench," Research Report 431, Department of Transportation, Division of Research, Lexington, Kentucky, August 1975.
25. Allen, D.L., and Russ, R.L., "Loads on Box Culverts under High Embankments: Analysis and Design Considerations," Research Report 491, Department of Transportation, Division of Research, Lexington, Kentucky, January 1978.

26. Kulhawy, F.H., J.M. Duncan, and H.B. Seed, "Finite Element Analysis of Stresses and Movements in Embankments during Construction," U.S. Army Eng. Waterways Experiment Station, Contract Report 569-8, Vicksburg, Miss., 1969.
27. Duncan, J.M., and C.Y. Chang, "Nonlinear Analysis of Stress and Strain in Soils, Journal of Soil Mechanics and Foundations Div., ASCE, vol. 96, No. SM5, Sept. 1970, pp. 1629-1653.
28. Wong, Kai S. and J.M. Duncan, "Hyperbolic Stress-Strain Parameters for Nonlinear Finite Element Analysis of Stresses and Movements in Soil Masses," Report No. TE-74-3, University of California, Berkeley, July 1974.
29. Duncan, J.M., et. al., "Strength, Stress-Strain and Bulk Modulus Parameters for Finite Element Analyses of Stresses and Movements in Soil Masses, Report No. UCB/GT/78-02 to National Science Foundation, April 1978.
30. Lee, Chee-Hai, "Evaluation of Duncan's Hyperbolic Soil Model," Master's Thesis, University of Notre Dame, May, 1979.
31. Katona, M.G., et. al., "Structural Evaluation of New Concepts for Long-Span Culverts and Culvert Installations," FHWA Report No. RD-79-115, Washington, D.C., December, 1979.



FEDERALLY COORDINATED PROGRAM (FCP) OF HIGHWAY RESEARCH AND DEVELOPMENT

The Offices of Research and Development (R&D) of the Federal Highway Administration (FHWA) are responsible for a broad program of staff and contract research and development and a Federal-aid program, conducted by or through the State highway transportation agencies, that includes the Highway Planning and Research (HP&R) program and the National Cooperative Highway Research Program (NCHRP) managed by the Transportation Research Board. The FCP is a carefully selected group of projects that uses research and development resources to obtain timely solutions to urgent national highway engineering problems.*

The diagonal double stripe on the cover of this report represents a highway and is color-coded to identify the FCP category that the report falls under. A red stripe is used for category 1, dark blue for category 2, light blue for category 3, brown for category 4, gray for category 5, green for categories 6 and 7, and an orange stripe identifies category 0.

FCP Category Descriptions

1. Improved Highway Design and Operation for Safety

Safety R&D addresses problems associated with the responsibilities of the FHWA under the Highway Safety Act and includes investigation of appropriate design standards, roadside hardware, signing, and physical and scientific data for the formulation of improved safety regulations.

2. Reduction of Traffic Congestion, and Improved Operational Efficiency

Traffic R&D is concerned with increasing the operational efficiency of existing highways by advancing technology, by improving designs for existing as well as new facilities, and by balancing the demand-capacity relationship through traffic management techniques such as bus and carpool preferential treatment, motorist information, and rerouting of traffic.

3. Environmental Considerations in Highway Design, Location, Construction, and Operation

Environmental R&D is directed toward identifying and evaluating highway elements that affect

the quality of the human environment. The goals are reduction of adverse highway and traffic impacts, and protection and enhancement of the environment.

4. Improved Materials Utilization and Durability

Materials R&D is concerned with expanding the knowledge and technology of materials properties, using available natural materials, improving structural foundation materials, recycling highway materials, converting industrial wastes into useful highway products, developing extender or substitute materials for those in short supply, and developing more rapid and reliable testing procedures. The goals are lower highway construction costs and extended maintenance-free operation.

5. Improved Design to Reduce Costs, Extend Life Expectancy, and Insure Structural Safety

Structural R&D is concerned with furthering the latest technological advances in structural and hydraulic designs, fabrication processes, and construction techniques to provide safe, efficient highways at reasonable costs.

6. Improved Technology for Highway Construction

This category is concerned with the research, development, and implementation of highway construction technology to increase productivity, reduce energy consumption, conserve dwindling resources, and reduce costs while improving the quality and methods of construction.

7. Improved Technology for Highway Maintenance

This category addresses problems in preserving the Nation's highways and includes activities in physical maintenance, traffic services, management, and equipment. The goal is to maximize operational efficiency and safety to the traveling public while conserving resources.

8. Other New Studies

This category, not included in the seven-volume official statement of the FCP, is concerned with HP&R and NCHRP studies not specifically related to FCP projects. These studies involve R&D support of other FHWA program office research.

*The complete seven-volume official statement of the FCP is available from the National Technical Information Service, Springfield, Va. 22161. Single copies of the introductory volume are available without charge from Program Analysis (HRD-3), Offices of Research and Development, Federal Highway Administration, Washington, D.C. 20590.



00056990